Optimisation et modélisation du traitement combiné biologique et physico-chimique du phosphore dans les stations d'épuration avec aération alternée

Erika Varga

A DISSERTATION

In order to obtain the title of

DOCTOR OF THE UNIVERSITY OF TOULOUSE

Issued by Institut National des Sciences Appliquées de Toulouse

---

Defended by

Erika VARGA

On 24 March 2022

Optimization and modeling of combined biological and physical-chemical phosphorus removal in wastewater treatment plants with intermittent aeration

---

PhD School: **MEGEP - Mécanique, Energétique, Génie civil, Procédés**

Department: **Génie des Procédés et de l'Environnement**

Research Laboratory:
TBI - Toulouse Biotechnology Institute, Bio & Chemical Engineering

Supervised by
Mathieu SPERANDIO

The jury members

Mrs. Anna MIKOLA, Referee
Mrs. Marion ALLIET, Examiner
Mrs. Sylvie GILLOT, Examiner
Mr. Mathieu SPERANDIO, PhD Supervisor
Mrs. Eveline VOLCKE, President

Abstract

The objective of this thesis was to study the combined biological and physical-chemical treatment of phosphorus in wastewater treatment plants using intermittent aeration in order to optimize performance and identify the potential for nutrient recovery. While combined treatment in alternating aeration activated sludge systems has become a standard in France, optimization scenarios to allow better nutrient recovery have been developed. The possibility of coupling treatment with ferric salts and producing a valuable iron phosphate product is an important target. One of the challenges of this work was to generate knowledge for a better understanding and modeling of these systems.

Firstly, a literature review presents the current state of knowledge in the field, especially regarding the combined biological and physical-chemical removal of phosphorus, the reaction mechanisms of iron, and the progress in the field of modeling.

An experimental study was then carried out on the scale of a real treatment plant using an intermittent aeration system (Villefranche de Lauragais). On this site, the aeration control was particularly optimized for the complete removal of nitrogen by nitrification and denitrification. Through an intensive measurement campaign, using on-line sensors and laboratory analysis, the performance and dynamics of phosphorus removal were characterized. This work was carried out within the framework of a European project (CircRural4.0) aiming at optimizing nutrient removal and recovery in rural plants while maintaining high energy efficiency. Dedicated periods were devoted to purely biological treatment, without iron input. This analysis showed that the requirement of an average concentration of less than 2 mg P/L can be met by biological treatment only. However, this result is only achieved by integrating constraints in the aeration cycles and sludge management. Indeed, kinetic experiments have shown that the anoxic phosphorus uptake rate is significantly lower than the aerobic uptake rate, and anaerobic periods can lead to disturbances in phosphate release. To ensure a more reliable removal and to achieve low phosphate concentrations, different levels of iron dosing were tested to complement the biological system. A minor dosage (50% lower than the theoretical recommended dosage) was found to be sufficient to maintain very good quality. After having noticed a peak in phosphate release during the extraction and sludge treatment periods, a specific dosing method on the dewatering liquors was successfully implemented.

This type of installation operates with extended solids retention times and the fate of iron and phosphates in the sludge stream was examined. For this reason, a series of specific experiments on iron reduction kinetics and its consequences was then carried out. These experiments confirmed the biological nature of the reduction process and showed that the reaction is not limited by the electron donors present in the activated sludge. Indeed, an additional substrate (lactate and acetate) only slightly increases the rates. Furthermore, the overall reactions were described with first-order kinetics, and most of the iron was reduced after 24 h and almost all after 48 h. The most influential parameter was the concentration of suspended solids (microbial biomass), the influence of which was introduced to a mathematical model. Throughout the experiments, the release of phosphate was observed in parallel with the reduction processes. This release was analyzed together with the iron and sulfate concentration in order to reveal the conditions favorable to the precipitation of vivianite (iron phosphate).

The impact of sulfate concentration on iron reduction was studied, and the results show that an increase in sulfate concentration does not influence the rate of Fe(III) reduction, but causes an increased release of phosphate, due to the appearance of sulfides and competitive precipitation processes with iron. This interaction requires detailed attention in activated sludge in order to profit from it to the fullest in phosphorus recovery processes.

Finally, in the last chapter, a complete model of the alternating aeration treatment plant was developed, based on the Sumo21 model. The challenge was to improve the predictive quality of the model for the biological treatment and the combined phosphorus treatment under these conditions. Some processes were refined such as the prediction of iron reduction and oxidation based on laboratory experiments. The parameters of the biological phosphorus removal model were calibrated, in particular the kinetics of phosphate release and reabsorption in anaerobic, aerobic, and anoxic conditions. A method for controlling intermittent aeration was developed and the influence of the degree of aeration on phosphorus removal was successfully described. The hypothesis of an inhibition of biological phosphorus removal by iron was evaluated and different iron dosing strategies were simulated. Finally, the perspectives for the improvement of the model were discussed. This model will constitute a basis for further work, the aim of which could be to numerically simulate operating solutions for the recovery of iron phosphate

Résumé

L'objectif de cette thèse était d'étudier le traitement combiné du phosphore, biologique et physico-chimique, dans des systèmes d'épuration de petite taille, afin d'optimiser les performances et d'identifier le potentiel de récupération des nutriments. Alors que le traitement combiné dans des systèmes de boues activées à aération alternée est devenu une norme en France, des scénarios d'optimisation pour permettre une meilleure valorisation des nutriments se sont développés. La possibilité de coupler le traitement à base de sels ferriques et de produire un produit valorisable de phosphate de fer est une perspective. L'un des enjeux de ce travail était de générer des connaissances permettant une meilleure compréhension et une meilleure modélisation de ces systèmes.

Tout d'abord une revue de la littérature présente l'état actuel des connaissances du domaine, notamment en ce qui concerne l'élimination biologique et physico-chimique combinée du phosphore, les mécanismes réactionnels du fer, et les progrès en termes de modélisation.

Une étude expérimentale a ensuite été menée à l'échelle d'une installation réelle de traitement utilisant un système d'aération intermittente (Villefranche de Lauragais). Sur ce site le contrôle de l'aération était particulièrement optimisé pour une élimination complète de l'azote par nitrification et dénitrification. Au travers d'une campagne intensive de mesure, par des capteurs en ligne et des analyses de laboratoire, les performances et la dynamique de l'élimination du phosphore ont été caractérisées. Ce travail était réalisé dans le cadre d'un projet européen (CircRural4.0) visant à optimiser l'élimination et la récupération des nutriments dans les usines rurales tout en maintenant une efficacité énergétique élevée. Des périodes dédiées ont été consacrées à un traitement purement biologique, sans apport de fer. Cette analyse a permis de montrer que l'exigence d'une moyenne de concentration inférieure à 2 mg P/L peut être satisfaite par un traitement biologique. Cependant, ce résultat n'est atteint qu'en intégrant des contraintes concernant les cycles d'aération et la gestion de l'extraction des boues. En effet les expériences cinétiques ont montré que la vitesse d'absorption anoxique est significativement plus faible que la vitesse d'absorption en aérobie, et les périodes anaérobies peuvent entraîner une libération perturbante de phosphate. Pour assurer une garantie plus forte et atteindre de faibles concentrations en phosphate, différents niveaux de dosage de Fer ont été testés pour compléter le système biologique. Une dose mineure (50% inférieure à la dose théorique recommandée) s'est avérée suffisante pour maintenir une très bonne qualité. Après avoir constaté un relargage de phosphate lors des périodes d'extraction et de traitement des boues, une méthode de dosage spécifique sur les liqueurs de déshydratation a été mise en place avec succès.

Ce type d'installation fonctionne avec des temps de rétention prolongés et le devenir du fer et des phosphates dans la filière boue était questionnée. Pour cette raison un travail spécifique sur les cinétiques de réduction du fer et ses conséquences a ensuite été réalisé. Ces expériences ont confirmé la nature biologique du processus de réduction et montrent que la réaction n'est pas limitée par les donneurs d'électrons présents dans les boues activées. En effet un substrat supplémentaire (lactate et acétate) n'augmente que très légèrement les taux. De plus, les réactions globales ont été décrites avec une cinétique de premier ordre, et la majorité du fer était réduite après 24 h et en quasi-totalité après 48 h.

Le paramètre le plus influent était la concentration en matières en suspension (biomasse microbienne) dont l'influence a été traduite par un modèle mathématique. Tout au long des expériences, la libération de phosphate a été observée parallèlement aux processus de réduction. Cette libération a été analysée conjointement avec les teneurs de fer et sulfate de manière à révéler les conditions favorables à l'apparition de vivianite (phosphate de fer). L'impact de la concentration en sulfate sur la réduction du fer a été étudié, et les résultats montrent qu'une augmentation de cette concentration en sulfate n'influence pas le taux de réduction du Fe(III), mais provoque une libération accrue de phosphate, due à l'apparition des sulfides et aux processus de précipitation compétitif avec le fer. Cette interaction nécessite une attention détaillée dans les boues activées afin de l'exploiter au mieux dans les processus de récupération du phosphore.

Enfin, dans le dernier chapitre, un modèle complet de la station d'épuration à aération alternée a été développé, sur la base du modèle Sumo21. L'enjeu était d'améliorer la qualité prédictive du modèle pour le traitement biologique et le traitement combiné du phosphore. Certains processus ont été affinés comme la prédiction de la réduction et oxydation du fer sur la base des expériences menées au laboratoire. Les paramètres du modèle de déphosphatation biologique ont été calibrés, en particulier les cinétiques de relargage et réabsorption des phosphates en anaérobie, aérobie et anoxie. Une méthode de contrôle de l'aération l'intermittente a été développée et l'influence du degré d'aération sur la déphosphatation a été décrit avec succès. L'hypothèse d'une inhibition de la déphosphatation biologique par le fer a été évaluée et les différentes stratégies de dosage du fer ont été simulées. Enfin les perspectives d'amélioration du modèle ont été discutées. Ce modèle constituera une base pour de futurs travaux plus approfondis dont le but pourrait être de simuler numériquement des solutions d'exploitation permettant de réaliser la récupération de phosphate de fer.

Acknowledgments

First and foremost I would like to express my sincere gratitude to my supervisor, professor Mathieu Sperandio. I thank him, for patiently supporting me during all these years. It was very inspiring to work with such an expert on this challenging project. I wholeheartedly thank him for the encouragement and advice that he gave me, I could not have wished for a better mentor. He guided me through my first stumbling steps in research and equipped me with the tools to develop ideas and be more confident.

I would also thank the support of the team of Réseau31 throughout the project. Their flexibility really helped my work to move along.

I would like to express my appreciation to all the participants of the CircRural 4.0 Interreg project, which made my research possible. I deeply appreciate the opportunity to join this program.

I have been really lucky with the surrounding team in the lab, Symbiose, where each member supported my work there in one way or another.

I would like to thank all the technicians on the team, who were always patient with me, especially Chantha and Mansour who taught me my way around the lab.

I am grateful to have worked together with some enthusiastic interns and students, it was a great experience for me, and I hope it was beneficial for them as well.

I would like to thank all the team members for their part in my (professional or personal) life in Toulouse, may that be help to adjust to the lab, countless advice in my work, conference prep-presentations, and (as a result) great conferences, snowball fight, kayak trips, hiking (beyond where the water meets the sky), horse-riding, handball games, trips to Ikea, little people on the wall, festivals or even just talking (we all know, that is probably my favorite…) there are countless memories of these years.

I am and always will be grateful to the team at Dynamita, where I started my carrier. They inspired me to embark on this journey and supported me all along with priceless advice and a lot of consultation. Special thanks to Hélène and Imre for making my transition easier (although it was not an easy decision to leave such an incredible team) and that I could always turn to them for guidance.

I hope to see all these colleagues, and friends around at conferences and in future projects.

Finally, I am most grateful to my friends and family for their encouragement and endless support.

There may be others who I invertedly have not mentioned here but contributed to my work leading up to the completion of this thesis, my humblest apologies and I am nonetheless grateful.

List of communications and publications

Journal publication

Varga, E., Hauduc, H., Barnard, J., Dunlap, P., Jimenez, J., Menniti, A., Schauer P., Lopez-Vazquez C. M., Gu A.Z., Sperandio M. & Takács, I. (2018). Recent advances in bio-P modelling–a new approach verified by full-scale observations. *Water Science and Technology*, *78*(10), 2119-2130.

Recent submission (chapter 3)

Varga, E., Bounouba, M., Hauduc, H., Takács, I., Azimi, S., Rocher, V., Sperandio, M. (2022). Iron reduction kinetics and influencing parameters in activated sludge. Submitted to *Chemosphere*.

Conference

Varga, E., Hauduc, H., Barnard, J., Dunlap, P., Jimenez, J., Menniti, A., Schauer P., Lopez-Vazquez C. M., Gu A.Z., Sperandio M. & Takács, I: Enhanced Biological Phosphorus Removal Session: Recent Advances in bio-P modelling: A new approach verified by full-scale observations. *6th IWA/WEF Water Resource Recovery Modelling Seminar 2018* (10-14 March 2018, Lac Beauport, Quebec, Canada). Oral presentation.

Varga E., Bounouba M., Takacs I., Sperandio M. P recovery end products session: Significance of Fe(III) reduction and Consequence on Phosphate Binding Capacities. *IWA Nutrient Removal and Recovery Virtual Conference* (1-3 September 2020). Oral presentation.

Varga E., Bounouba M., Hauduc H., Takacs I., Azimi S., Rocher V., Sperandio M.: Analysis and modeling of iron reduction kinetics in activated sludge 7th IWA/WEF Water Resource Recovery Modelling Seminar 2021 (20-25 August 2021). Poster presentation (3rd place in best poster competition).

Webinar, Workshops, and others

IWA MIA Webinar: New Advances in Enhanced Biological Phosphorus Removal (EBPR) Modelling (9 July 2018). Panelist.

YWP Workshop: New model developments for Bio-P. *6th IWA/WEF Water Resource Recovery Modelling Seminar 2018.*

WEFTEC 2018. Menniti et al., Novel Treatment processes Pose Challenges for Standard Process Models

IWA LET 2019 Takacs et al., New Directions in Process Modelling – Catching up with the Industry

General introduction

The Phosphorus challenge

Phosphorus is an essential micronutrient for all organisms. Human phosphorus consumption has been linear thus far: consumption via food and disposal via waste and wastewater. This approach with increasing population and thus demand is unsustainable for numerous reasons. There are various aspects supporting the need for a circular P economy from the general necessity of P for food production (and increasing demand for efficient fertilizers), widespread environmental concerns (eutrophication) to geopolitical questions (regarding phosphate rock deposits, inequality caused by unstable food prices) (Roy, 2017). P cycle in nature through weathering, biological use, sedimentation, and eventual geologic uplift is a very slow process, while the rate of consumption is ever-increasing. With an integrated approach, this negative effect can be mitigated (Vaccari, 2009). As pollution from wastewater was linked to eutrophication, significant effort was invested into properly treating collected wastewater, and eventually, the need for nutrient recovery encourages researchers to find pathways for various removal technologies to the recovery of a safe, pure economically feasible product.

Often even the primary goals (i.e. reducing effluent concentrations to protect the receiving waters) meet challenges and the result of mitigation of these effects takes time (often due to the diffuse pollution from agricultural lands). According to an assessment of the ecological status of the European surface waters, in Adour-Garonne River Basin/Watershed (France), up to 60% of water bodies are still considered as not in a good ecological status or potential, and this is mainly due to high nitrogen and phosphorus content. At the same time, the agricultural soil in France is often P deficient, which indicates inefficient fertilizer use. While the European regulation determines effluent limits based on the receiving water, increasing constraints are imposed even in small water bodies.

Several small plants face challenges with efficient P removal, as they often face difficulties with the resources for monitoring, optimization, and operation. A retrofitted facility for example may not perform efficiently biological P removal, and it needs to be supplemented with chemicals.

Nutrient recovery from wastewater has received increasing attention recently. Indeed, phosphorus recovery from wastewater was selected as one of the top one hundred green activities by an EU-wide technical classification system (EU Taxonomy) to assess different economical activities that may contribute to the achievement of the EU Green Deal. Although this report may not consider all applicable technologies and is limited to phosphorus, it shows that P recovery gains a new level of significance on an international legislative level as well.

In France, the frequently used chemical addition during P removal leads to the poor development of P recovery, as struvite recovery is better suited for purely biological systems (often with digester) without metal dosage, and this is quite rare with stringent phosphorus limits. It is essential to re-examine the chemical use and/or evaluate different potential recovery products.

The need for a better understanding of combined P removal strategies

Several plant configurations have been developed for biological nutrient removal. Conventional multiple basin systems (such as Bardenpho, UCT) are efficient and reliable for purely biological P removal. However, they are not a common design for small/medium facilities. Indeed, in France, intermittent aerated systems are more widespread, usually optimized for complete nitrogen removal via nitrification/denitrification. While these facilities are efficient and robust regarding nitrogen removal, often face challenges with biological P removal. In order to comply with the effluent limits, these systems are supplemented with chemical dose (commonly Fe(III) salts). However, the interaction between biological and physical-chemical P removal in these types of facilities is not well understood. This leads to suboptimal operation and difficulties to reach effluent limits in case of a system disruption.

Besides the interactions between chemical dose and biological processes, it is important to consider the interactions between iron and phosphorus (and sulfur), especially for recovery purposes, for which the mobility of P is crucial for the recovery product.

Iron is widely used for different purposes (prevention of H_2S formation, coagulation, and phosphate removal) in WRRF. The use of aluminum is also considered to be efficient during wastewater treatment, but the use is often debated as the direct spreading of sludge for agricultural purposes is restricted in many countries due to the bio-availability and toxicity of the metal.

The main interest of this thesis is to assess iron-interaction, as it is a more commonly used coagulant in France and increased attention for P recovery via vivianite. Vivianite ($Fe_3(PO_4)_2 \bullet 8(H_2O)$) is a Fe(II) precipitate, therefore it is important to examine reductive conditions at the facilities. The obvious zone for vivianite recovery would be an anaerobic digester, however, it is not common to have anaerobic digesters at small facilities. With the clarification of the reduction kinetics, alternative ways can be found even at small facilities.

Functional groups of microorganisms use energetically more favorable electron acceptors. It is important to clarify these relations as typically various electron acceptors are available in activated sludge. Sulphate reduction needs to be considered, as a competing process, not only in the scope of the hierarchy of terminal electron-accepting processes but also in the subsequent precipitation processes as it can cause additional P release.

Iron reduction can be an important mechanism for modeling systems with long anaerobic periods, sidestream fermentation, as well as intermittent aeration systems. In various full-plant models, iron reactions are already included, these reactions are revisited and evaluated in this thesis.

The thesis outline and objectives

The aim of the thesis was to investigate phosphorus removal technologies for small/medium facilities applying combined biological and physical-chemical phosphorus removal. The objectives were either to better quantify the dynamic phenomenon and to give new insight into dynamic modeling which is a powerful approach for optimizing activated sludge systems. Each chapter represents a different approach highlighting the areas that need to be further investigated and proposing enhancement on the efficiency of currently/widely used strategies.

Chapter 1 explores the status quo and recent developments in the field. A detailed literature review is given on phosphorus removal technologies, focusing specifically on biological P removal mechanisms and configurations, as well as physical-chemical removal using iron salts.

Nutrient recovery technologies are also presented, specifically struvite and vivianite recovery, these having the highest recovery potential for the discussed facility-types. As vivianite recovery requires reduced iron forms, known reduction mechanisms and kinetics are presented in natural and engineered aquatic environments.

Redox cycling of different elements may impact plant operation and removal efficiency, therefore research exploring relevant topics such as terminal electron accepting processes is also introduced. Available and widely used biokinetic models are also described.

This chapter provides an overview of the recent and ongoing research related to the further chapters of the thesis. While in the introduction of each chapter a relevant literature background is given, more detailed information is provided in Chapter 1.

Chapter 2 is a case study of a rural wastewater treatment plant where nutrient removal is carried out via combined biological and physical-chemical techniques. This chapter addresses the related operating challenges and aims to identify the biological contribution to the overall phosphorus removal, correlation with aeration and solids concentration (including wastage strategies), and finally the optimization of chemical use.

Combined biological and physical-chemical phosphorus removal is fairly common in France. Through the example of this facility, common practices are presented with high efficiency and robust nitrogen removal as well as operating challenges. A specific monitoring campaign was realized in the framework of the CIRCURURAL4.0 Sudoe-Interreg project, in order to collect some data for almost three years. The aeration control system named *Inflex* developed by INSA-TBI was also installed and assessed during this period.

The impact of different factors (aeration strategies, influent loads, mixed liquor suspended solids (MLSS) concentration, sludge retention time (SRT), chemical dose strategies) is evaluated on the nutrient removal efficiency. Secondary P release locations and scenarios are identified and different remediations are implemented/piloted (such as aiming Fe dose specifically at these loads). As chemical dose and dosage point are important parameters, considering redox transformations of major interacting components (SO_4^{2-}, Fe(III)) is important.

Despite the plant does not include anaerobic digestion, PO_4 release in the sludge line is observed and an original iron dosing on the sludge liquor recirculation is evaluated.

Chapter 3 examines iron reduction mechanisms in activated sludge through a comprehensive series of experiments in order to define Fe(III) reduction in activated sludge and identify key influencing parameters. A detailed understanding of Fe(III) reduction processes can give an insight into the P retaining capacities throughout the process and the implications for removal and recovery potential.

Even though it was already established that extended anaerobic retention time such as in an anaerobic digester results in a complete reduction of Fe(III), the information on the activated sludge reactors with shorter (<24h) anaerobic retention time needed to be clarified. The experiments are designed to closely observe the beginning of the reaction as well as the complete reaction. Sludge was collected from two different plants for comparison, further scenarios were completed with sludge from the mainly discussed reference facility.

Under anaerobic conditions, the major electron acceptor in activated sludge is sulphate. For understanding the interactions/order of terminal electron-accepting processes, anaerobic kinetic tests are carried out with various initial sulphate to ferric iron ratios.

Chapter 4 summarizes the findings of the field observations and laboratory measurements and attempts to integrate them into the full plant Sumo model using the Sumo2S model as a basis, in which several sulfur and iron reactions are already included with special regard to the observed interactions of phosphorus and iron and the configuration of the partner facility.

Influent characterization was carried out by a dedicated measurement campaign and a specific process unit was developed for the configuration to describe aeration control.

Based on the findings, a calibrated process model extension is presented with a specific focus on the main challenges of the facility regarding phosphorus removal modeling.

Several questions and theories were met during the model development, and conceptual model extension and suggestions for future development are also presented.

Contents

Abstract I

Résumé III

Acknowledgments V

List of communications and publications VI

General introduction VII

The Phosphorus challenge VII

The need for a better understanding of combined P removal strategies VIII

The thesis outline and objectives IX

Chapter 1 - Recent advances in biological and physical-chemical P removal and recovery 1

1.1. Introduction and context 2

1.2. Biological Phosphorus removal 3

1.2.1. Recent knowledge on biological phosphorus removal optimization 3

1.2.2. Optimization of EBPR configuration 6

1.2.3. Modeling Biological Phosphorus Removal 9

1.3. Iron chemistry in water and wastewater treatment 12

1.3.1. Role of iron in wastewater treatment 12

1.3.2. Physical-chemical mechanisms of phosphate removal with iron 13

1.3.3. Iron species in aquatic environments and particulate iron forms 14

1.3.4. Iron redox-cycling in aquatic environments 16

1.3.5. Microbial community and Fe(III) reduction 18

1.3.6. Iron reduction mechanisms 18

1.3.7. Iron reduction kinetics 19

1.3.8. Recent models for describing iron-based phosphate removal 21

1.4. Combined chemical and biological treatment in alternated aeration systems 23

1.4.1. Alternated aeration systems 23

1.4.2. Terminal electron-accepting processes 26

1.4.3. Common practices with combined biological and physical-chemical removal 26

1.4.4. Recent routes for phosphate recovery in the presence of iron 28

1.4.5. Interaction between iron dosage and biological processes 30

1.5. Conclusion and thesis contribution 31

1.6. References 34
Chapter 2 - Optimization of P removal in activated sludge process with intermittent aeration at a rural facility – a case study 42
2.1. Introduction 44
2.2. Materials and Methods 48
2.2.1. Plant description 48
2.2.2. Aeration control 50
2.2.3. Data monitoring 51
2.2.4. Influent characterization 52
2.2.5. Phosphorus release and uptake tests 52
2.2.6. Description of iron dosage 53
2.3. Results and discussion 54
2.3.1. Influent characteristics 54
2.3.2. Plant load and overview of overall nutrient removal 55
2.3.3. Biological P removal dynamics during intermittent aeration 58
2.3.4. Relation between sludge management and P removal 61
2.3.5. Toward an optimal Fe dose 64
2.4. Conclusions 66
2.5. Acknowledgment 67
2.6. References 68
2.7. Supplementary material 71
Chapter 3 - Iron reduction kinetics and influencing parameters in activated sludge 73
3.1. Introduction 75
3.2. Materials and methods 77
3.2.1. Batch assay setup 77
3.2.2. Analysis 79
3.2.3. Calculation 80
3.3. Results 80
3.3.1. Iron reduction kinetics 80
3.3.2. Influence of sludge concentration on the kinetic rate 83
3.3.3. Effect of sulphate on reduction kinetics and phosphate release 84
3.3.4. Calculation of iron and phosphorus speciation 86
3.4. Discussion 88

3.4.1. Iron reduction kinetic rates 88
3.4.2. Relation and comparison between iron and sulphate reduction 90
3.4.3. Implications for phosphate and iron recovery 91
3.5. Conclusions 92
3.6. References 93
3.7. Supplementary material 96
Chapter 4 - Modelling combined biological and physical-chemical P removal in an intermittent aeration system 99
4.1. Introduction 101
4.2. Process unit development 103
4.2.1. Influent characterization and influent Process Unit 103
4.2.2. Operational inputs: alternated aeration and sludge wastage 104
4.3. Process model basis and extension 106
4.3.1. Calibration Overview 106
4.3.2. Biological P removal processes 107
4.3.3. Hydrolysis 108
4.3.4. HFO kinetics 108
4.3.5. Fe reduction 109
4.3.6. Iron oxidation 109
4.4. Results and discussion 114
4.4.1. Modeling aeration control and nitrogen removal 114
4.4.2. Initial results for phosphorus removal with default parameters and calibration approach 116
4.4.3. Phosphorus release and uptake tests 119
4.4.4. Intermittent aeration and phosphorus removal 121
4.4.5. Modeling the effect of iron dose on P removal efficiency 123
4.4.6. Effect of sludge wastage and MLSS concentration on P removal 125
4.4.7. Model complexity and remaining challenges 126
4.5. Conclusions and outlook 128
4.6. References 129
4.7. Supplementary material 131
Conclusion and perspectives 135
List of Figures 140
List of Tables 143

Chapter 1 - Recent advances in biological and physical-chemical P removal and recovery

1.1. Introduction and context

After eutrophication of receiving waters has been clearly linked to excess nutrients from effluents (as a point source of pollution), there has been a long tradition to remove nitrogen and phosphorus (P being often the limiting nutrient) from wastewater. Specifically, phosphorus removal has been carried out by biological, physical-chemical means (precipitation with Fe, Al, or Ca being the most common) or the combination of the two.

In the European Union (EU), a common collection and treatment legislation has been introduced in 1991 for effluent quality to protect receiving waters and prevent/mitigate eutrophication (Council Directive 91/271/EEC). The document specifies planning, regulation, monitoring, and report principles, and requires and defines collection and treatment levels, domestic and industrial discharges into the collection system, monitoring of the facilities and receiving water, and the conditions of sludge disposal and reuse as well as water reuse. Within high compliance with these regulations, according to a 2020 implementation report (Technical Assessment, 2020), by 2016, the majority of EU citizens have access to basic sanitation (95% compliance rate to connection, 88% to secondary, and 86% to more stringent treatment), challenges remain and further development is necessary, especially regarding sensitive areas.

Moreover, new legislation is in preparation aiming to promote a circular economy in the water industry as well (European Commission, 2020). There are different estimations on what amount of mineral fertilizers could be replaced by P recovery from sewage sludge. According to a model-based calculation provided by Kok *et al* (2018), human discharge into wastewater could cover 20% of the fertilizer demand, while a press release by the European Commission (EC) in 2018 (IP/18/6161) estimates that 30% of mineral P fertilizers could be replaced by bio-waste recycling (including domestic sewage sludge, biodegradable waste, and agricultural waste). However, fertilizer trade regulations need to be revised to achieve progress in the circular economy. As the economic feasibility of P recovery from sewage sludge is debated, legislation can stimulate the transition process. In some member states such as Finland, Germany, and Sweden authorities have taken specific steps to define and accomplish P recovery targets (Stark, 2004).

1.2. Biological Phosphorus removal

1.2.1. Recent knowledge on biological phosphorus removal optimization

Since the early studies of the last fifty years (Milbury *et al*., 1971; Barnard, 1976; Ekama *et al*., 1983; Wentzel *et al*., 1986; Comeau 1990a, 1990b) biological phosphorus removal has been extensively studied. These studies established the major mechanisms of P removal and provided fundamental observations and proposals of configurations that are still of major interest.

Biological P removal requires two distinct steps regarding operation (Figure 1.2-1). Under anaerobic conditions, Phosphorus Accumulating Organisms (PAO) can store carbon in a readily biodegradable form (such as volatile fatty acids (VFA)) using the energy available from stored polyphosphate (PP) cleavage to produce intracellular polyhydroxy alkanoates (PHA) and consequently release orthophosphate during the process. At this stage, the PHA content of the PAOs increases and the PP decreases. Under aerobic conditions, stored PHA is oxidized by an available electron acceptor (oxygen or nitrate) providing energy for cell growth and PP storage (luxury uptake) along with stabilizing counter-cations. The net accumulation of PP is greater than the release during the anaerobic phase, resulting in efficient P removal under the right conditions.

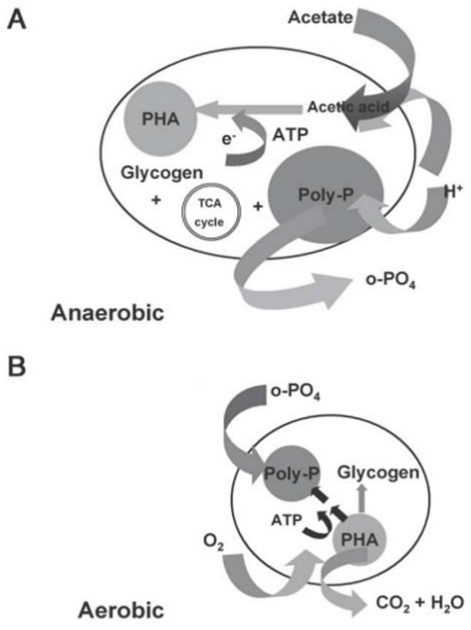

Figure 1.2-1. Simplified visualization of anaerobic (A) and aerobic (B) processes of PAO (Seviour et al., 2003)

Accumulated PP, as an energy reserve for growth and maintenance, gives an advantage to PAOs over heterotrophs as soon as alternance between anaerobic and aerobic conditions is provided. However, glycogen accumulating organisms (GAO), facultative anaerobes as well, have similar metabolism as PAOs, and certain conditions may favor GAO growth over PAO growth. PAO and GAO have been found to coexist in EBPR activated sludge but GAOs do not contribute to phosphorus accumulation and removal.

Mino *et al.* (1998) investigated the diversity of enhanced biological phosphorus removal (EBPR) sludge biomass and summarized, that PAO and GAO metabolisms are very similar, with the extension, that GAOs use glycogen as their sole energy source, and store without P release. It was confirmed, that a fraction of PAO is able to use nitrate as an electron acceptor. Saunders *et al.* (2003) identified *Candidatus Accumulibacter phosphatis* (*Accumulibacter*) and *Candidatus Competibacter phosphatis* (*Competibacter*) to be the most abundant PAO and GAO (respectively) present in their EBPR study, suggesting that with significant GAO present, carbon demand would increase due to the VFA uptake of GAO. *Acinetobacter* was also isolated as PAO in various facilities (Wagner *et al.*1994, Kong *et al.*2005) including *Actinobacteria* which was later defined as *Tetrasphaera* (Liu *et al.*2019). As this review summarized, the *Tetrasphaera* genus consists at least of four isolated species and holds various characteristics: the ability to metabolize and/or ferment glucose and amino acids, and their metabolic pathways are adaptable to the conditions. While the extent of PP storage of *Tetrasphaera* is still under investigation, it was shown that in synergy with *Accumulibacter*, a high level of P removal can be achieved (Figure 1.2-2).

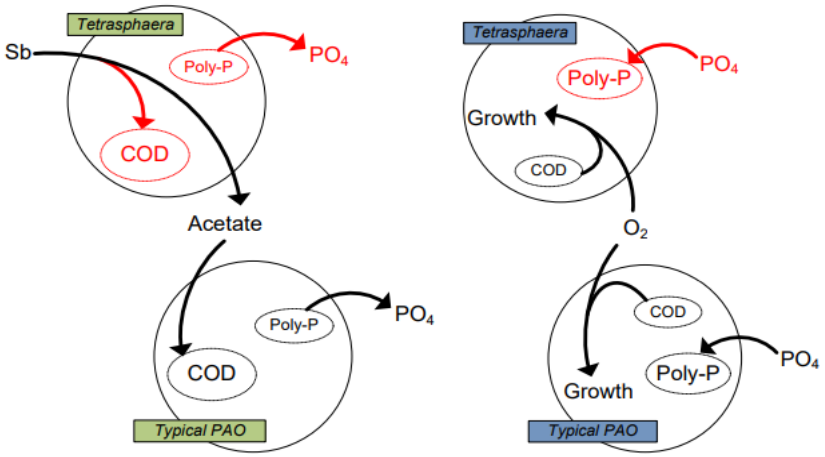

Figure 1.2-2. Simplified presentation of Tetrasphaera and typical PAO processes and interactions under anaerobic and aerobic conditions (Barnard et al., 2017)

The main drivers of the competition between PAO and GAO have been widely investigated. It was clarified earlier that VFA is a suitable carbon source for both groups. However, fractionation revealed that while acetate is readily available for both PAO and GAO, propionate was poorly utilized by GAO (Oehmen *et al.*2004). Different GAO such as *Alphaproteobacteria Defluviicoccus Vanus* (*Defluviicoccus*) was also shown to be abundant in EBPR facilities and may metabolize propionate but as Taya *et al.* (2013) showed, not able to use nitrite as electron acceptor. A different study (Rubio-Rincon *et al.*2017) showed, that PAO and GAO do not compete in every case, but for example, may form a synergic relationship through two steps of denitrification, where the different groups utilize different electron acceptors (Figure 1.2-3).

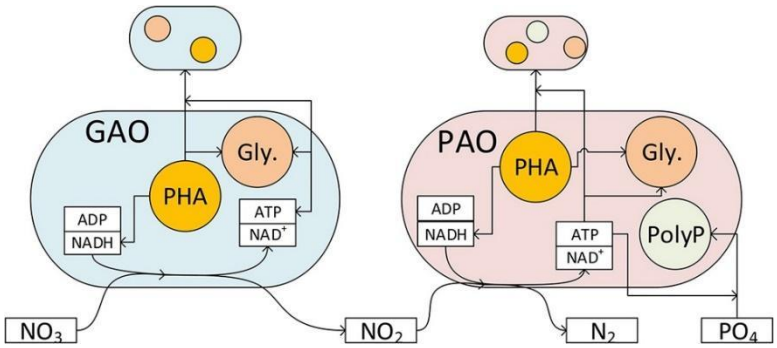

Figure 1.2-3 Anoxic processes of denitrifying GAO and PAO synergy according to Rubio-Rincon et al. (2017)

Lopez-Vazquez *et al.* (2008) examined the effect of various parameters on the PAO-GAO competition. They reported that despite VFA dosing being an important factor to consider (if an external carbon source is necessary) the composition did not result in significant changes between the different organisms. Therefore they concluded that overdosing of VFA could be detrimental to P removal efficiency, and they did not find evidence of a preferred VFA fraction in the investigated samples. As previous studies (Smolder *et al.*, 1993; Felipe *et al.*, 2001) have established, higher pH favor PAO metabolism over GAO. To take advantage of this, considering influent total nitrogen (TN) / pH in the anaerobic tank, a well-defined denitrification step is proposed by the authors. On the contrary, higher temperature appears to benefit GAO growth, which may be problematic for summer conditions (>20°C) but explain good performance at relatively low temperatures (Lopez-Vazquez *et al*., 2008). However, PAO like *Tetrasphaera* which can utilize more complex carbon compounds from the influent can possibly ameliorate bio-P removal efficiency in such conditions.

Low dissolved oxygen (DO) conditions also appear to favor PAO growth over GAO. Keene *et al.* (2017) found that with a low DO environment, GAO relative abundance is negligible (<0.2%) while identified *Accumulibacter* as the dominant PAO species. Multiple studies have demonstrated efficient P removal with low DO concentration (Downing *et al.,* 2014, Jimenez *et al.*, 2014, Jimenez *et al.,* 2017) and found that anoxic/micro-aerated P uptake in some cases is comparable to conventional aerobic conditions.

Erdel *et al.* (2007) found that PAO may alter their metabolism, using a glycolytic pathway to generate energy under anaerobic conditions. Temperature can be a controller for such a shift resulting in lower P removal efficiency in higher temperatures. They argued, therefore the loss in P removal efficiency may not be a result of PAO-GAO competition in every case, but rather the metabolic shift in PAOs. Acevedo *et al.* (2017) also observed the metabolic shift phenomena when PP was limited.

1.2.2. Optimization of EBPR configuration

Four conventional EBPR configurations are presented on Figure 1.2-4. These are implemented for complete biological nutrient removal (biological phosphorus removal and nitrogen removal via nitrification-denitrification). Anaerobic-anoxic-aerobic (A2O) (Spector, 1979) is a commonly used configuration with an anaerobic – anoxic and aerated (oxic) tank, where internal mixed-liquor return sludge is directed from the aerated to the anoxic tank to ensure minimal nitrate recycling to the anaerobic tank via return activated sludge (RAS). The 5-stage (modified) Bardenpho (Barnard, 1978) configuration operates with five zones – anaerobic, anoxic, aerobic, anoxic, and aerobic – which provides highly efficient and reliable nutrient removal. The Modified University of Cape Town (mUCT) configuration consists of a series of four reactors; anaerobic, two consecutive anoxic, and an aerobic tank with internal nitrate-free sludge recycling from the first anoxic to the anaerobic and to the second anoxic from the aerobic zone, and RAS to the first anoxic zone. Similarly to A2O, Virginia Initiative Plant (VIP) process (Mines and Thomas, 1996) also uses three reactors (anaerobic, anoxic, and oxic zones), however, it operates with two internal recycling routes: anoxic zone recycle (ARCY) from the anoxic to anaerobic zone and nitrified recycle (NRCY) from aerobic to anoxic zone and RAS is directed to the anoxic tank.

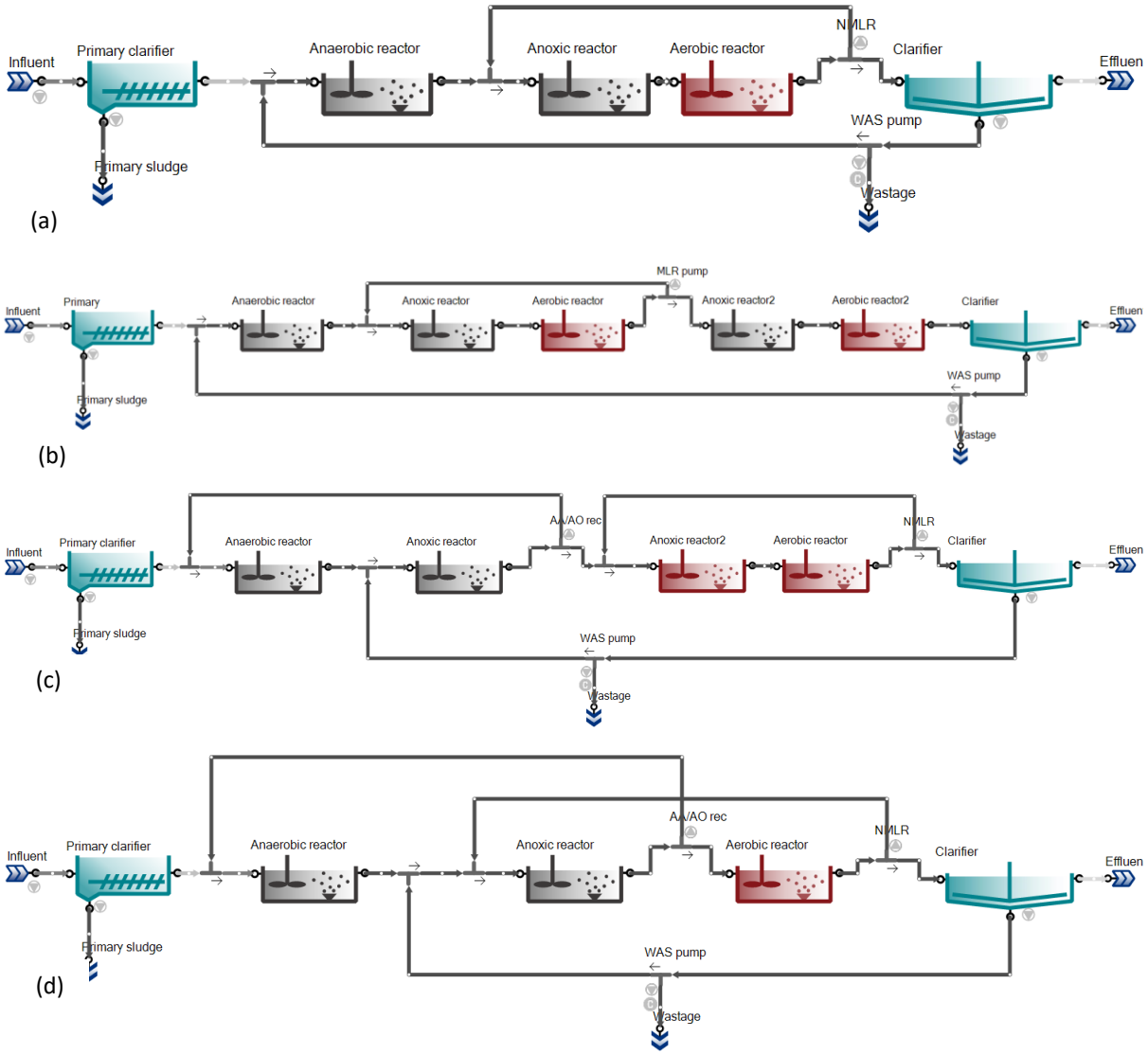

Figure 1.2-4 Conventional EBPR configurations (a) A2O (b) Bardenpho (c) mUCT (d) VIP, designed in SUMO21 software

To ensure proper effluent quality, several operational parameters need to be considered, such as sufficient carbon source for P and N removal (configurations designed according to minimize supplementation), hydraulic retention time (HRT), and sludge retention time (SRT) (too long SRT can be detrimental for PAO and result in secondary release), internal recycle flows (minimize nitrate and oxygen recycle to anaerobic zone).

Biological phosphorus removal efficiency relies on the influent VFA and the overall potential can be calculated (Houweling *et al.,* 2010). A widespread practice to improve EBPR is the addition of VFA.

A convenient and economically efficient way to provide additional VFA is through on-site fermentation through pre-fermenters, RAS/WAS, or mixed-liquor fermentation. Barnard *et al. (*2017) summarized the development and understanding of mixed-liquor sludge fermentation which produces enough VFA to ameliorate P removal and consequently the development of side-stream enhanced biological phosphorus removal (S2EBPR).In an early S2EBPR configuration (Lamb, 1994), a nonconventional flowsheet is implemented, such as a portion of RAS being directed to a sidestream fermenter. The effluent of this fermenter is directed to the anaerobic zone and provides substrate for PHA storage, while primary effluent is directed to the anoxic zone.

Barnard *et al* (2017) concluded that S2EBPR configurations are more efficient in certain PAO selection, such as Tetrasphaera. To optimize the process, they pointed out some important operating parameters, namely the importance of mixing and control of flows (primary effluent as well as RAS) recommended HRT and SRT. Moreover, ORP was also considered a good indicator, as low ORP conditions are required for these processes, but absolute values may vary significantly at different facilities.

Tooker *et al.* (2018) summarized the main mechanisms of S2EBPR processes on lab-scale and full-scale examples (Figure 1.2-5). They demonstrated that with sufficient HRT, side stream fermenters can provide enough VFA for stable P removal. Under extended anaerobic retention time, increase PHA accumulation was observed for PAOs. Additionally, they can outcompete GAOs due to the anaerobic maintenance of PAOs via PP cleavage. Various genera of PAOs were identified which may also be beneficial for P removal stability.

There are several case studies of different sludge fermentation strategies, such as primary sludge fermentation (PSF) (Bratby *et al.,* 2012), Unmixed inline MLSS fermentation (UMIF) (Barnard *et al.,* 2010, Dunlap *et al.,* 2017), side-stream MLSS fermentation (SSM) (Tremblay *et al.,* 2005), side-stream RAS fermentation (SSR). Fan *et al.* (2021) demonstrated the efficiency of these interactions with a completely eliminated P and significantly reduced sludge in SBR using WAS fermentation while reaching a high (91.4%) relative abundance of Tetrasphaera.

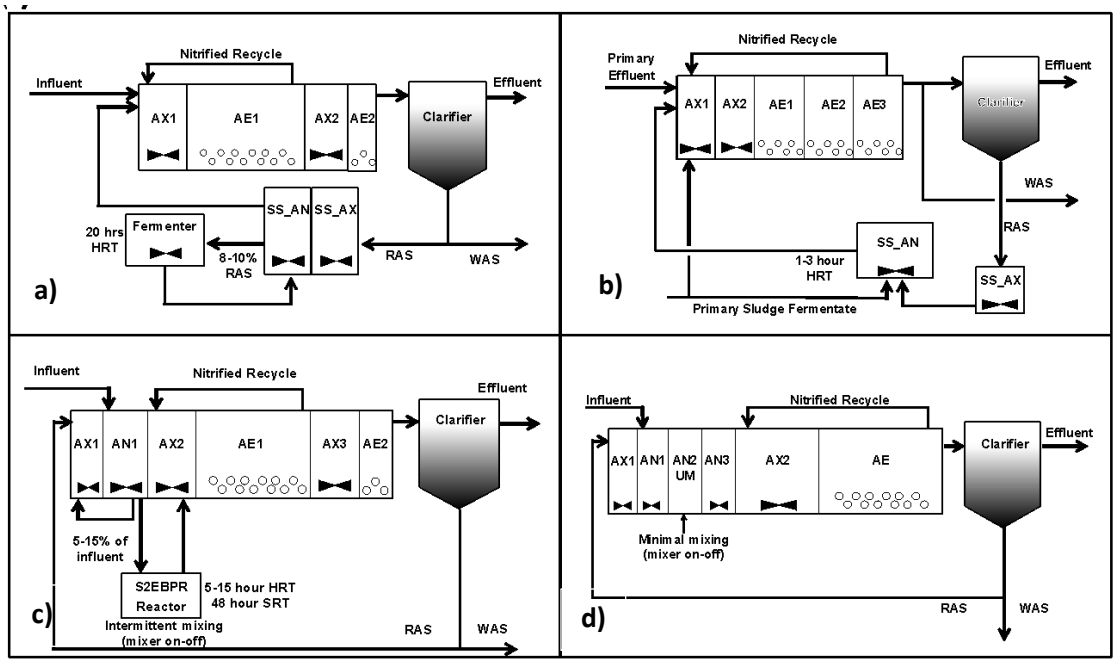

Figure 1.2-5 Examples of S2EBPR configurations (Tooker et al., 2018). (a) Side-stream RAS fermentation (SSR) (b) Side-stream RAS fermentation with external carbon addition (SSRC) (c) Side-stream MLSS fermentation (SSM), (d) Unmixed, in-line MLSS fermentation (UMIF)

1.2.3. Modeling Biological Phosphorus Removal

Activated Sludge Model No. 2d (Henze *et al.,* 1999) introduced biological phosphorus removal processes to the general ASM model describing anaerobic and aerobic processes of EBPR, including PHA storage (anaerobic P release) and PP storage as well as aerobic growth and lysis of PAOs and PP and PHA lysis.

In the General model of Barker and Dold (1997) further processes were included, introducing denitrifying fraction of PAOs and the use (albeit not equivalent to oxygen) of nitrate as an electron acceptor.

More detailed metabolic models (Smolders *et al.,* 1993) include the Tricarboxylic Acid (TCA) cycle and Embden-Meyerhof (EM) pathways of intracellular glycogen storage, to consider the reasons beyond the variation of VFA uptake to P release ratio and also accounting for the effect of pH. In addition, Kuba *et al.* (1995) included denitrifying phosphorus removal in the metabolic model, demonstrating the use of different electron acceptors.

PAO and GAO competition has been also included in metabolic models, Oehmen *et al.* (2010) classified different species with reported abundance at EBPR facilities by substrate uptake mechanism, preferred VFA, source of reducing power, and the ability to use nitrite and/or nitrate as electron acceptor (Figure 1.2-6).

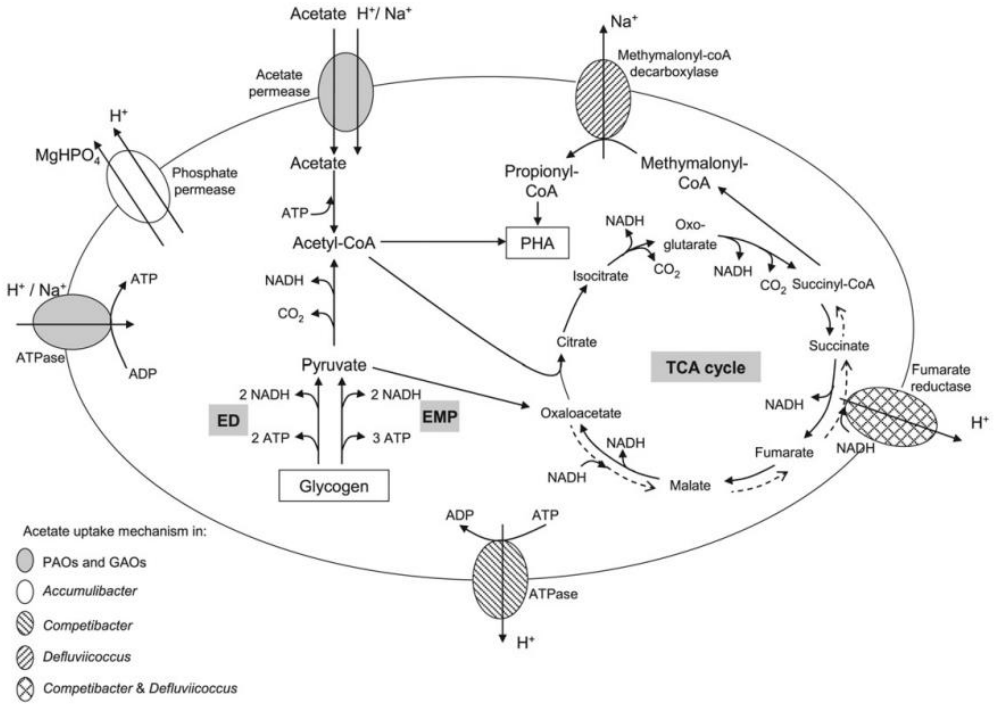

Figure 1.2-6 Detailed anaerobic metabolism of different PAO and GAO by Oehmen et al. (2010)

As phosphorus removal techniques evolved through time, conventional models required more calibration to fit specific configurations such as side stream EBPR. Based on S2EBPR observations on PAO mechanisms and PAO parameters, Dunlap *et al.* (2016) proposed a new model framework (Figure 1.2-7) to improve EBPR models. Their work included two distinct groups of PAOs with different mechanisms, representing a conventionally included in models as a mixed culture of PAO and GAO and a specific group of PAO with a separate parameter set. A conventional group of PAOs (PAO1) describes a wide range of processes observed in conventional EBPR systems. In contrast side-stream conditions, operating with extended anaerobic HRT and therefore low ORP, are dominated by a different group (PAO2) with fermenting ability. Here, GAOs are outcompeted by present PAOs, with *Tetrasphaera* assumed to be the dominant species.

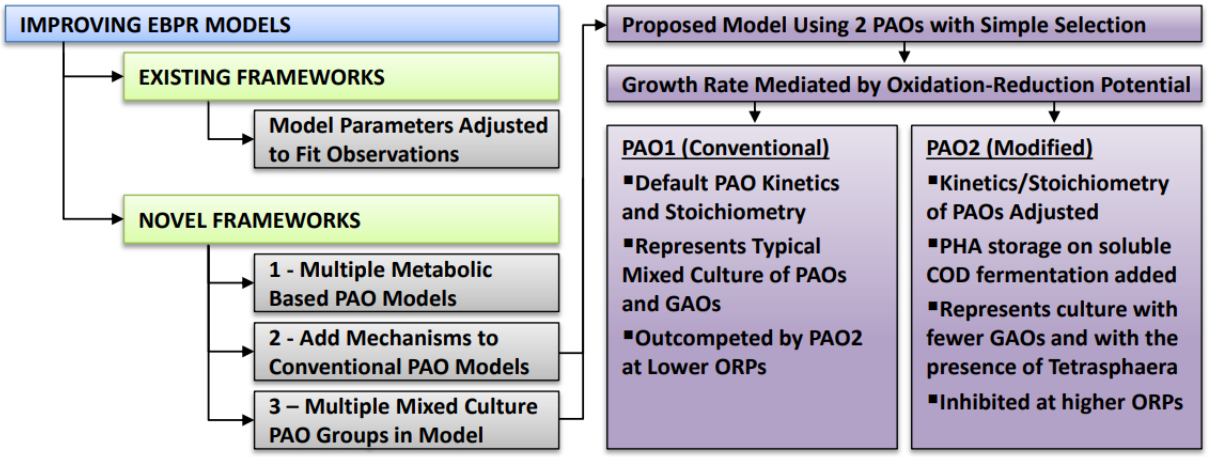

Figure 1.2-7 EBPR model framework proposed by Dunlap et al. (2016)

Varga *et al.* (2018) extended this approach, modifying the two groups of PAOs to separate, competing PAO and GAO groups in the full plant *SUMO* model. GAOs (previously included in PAOs, therefore altering observed parameters) are not able to accumulate PP and PAOs have different metabolism according to the conditions. In this model, both PAOs and GAOs use a single carbon source (VFA) and store one carbon storage component (PHA and GLY respectively) under anaerobic conditions. A fraction of both groups is able to denitrify. Under low ORP conditions, PAOs are able to ferment and outcompete GAOs. Certain conditions such as high temperatures favor GAOs, while micro aeration favor PAO growth. These complex interactions enable the model to describe sufficiently well a wide range of configurations but are especially useful in S2EBPR simulations.

Santos *et al.* (2020) presented most recently a detailed metabolic model, including different subgroups of PAO and GAO (relating to their denitrifying capability), describing their competition through operating conditions and metabolic shifts, endogenous processes, and anaerobic and aerobic maintenance processes, PAO fermentation as well as their interactions within the microbial ecology in the activated sludge. This detailed model increased the ability to predict complex dynamic interactions and EBPR performance.

1.3. Iron chemistry in water and wastewater treatment

1.3.1. Role of iron in wastewater treatment

Iron salts are frequently used in various steps of the wastewater collecting and treatment system to avoid operational problems and meet effluent requirements. In general, at different dosage points, the chemical addition serves different purposes:

- *Sewer system* – to prevent H_2S-derived corrosion and odor (more details)
    - Prevention of toxic sulfide formation in order to protect sewer workers and limit unpleasant smells in an urban area and sewer corrosion (WERF, 2007)
    - Recent studies have been conducted that sewer-dosed iron has a positive impact on P removal and even H_2S formation in digesters (Rebosura *et al.,* 2018)
    - retention time: a few hours
- *Mainstream wastewater treatment* – Chemically enhanced primary treatment and phosphorus removal. Depending on the dosage point and design, the P removal can be classified as (Metcalf & Eddy, 2014):
    - *Pre-precipitation:* the chemical is dosed into the primary settler and the P is removed with the primary sludge. This solution is widely applicable and ensures low metal leakage however the least efficient dosage point and may cause dewatering problems and requires polymer addition.
    - *Simultaneous precipitation*: the chemical is dosed to the primary clarifier effluent, the mixed liquor, or the effluent of the activated sludge process, before sedimentation, and removed with the wasted activated sludge. This solution requires low capital costs and is highly efficient, improving the stability of the activated sludge, however, the overdose of the metal may cause pH toxicity in low alkalinity wastewaters therefore pH control may be necessary.
    - *Post-precipitation*: the chemical is dosed to the effluent of the secondary clarifier and removed in subsequent sedimentation or effluent filters. The lowest P effluent of the mentioned methods can be achieved with this precipitation as well as the most efficient metal use occurs here, however, this dosage point represents the highest capital costs and highest risk of metal leakage.

- *Digester* – to prevent H_2S formation and biogas contamination, and to prevent unwanted struvite precipitation. While unwanted struvite precipitation can be minimized with the immobilization of phosphorus and alternative scaling problems of vivianite formation may also occur. Prot *et al* (2021) observed significant scaling in digesters, attributed to the temperature dependency of vivianite solubility.

1.3.2. Physical-chemical mechanisms of phosphate removal with iron

The mechanism of iron dosage had been considered for a long time as double precipitation ($FePO_4$ + $Fe(OH)_3$) where the iron hydroxide would be a parasite reaction (Deronzier and Choubert, 2004). However, more recent works recognized that iron hydroxide, or more accurately hydrous ferric oxides (HFO), precursors of ferrihydrite, play a major role in phosphate removal as a substrate for P adsorption and incorporation of P in the HFO structure along with the formation of mixed cation phosphates (Metcalf and Eddy, 2014). The surface complexation model (Smith *et al*., 2008) describes how the precipitation of XHFO provides a number of adsorption sites for ions on its surface. Hauduc *et al*. (2015) adapted this approach focusing only on phosphates adsorption and co-precipitation.

More generally Szabo *et al.* (2008) found that when dosing Fe(III) salts, the dominant process is co-precipitation of phosphate into the HFO structure in case of pre- and post-precipitation due to intensive mixing, whereas during simultaneous precipitation (in activated sludge), the main process is adsorption of phosphate (chemisorption, physisorption) onto the surface of formed HFO. In this case, the effect of aging seems to be very significant, as with the structural changes of HFO - increasing density - fewer active sites are available for reaction (Smith *et al.*, 2008).

Typically the chemicals are proposed to be dosed into the secondary clarifier influent, this way the interference with activated sludge processes can be minimized (due to alkalinity consumption). The major fraction of P is orthophosphate, which can be precipitated and separated during the settling process. However, the current practice is to dose iron directly in the aeration basin.

Szabo *et al.* (2008) investigated the effect of mixing, reaction types, aging of flocs, pH, alkalinity, metal dose, metal type, initial P content, residual P, and organic content of wastewater. They found that instantaneous P removal happens within 1 minute, the majority of removal (90%) within 30 minutes, and the rest in the next few hours. When mixing intensity is low, the instant removal is impaired but slow adsorption reactions continue (surface complexation). Ideally, high mixing intensity at the dosage point, where metal hydroxides are formed, provides sufficient contact between ferric and phosphate ions. Low effluent P can be achieved in a wide range of pH (optimal pH is 5-7) if other parameters (e.g. mixing) are sufficient. With extremely low pH, precipitation of metal hydroxide is limited, mostly soluble phosphate complexes form, and redissolution occurs even with a higher coagulant dose. At high pH, the surface of metal hydroxides is more negatively charged, and soluble iron hydroxides form, resulting in decreasing phosphate removal efficiency. However, for pH>10, calcium and magnesium can form precipitates with phosphate, and low P effluent can be achieved without metal salts.

Phosphate removal with aluminum and ferric salts shows similar efficiency, and pH dependency is comparable, whereas pre-polymerized salts show lower efficiency. Phosphate removal is negatively affected by high influent COD (both soluble and total) and also higher TSS, as carboxylic and phenolic groups may compete with phosphate for binding sites. Generally, the required metal-to-phosphate ratio exceeds the stoichiometric Me: P=1 ratio, and typical influent P concentrations require doses above 1.5 – 2 depending on the effluent limits. The optimal case is when the initial Me:P ratio is the same in the precipitate, meaning negligible residual phosphate in the effluent. Relative phosphate removal efficiency increases with increasing influent phosphate concentration, while to achieve low effluent P, a higher metal dosage is required. A tertiary dosage of iron salts (paired simultaneous dose) can be an efficient way to significantly reduce iron dose while achieving a very low level of effluent P concentration, due to the assumed high active HFO content of the recycled sludge (Takacs *et al.,* 2006).

1.3.3. Iron species in aquatic environments and particulate iron forms

Iron speciation in aqueous systems is controlled by oxidation-reduction, complexation, and solids formation and dissolution. The level of oxidation is basically imposed by pH and redox potential (Figure 1.3-1), which are both influenced by the presence of acid-base reactions, various electro-active couples as well as microbial reactions. Both iron(II) and iron(III) domains are found in aquatic environments, and similarly in wastewater treatment plants. As iron species are examined in the thesis in detail, the illustration of a Pourbaix diagram is limited to iron species.

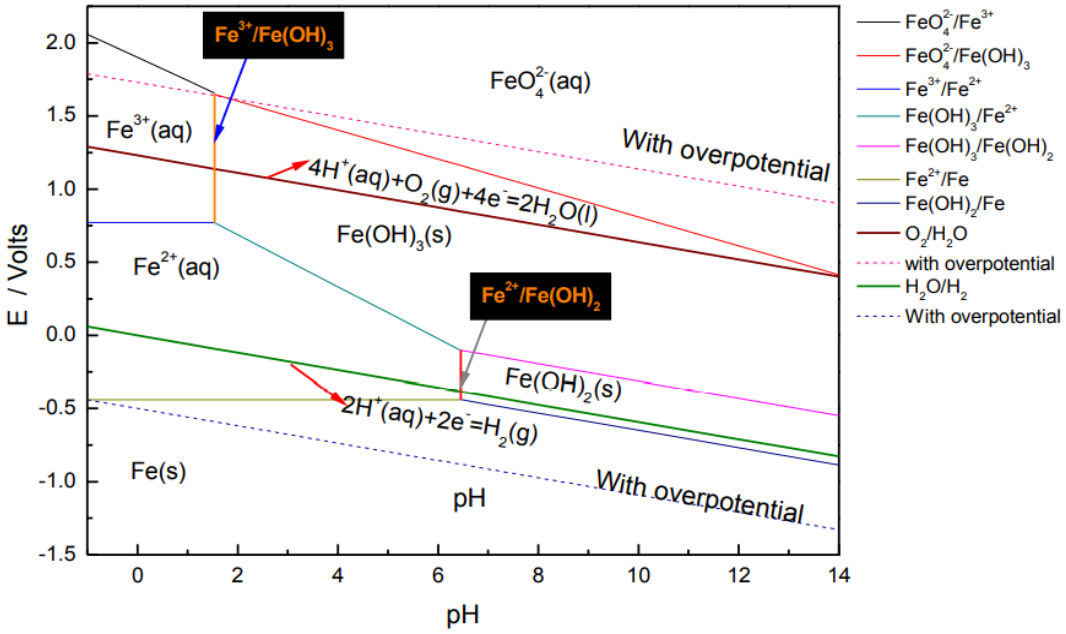

Figure 1.3-1 Pourbaix diagram for iron, adapted from Kappler and Straub (2005)

Regarding the solid forms, there are 16 different kinds of iron oxides with various crystal structures (Cornell and Schwertmann, 2003) which generally have low solubility. Almost all Fe oxides are crystalline (the degree of crystallization depends on the conditions of their formation). Ferrihydrite is a poorly crystalline precipitate, that transforms into more crystalline iron oxides and therefore an important precursor. The composition seems to be variable, especially regarding OH and H_2O, the preliminary formula is $Fe_5O_8H*H_2O$ (Cornell and Schwertmann, 2003). Due to their high specific surface area, they are effective sorbents. The most widespread in WRRFs (and also abundant in natural surface environments) is ferrihydrite, whose composition (regarding OH and H_2O) seems to be variable. As it only exists in nano-crystals, without other kinds of stabilization, it may transform into a more thermodynamically stable iron oxide with time.

There are Fe oxides (e.g. magnetite) that contain Fe(II) and Fe(III) as well, and Wüstite (FeO) only contains Fe(II). The structure of wüstite is usually non-stoichiometric (O-deficient) and an important intermediate for iron reduction. It is generally considered that iron(II) forms more stable crystals under reductive conditions. With regards to WRRFs, the most significant ones are vivianite ($Fe_3(PO4)_2$), pyrite (FeS_2), and siderite ($FeCO_2$).

1.3.4. Iron redox-cycling in aquatic environments

Iron may occur in both oxidized and reduced forms in natural or engineered aquatic environments depending on the conditions. In some cases, these conditions are variable due to biological or chemical reactions and diffusion, e.g. in the sediments transition zone or in a WRRF, causing redox transformation of iron species (Figure 1.3-2).

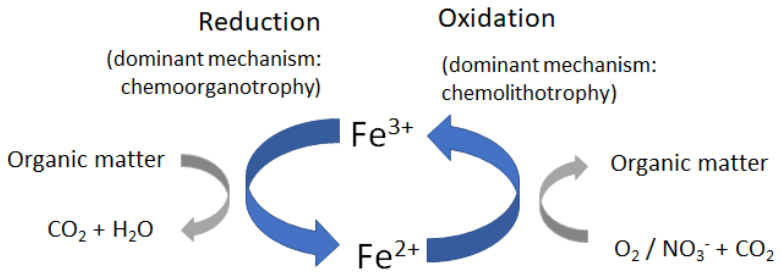

Figure 1.3-2 Basic presentation of iron redox mechanism

At circumneutral pH conditions, abiotic Fe(II) oxidation is rapid therefore Fe(II) oxidizers must compete with abiotic oxidation. One mechanism occurring in micro-aerated conditions is that iron oxidizing bacteria (FeOBs) are able to form amorphous ferrihydrites or oxy-hydroxides which then provide suitable electron acceptor for dissimilatory Fe(III) reduction (Roden 2012). These processes can be observed in situ in complex soil matrices and freshwater sediments. Blöthe and Roden (2009) suggested that under circumneutral pH conditions, redox-cycling of iron is likely to take place in virtually all redox interfacial environments. Based on these observations, these principals can be applied to the dynamically changing conditions of water resource recovery facilities.

Under anoxic conditions, it was observed, that Fe(II) oxidation occurs (Nielsen and Nielsen, 1998). Nitrate does not react directly with Fe(II) so there is no competition between abiotic and biotic nitrate-dependent Fe(II) oxidation. This oxidation is mostly due to denitrifiers, even if there are some cases of nitrate-dependent Fe(II) oxidation without the addition of organic compounds (chemolithotrophs) as reported by Straub *et al.1996*. In experimental nitrate-dependent redox cycling, it was demonstrated that for 75% of Fe(II) oxidation cases, nitrate got reduced to ammonium (Coby *et al.*2011) which means the production of ammonium to some extent needs attention in WRRF.

Table 1.3-1 Microbial groups catalyzing iron redox transformations (Kappler and Staub, 2005)

Habitat/Conditions	Electron donor	Electron acceptor	pH	Microbial metabolism	Representative strains
Oxic	Fe(II)	O_2	Acidic	Fe(II) oxidation	Thiobacillus ferrooxidans Sulfobacillus acidophilus
	Fe(II)	O_2	Neutral		Gallionella ferrugmea Leptothrix ochracea
Anoxic	Fe(II)	NO_3^-	Neutral	NO_3^- dependent Fe(II) oxidation	Acidovorax sp. Strain BrG1 Azospira oryzae strain PS
	Fe(II)	CO_2	Neutral	Phototrophic Fe(II) oxidation	Rhodobacter ferrooxidans strain SW2 Rhodovulum iodosum
	Organic or inorganic compounds	Fe(III)	Acidic	Fe(III) reduction	Acidiphilium cryptum sp JF-5 Thiobacillus thiooxidans
	Organic or inorganic compound	Fe(III)	neutral	Fe(III) reduction	Geobacter metallireducer Shewanella oneidensis

There are several groups of prokaryotes that use Fe as a source of energy generation in their catabolism. Table 1.3-1 highlights the relevant groups according to Kappler and Staub (2005) with representative strains taking part in Fe redox cycling. Such microbial processes can be classified according to metabolism as follows (Roden, 2008):

- Chemoorganotrophy (using organic electron donor)
    - Oxidation of particulate organic matter
    - Reductive dissolution of Fe(III) at circumneutral pH coupled with organic acid and H_2 oxidation
    - Formation of magnetite, siderite, vivianite, pyrite, and other metal-sulfides
- Chemolithotrophy (using an inorganic electron donor)
    - Aerobic and nitrate-dependent FeS oxidation
    - Oxidation of Fe(II) in FeS
    - Nitrate-dependent Fe(II) oxidation (soluble and particulate)
- Mixotropy
    - Oxidative precipitation of Fe(III) oxides
    - Aerobic and nitrate-dependent oxidation of FeS
    - Nitrate-dependent Fe(II) oxidation (soluble and particulate)

1.3.5. Microbial community and Fe(III) reduction

Diverse groups of microorganisms take part in Fe(III) reduction. The ability of Fe(III) reducing organisms to outcompete sulfate reducers and methanogens has been demonstrated and has significance for WRRF operation and maintenance. Under the conditions that occur during wastewater treatment, several types of organisms of Fe(III) reducing capabilities can be found. Lovely (2006) summarized the metabolic and phylogenetic diversity of these organisms. Many fermentative bacteria can grow with Fe(III) as a minor electron acceptor, but growth is also possible without the presence of iron. Respiratory bacteria that grow with sulfate as an electron acceptor in anaerobic conditions may also reduce iron.

There are also bacteria that conserve energy from Fe(III) reduction, using organic carbon (mainly acetate) or hydrogen. For example, the *Geobacteraceae* family can oxidize organic compounds completely to CO_2, using Fe(III) as the sole electron acceptor. Moreover, most strains can oxidize acetate completely. *Gheothrix fermentants* can oxidize short-chain fatty acids completely and they can grow fermentatively on organic acids. There are also many thermophilic and acidophilic organisms that will not be discussed.

Unlike the aforementioned groups of strictly anaerobic bacteria, there are several facultative genera (including *Shewanella*, *Ferrimonas*, and *Aeromonas*) that can grow aerobically and under anaerobic conditions using Fe(III) as an electron acceptor. When oxygen is present, they can usually use a diverse range of electron donors, but anaerobically for Fe(III) reduction only hydrogen and small chained organic acids are available electron donors. *Shewanella* species are able to incompletely oxidize organic acids to acetate.

1.3.6. Iron reduction mechanisms

Iron(III) reduction in aquatic environments can happen both through abiotic and biotic pathways (Roden 2008, Lovely 2006). However, under the conditions that occur at WRRFs, microbial Fe(III) reduction seems to be dominant.

Mineral-water interactions occur through three basic mechanisms (Roden 2008):

1. Enzymatic reactions for energy generation or biochemical processes of the production/consumption of the dissolved or solid phase compound
2. Non-enzymatic reactions in the bulk phase (promoted by enzymatic production/consumption of compounds)

3. Non-enzymatic reactions promoted by cell-surface ligands (e.g. cell-surface adsorption or surface nucleation/precipitation)

The Fe(III) reducing organisms are able to produce redox-active proteins on the outer surface of the cell that facilitates the electron transfer of stored organic carbon to Fe(III) oxides outside the cell. In the absence of the enzyme, a spontaneous reaction between intracellular organic carbon and extracellular Fe(III) oxides does not occur. These prokaryotes also have the capability to provide a surface for the sorption of metal ions on the cell membrane which then can nucleate creating small particles through this reaction (Schultze-Lam *et al.*, 1996).

The formation of these fine-grain minerals occurs in two different ways: passive microbially induced formation, where the cations bind to the surface anions creating a surface nucleation site, or active microbially induced mineral formation, where the enzymatic electron transfer the metabolic end product forms mineral on the cells (Southam, 2000). These observations have significance for activated sludge processes where the relatively homogenous, small particle distribution may impact the reduction rates (as opposed to sediments and soil matrices).

To combine earlier observations and models, Roden (2008) proposed a model for direct enzymatic Fe(III) reduction. According to their summary, the three mechanisms include: 1) Direct reduction 2) Chelator promoted reduction 3) Electron-shuttling promoted reduction, including “geopilins” that may facilitate the process.

1.3.7. Iron reduction kinetics

In the conditions that occur during wastewater treatment, iron can be found in both oxidized (Fe(III)) and reduced (Fe(II)) forms. The most current practice is to dose Fe(III) salts (e.g. ferric chloride) whereas Fe(II) salts can be also used (e.g. Ferrous sulfate). The dosage point signifies the initial conditions and expected retention time of the iron salts in unaerated or aerated zones. Therefore the reaction rates can be determined, their significance assessed in plant operation, and incorporated into models, as soon as the oxidation level is known. According to the conditions iron forms different amorphous precipitates or crystals with various structure that impacts bio-availability and the phosphate-removing capacity.
Understanding the iron redox cycle seems therefore a crucial issue to optimize chemical use (regarding both the dosage point and the iron species) and increase nutrient recovery potential.

Previous studies on activated sludge systems show that iron reduction begins under anaerobic conditions (Nielsen, 1996; Lovley, 2013; Chen *et al.,* 2018) and confirmed that complete reduction is carried out after long anaerobic HRT (~20 days) which explains the observations of Fe(II) mineral (such as vivianite and pyrite) formation in digested sludge (Wilfert *et al.,* 2016).

The kinetic reduction rates determined by these studies are summarized in Table 1.3-2. Wilfert *et al.* (2016) confirmed that after extended anaerobic retention time (e.g. which occurs in an anaerobic digester), the dominant iron species becomes Fe(II) and the major precipitates are stable crystals formed with phosphate (vivianite) or sulfide (e.g. pyrite). Considering phosphorus recovery potential from sludge, iron(II) mineral (vivianite) was preferred due to the separating possibilities of the crystals with magnetic properties and crystal growth dynamics as opposed to the amorphous flocs of iron(III) precipitates.

Table 1.3-2 Kinetic rates for iron reduction in different studies

Reference/study	Unit (First order / zero order)	Reduction rate	Comment
Roden and Wetzel (2002)	d^{-1}	0.178 – 0.392	Slurries, natural water sediments
Chen *et al.* (2003)	d^{-1}	3.312 – 10.944	S. putrefaciens CN32 in PIPES-phosphate buffer solution
Wang *et al.* (2019)	d^{-1}	1.2 – 1.44	First order constant, Biological and chemical activated sludge (linear fitting 24 h)
Frederickson *et al.* (2003)	µmol/h	14.3 – 50	Initial rate for the first 50h, with variable lactate addition
Nielsen (1996)	mg Fe/g VSS.h	0.9 – 3.7 (5.4)	Potential reduction rates in activated sludge
Wang *et al.* (2019)	mg Fe/g VSS.h	1.02 – 2.99	Biological and chemical activated sludge (linear fitting 24 h)

In the mainstream, the typical anaerobic HRT (a few hours) is much lower than digester and the primary goal of iron addition is to reach low phosphate concentration. Usually, Fe(III) is dosed in the aeration tank where it forms ferrihydrites and more stable iron-hydroxides. Adhikari (2017) suggests that ferrihydrite has a high organic carbon binding capacity (surface adsorption) and due to the poorly crystalline structure, should be more available for reduction than other more structured crystalline Fe(III) oxides.

The reduction of Fe(III) may cause phosphate release (secondary phosphate release, desorption, and anaerobic polyphosphate breakdown), and therefore impacts the global phosphate removal performance of the facility. Nielsen and Keiding (1998) found that the FeS formation (subsequent to iron reduction) may also cause the disintegration of flocs which has detrimental effects on phase separation.

1.3.8. Recent models for describing iron-based phosphate removal

Different models describing chemical P removal have been focusing on the interaction between amorphous ferrihydrite and orthophosphate. There has been a long history of chemical equilibrium (Luedecke *et al.,* 1988; WEF, 1998) and kinetics (Henze *et al.,* 1995) approaches (and the combination of the two) to describe the precipitation of ferric hydroxy-orthophosphate (formulated as $Fe_rPO_4(OH)_{3r-3}$ by Stumm and Morgan, 1970) and hydrous ferric oxide (HFO) and subsequent adsorption of P on the surface.

Smith *et al.* (2008) introduced the surface complexation model (SCM) which defines the main precipitation and P removal mechanisms: adsorption of phosphate onto HFO and the co-precipitation of ferric phosphates. The fraction of these precipitates depends on operating conditions (eg. co-precipitation requires rapid mixing). The model incorporates structural changes of HFO with time ("aging") as the particles get more dense (however, not crystalline, as the typical aerobic HRT would not be sufficient for crystallization) and fewer active surface sites are available. Hauduc *et al.* (2015) extended and validated this concept in the full plant model (SUMO) as this is summarized on Figure 1.3-3.

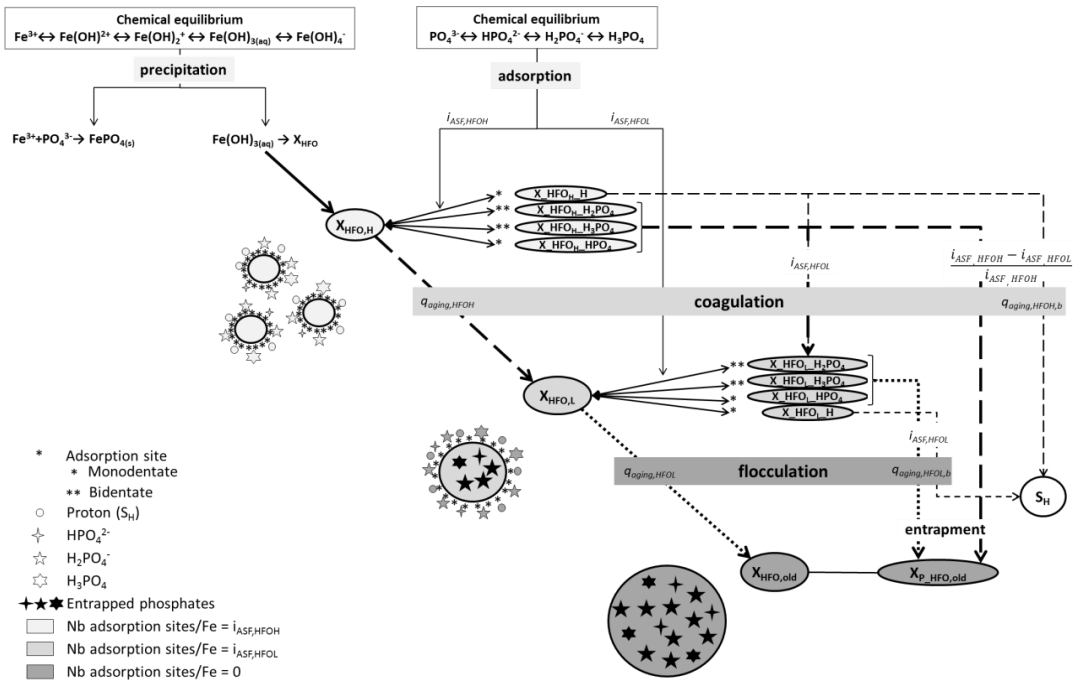

Figure 1.3-3 Description of adsorption and co-precipitation of phosphate on hydrous ferric oxides - HFO (Hauduc et al., 2015)

Recent full plant models, developed for plant-wide modeling, incorporating multiple mineral precipitates were proposed in the last decade (Mbamba *et al.,* 2016, 2019; Solon *et al.,* 2017; Hauduc *et al.*, 2019). These models present links between Fe – P – S reactions in wastewater treatment, both in mainstream and sidestreams.

Solon *et al. (*2017) incorporated a simplified version of the HFO model in a full-plant model (ADM, ASM2d, and PCM type with interfaces) to describe chemical P removal, including the formation of HFO and adsorption of phosphate subsequent formation of FeS in the digester, multiple mineral formation to describe nutrient recovery processes.

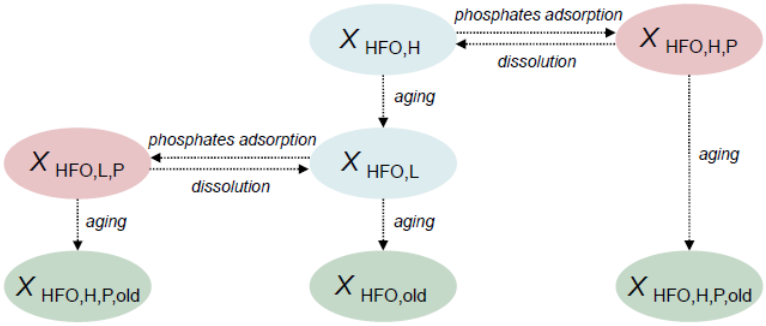

Figure 1.3-4 A simplified version of the HFO model coupled to ASM2d (Solon thesis, 2017)

Hauduc *et al.* (2019) incorporated iron and sulfur reactions in the SUMO model (Dynamita, SUMO2S full-plant model) where detailed biological and chemical interactions were included (Figure 1.3-5). Aside from the complete sulfur cycle, iron reduction and oxidation processes, precipitation of vivianite, ferric sulfide, struvite, and calcium phosphate were also included. The model is further discussed in Chapter 4.

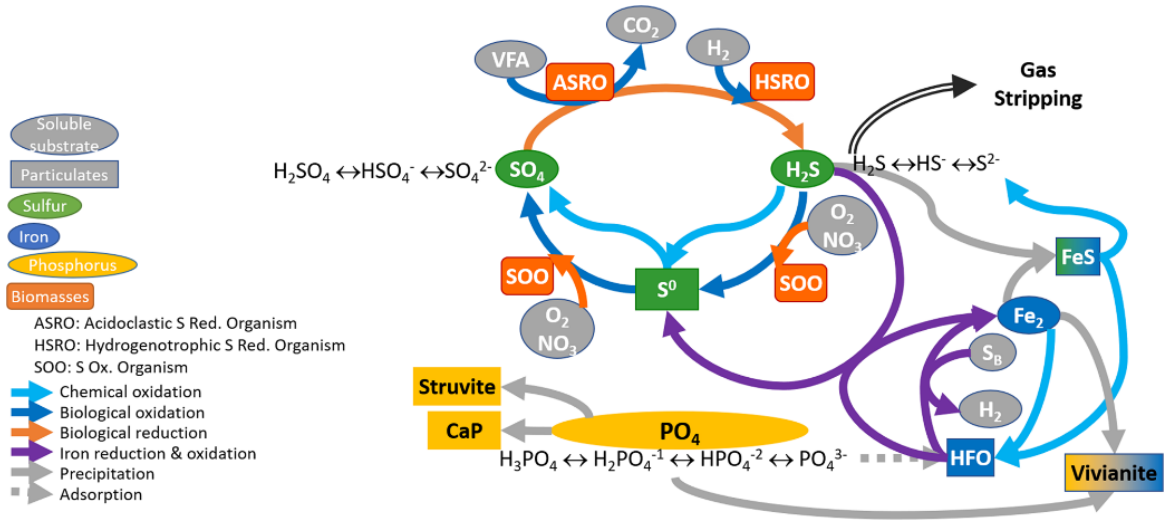

Figure 1.3-5 Fe-P-S interactions by Hauduc et al. (2019)

1.4. Combined chemical and biological treatment in alternated aeration systems

1.4.1. Alternated aeration systems

Alongside achieving low effluent nutrient concentration, energy efficiency has been a major driving force of design optimization. Aeration accounts for the majority of energy use in a WRRF. Therefore it has been a common interest to optimize aeration for each specific activated sludge configuration. While the multiple basin systems (Modified Ludzack-Ettinger process (MLE), Bardenpho, Phoredox, UCT) are recognized as the most efficient configurations for nutrient removal, the single tank or two tank systems with intermittent aeration has also become a standard, especially in rural areas and small or medium WRRFs in France. The advantage of intermittent systems is their (apparent) simplicity, avoiding internal recirculation pumps, and being adaptable with a variable aeration frequency.

It should be mentioned that such intermittently aerated AS with continuous feeding can achieve a low level of nitrate and ammonia because the dilution rate is sufficiently high, as for most of the AS designed with a low loading rate (e.g.: in France: 0.1 $KgBOD_5/KgSS^{-1}.m^{-3}$ and HRT around 24 hours, as a standard).

Due to the seasonal, weekly, and diurnal variations (flow and temperature), such intermittent systems need good aeration frequency regulation. ORP regulation in activated sludge is an example of using a very universal physical parameter to define specific processes. Charpentier *et al.* (1998) showed that carbon, sulfur, and nitrogen components go under redox transformations in an activated sludge system and defined a "biological window" of the Pourbaix-diagram (Potential EH-pH graph) in which these reactions occur (Figure 1.4-1). This study demonstrated that with proper mixing, chemical additions (such as a moderate amount of iron salts for P removal or chlorination to prevent bulking) do not present notable interference. ORP control is especially recommended for small and medium facilities to ensure the stability of the processes but is also advantageous in larger plants.

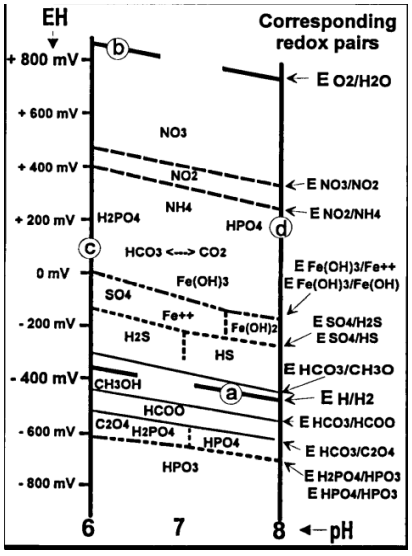

Figure 1.4-1 "Biological window" of Eh-pH diagram where redox transformation occurs in AS systems (Charpentier et al., 1998)

Paul *et al.* (1998) demonstrated the validity of using the bending point of DO to indicate the end of nitrification ("ammonia valley") and the bending point of the ORP curve to indicate the beginning and the end of denitrification ("nitrate knee") with different system loads. They found that in specific cases, these bending points may not appear, however, this still gives information on the operating conditions of the facility.

These principles have been successfully used in DO/ORP control systems (Figure 1.4-2) and implemented in various facilities (e.g. in France for instance within the *inflex* system developed by BIOTRADE in collaboration with INSA). Additionally, de la Vega (2012) introduced new parameters to further optimize the control: ORP arrow to characterize the anoxic phase and Oxygen Rise Average Slope (ORAS) which includes oxygen utilization rate (OUR) during the aeration phase.

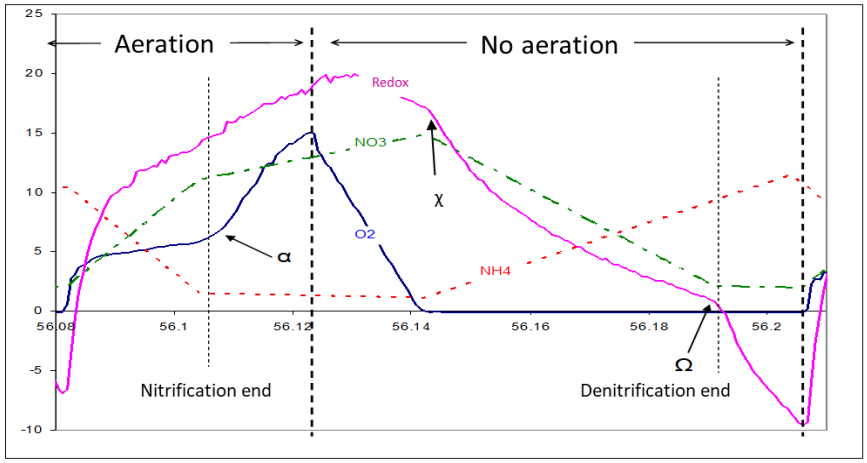

Figure 1.4-2 ORP, DO and pH curves presenting specific bending points associated with nitrogen removal (α: end of nitrification, β beginning of denitrification, and χ end of denitrification) in aeration cycles (figure by Michel Mauret, personal communication, 2018)

Aside from complete nitrogen removal, Sasaki *et al.* (1993) demonstrated over 95% TP removal (effluent TP<0,2 mg P/L) on a pilot scale, with consecutive intermittent aeration reactors, allowing extended cycles in the first reactor and therefore ensuring P release and sufficient PHA storage while maintaining aerobic/anoxic conditions in the second. They suggest that this strategy is advantageous to small and medium facilities and it requires relatively low additional investments for retrofitting existing plants.

In practice, biological removal efficiency is highly variable and not systematically estimated in full-scale intermittent aerated AS, because simultaneous metal addition is performed in most facilities.

Some recommendations were given in the FNDAE report n°29 (Deronzier and Choubert, 2004) for phosphorus removal in rural plants in France. From the study of 6 different A/O activated sludge plants the efficiency of biological P removal varies from 56 to 89% (Deronzier and Choubert, 2004).

The biological removal efficiency was estimated to be 60-70% for dry weather conditions but only in the range of 30-50 % for diluted water (rain period or groundwater infiltration). A recommendation was to maintain good denitrification in order to limit nitrate recirculation in the anaerobic zone, which is known to be detrimental to polyphosphate accumulation.

The survey contains several plants implementing intermittent aeration, however, the exact mechanism and the effect of intermittent aeration on P removal are not discussed. Nonetheless, these varying conditions may explain the significant variation of the biological fraction of the P removal and the related issues (such as the unstable period in performance, and the need for re-adjustment of chemical dose).

1.4.2. Terminal electron-accepting processes

When considering (biological) iron transformations in wastewater, it is essential to incorporate them into the entire ecology of activated sludge systems. As functional groups of microorganisms capture energy from a specific reaction (e.g. oxidation of acetate by sulfate) either by catalyzing the full reaction or a specific step of the reaction in a symbiotic community it is important to consider which available electron acceptor is the most energetically favorable. This may drive competition between different microorganisms (competitive exclusion) as the ecological advantage depends on the ability to capture more energy. It is generally assumed, that the functional groups follow a thermodynamic hierarchy for the competition for the same electron donor. However, Bethke *et al.* (2011) found an instance of mutualism, namely in the formation of iron sulfide (FeS_x).

Finally, in WRRF, the consideration of the sequence of the dominant electron-accepting processes (Figure 1.4-3) may be helpful as an indicator of the conditions and the system state in general.

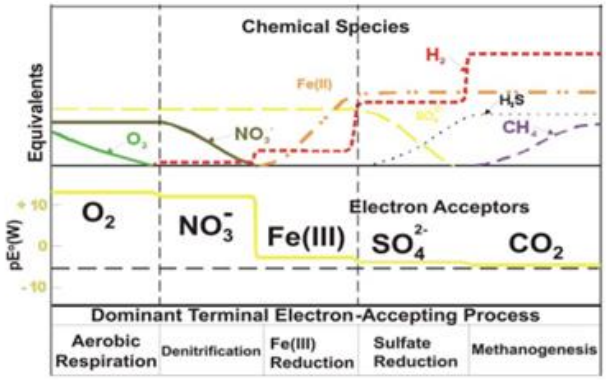

Figure 1.4-3 Dominant electron-accepting processes (EPA 542-R-13-018)

1.4.3. Common practices with combined biological and physical-chemical removal

Minton and Carlson (1972) summarized typical combined biological and physical-chemical phosphorus removal strategies by dosage points as primary, simultaneous, and tertiary (Figure 1.4-4).

They suggest considering several parameters when optimizing the process: pH (sensitivity of the precipitates), alkalinity (e.g. nitrification depends on alkalinity) formation and settleability of biological-chemical flocs (reconsidering dosage strategy during high hydraulic loads), hydraulic conditions in the final clarifier and retention time. It is also a common practice to temporarily use chemical dosage (e.g. during summer to meet effluent requirements to supplement EBPR).

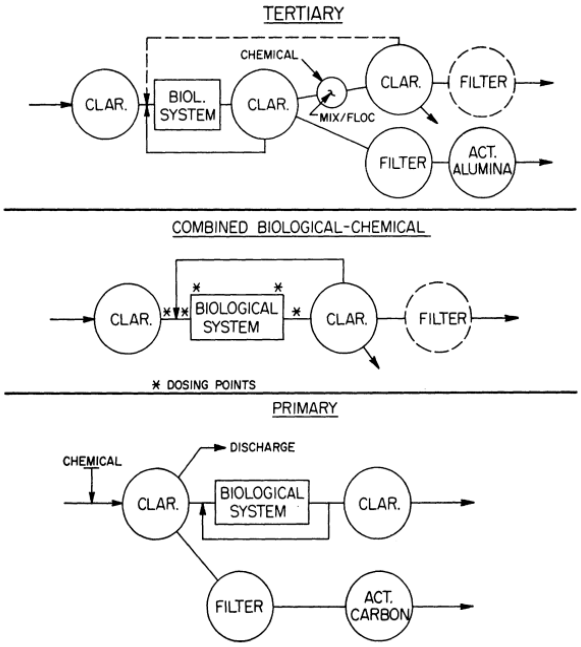

Figure 1.4-4 Chemical dosage strategies presented by Minton and Carlson (1972)

Paul *et al.* (2001) investigated the effect of the type of P removal on excess sludge at several French facilities. As they found, the majority of the facilities (83%) implement some sort of chemical dosage (88% iron and 12% alum) which have important implications not only on the sludge production itself, but the sludge handling as well, since direct spreading for agricultural purposes was (and still is) a common practice in France. The excess sludge production as well as the chemical use itself represent a significant cost in the operation of the facilities. After analyzing the data from 35 different facilities, and based on a rational model considering the typical French sewage characteristics, it was concluded that EBPR alone can achieve 58% removal for a BOD:P ratio of 25 (typical ratio in the nineties). However, the biological P removal performance would increase up to 80% for a BOD:P ratio of 36, as soon as the phosphorus from detergents would be removed (decreasing from 2.5 to 1.7 g P/PE.d). This last situation is certainly reached today but metals are still widely used in practice for complementing biological P removal.

Regarding the global operating cost and the environmental impacts of wastewater treatment, it seems logical to encourage biological P removal and minimize the use of chemicals. Paul *et al*. (2001) showed that the operating cost of pure physical-chemical treatment is 6 times higher than EBPR, considering chemicals and sludge disposal costs. The combined treatment allows a reduction of 50% of the costs compared to pure physicochemical. For typical domestic sewage with BOD: P=30, phosphorus removal generates 10% of supplementary sludge with EBPR but an excess of 20% for physical-chemical treatment (Paul *et al.*, 2001). Coats *et al.* (2011) concluded with a comprehensive life cycle assessment (LCA) that with increasing chemical usage also the adverse environmental impact of the chemical treatment also increased, therefore, from a holistic environmental point of view chemical dose should be minimized while maintaining the effluent quality with encouraging biological processes. Considering the extra costs and potential harm to biological processes, it is clear that optimizing combined biological and physical-chemical P removal would require maximizing EBPR and controlling chemical dose precisely while maintaining proper operating conditions (mixing, pH regulation if necessary) (Thomas *et al.* 1996).

1.4.4. Recent routes for phosphate recovery in the presence of iron

Nutrient recovery from wastewater has received increasing attention recently. Indeed the finality of the world's mineral phosphorus deposit and its implications were pointed out (Vaccari, 2009; Cordell, 2011; Descmidt *et al.,* 2015) and the linear usage of phosphorus is not only wasteful but causes pollution (point and dispersed) to natural waters, causing eutrophication. Phosphorus can be recovered from wastewater by different technologies and could theoretically provide up to 20% of the agricultural phosphorus needs to replace mineral P. However, the development and commercialization of these technologies face different constraints (economic feasibility, product safety, and recovery technologies). One significant aspect was the presence of iron in the sewage sludge, lowering P availability.

Numerous studies have reviewed P recovery processes (Morse *et al*, 1998; Stark, 2005, Descmidt *et al*, 2015; Egle *et al*, 2015; Cieslik and Konieczka, 2017). Based on recovery points, they can be categorized as 1) direct application of waste sludge 2) recovery from sewage sludge or leachate 3) Recovery from sewage sludge ashes (after incineration), or 4) Recovery from urine (after source separation).

There are several technologies optimized for different configurations. The simplest method for phosphorus recovery is the direct application of dewatered sludge on agricultural fields. This may raise concerns and needs careful monitoring regarding pathogens and heavy metal pollutants and may not be applicable in some countries. Indeed there is an increasing tendency in Europe to limit direct sludge spreading. Moreover, plant availability, especially in the case of some chemical treatments is also an issue. To achieve a higher concentration of nutrients and enhanced plant availability, several technologies to recover different products have been developed.

Outside of the direct use of sewage sludge, the most relevant due to reasonable (but still significant) investment costs is the recovery from sewage sludge and leachate. This technology requires the solubilization of phosphorus in order to precipitate/crystallize as struvite ($MgNH_4PO_4.6H_2O$) usually on the anaerobically digested sludge liquor using magnesium addition or hydroxyapatite ($Ca_5(PO_4)_3(OH)$) can be alternatively produced with calcium addition.

Kabbe (2017) summarized wastewater treatment facilities where P recovery is implemented and the majority recovered struvite. Struvite was known for causing operational problems by spontaneous precipitation in digestors (Borgerding, 1972). However, later crystalization technologies were developed to create a fertilizer product. There are several techniques for struvite crystalization (such as Phospaq, Ostara Pearl technology, and AirPrex) but the efficiency depends on the P mobility. There are different methods to solubilize phosphorus (Kataki *et al*. 2016): anaerobic digestion; acid-base leaching; use of chelating agents; microwave heating or P release during EBPR processes. This latter allows a simple way to release stored polyphosphate via anaerobic processes such as WASSTRIP. However, in the case of chemical phosphorus removal, this method does not provide high efficiency.
In order to increase the recovery potential from chemical sludge, iron-phosphate interactions need to be examined. P release upon iron reduction has been reported previously. As extended low ORP conditions occur in anaerobic digesters, digested chemical sludge may represent a recovery source. Typical Fe(II) precipitates in an anaerobic digester are FeS and vivianite (Roussel and Carliell-Marquet, 2016). Vivianite formation had been reported in FeSO4 flocculated sludges in both digested and activated sludge (60-67% and 43% of total iron respectively (Frossard *et al.*, 1997).

Vivianite has been known for its coloring properties and used as paint but for agricultural purposes, it may be applied as fertilizer and is especially beneficial in iron-deficient soils. There are other potential uses of vivianite (such as in the battery industry).

Wilfert *et al.* (2018) and later Prot *et al.* (2019) investigated the possibility of ferrous phosphate recovery from digested sludge, and more specifically the role of vivianite in nutrient recovery. They found that the omnipresence of iron in WWTPs (either by metal addition or from influent) has an effect on the recovery process, may that be positive (more advantageous acid consumption than aluminum during wet digestion), negative (lower efficiency in recovering specific products such as struvite) or indifferent/inconclusive (e.g. thermochemical treatment of sludge). The author suggests that iron dosage to remove P and COD is overall advantageous regarding plant performance and energy efficiency.

It was found that 70-90 % of P is bound to vivianite in digested sludge and therefore makes vivianite desirable to separate from the sludge. One suggested method is magnetic separation. Another investigated option for P recovery from digested chemical sludge was the release by sulfide addition in order to encourage FeS formation as opposed to vivianite.

However, this method had limited applicability. The author recommends further investigation on vivianite formation in order to enhance characteristics (particle size, impurities, etc). Prot *et al.* (2019) demonstrated the possibility to recover vivianite from digested sludge via wet magnetic separation. The recovered material has a high content in vivianite and can be further processed for agricultural or other products.

While the long retention time in digesters ensures the complete reduction of iron, further reduction studies showed that shorter (2-3 days) anaerobic retention time is sufficient to form vivianite (Prot *et al*., 2021). With excess iron dose, the authors demonstrated that 50-55% of iron was in the form of vivianite (up to 4 days of anaerobic retention time). But vivianite could be theoretically formed with a low retention time as soon as the iron is in a ferrous state and saturation level is reached. Indeed Primadoro *et al.* (2017) achieved high-purity vivianite from activated sludge using fluidized bed crystallization.

1.4.5. Interaction between iron dosage and biological processes

The biological and physical-chemical removal processes have been extensively described, however, the interaction between chemical dose and related (or non-related) biological processes need also to be considered.

De Haas *et al.* (2000) dedicated extensive work to investigating such interactions, considering aluminum, ferric solution, and ferrous-ferric blend as a chemical addition to biological processes. They observed the precipitation mechanisms as well as the potential inhibition effect on specific processes of EBPR.

They found that with ferric addition, anaerobic P release was reduced (both in P-limiting and non-limiting conditions, however, in limiting conditions the inhibition effect was higher).

An important implication of Fe dosing is the lowering of the pH (and consumption of alkalinity) but this did not inhibit the biological processes. Total suspended solids (TSS) production increased, partially due to the increased inorganic suspended solids (ISS) but also somewhat increased VSS was observed, which suggests that ferric iron addition affects the biomass production yield. Valve *et al.* (2002) also found that at simultaneous biological and physical-chemical P removal, chemical precipitation competes with the biological processes and even inhibits them with increased concentration (they dosed ferrous sulphate to aerobic tank and mainly ferric/HFO needs to be considered as precipitates). Liu *et al.* (2011) conducted a series of experiments and confirmed the detrimental effect of chemical use on biological processes (although ferric to a lower extent than alum). With the accumulated precipitates, the inhibition effect is maintained even after the cessation of the dose.

Fan *et al.* (2018) confirm the observation on increased MLSS, decreased pH, and altered anaerobic P release. They dosed ferrous sulphate and followed the effects of two precipitates: $FePO_4$ and HFO, both deteriorating EBPR. They found that $FePO_4$ dissolved rather quickly during anaerobic transformations and the released phosphate was not re-absorbed in the following processes. $FePO_4$ inhibited potassium uptake (important counter-cation for phosphate). Similarly to de Haas *et al.* (2000), Fan *et al.* (2018) also observed lower phosphate release in the presence of HFO. Moreover, potassium and phosphate uptake was reduced as well. Accumulated Fe concentration of 0,14 mM FePO4 or 0,1 mM HFO resulted in these inhibitions. An Increase K/P ratio can be an indicator of residual iron. To avoid these detrimental effects, the authors suggested intermittent chemical dose when possible.

1.5. Conclusion and thesis contribution

There have been decades of a long development in biological nutrient removal and new advances lead to more efficient removal technologies and increased recovery potential. As more and more mechanisms are described in EBPR systems, activated sludge modeling also becomes more detailed and complex. Starting from three P-related processes in the initial ASM2d model, recent agent-based and metabolic models include several groups of organisms with detailed interactions with one other under different conditions.

Alongside biological processes, chemical processes have also been investigated, and similarly, modeling efforts followed the recent discoveries: a comprehensive surface complexation model has been developed for HFOs including precipitation and transformation processes (adsorption, aging). Moreover, several precipitation processes have been described in current models, such as struvite, hydroxy-apatite, iron sulfide, and vivianite. The prediction of such precipitates is crucial from an operational and maintenance standpoint as well as for estimating recovery potential.

The interactions between these two major types of P removal are not well described in activated sludge models, even though combined systems are fairly common and literature suggests that chemical dose has more impacts on biological processes apart from P limitation. It is important to consider possible inhibitory effects as well as estimate the overall benefit of a certain chemical dosage strategy.

Iron dosage at different points of dosage serves different direct purposes, however, with the dynamic nature of the wastewater collection and treatment system as well as sludge handling, iron may undergo (multiple) redox transformations depending on the conditions. It is important to consider these reactions, especially iron reduction, as they may have an impact on P removal efficiency and settling and separating processes (Fe^{2+} may form colloids which are detrimental for settling and dewatering).

Moreover, under reductive conditions iron(II) forms vivianite, a precipitation product receiving increasing interest due to its recovery potential. In case an anaerobic digester is not in operation at the plant (which would provide long enough anaerobic retention time for reduction), it is important to understand reduction processes in detail in order to efficiently control processes (HRT) to maximize vivianite recovery.

When discussing reduction processes, it is important to consider other available electron acceptors in the same system. In the context of wastewater treatment, sulfur species play an important role and also undergo redox transformations (usually mediated by microorganisms). To understand and assess precipitation products (iron precipitates with P or S in reductive zones) the hierarchy (or interactions) of terminal electron-accepting processes need to be examined.

While the general full-plant models are well calibrated for steady-state conditions, alternating aeration processes became a standard in France for small and medium facilities and these systems may require a specific approach for the model configuration.

Moreover, these systems are optimized for nitrogen removal but few studies deal with P removal in such a process. Usually, to a certain extent chemical (iron) dose is applied to meet effluent quality standards, however, the exact contributions of biological and chemical P removal are not well characterized.

The aim of this thesis is to observe and evaluate a combined biological and physical-chemical P removal system at a rural French facility using intermittent aeration. One objective was also to provide more knowledge relative to iron speciation and interaction in such a complex biological system.

The following chapters provide further insights using three different approaches. Beginning with the operational monitoring campaign and day-to-day challenges of the partner facility, a specific set of challenges is examined (Chapter 2). This case study brings attention to the main issues that these types of plants face and attempts to ameliorate the efficiency of chemical use integrating previously gained theoretical knowledge and the valuable observations collected from online monitoring and some lab scale characterizations.

To deeper characterize certain interactions, several laboratory experiments were carried out, providing the second basis of the work (Chapter 3). Regarding the questions of the thesis, specific questions were defined when preparing the experiments: especially focusing on iron reduction kinetics and terminal electron-accepting processes in activated sludge. As it is uncommon to have an anaerobic digester in such a facility but in short-term anaerobic periods, it is important to carefully consider reduction kinetics (and evaluate possible P release during the reaction) under different conditions that occur in activated sludge. Moreover, P release is also evaluated under different conditions. This is an important question for both removal and recovery aspects.

Finally, a dynamic simulation is presented with a specific calibrated model extension to describe previous observations in detail (Chapter 4). The model extension is implemented in the Sumo2S framework (Sumo21 version software) an extensive and complex full-plant model including several of the discussed processes. This model extension is aimed to be “as simple as possible but no simpler”. Indeed as process modeling is an ever-increasing area with new ideas and different frameworks leading regularly to new complex questions regarding calibration, any additional conceptual process needs to present a proportional benefit and/or be provided as an add-on extension to be used for specific focus cases only. While the development of these processes presents an interest (according to the author at least) it is important to evaluate if the additional complexity also provides corresponding benefits, and consider the simplifications which can make the model easier to use.

1.6. References

10th Technical assessment of information on the implementation of Council Directive 91/271/EEC

Acevedo, B., Oehmen, A., Carvalho, G., Seco, A., Borrás, L., & Barat, R. (2012). Metabolic shift of polyphosphate-accumulating organisms with different levels of polyphosphate storage. *Water research*, *46*(6), 1889-1900.

Acevedo, B., Murgui, M., Borrás, L., & Barat, R. (2017). New insights in the metabolic behaviour of PAO under negligible poly-P reserves. *Chemical Engineering Journal*, *311*, 82-90.

Azam H. M. and Finneran K. T. (2014) Fe(III) reduction-mediated phosphate removal as vivianite (Fe3(PO4)2·8H2O) in septic system wastewater *Chemosphere*, vol. 97, p. 1-9

Barker, P. S., & Dold, P. L. (1997). General model for biological nutrient removal activated-sludge systems: model presentation. *Water Environment Research*, *69*(5), 969-984.

Barnard J. L. (1976) A review of biological phosphorus removal in activated sludge process. *Water SA,* 2(3), 136-144)

Barnard, J. L. (1978). The Bardenpho Process. In *Conf. Biol. Nutrient Rem. Alternatives* (pp. 79-113).

Barnard, J., Houweling, D., Analla, H., Steichen, M., 2010. Fermentation of mixed liquor for phosphorus removal. *Proceedings of the Water Environment Federation, 2010*, pp. 59-71

Barnard J. L., Dunlap P. J., Steichen M. (2017) Rethinking the mechanisms of biological phosphorus removal *Water Environment Research,* 89(11) 2043 – 2054

Bartlomiej Cieslik, Piotr Konieczka (2017) A review of phosphorus recovery methods at various steps of wastewater treatment and sewage sludge management. The concept of "no solid waste generation" and analytical methods. *Journal of Cleaner Production* 142 (2017) 1728-1740

Bethke, C. M., Sanford, R. A., Kirk, M. F., Jin, Q., & Flynn, T. M. (2011). The thermodynamic ladder in geomicrobiology. *American Journal of Science*, *311*(3), 183-210.

Blöthe, M., & Roden, E. E. (2009). Microbial iron redox cycling in a circumneutral-pH groundwater seep. *Applied and environmental microbiology*, *75*(2), 468-473.

Borgerding, J. (1972). Phosphate deposits in digestion systems. *J. Wat. Pollut. Control Fed.*, *44*(5), 813-819.

Bratby, J., Fevig, S., & Jimenez, J. (2012). The dirty secret of primary sludge prefermenters. *Proceedings of the Water Environment Federation*, *2012*(10), 5660-5671.

Charpentier, J., Martin, G., Wacheux, H., & Gilles, P. (1998). ORP regulation and activated sludge: 15 years of experience. *Water science and technology*, *38*(3), 197-208.

Chen R. Liu H., Tong M., Zhao L., Zhang P., Liu D., Yuan S. (2018) Impact of Fe(II) oxidation in the presence of iron-reducing bacteria on subsequent Fe(III) bio-reduction *Science of The Total Environment Volume 639, 15 October 2018, Pages 1007-1014*

Chen, J., Gu, B., Royer, R. A., & Burgos, W. D. (2003). The roles of natural organic matter in chemical and microbial reduction of ferric iron. Science of the total environment, 307(1-3), 167-178.

Coats, E. R., Watkins, D. L., & Kranenburg, D. (2011). A Comparative Environmental Life-Cycle Analysis for Removing Phosphorus from Wastewater: Biological versus Physical/Chemical Processes. *Water Environment Research*, *83*(8), 750-760.

Coby, A.J., Picardal, F., Shelobolina, E.S., Xu, H. and Roden, E.E. (2011) Repeated anaerobic microbial redox cycling of iron. Appl. Environ. Microbiol. 77, 6036–6042

Comeau Y., 1990a, La déphosphatation biologique, métabolisme microbien, Sciences et Techniques de l'eau 23(1): 47-60.

Comeau Y., 1990b, La déphosphatation biologique, procédés et conception, Sciences et Techniques de l'eau 23(2): 199-216.

Cordell, D., Rosemarin, A., Schröder, J. J., & Smit, A. L. (2011). Towards global phosphorus security: A systems framework for phosphorus recovery and reuse options. *Chemosphere*, *84*(6), 747-758.

Cornell R.M. and Schwertmann U. (2003) The iron oxides – Structure, Properties, Reactions, Occurrences and Uses *Wiley-VCH GmbH&Co publication*

Council, E. E. C., & Directive, C. (1991). 91/271/EEC of 21 May 1991 concerning urban waste-water treatment. *European Environment Agency, Copenhagen*.

de Haas, DW, Wentzel, MC & Ekama, G. A. (2000). The use of simultaneous chemical precipitation in modified activated sludge systems exhibiting biological excess phosphate removal Part 4: Experimental periods using ferric chloride. *Water Sa*, *26*(4), 485-504.

de la Vega, P. M., de Salazar, E. M., Jaramillo, M. A., & Cros, J. (2012). New contributions to the ORP & DO time profile characterization to improve biological nutrient removal. *Bioresource technology*, *114*, 160-167.

Deronzier, Gaëlle, Choubert, Jean-Marc. 2004. Traitement du phosphore dans les petites stations d'épuration à boues activées. Cemagref, Document Technique FNDAE, n° 29.

Desmidt, E., Ghyselbrecht, K., Zhang, Y., Pinoy, L., Van der Bruggen, B., Verstraete, W., ... & Meesschaert, B. (2015). Global phosphorus scarcity and full-scale P-recovery techniques: a review. *Critical Reviews in Environmental Science and Technology*, *45*(4), 336-384.

Downing, L., Young, M., Cramer, J., Nerenberg, R., & Bruce, S. (2014). Low level DO operation: impacts on energy, nutrients, and ecology. *Proceedings of the Water Environment Federation*, *2014*(19), 6771-6783.

Dunlap, P., Robinson, C., Mach, E., Easley, M., Barnard, J., Jordan, B., & Caffey, J. (2017). Demonstration Scale Mixed Liquor Fermentation Investigation at TRA's Ten Mile Creek WWTP–Operation, Performance, and Modeling. *Proceedings of the Water Environment Federation*, *2017*(10), 2735-2751.

Egle, L., Rechberger, H., & Zessner, M. (2015). Overview and description of technologies for recovering phosphorus from municipal wastewater. *Resources, Conservation and Recycling*, *105*, 325-346.

Ekama, G. A., Siebritz, I. P., Marais, G. v. R., 1983, Considerations in the process design of nutrient removal activated sludge processes, Wat. Sci. Tech., 15 283-318.

Erdal, U. G., Erdal, Z. K., Daigger, G. T., & Randall, C. W. (2008). Is it PAO-GAO competition or metabolic shift in EBPR system? Evidence from an experimental study. *Water science and technology*, *58*(6), 1329-1334.

EU Taxonomy, Annex B 12.2: Phosphorus recovery from waste water p922-926

European Commission (2020) COMMUNICATION FROM THE COMMISSION TO THE EUROPEAN PARLIAMENT, THE COUNCIL, THE EUROPEAN ECONOMIC AND SOCIAL COMMITTEE AND THE COMMITTEE OF THE REGIONS A new Circular Economy Action Plan For a cleaner and more competitive Europe, COM/2020/98 final

Fan, J., Zhang, H., Ye, J., & Ji, B. (2018). Chemical stress from Fe salts dosing on biological phosphorus and potassium behavior. *Water Science and Technology*, *77*(5), 1222-1229.

Fan, Z., Zeng, W., Meng, Q., Liu, H., Liu, H., & Peng, Y. (2021). Achieving enhanced biological phosphorus removal utilizing waste activated sludge as sole carbon source and simultaneous sludge reduction in sequencing batch reactor. *Science of The Total Environment*, *799*, 149291.

Filipe, C. D., Daigger, G. T., & Grady Jr, C. L. (2001). pH as a key factor in the competition between glycogen-accumulating organisms and phosphorus-accumulating organisms. *Water Environment Research*, *73*(2), 223-232.

Fredrickson, J. K., Kota, S., Kukkadapu, R. K., Liu, C., & Zachara, J. M. (2003). Influence of electron donor/acceptor concentrations on hydrous ferric oxide (HFO) bioreduction. *Biodegradation*, *14*(2), 91-103.

Hauduc, H., Takács, I., Smith, S., Szabó, A., Murthy, S., Daigger, G. T., & Spérandio, M. (2015). A dynamic physicochemical model for chemical phosphorus removal. *Water Research*, *73*, 157-170.

Hauduc, H., Wadhawan, T., Johnson, B., Bott, C., Ward, M., & Takács, I. (2019). Incorporating sulfur reactions and interactions with iron and phosphorus into a general plant-wide model. *Water Science and Technology*, *79*(1), 26-34.

Henze, M., Gujer, W., Mino, T., Matsuo, T., Wentzel, M. C., Marais, G. V. R., & Van Loosdrecht, M. C. (1999). Activated sludge model no. 2d, ASM2d. *Water science and technology*, *39*(1), 165-182.

Houweling, D., Dold, P., & Barnard, J. (2010). Theoretical limits to biological phosphorus removal: rethinking the influent COD: N: P ratio. *Proceedings of the Water Environment Federation*, *2010*(9), 7044-7059.

Jimenez, J., Wise, G., Burger, G., Du, W., & Dold, P. (2014). Mainstream nitrite-shunt with biological phosphorus removal at the City of St. Petersburg Southwest WRF. *Proceedings of the Water Environment Federation*, *6*, 696-711.

Jimenez, J., Stensel, D., & Daigger, G. (2017). Simultaneous nutrient removal through low dissolved oxygen operation: application, pitfalls and design. *Proceedings of the Water Environment Federation*, *2017*(13), 1308-1313.

Kabbe, C. (2017). Overview of phosphorus recovery from the wastewater stream facilities operating or under construction. *Phosphorus Recovery and Recycling*.

Kappler, A., & Straub, K. L. (2005). Geomicrobiological cycling of iron. *Reviews in Mineralogy and Geochemistry*, *59*(1), 85-108.

Kataki, S., West, H., Clarke, M., & Baruah, D. C. (2016). Phosphorus recovery as struvite: Recent concerns for use of seed, alternative Mg source, nitrogen conservation and fertilizer potential. *Resources, Conservation and Recycling*, *107*, 142-156.

Keene, N. A., Reusser, S. R., Scarborough, M. J., Grooms, A. L., Seib, M., Santo Domingo, J., & Noguera, D. R. (2017). Pilot plant demonstration of stable and efficient high rate biological nutrient removal with low dissolved oxygen conditions. *Water research*, *121*, 72-85.

Kok, D. J. D., Pande, S., Lier, J. B. V., Ortigara, A. R., Savenije, H., & Uhlenbrook, S. (2018). Global phosphorus recovery from wastewater for agricultural reuse. *Hydrology and Earth System Sciences*, *22*(11), 5781-5799.

Kong, Y., Nielsen, J. L., & Nielsen, P. H. (2005). Identity and ecophysiology of uncultured actinobacterial polyphosphate-accumulating organisms in full-scale enhanced biological phosphorus removal plants. *Applied and environmental microbiology*, *71*(7), 4076-4085.

Kuba, T., Murnleitner, E., Van Loosdrecht, M. C. M., & Heijnen, J. J. (1996). A metabolic model for biological phosphorus removal by denitrifying organisms. *Biotechnology and bioengineering*, *52*(6), 685-695.

Lamb, J., (1994). Wastewater treatment with enhanced biological phosphorus removal and related purification processes. *U.S. Patent US 5288405A*. February 22, 1994

Liu, R., Hao, X., Chen, Q., & Li, J. (2019). Research advances of Tetrasphaera in enhanced biological phosphorus removal: a review. *Water research*, *166*, 115003.

López-Vázquez, C. M., Hooijmans, C. M., Brdjanovic, D., Gijzen, H. J., & van Loosdrecht, M. C. (2008). Factors affecting the microbial populations at full-scale enhanced biological phosphorus removal (EBPR) wastewater treatment plants in The Netherlands. *Water research*, *42*(10-11), 2349-2360.

Lovley, D. (2006). Dissimilatory Fe (III)-and Mn (IV)-reducing prokaryotes. *Prokaryotes*, *2*, 635-658.

Lovley D. (2013) Dissimilatory Fe(III)- and Mn(IV)-Reducing Prokaryotes. In: Rosenberg E., DeLong E.F., Lory S., Stackebrandt E., Thompson F. (eds) *The Prokaryotes. Springer, Berlin, Heidelberg*

Luedecke, C., Hermanowicz, S. W., & Jenkins, D. (1988). Precipitation of ferric phosphate in activated sludge: a chemical model and its verification. In *Water Pollution Research and Control Brighton* (pp. 325-337). Pergamon.

Mbamba, C. K., Flores-Alsina, X., Batstone, D. J., & Tait, S. (2016). Validation of a plant-wide phosphorus modelling approach with minerals precipitation in a full-scale WWTP. *Water Research*, *100*, 169-183.

Mbamba, C. K., Lindblom, E., Flores-Alsina, X., Tait, S., Anderson, S., Saagi, R., ... & Jeppsson, U. (2019). Plant-wide model-based analysis of iron dosage strategies for chemical phosphorus removal in wastewater treatment systems. *Water research*, *155*, 12-25.

Metcalf & Eddy, Abu-Orf, M., Bowden, G., Burton, F. L., Pfrang, W., Stensel, H. D., ... & AECOM (Firm). (2014). *Wastewater engineering: treatment and resource recovery*. McGraw Hill Education.

Milbury, W. F., McCaluley D., Hawthorne, C. H. (1971) Operation of conventional activated sludge for maximum phosphorus removal. Water Poll. Control. Fed. 43(9), 1890-1901.

Mines Jr, R. O., & Thomas IV, W. C. (1996). Biological nutrient removal using the VIP process. *Journal of Environmental Science & Health Part A*, *31*(10), 2557-2575.

Mino, T. M. C. M., Van Loosdrecht, M. C. M., & Heijnen, J. J. (1998). Microbiology and biochemistry of the enhanced biological phosphate removal process. *Water research*, *32*(11), 3193-3207.

Minton, G. R., & Carlson, D. A. (1972). Combined biological-chemical phosphorus removal. *Journal (Water Pollution Control Federation)*, 1736-1755.

Morse, G. K., Brett, S. W., Guy, J. A., & Lester, J. N. (1998). Phosphorus removal and recovery technologies. *Science of the total environment*, *212*(1), 69-81.

Nielsen P. H. (1996) The significance of microbial Fe(III) reduction in the activated sludge process. *Wat. Sci. Tech. Vol. 34. No.s-e. pp. 129-136.*

Nielsen, J. L., & Nielsen, P. H. (1998). Microbial Fe (II)-oxidation by nitrate in activated sludge. *Water Science and Technology*, *37*(4-5), 403-406.

Nielsen, P. H., & Keiding, K. (1998). Disintegration of activated sludge flocs in presence of sulfide. *Water Research*, *32*(2), 313-320.

Oehmen, A., Yuan, Z., Blackall, L. L., & Keller, J. (2004). Short-term effects of carbon source on the competition of polyphosphate accumulating organisms and glycogen accumulating organisms. *Water Science and Technology*, *50*(10), 139-144.

Oehmen, A., Carvalho, G., Lopez-Vazquez, C. M., Van Loosdrecht, M. C. M., & Reis, M. A. M. (2010). Incorporating microbial ecology into the metabolic modelling of polyphosphate accumulating organisms and glycogen accumulating organisms. *Water research*, *44*(17), 4992-5004.

Paul, E., Plisson-Saune, S., Mauret, M., & Cantet, J. (1998). Process state evaluation of alternating oxic-anoxic activated sludge using ORP, pH and DO. *Water Science and Technology*, *38*(3), 299-306.

Paul, E., Laval, M. L., & Sperandio, M. (2001). Excess sludge production and costs due to phosphorus removal. *Environmental technology*, *22*(11), 1363-1371.

Prot, T., Korving, L., Dugulan, A. I., Goubitz, K., & van Loosdrecht, M. C. M. (2021). Vivianite scaling in wastewater treatment plants: Occurrence, formation mechanisms and mitigation solutions. *Water Research*, *197*, 117045.

Rebosura Jr, M., Salehin, S., Pikaar, I., Sun, X., Keller, J., Sharma, K., & Yuan, Z. (2018). A comprehensive laboratory assessment of the effects of sewer-dosed iron salts on wastewater treatment processes. *Water research*, *146*, 109-117.

Roden E. (2008) Microbiological Controls on Geochemical Kinetics 1: Fundamentals and Case Study on Microbial Fe(III) Oxide Reduction. In: Brantley S., Kubicki J., White A. (eds) Kinetics of Water-Rock Interaction. Springer, New York, NY. https://doi.org/10.1007/978-0-387-73563-4_8

Roden, E. E. (2012). Microbial iron-redox cycling in subsurface environments. *Biochemical Society Transactions*, *40*(6), 1249-1256.

Roussel, J., & Carliell-Marquet, C. (2016). Significance of vivianite precipitation on the mobility of iron in anaerobically digested sludge. *Frontiers in Environmental Science*, *4*, 60.

Roy, E. D. (2017). Phosphorus recovery and recycling with ecological engineering: A review. *Ecological engineering*, *98*, 213-227.

Rubio-Rincón, F. J., Lopez-Vazquez, C. M., Welles, L., Van Loosdrecht, M. C. M., & Brdjanovic, D. (2017). Cooperation between Candidatus Competibacter and Candidatus Accumulibacter clade I, in denitrification and phosphate removal processes. *Water Research*, *120*, 156-164.

Santos, J. M., Rieger, L., Lanham, A. B., Carvalheira, M., Reis, M. A., & Oehmen, A. (2020). A novel metabolic-ASM model for full-scale biological nutrient removal systems. *Water research*, *171*, 115373.

Sasaki, K., Yamamoto, Y., Tsumura, K., Hatsumata, S., & Tatewaki, M. (1993). Simultaneous removal of nitrogen and phosphorus in intermittently aerated 2-tank activated sludge process using DO and ORP-bending-point control. *Water Science and Technology*, *28*(11-12), 513-521.

Saunders, A. M., Oehmen, A., Blackall, L. L., Yuan, Z., & Keller, J. (2003). The effect of GAOs (glycogen accumulating organisms) on anaerobic carbon requirements in full-scale Australian EBPR (enhanced biological phosphorus removal) plants. *Water Science and Technology*, *47*(11), 37-43.

Schultze-Lam, S., Fortin, D., Davis, B. S., & Beveridge, T. J. (1996). Mineralization of bacterial surfaces. *Chemical Geology*, *132*(1-4), 171-181.

Seviour, R. J., Mino, T., & Onuki, M. (2003). The microbiology of biological phosphorus removal in activated sludge systems. *FEMS microbiology reviews*, *27*(1), 99-127.

Smith S., Takács I., Murthy S., Daigger G. T. and Szabó A., (2008) Phosphate complexation model and its implications for chemical phosphorus removal. *Water Environment Research Vol. 80, No. 5, Nutrient Removal, pp. 428-438*

Smolders, G. J. F., Van der Meij, J., Van Loosdrecht, M. C. M., & Heijnen, J. J. (1994). Model of the anaerobic metabolism of the biological phosphorus removal process: stoichiometry and pH influence. *Biotechnology and bioengineering*, *43*(6), 461-470.

Solon, K., Flores-Alsina, X., Mbamba, C. K., Ikumi, D., Volcke, E. I. P., Vaneeckhaute, C., ... & Jeppsson, U. (2017). Plant-wide modelling of phosphorus transformations in wastewater treatment systems: Impacts of control and operational strategies. *Water Research*, *113*, 97-110.

Southam, G. (2000). Bacterial surface-mediated mineral formation. *Environmental microbe-metal interactions*, 257-276.

Spector, M. L. (1979). *U.S. Patent No. 4,162,153*. Washington, DC: U.S. Patent and Trademark Office.

Stark, K. (2004, June). Phosphorus recovery–Experience from European countries. In *Proceedings of Polish-Swedish seminars, Stockholm June 6-8*.

Straub, K.L., Benz, M., Schink, B. and Widdel, F. (1996) Anaerobic, nitrate-dependent microbial oxidation of ferrous iron. Environ. Microbiol. 62, 1458–1460

Stumm, W., & Morgan, J. J. (1970). *Aquatic chemistry; an introduction emphasizing chemical equilibria in natural waters*.

Szabo A., Takács I., Murthy S., Daigger G. T. and Smith S. (2006) The importance of slow kinetic reactions in simultaneous chemical P removal *Water Environment Research Vol. 80, No. 5, Nutrient Removal, pp. 407-416*

Szabó, A., Takács, I., Murthy, S., Daigger, G. T., Licsko, I., & Smith, S. (2008). Significance of design and operational variables in chemical phosphorus removal. *Water Environment Research*, *80*(5), 407-416.

Takács, I., Murthy, S., Smith, S., & McGrath, M. (2006). Chemical phosphorus removal to extremely low levels: experience of two plants in the Washington, DC area. *Water Science and Technology*, *53*(12), 21-28.

Tayà, C., Garlapati, V. K., Guisasola, A., & Baeza, J. A. (2013). The selective role of nitrite in the PAO/GAO competition. *Chemosphere*, *93*(4), 612-618.

Tooker, N. B., Li, G., Srinivasan, V., Barnard, J. L., Bott, C., Dombrowski, P., Schauer P., Menniti A., Shaw A., Stinson B., Stevens G., Dunlap P., Takàcs I., Phillips H., Analla H., Russell A., Lambrecht A., McQuarrie J., Onnis-Hayden A. & Gu. A. Z. (2018). Side-Stream EBPR Practices and Fundamentals–Rethinking and Reforming the Enhanced Biological Phosphorus Removal Process. *Proceedings of the Water Environment Federation*, *2018*(5), 223-239.

Tremblay, S., Hilger, H., Barnard, J. L., DeBarbadillo, C., & Goins, P. (2005, January). Phosphorus accumulating organisms utilization of volatile fatty acids produced by fermentation of anaerobic mixed liquor. In *Proceedings of the 78th Annual Water Environment Federation Technical Exhibition and Conference [CD-ROM]* (pp. 5971-5986).

Union, E. (1991). Council directive 91/271/EEC concerning urban wastewater treatment. *Brussels, Belgium*.

Vaccari, D. A. (2009). Phosphorus: a looming crisis. *Scientific American*, *300*(6), 54-59.

Valve, M., Rantanen, P., & Kallio, J. (2002). Enhancing biological phosphorus removal from municipal wastewater with partial simultaneous precipitation. *Water science and technology*, *46*(4-5), 249-255.

Varga, E., Hauduc, H., Barnard, J., Dunlap, P., Jimenez, J., Menniti, A., ... & Takács, I. (2018). Recent advances in bio-P modelling–a new approach verified by full-scale observations. *Water Science and Technology*, *78*(10), 2119-2130.

Wagner, M., Erhart, R., Manz, W., Amann, R., Lemmer, H., Wedi, D., & Schleifer, K. (1994). Development of an rRNA-targeted oligonucleotide probe specific for the genus Acinetobacter and its application for in situ monitoring in activated sludge. *Applied and Environmental Microbiology*, *60*(3), 792-800.

Wang, R., Wilfert, P., Dugulan, I., Goubitz, K., Korving, L., Witkamp, G.J., van Loosdrecht, M.C.M., (2019). Fe(III) reduction and vivianite formation in activated sludge. *Separation and Purification Technology Vol 220, P 126-135*

Wentzel, M. C., Lötter, L. H., Loewenthal, R. E., Marais, G. v. R., 1986, Metabolic behaviour of Acinetobacter spp. in enhanced biological phosphorus removal - a biochemical model, *Water SA* 12 (4) 209-224.

Wilfert, P., Mandalidis, A., Dugulan, I., Goubitz, K., Korving, L., Temmink, H., Witkamp, G.J., van Loosdrecht, M.C.M., (2016). Vivianite as an important iron phosphate precipitate in sewage treatment plants. *Water research 104, 449–460*

Chapter 2 - Optimization of P removal in activated sludge process with intermittent aeration at a rural facility – a case study

Highlights

- Phosphorus removal was monitored and scrutinized in detail for 3 years in a real plant
- Phosphate uptake and removal depend on the aeration time ratio
- Adequate control of intermittent aeration allows biological P removal to reach 71% (1.61 mgPO_4-P/L on average)
- Optimization of aeration and sludge wastage allowed to reduce by more than 50% the iron dose
- Some phosphate peaks were due to sludge dewatering liquor recirculation
- Side-stream iron dosage on sludge liquor allows reaching the P removal requirements

Keywords

Phosphorus removal, aeration control, iron dose, intermittent aeration, P release, and uptake

2.1. Introduction

With the advancements in wastewater treatment, more and more stringent effluent limits for nutrients and contaminants of emerging concern (CEC) are in place to protect the environment. However, outside of direct prevention of pollution, indirect emission also needs to be reduced. Conventional wastewater treatment represents a significant fraction of global energy use, with estimates of 1-4 % (Longo et al, 2016, IEA, 2018, Christoforidou et al, 2020). Moreover, greenhouse gas (GHG) emissions can be also substantial as N_2O is a by-product of biological nitrogen removal.

Chemical use also contributes to the negative impact of wastewater treatment plants as Coats *et al.* (2011) demonstrated in a comprehensive life-cycle analysis (LCA). In the case of phosphorus removal, the consumption of iron chloride is a major contributor to the global LCA impacts (Bisinella *et al.*, 2016) Therefore, it is imperative to optimize these chemical consuming processes to reduce anthropogenic emissions.

Advanced nitrification and denitrification are commonly carried out through alternated aeration in activated sludge systems called 'extended aeration systems' i.e. designed with high sludge age and low loading rate. In addition, combined biological and physical-chemical phosphorus removal is performed as well in the same facility by adding a first anaerobic zone and a coagulant dosage point. This work is focused on a two-stage activated sludge process (A/O) with a first non-aerated zone combined with an intermittently aerated basin.

This type of facility is now very common in France. Iron chloride is the most widely used chemical whereas aluminum salts are also alternatives. According to a 2019 database from the French government website, the small/medium size treatment facilities (2000-10000 PE) account for 12% of the number of active facilities and 12% of served population equivalent (PE) in France. A similar level of treatment is generally expected regarding nitrogen and phosphorus but it can be specifically adapted to the local sensitivity of receiving water body. Even though the removal of pollutants is up to international standards, nutrient recovery is an area with large development potential. According to a European Sustainable Phosphorus Platform (ESPP) report (2021), currently, only 3 facilities in France recover phosphorus (Kabbe, 2021).

Whereas the A/O process with intermittent aeration has become a standard in France, biological phosphorus removal is not necessarily optimal in that system but is generally complemented by coagulant dosage. However, the respective contributions of biological and physical-chemical processes have been poorly evaluated. The iron dosage is often adapted in a way to reach the target of 1 or 2 mg TP/L without necessarily optimal conditions for biological P removal. Finally, the minimization of iron dosage needs a good understanding of bio-P capacity in such a configuration. Moreover, an additional recovery route for phosphorus recovery is dependent on iron dosage. The struvite recovery route needs a low level of iron whereas the vivianite recovery route would be enhanced by a high iron dosage. Therefore good knowledge and control of biological and physical-chemical processes are really important to adapt the practical dosage to a chosen strategy.

Until now, intermittent aeration has been always controlled for regulating nitrogen removal in priority, whereas biological phosphorus removal was considered to adapt with the complement of chemical dosage to reach a phosphate objective. To achieve low total nitrogen in effluent with reduced energy use, it is essential to adapt the aeration cycles to incoming load and biological activity. In alternated aeration systems, aeration can be controlled with different approaches and sensors. The following methods, with increasing complexity and cost, can be listed: (1) timetables, (2) dissolved oxygen (DO) and oxidoreduction potential (ORP) limits (Charpentier, 1987, Charpentier, 1989), (3) dissolved oxygen and redox potential bending points (Paul *et al*. 1998; de la Vega *et al*. 2012), (4) ammonia and nitrate limits (David and Carpentier, 1984).

Olsson *et al*. (2014) summarized the development and experience of such instrumentation and control strategies. The later nitrogen sensors are based on potentiometric or spectrophotometric techniques which need more maintenance than optical DO probes or platine-based ORP sensors. As a consequence, only methods (1), (2), and (3) are found in small WWTPs (<10000 PE). Bending point detection can be considered a robust method for complete nitrogen removal via nitrification and denitrification. In previous research (Charpentier *et al*., 1998; Paul *et al*. 1998; de la Vega *et al.* 2012) bending points of the ORP and pH curves have been recognized in connection with the nitrification-denitrification cycle. Paul *et al*. (1998) demonstrated the validity of using the bending point of DO to indicate the end of nitrification and the bending point of the ORP curve (“nitrate knee”) to indicate the end of denitrification with different system loads.

In A/O system biological phosphorus removal is carried out by phosphorus accumulating organisms (PAOs). These are facultative anaerobic organisms, which under anaerobic conditions store carbon compounds (as intracellular polyhydroxyalkanoates (PHAs) and glycogen) while releasing phosphorus (energy is generated by the cleavage of intracellular polyphosphates (PP)). During aerobic and anoxic conditions there is a luxury phosphorus uptake, during which the PAO stores PP while depleting their carbon storage pools. Several PAO genera have been identified over the years, some with denitrifying (Kuba *et al*. 1997, Rubio-Rincon *et al*. 2017) and others with fermenting (Marques *et al*., 2017) capabilities. But all the PAOs are not able to denitrify and it is considered that both denitrifying and non-denitrifying PAO coexist in activated sludge. The provided conditions at the facilities can also give an advantage over other species whose storage capacities do not contribute to P removal (eg. GAO for glycogen accumulating organisms).

Conducting studies on livestock wastewater, Osada *et al*. (1991) found that with intermittent aeration, during optimal process control, high nitrate removal creates beneficial (anaerobic) conditions for P release and subsequent uptake, resulting in low effluent concentration. Nonetheless, removal efficiencies decreased with increasing N/BOD_5 ratio, probably due to the residual nitrate concentrations. With adequate aeration control, high removal of organic matter, nitrogen, and phosphorus can be achieved. Liu and Wang (2017) demonstrated the efficiency of intermittent aeration systems (specifically intermittent aeration of MLE) in a pilot scale study, considering total nitrogen and phosphorus removal. They found that alternated aeration showed higher removal efficiency than conventional MLE operation, over 90% of TN and TP were removed under regular conditions. Moreover, under unfavorable conditions (low temperature and low C/N ratio) removal efficiency was still 76% and 56% of TN and TP respectively.

Outside of obvious operational parameters such as the aeration cycles, SRT is also an important parameter for biological P removal. From the early studies in the eighties (Ekama *et al*., 1983; Wentzel, 1986) it came out that biological phosphorus removal deteriorated for SRT higher than 35 days due to saturation of biomass in polyphosphate and endogenous release, while SRT of 20 days was considered as optimal. Lee *et al*. (2007) found that with increasing SRT, the relative abundance of PAO increased as well (up until endogenous decomposition of PAOs occurs) but suggested that GAO may compete with PAO under these conditions, which can negatively impact biological phosphorus removal (BPR) performance. In their scenarios (SRT=10, 20, 30 d) 20 days of SRT proved to be the most advantageous for bio-P removal. The activated sludge systems are generally designed in France with a low loading rate (0.10 kg DBO5 / kg VSS . d) and an SRT of around 20 days.

However, usually designed for 20 years and running under that design load, such systems could have problems with biological P removal if the sludge extraction was not sufficient to maintain a proper SRT.

Simultaneous chemical P removal is a widely used process, typically chemicals are dosed to supplement bioP removal. For the optimization of chemical dose, several operational parameters need to be considered. Szabo *et al*. (2006) defined that during simultaneous iron dosage, the main process of P immobilization is adsorption onto the surface of formed hydrous ferric oxide (HFO) due to less intense mixing and longer HRT (as opposed to pre- and post-precipitation, where intensive mixing causes co-precipitation of phosphorus into the structure. The current practice is to choose the iron dosing rate considering a stoichiometry Fe:P ratio of 1.5 moles of iron per mole of phosphate removed (Deronzier and Choubert, 2004; Metcalf and Eddy, 2003).

For activated sludge using combined biological and chemical removal, the contribution of biology should be estimated theoretically or practically to know the chemical needs. Different methods exist using BOD:P or COD:P ratios and design criteria. However, in practice, biological removal efficiency is highly variable and not systematically well estimated. In the study of Deronzier and Choubert (2004) the efficiency of biological P removal varies from 56 to 89% in 6 different A2O activated sludge plants. A range of efficiency of 60-70% for bio-P removal was proposed for dry weather conditions (Deronzier and Choubert, 2004), falling to 30-50 % for diluted water in case of rainwater or groundwater infiltration. A recommendation was to maintain good denitrification in order to limit the nitrate recirculation in the anaerobic zone which is detrimental to good polyphosphate storage. However aeration intermittency was not considered to give that recommendation while it is expected to affect biological P uptake, and intermittent aeration became the most common system observed in small AS plants in France. Additionally, De Haas *et al*. (2000) studied the interactions between biological and chemical processes in combined P removal. They suggested that anaerobic P release may be used as an indicator of the estimation of the biological fraction of P removal (outside of specific speciation studies). They found that the presence of iron partially inhibited microbial processes, specifically PHA storage, especially under P-limiting conditions.

This study aims to optimize the biological and physical-chemical treatment of phosphorus in A/O activated sludge with intermittent aeration. The case study is a real WWTP with a design capacity of 9500 population equivalents (PE). Online monitoring systems were installed to follow nutrient removal dynamics for more than 3 years. The work was first focused on the interaction between aeration control, nitrogen removal, and biological phosphate release and uptake.

One objective was to save energy (aeration) and chemical dosing with the guarantee of good nutrient removal performance. Then the role of sludge wastage in phosphate dynamics was assessed and finally different specific iron dosage strategies were compared.

2.2. Materials and Methods

2.2.1. Plant description

Villefranche de Lauragais wastewater treatment facility (design capacity: 9500PE) receives primarily domestic wastewater from the municipality, as well as wastewater from Monié Clinic (350 PE) and 3A factory (dairy industry – 500 PE). The facility also regularly receives sludge from household septic tanks. This sludge represents low hydraulic load, but due to the high concentrations, it is fed during low load periods. The wastewater collection is carried out by separated gravity sewer (90 %) with 5 pumping stations. However, significant groundwater infiltration is observed with the surplus hydraulic load as delayed inflow during and after high precipitation periods. The facility is on the catchment area of Mares creek, a sensitive area with low overall ecological status. The treatment technology is designed to reliably fulfill the legal requirements to protect the receiving water with TN imposed at 15 mg/L and TP at 2 mg/L. The prefectural decree N°31-2008-00121 defines effluent limits and sampling obligations of the facility, which is operated by Réseau31.

The pumping station at the entrance of the plant has a maximum capacity of 412 m^3/h and a bypass pump directed to Mares creek. An equalization buffer tank (600 m^3) is available for the temporary storage of excess influent/external load. Mechanical pre-treatments are composed of an automatic screen (6 mm spacings) with a grit and grease removal tank. Grease is treated in a separate aerobic biological tank from which the effluent is directed back to the water treatment line. Dewatered and compacted waste from mechanical treatment is forwarded to a landfill or incineration.

Secondary treatment is carried out by an activated sludge basin including a small contact zone (32 m^3), an unaerated zone (350 m^3), and an aerobic zone with intermittent aeration (2410 m^3). A physical-chemical treatment for phosphorus removal is performed simultaneously by dosing $FeCl_3$ just before the degasser, an unaerated zone to avoid oxygen recirculation to the anaerobic reactor (20 m^3), and the clarifiers. Then the flow is divided equally into two secondary clarifiers (surface area of 120 m^2 each).

Sludge is recirculated at an average flow rate of 1400 m^3/d (1.23* influent flow) and 55% directed to the aeration basin and 45% to the contact zone where influent and mixed liquor return sludge is intensely mixed in an unaerated zone. Sludge wastage was generally performed once or twice a week.

Wasted sludge was subjected to chemical conditioning (polyacrylamide polymer) and then dewatered by centrifuge (up to 20% TSS) most frequently, or by dewatering table/belt filter (up to 5% TSS). There are on-site storage units for sludge: 2 units for soft sludge (300 m^3 each) and a silo for dewatered sludge (1000 m^3). The dewatered sludge is then either composted or spread directly on agricultural fields. Sludge liquor is directed back to the entering flow before the activated sludge basin.

The activated sludge process actually receives about 50% of the design load. Therefore, operational characteristics correspond to a very low-loaded system: OLR=0.05 KgCOD/KgVSS.d, HRT= 48 h, SRT=40-50 days.

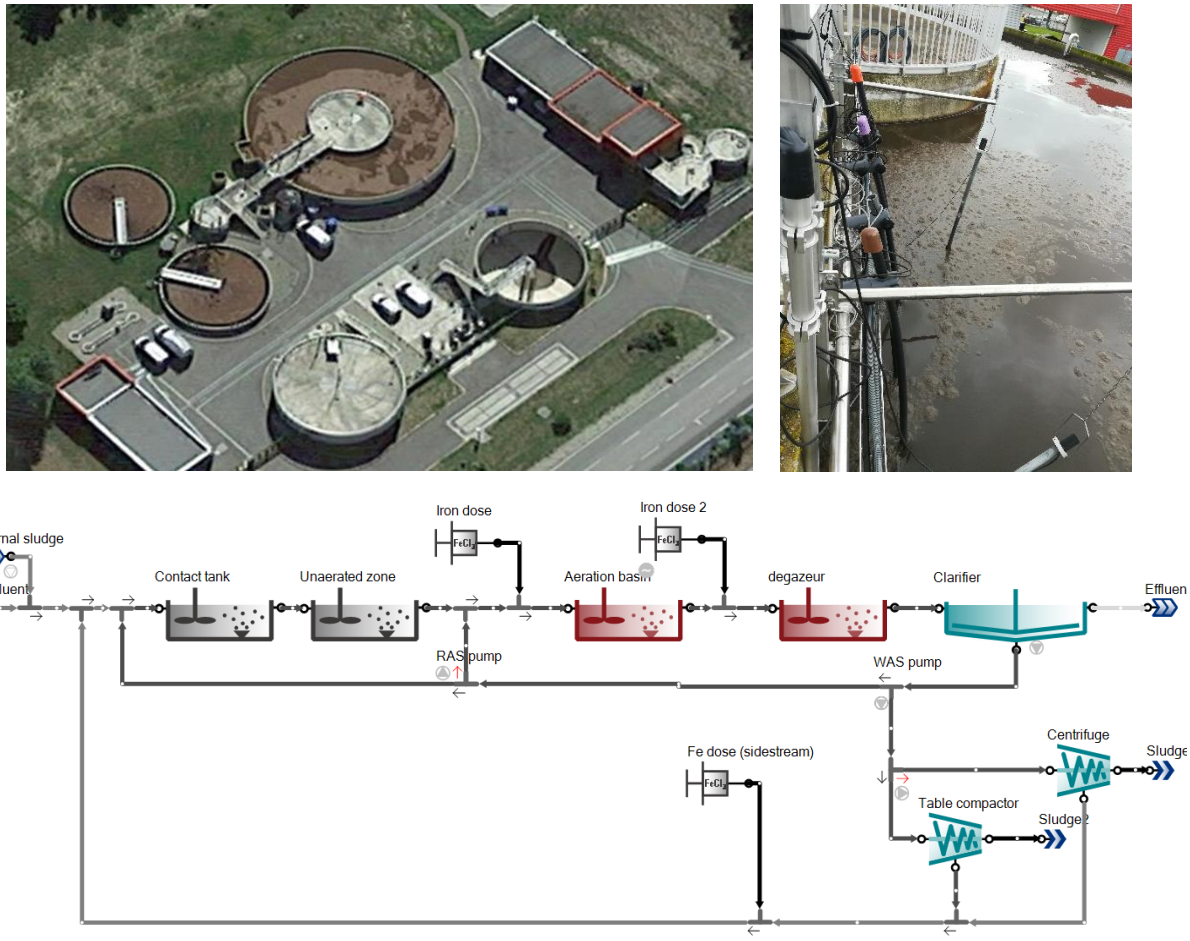

Figure 2.2-1 Picture (site and sensors) and Flow scheme of Villefranche de Lauragais wastewater treatment plant with potential iron dosage points

2.2.2. Aeration control

In the current operation, the aeration was controlled via bending points detection (*inflex* system developed by INSA and licensed by Biotrade) for complete nitrogen removal via nitrification and denitrification. The bending point of the oxygen concentration indicates the end of nitrification and similarly, the bending point of ORP indicates the end of denitrification (observed as “nitrate knee” on the displayed ORP).

To achieve low effluent of total nitrogen with reduced energy use, the aeration cycles are adapted to biological activity and variation of influent loading rate therefore the cycle length may vary according to the conditions. *Inflex* control system is based on the real-time data of the DO and ORP sensors. Figure 2.2-2 shows DO and ORP curves corresponding with ammonia and nitrate concentrations. In case of an overload in the system, the maximum time for aerobic and anoxic phases was determined as 60 and 90 minutes respectively.

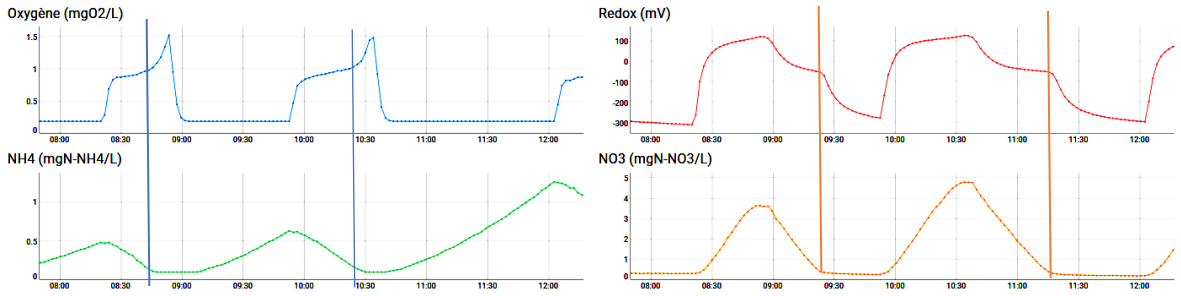

Figure 2.2-2. Typical cycles (DO, ORP, NH4, NO3) with various phase lengths (aerated and unaerated), and associated DO and ORP bending point corresponding to NH4 or NO3 removal indicators (downloaded form: myinflex.com)

To avoid measurement insecurities and noise in the data and simplify operations, the cycles have been redefined (in 2019), from the initial DO/ORP system to a simpler DO – time-based one. In this system, as before, the end of nitrification is indicated by the bending point in the DO curve and simultaneously a maximum aeration time is set. In case of a high load, if after this maximum aeration time the bending point is not detectable then the following anoxic time is shortened.

The cycles were, therefore: 1) aerated period until DO bending point, but minimum 15 min and maximum 60 min, 2) unaerated period, minimum 60 and maximum 90 min depending on the aerated phase. In case the aerated period is less than the maximum time (meaning the nitrification is completed), the unaerated time is shorter, if the aeration time is maximum (meaning incomplete nitrification) the unaerated time is also maximum.

This gives on average systematic aerated/unaerated periods and ensures effluent quality, but easier to manage and avoids problems connected to possible faulty data.

2.2.3. Data monitoring

The utility is required to carry out official monitoring with composite samples of 24 hours including influent and effluent and sludge production (Table 2.2.1). This gives a general overview of the performance of the facility. During the study, this legal analysis was complemented with monthly measurements and online monitoring.

During the entire study, from September 2018 to September 2021, sensors were installed and used for continuous monitoring of nitrogen forms, phosphate, and suspended solids in the activated sludge system (aerated basin). The following systems were used: ammonia and nitrate (Multi parameter SC1000, Hach Lange), phosphates (Phosphax sc, Hach Lange, with filtration system Filtrax), suspended solids (Solitax TS-line sc 'TSS', Hach Lange). These sensors were verified once a week and recalibrated if needed. All the sensor data were collected online on a web platform designed by Biotrade (*My Inflex*).

Hydraulic-related data were registered continuously (influent and recycled flows), sludge wastage, and chemicals flow rate. In this study, operational data is presented to demonstrate the correlation between aeration efficiency (specifically aeration time) and MLSS concentration.

Table 2.2-1 Data monitoring during the 3-year study

Parameter	Mandatory frequency by utility, 24h average samples, Inlet – outlet (days/year)	Campaign frequency 24h average samples Inlet – outlet (days/year)	Daily profile inlet (laboratory)	Continuous monitoring in aeration tank (2 min^{-1})
Flow	365	365	3 campaigns	*
TSS	12	12	3 campaigns	*
BOD5	12	12		
COD	12	12	3 campaigns	
TKN	4	6-12	3 campaigns	
NH4-N	4	6-12	3 campaigns	*
NO2-N	4	4		
NO3-N	4	6-12		*
TP	4	6-12	3 campaigns	
PO4-P		6-12	3 campaigns	*
Sludge (Dry matter and flow)	4	4		

2.2.4. Influent characterization

In addition, specific campaigns were performed on three separate occasions to obtain daily hourly variation in the influent characteristics (it was not raining the day prior to the sampling to avoid diluting effect). The following parameters were measured in the influent hourly samples according to Standard Methods (APHA, 1992): Total chemical oxygen demand (TCOD) soluble chemical oxygen demand (SCOD) Total Kjeldahl nitrogen (TKN), Total suspended solids (TSS), Total phosphorus (TP), orthophosphate (SPO4), ammonia (SNHx) nitrite (SNO2) and nitrate (SNO3). These parameters give an insight into the general composition of the influent and represent the daily variation. Moreover, seasonal variation also needs to be considered as significant infiltration is observed during rainy periods (typically during the winter), which dilute the influent and impact the performance.

2.2.5. Phosphorus release and uptake tests

As the configuration of the facility fosters biological phosphorus removal, P release and uptake tests were performed to evaluate the biological contribution to the overall P removal. One set of experiments was designed to evaluate the anaerobic phosphate release, as well as aerobic and anoxic phosphate uptake (to estimate the impact of denitrifying PAOs) with the following schedule illustrated on Figure 2.2-3. During these tests, SCOD and SPO4 concentrations were analyzed.

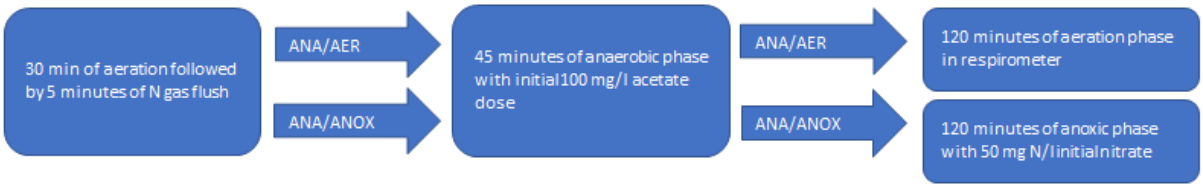

Figure 2.2-3 P release and uptake test schedule

Similarly, additional P release tests were carried out, with the same initial acetate addition but a longer period of anaerobic time (180 min) in order to estimate the maximum releasable phosphate. These experiments were performed only under anaerobic conditions. In preparation of the sample, 30 min of aerated time was provided in order to stimulate PP storage to avoid the interference of possible release during storage. The aeration phase, prior to the anaerobic phase is followed by a nitrogen gas flush to strip out oxygen and ensure that the initial kinetics are admissible.

2.2.6. Description of iron dosage

The phosphorus removal at the facility is carried out by combined biological and physical-chemical methods. In general operation, $FeCl_3$ (Kemira PIX 511, 40%, d=1,4) is dosed in the aerated basin. The supplementary iron dose was calculated based on the previous year's data from the facility and the schedule was determined as seen in Table 2.2-2. As the configuration of the plant is suitable for bio-P and the iron dose does not create P-limiting conditions, it was assumed that PAO activity also takes place at the facility. In order to estimate the potential for bio-P removal, the iron dosage was stopped during two dedicated periods.

The different dosage strategies have been named *Iron dose A* for regular dose, with 13.5 l/d, *Iron dose B*, with a higher dose, 33.3 l/d (corresponding to the calculated dose considering 50% of biological P removal), and *Iron dose C* when the dose was specifically adjusted to the recycled flow, 4.5 l/d on average. In that last case, the side-stream dose was calculated based on the measured recycled phosphate concentration and assumed a 1.5 Fe:P molar ratio for removal.

Table 2.2-2 $FeCl_3$ dose during different periods of the study

Start	Stop	$FeCl_3$ (l/d)	Dosage strategy
28/01/2018	25/08/2018	13.5	A
26/08/2018	30/10/2018	0	
31/10/2018	13/06/2019	13.5	A
14/06/2019	28/08/2019	0	
29/08/2019	11/02/2021	13.5	A
20/06/2020	08/12/2020	33.3	B
09/12/2020	10/02/2021	17.5	C
10/02/2021	16/05/2021	0	
17/05/2021	Present	4.5*	

* Dosed directly on sludge liquor

2.3. Results and discussion

2.3.1. Influent characteristics

The average characteristics of the influent wastewater measured by the facility are given in Table 2.3-1. The daily pattern, measured during the measurement campaign is given in supplementary material, Figure S2. 1. This pattern is fairly typical for a municipal treatment facility of this size, with distinct morning and afternoon peak loads.

Calculating typical ratios of the influent concentrations can help to gain insight into potential challenges in the system (eg. sufficient available carbon for nutrient removal). Rieger *et al*. (2012) provided typical ratios observed in various facilities, and it is clear that Villefranche de Lauragais wastewater aligns with other municipal sewage on average (Table 2.3-1).

Table 2.3-1 Villefranche raw influent concentration ratios compared to typical ratios from Rieger et al. (2012)

Ratio	Villefranche mean	Reference (GMP) mean	Min	Max
TN/TCOD	**0,1098**	0,095	0,05	0,15
SNHx/TKN	**0,5746**	0,684	0,5	0,9
TP/TCOD	**0,0110**	0,016	0,007	0,025
SPO4/TP	**0,6604**	0,6	0,39	0,8
SCOD/TCOD	**0,2164**	0,343	0,12	0,75
TSS/TCOD	**0,3729**	0,503	0,35	0,7
VSS/TSS	**0,7054**	0,74	0,3	0,9

An important parameter for biological P removal is SCOD/TCOD which indicates the available readily biodegradable substrate for nutrient removal, the values of the facility are within the range but on the lower side. The observed variation (Figure 2.3-1) indicates an even lower availability during the daily peak load. It is clear that during the night (low load) hours, the fraction of soluble COD increases due to lower TSS, whereas, by the morning peak hours, the TP to SCOD ratio increases.

Seasonal variations are also important to consider. The influent monitoring during the three years clearly showed that significant dilution was observed in winter months due to rain events and significant underground water infiltration.

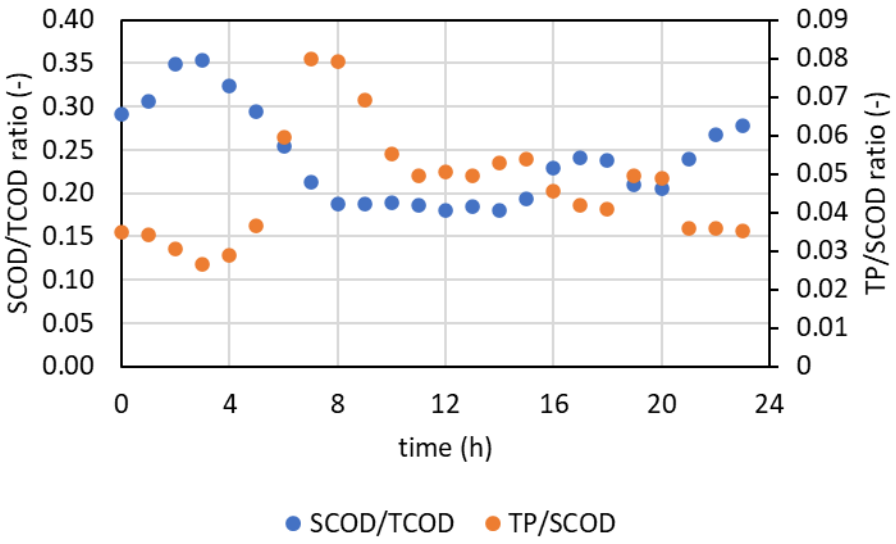

Figure 2.3-1 daily pattern of soluble COD to total COD, and total phosphorus to soluble COD ratio in Villefranche de Lauragais wastewater

2.3.2. Plant load and overview of overall nutrient removal

Figure 2.2-2 shows a typical pattern for daily variation and the concentration changes within cycles. It is visible that during high load periods (typically in the afternoons) the aeration phase is longer, and the limited DO indicates incomplete nitrification (corresponds to the higher measured ammonia concentration). Even during these periods, nitrogen removal is highly efficient, with a removal rate of 96% during the four years of the project.

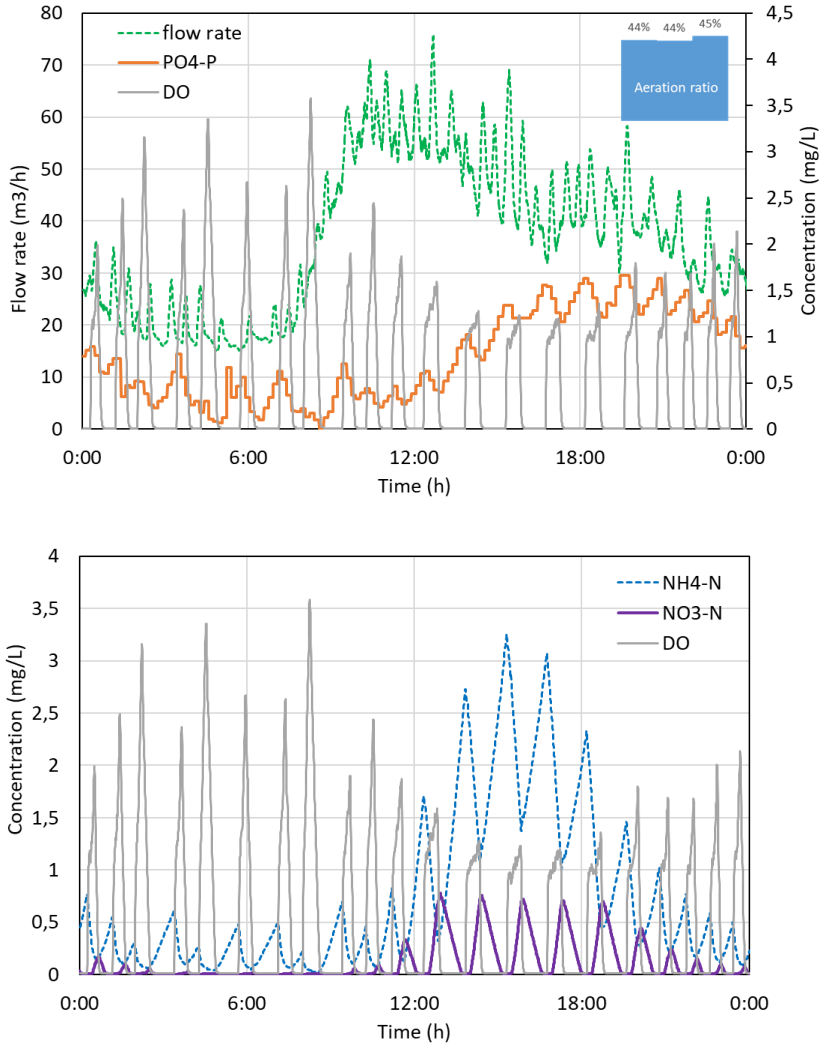

Figure 2.3-2 Typical daily variation and cycles in the aeration tank (01/12/2018, iron dose A). Aeration time ratios are indicated for three periods: 0-8h, 8h-20h, and 20h-24h.

Figure 2.3-3 shows N and P removal rates as a function of influent loading rates. With proper operation, the total nitrogen removal at the facility was impeccable (96% on average) and performs beyond the legal requirements. It can be observed that the configuration and the aeration strategy are robust, and changes in other parameters (e.g. MLSS concentration) do not seem to interfere with nitrogen removal efficiency. Regarding the total phosphorus removal, the average effluent concentration was 1.12 mg P/l during the entire period of observation (2018-2020) which corresponds to an average removal efficiency of 78.9%, and a variation from 45% to 95%.

Major variations were observed during the period of dilution by infiltrated water in winter during which the retention time was lowered and the influent concentration lesser (Figure 2.3-4). During such dilution periods the outlet concentration was generally below the rejection limit (2 mgP/L) but the removal efficiency decreased.

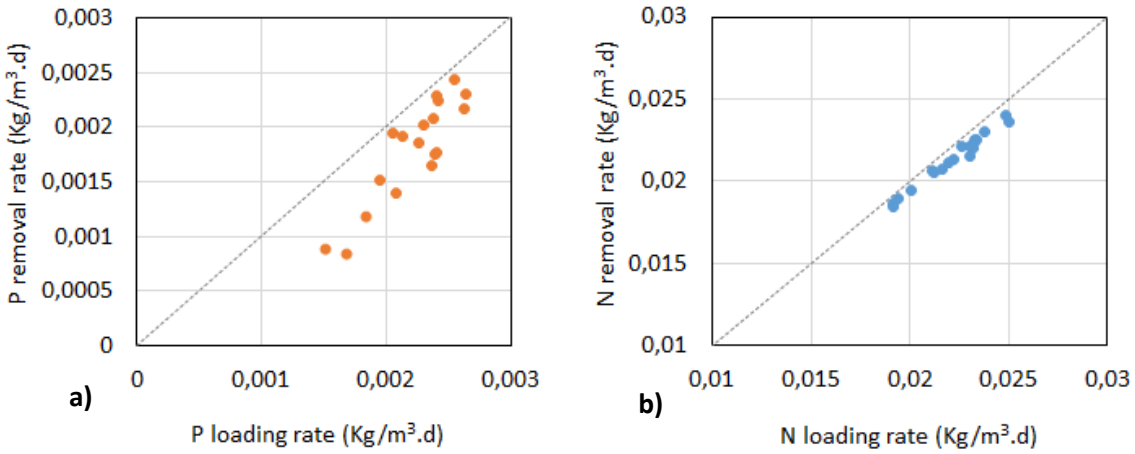

Figure 2.3-3 a) Phosphorus and b) nitrogen removal efficiency as a function of loading rate

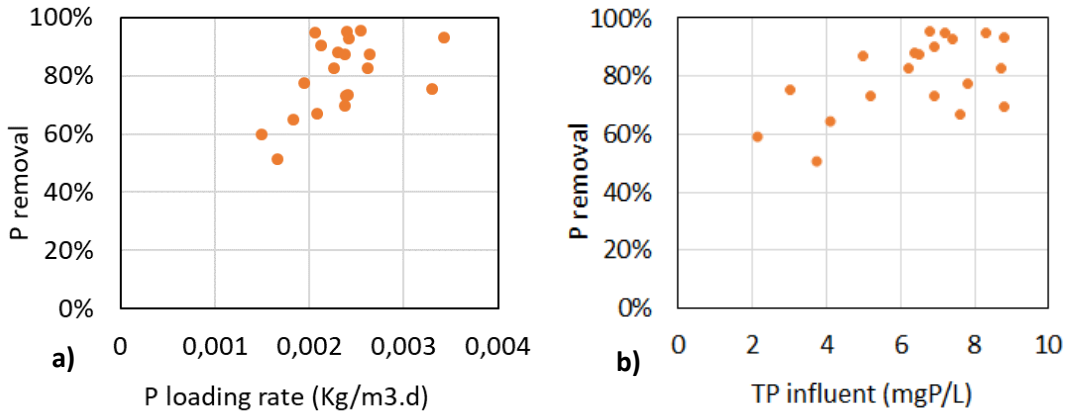

Figure 2.3-4 Phosphate removal as a function of a) P loading rate and b) influent TP concentration (2019-2021)

As shown on Figure 2.3-5 phosphate concentration in the effluent was linearly correlated to total phosphorus, the phosphate concentration representing 90% of the TP in the treated effluent. This supports the fact that the online monitoring of phosphate is a good indicator of P removal performance.

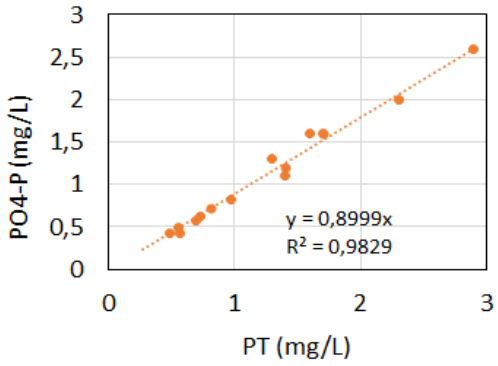

Figure 2.3-5 Phosphate versus total phosphorus concentration in the effluent (2019-2021)

2.3.3. Biological P removal dynamics during intermittent aeration

The Villefranche WRRF is a highly dynamic system regarding operations with daily variations typical to small treatment plants and seasonal variations that are markedly impacted by precipitation in the catchment area.

Figure 2.3-6 presents the daily pattern of nutrients in two different periods without iron dose. As the aeration is aligned with the nitrogen removal, it can be observed that the longer aerated phase systematically occurs during high load times and the shorter aerated (longer unaerated) phase during low load periods (e.g. night). The aeration time ratio is calculated for three periods of the day: 0-8 h (low load), 8-20 h (morning peak and midday idle time) 20-24 h (evening peak and night idle). This aeration time ratio depends on controller set-up (*inflex*) and was fixed at different levels during the study. The aeration time ratio was initially high (44%) and relatively similar during night and day (Figure 2.2-2). Then the aeration control was adapted, leading to lower aeration time in a low load period (night), as in the example presented in Figure 2.3-6 (a, b), with an average aeration time ratio of 34%. Finally, a more homogeneous aeration ratio was reached (Figure 2.3-6 (c, d)), with an average ratio of 36-39% leading to the best performance for biological P removal (average daily phosphate concentration around 1 mgP/L).

As the aeration cycles are adapted for optimal nitrogen removal (*Inflex* aeration control system), the cycle length may change according to the influent ammonia load. The phosphate variation within the cycles corresponds to the aeration cycles too: decreasing during the aerobic period and increasing during the non-aerated period.

During high load periods, the extended aeration and shorter unaerated periods can result in incomplete denitrification, which means that during the entire cycle, P removal (with either oxygen or nitrate as an electron acceptor) is carried out. In contrast, for extended unaerated times, anaerobic conditions may occur with the complete depletion of nitrate and therefore P uptake is ceased and even P release may occur. This type of P release during unaerated periods is not confirmed, but just the depletion of electron acceptors can cause the observed higher amplitudes within cycles.

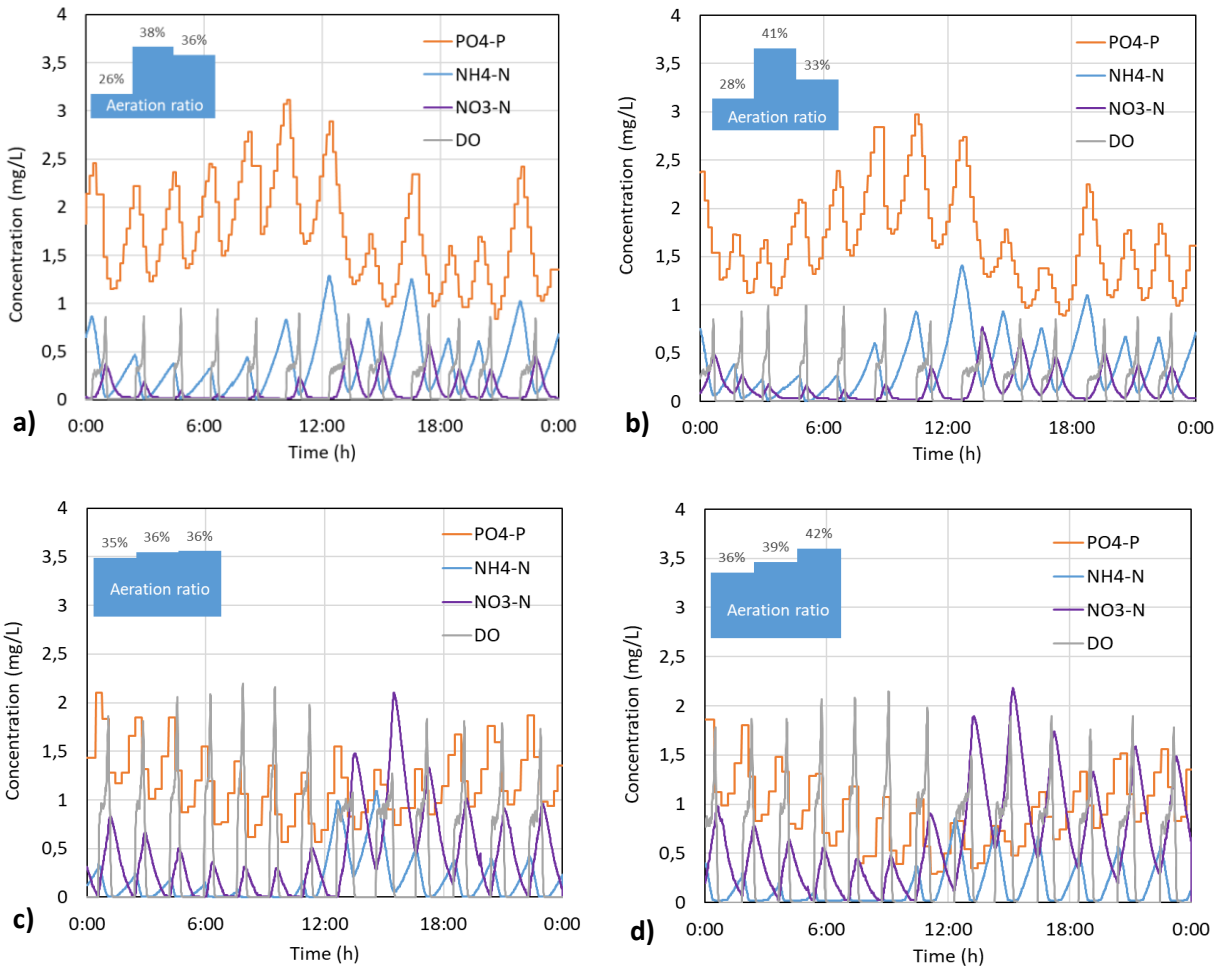

Figure 2.3-6 Two periods with zero iron dosage. (a) 24/07/2019 $P_{average}$ = 1.74 mg P/l (b) 25/07/2021 $P_{average}$ = 1.61mg P/l. (c) 04/04/2021 $P_{average}$ = 1.16 mg P/l (d) 06/04/2021 $P_{average}$ = 0.92 mg P/l. The aeration time ratio is given for 0-8h, 8-20h, 20-24h.

From earlier monitoring (04-07 June 2019 and 04-08 August 2019) P release was measured between 10-15 mg P/l in the anaerobic reactor, indicating P release due to PP cleavage by PAOs.

Moreover, rapid P uptake after aeration disturbance (and therefore extended anaerobic time which resulted in higher P concentration) also confirms significant biological contribution in the P removal.

Laboratory P release and uptake tests were performed to estimate independently the PAO activity at the facility. The phosphate release and uptake measured in specific batch tests are summarized in Figure 2.3-7. The average release rate was around 19,2 ± 4,5 mg P/L.h, while the anoxic uptake rate was 4,6 ± 0,9 mg P/L.h and the aerobic uptake rate was 7,55 ± 0,9 mg P/L.h. These kinetics were actually better described by a first-order kinetic (k = 1,33 h^{-1}; 0,194 h^{-1}; 0,509 h^{-1} respectively for release, anoxic and aerobic uptake rate). Overall laboratory batch tests confirmed that denitrifying PAOs are present in the sludge of Villefranche de Lauragais, but they also confirmed that the P uptake rate is lower in anoxic than in aerobic conditions. It is due either to the fact that only a fraction of PAO are able to denitrify or their uptake rate is lower than aerobic ones. Basically, these uptake rates are controlled by internal carbon stored in previous anaerobic periods which is consumed while recovering internal polyphosphate stock.

During the anaerobic batch test around 22 mgPO_4-P/L was released, whereas around 50 mgCOD/L (as acetate) was consumed. In the anaerobic tank, the release of phosphate was generally lower than 15 mgPO4-P/L. Measurements were performed during three periods in the anaerobic tank and the phosphate concentration was varying in the range from 10 to 15 mgPO_4-P/L. In the activated sludge the release is based on the usage of easily biodegradable carbon coming from influent which is made of fermentation products (like acetate) but also substrates that need to be fermented in the anaerobic tank. The fermentation rate is slower than the acetate uptake rate by PAO, this explains why the release rate is lower in the tank than in the batch test performed without acetate limitation.

In the activated sludge basin, the anoxic increase rates (0,75 ± 0,16 mg P/L.h) and aerobic decrease rates (0,85 ± 0,12 mg P/L.h) observed were much lower than the batch test rates. It is important to clarify that actual variation rates in the tank are related to entering the flow and are not directly comparable to the outline tests. The apparent P release (named here *increase rate*) during the unaerated period is due to the continuous influent and a lowered uptake rate in anoxic conditions, also possibly the release of polyphosphate with the depletion of nitrate. Aerobic P uptake rates (called here decrease rates) are linked to the reabsorption of phosphate as polyphosphate by the same microorganisms but at a low rate because their internal carbon storage has been highly reduced due to long retention time. Moreover, the rates are observed here for a low range of concentration (0,1-2 mgP/L) much lower than in batch tests, and rates become limited by phosphate concentration.

Finally, tests confirmed that the anoxic condition is not optimal for phosphate capture as the PO4 uptake rate is 39% lower than in aerobic conditions. Too long unaerated time is detrimental not only because of lower phosphate uptake rate but also because of the risk of anaerobic P release. Fortunately, the anaerobic release in the principal basin during the unaerated period is not that high (compared to pre anaerobic zone) because the available external carbon substrate is low and fermentation is a slow process.

As a consequence aeration control strategy should take this phenomenon into account. To maintain the biological phosphorus removal at a higher level, the unaerated time should not be maintained too longer after nitrate depletion. Finally regarding the energy saving the results confirmed that a different parametrization of the *inflex* automate during high load (day) and low load (night) periods is a good method but should include specific constraints to avoid a detrimental effect on phosphate concentration.

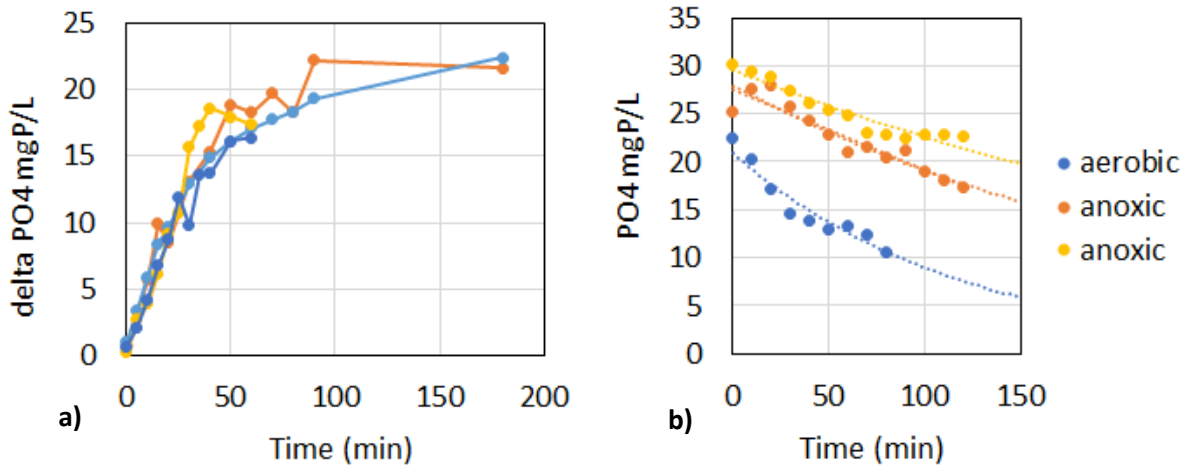

Figure 2.3-7 Batch tests (a) anaerobic for phosphate release (Sept 2019, June 2020) ; (b) anoxic and aerobic for phosphate uptake after anaerobic release (Sept 2019). Dot lines for the first-order model.

2.3.4. Relation between sludge management and P removal

Sludge extraction is a manual operation in such a relatively small treatment plant and depends on human constraints. Sludge dewatering processes are operated with the presence of the operator for a sequence of 8 hours a day generally, one or two days per week. Several observations can be pointed out regarding the correlation between sludge management and phosphorus removal during the 3 years of observation.

First, it appears that phosphate removal was generally better for periods with a regular wastage and relatively low MLSS range (3,5-4,5 g/L) compared to periods with no wastage and progressive sludge accumulation in the basin (up to 6-7 g/L). Indeed the average phosphate concentration in the aerated basin (and effluent) was observed to progressively increase as MLSS accumulated. This is relatively in line with theoretical knowledge regarding bioP processes, as too long sludge retention is known to be detrimental for bioP in alternated aeration facilities (Lee *et al.*, 2007). A good biological P removal is based on the extraction of biomass with a high phosphorus content as polyphosphate. The sludge of Villefranche-de-Lauragais WRRF has an average total P content of 32.3 g P/Kg VSS for normal operation.

In the intermittent aeration system with automatic adaptation of aeration time, the variation of MLSS in the basin also affects aeration. Indeed a clear correlation was observed between MLSS and daily aerated time (Figure 2.3-8) because the system automatically adapts by extending aeration during sludge accumulation. This was due to the decrease of DO resulting from an increase of endogenous oxygen demand and reduction of oxygen transfer coefficient at a high MLSS level, which naturally decreased the nitrification rate. The effect on phosphate removal is difficult to predict: on one hand increasing aerated periods is beneficial, but on the other hand, the reduction of DO can limit the P uptake, and lower denitrification could be detrimental to biological phosphorus removal. Hence multiple effects can be observed when the system is operated with too low sludge retention and it is highly recommended to perform a regular sludge wastage to efficiently maintain the biological P removal.

In terms of energy, it is clear that maintaining MLSS concentration to a lower level allows for reducing aeration time and saving energy (Figure 2.3-8, b). Maintaining the concentration around 4 gSS/L was thus recommended, as 40% more aeration energy is needed for a concentration around 6g/L. At the same MLSS level, it is important to point out that aeration time and associated energy vary from 450 to 600 kWh per day, depending on the aeration control parametrization and the resulting aeration time ratio (28% to 40%).

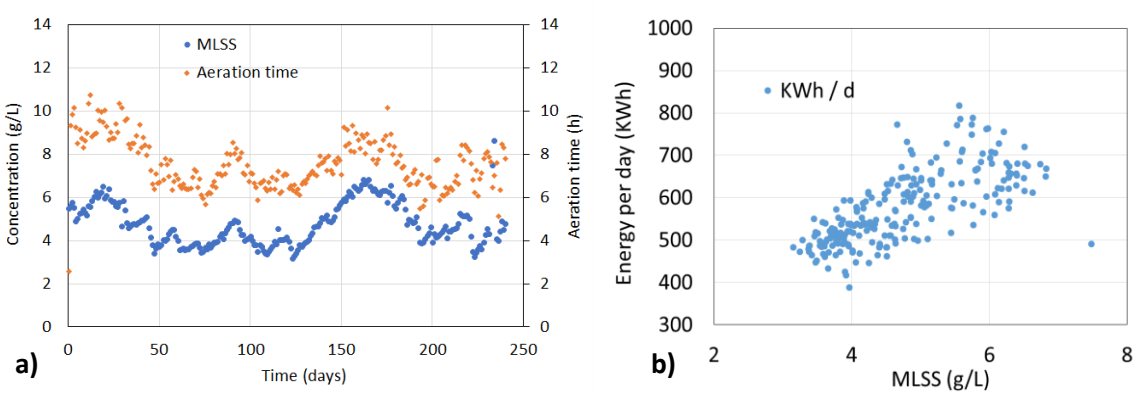

Figure 2.3-8 a) Correlation between MLSS concentration (g/L) and cumulated aeration time per day (h/days) in 2019 and b) related energy demand for aeration

The last observation is that phosphate peaks (from 1 to 3 mgP/L) were systematically observed for several days after each wastage and sludge dewatering sequence (Figure 2.3-8). After measurements were performed in the liquor from the centrifuge (12-15 mg P-PO_4/L), it was deduced that phosphate release occurred during sludge dewatering provoking some return P load into the activated sludge basin. This can be related to both phosphate desorption from HFO (hydrous ferric oxides) or polyphosphate cleavage. This observation was really unexpected as the sludge retention time in the side stream dewatering process is short, and phosphate release is generally associated with long anaerobic conditions.

Considering the stability of phosphate capture in both chemical and biological pathways, the question regarding the iron reduction in anaerobic conditions and secondary P release (ex: in clarifier sludge bed) could be important to consider.

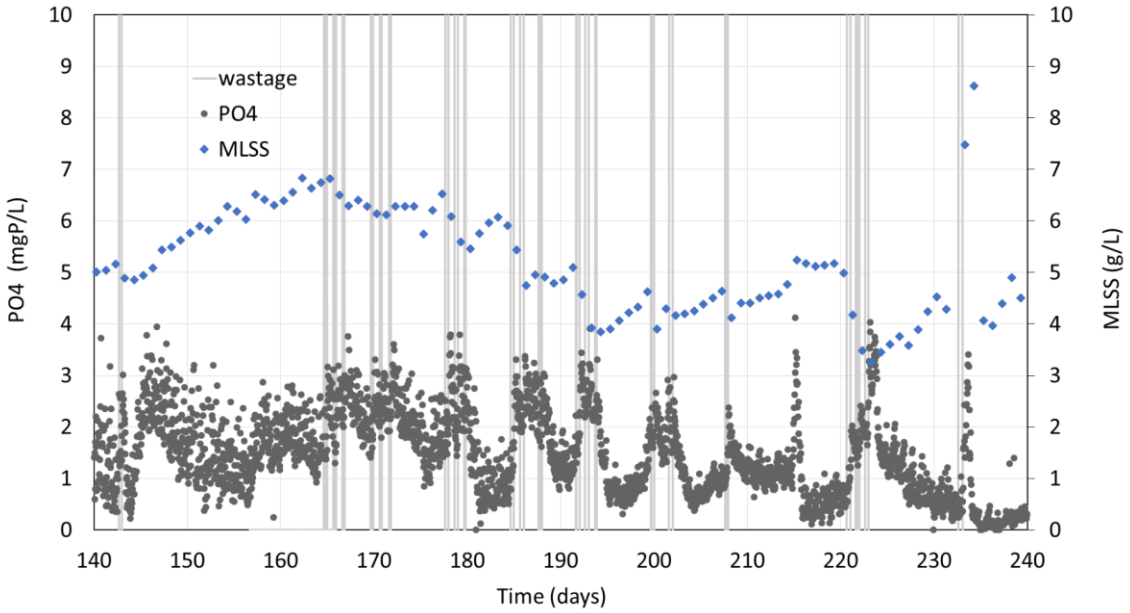

Figure 2.3-9 Effect of sludge wastage and centrifuge (grey lines) on PO4 (mgP/L) and MLSS concentration (g TSS/l)

2.3.5. Toward an optimal Fe dose

The 24h average phosphate concentration measured in the aerated tank for different iron dosage strategies is presented on Figure 2.3-10 (a legal requirement of 2 mg P/l yearly average is indicated with a blue line on the figure) and Table 2.3-2.

For pure biological treatment, the system was allowed to reach an average of 1,96 and 1,61 mgPO_4-P/L respectively during the two periods 2019 and 2021. During the first period, 50.7% of the analysis showed phosphate analysis higher than 2 mgP/L, whereas only 20,2% were above that limit is 2021 indicating that the rejection limit could be respected for 80% of the time. As explained before, this can be attributed to some improvements in the aeration control system to avoid too long anoxic time.

During the period 2019-2021, different $FeCl_3$ dosages were compared. It came that a Fe:P ratio of 0.22 mol Fe/mol P_{load} (dose A) allowed it to reach an average concentration of 1.08 mg P/L, and only 3.4% of the measurements were higher than 2 mg P/L. With a Fe:P ratio of 0.55 mol Fe/mol P_{load} (dose B) the concentration was 0.49 mgP/L on average whereas only 8.2% is higher than 1 mg P/L.

Finally, a specific dosage method was set up to remove only the phosphate released by sludge dewatering by direct addition of the ferric chloride to the sludge liquor.

This dosage (2 L/h during 8 hours of wastage) corresponds on average to the ratio Fe:P of 0.076 considering the P loading rate received by the plant. This strategy allowed us to reach average performances comparable to dose A. It means that significant chemicals saving could be obtained by dosing directly and specifically the iron in the sidestream liquor.

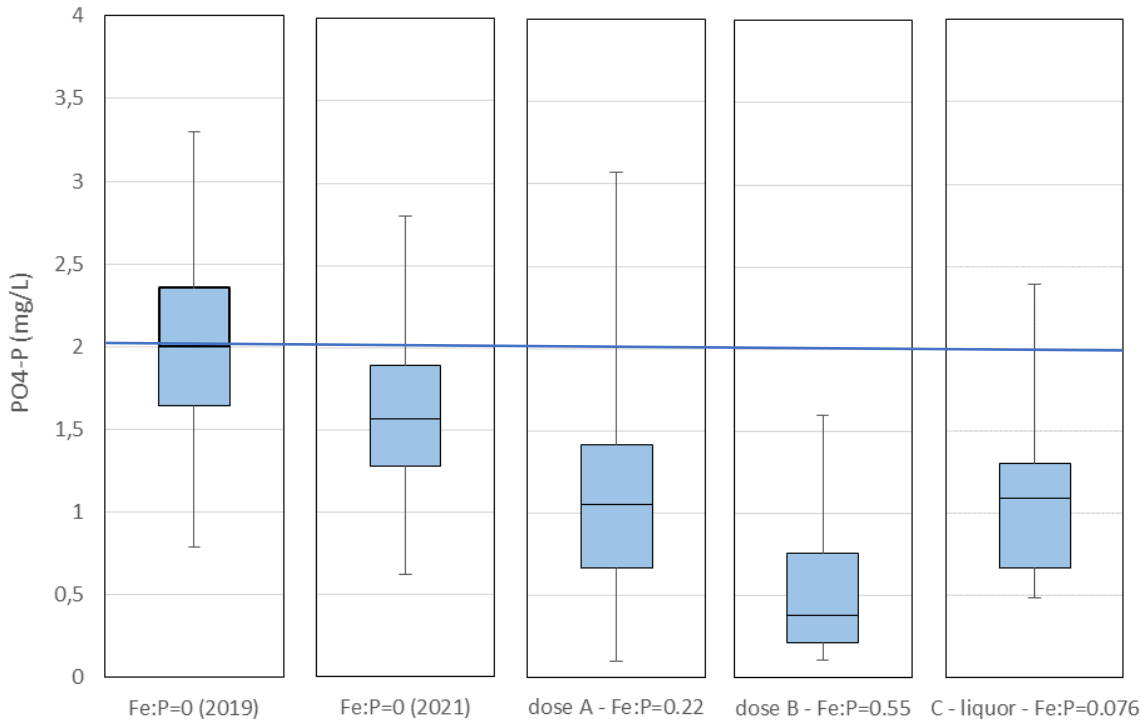

Figure 2.3-10 Phosphate levels for different periods with various iron dosages. Pure biological treatment (Fe: P=0) during two periods in 2019 and 2021; dosage in the biological reactor at two dosage levels (A, B); the dosage on sludge liquor only (C).

Table 2.3-2 Summary of phosphate concentration (based on a daily average, i.e. 24h average measurement in the aerated basin) for different periods with various iron dosages.

	Fe=0	Fe=0	Fe dose A	Fe dose B	Fe dose C liquor
Period (nb data - days)	2019 (71)	2021 (84)	2020 (147)	2020 (98)	2021 (28)
Fe:P (mol Fe/mol P_{load})	0	0	0,223	0,550	0,076
Average Concentration (mgP/L)	1,960	1,607	1,081	0,494	1,035
Standard Deviation	0,583	0,490	0,531	0,351	0,446
NB(%) >2 mg PO4-P/L	50,7%	20,2%	3,4%	0,0%	3,6%
NB(%) >1 mg PO4-P/L	93,0%	89,3%	52,4%	8,2%	53,6%

Based on the iron dose and overall removed phosphorus, the biological and physical-chemical fraction of P removal was estimated for different iron dose strategies. Whereas the removal efficiency for pure biological treatment was 65% and 71% respectively in the 2019 and 2021 campaigns, the overall efficiency increased to 80,7% and 91,3% with iron dosage respectively with dose A and dose B.

Considering the contribution of chemical removal and assuming that the biological processes were similar in presence of iron, the chemical removal of phosphorus followed a stoichiometry ranging from 1.7 to 2.3 mol Fe/mol P removed respectively for dose A and dose B. This is higher than the Fe/P ratio (1.5) which is normally applied to calculate iron dosing. Such observation can be explained either by a lower efficiency of chemical capture at low phosphate concentration or a possible detrimental effect of iron on biological phosphorus removal. Indeed Smith *et al*. (2008) and Szabo *et al*. (2008) demonstrated that the Fe/P ratio depends on the desired residual P concentration. The stoichiometry increases at low phosphate concentration which means that the iron needs are higher.

The newly implemented side-stream Fe dose was shown to fulfill effluent requirements during the experimental period. This new strategy needs to be validated on longer term. Iron is directly dosed to the return sludge liquor to mitigate the interference of the additional load that was observed before. It was estimated to reduce 65% of the dosed iron compared to the same period of the previous year (with dose A).

2.4. Conclusions

In this study, biological and physical-chemical phosphorus removal in intermittently aerated activated sludge was deeply investigated with a monitoring campaign for three years.

Results revealed that biological removal based on excess accumulation (PAO activity) contributes very significantly to the performance in the system but that performance was depending on aeration pattern (aeration time ratio) and sludge wastage management.

It was observed that the anoxic P uptake rate was significantly lower than the aerobic one and that anaerobic periods provoke phosphate release in the intermittently aerated tank.

As a consequence, a sufficient minimal aeration time ratio is necessary to maintain good biological phosphate removal in the system. After considering this observation a proper parametrization of the aeration controller was used (based on bending point detection and two load periods within the day) and biological P removal reached 71%, leading to a phosphate concentration of 1.61±0.49 mg P/L.

Finally, as the effluent target is 2 mg P/l in such a facility, the pure biological can fulfill this requirement on average, as soon as aeration intermittency and MLSS are both controlled adequately. However, on a daily average, this result is guaranteed only 80% of the time. Therefore, the complementary iron dosage help to fulfill the requirement with perfect reliability.

Thanks to proper aeration control for both biological phosphorus and nitrogen removal, a very low dose of chemicals was sufficient to reach the requirements. The dose was more than 50% lower than the theoretical dose recommended by the initial design method. Even more chemical saving was obtained by dosing the ferric chloride on the sludge liquor produced during the dewatering process.

The global ecological optimization of such a system should consider energy needs, chemical dosing, and direct and indirect emissions. This study allowed us to find threshold limits and recommendations for such global eco-design. It reveals that regular sludge wastage for good control of MLSS concentration, accurate process assessment by dissolved oxygen and ORP sensors for aeration control, as well as optimization of ion dosing point and quantity are all important to make such important progress in minimizing economic and environmental costs.

2.5. Acknowledgment

This work was supported by the European project Interreg SUDOE, named CIRCRURAL4.0 (2018-2021). The authors would like to thank the team of Reseau31 utility for their contribution to the monitoring campaigns.

2.6. References

APHA (1992). Standard Methods for the examination of water and wastewater *18th Edition. American Public Health Association, Washington D.C.*

Bisinella de Faria, A., Ahamadi, A., Tiruta-Barna, L., Spérandio, M. (2016). Feasibility of rigorous multi-objective optimization of wastewater management and treatment plants. Chemical Engineering Research and Design, Volume 115, 394-406.

Charpentier, J., Florentz, M., & David, G. (1987). Oxidation-reduction potential (ORP) regulation: a way to optimize pollution removal and energy savings in the low load activated sludge process. *Water Science and Technology*, *19*(3-4), 645-655.

Charpentier, J., Godart, H., Martin, G., & Mogno, Y. (1988). Oxidation-reduction potential (ORP) regulation as a way to optimize aeration and C, N and P removal: experimental basis and various full-scale examples. In *Water Pollution Research and Control Brighton* (pp. 1209-1223). Pergamon.

Charpentier, J., Martin, G., Wacheux, H., & Gilles, P. (1998). ORP regulation and activated sludge: 15 years of experience. *Water science and technology*, *38*(3), 197-208.

Christoforidou, P., Bariamis, G., Iosifidou, M., Nikolaidou, E., & Samaras, P. (2020). Energy benchmarking and optimization of wastewater treatment plants in Greece. *Environmental Sciences Proceedings*, *2*(1), 36.

Coats, E. R., Watkins, D. L., & Kranenburg, D. (2011). A Comparative Environmental Life-Cycle Analysis for Removing Phosphorus from Wastewater: Biological versus Physical/Chemical Processes. *Water Environment Research*, *83*(8), 750-760.

David, G., & Charpentier, J. (1984). Un graphique pour l'utilisation optimale de l'énergie en liaison avec l'élimination de la pollution carbonée et azotée. *Techniques et sciences municipales (1971)*, (2), 63-72.

de Haas, DW, Wentzel, MC & Ekama, G. A. (2000). The use of simultaneous chemical precipitation in modified activated sludge systems exhibiting biological excess phosphate removal Part 4: Experimental periods using ferric chloride. *Water Sa*, *26*(4), 485-504.

de la Vega, P. M., de Salazar, E. M., Jaramillo, M. A., & Cros, J. (2012). New contributions to the ORP & DO time profile characterization to improve biological nutrient removal. *Bioresource technology*, *114*, 160-167.

Deronzier, Gaëlle, Choubert, Jean-Marc. 2004. Traitement du phosphore dans les petites stations d'épuration à boues activées. Cemagref, Document Technique FNDAE, n° 29.

Ekama, G. A., Siebritz, I. P., Marais, G. v. R., 1983, Considerations in the process design of nutrient removal activated sludge processes, Wat. Sci. Tech., 15 283-318.

IEA (2018), The energy sector should care about wastewater, IEA, Paris https://www.iea.org/commentaries/the-energy-sector-should-care-about-wastewater

Kuba, T. M. C. M., Van Loosdrecht, M. C. M., Brandse, F. A., & Heijnen, J. J. (1997). Occurrence of denitrifying phosphorus removing bacteria in modified UCT-type wastewater treatment plants. *Water Research*, *31*(4), 777-786.

Lee, D., Kim, M., & Chung, J. (2007). Relationship between solid retention time and phosphorus removal in anaerobic-intermittent aeration process. *Journal of bioscience and bioengineering*, *103*(4), 338-344.

Liu, G., & Wang, J. (2017). Enhanced removal of total nitrogen and total phosphorus by applying intermittent aeration to the Modified Ludzack-Ettinger (MLE) process. *Journal of Cleaner Production*, *166*, 163-171.

Longo, S., d'Antoni, B. M., Bongards, M., Chaparro, A., Cronrath, A., Fatone, F., ... & Hospido, A. (2016). Monitoring and diagnosis of energy consumption in wastewater treatment plants. A state of the art and proposals for improvement. *Applied energy*, *179*, 1251-1268.

Marques, R., Santos, J., Nguyen, H., Carvalho, G., Noronha, J. P., Nielsen, P. H., Reis M.A.M. & Oehmen, A. (2017). Metabolism and ecological niche of Tetrasphaera and Ca. Accumulibacter in enhanced biological phosphorus removal. *Water research*, *122*, 159-171.

Metcalf and Eddy, Wastewater Engineering, 4th edition, 2003, McGraw-Hill Publishing Company

Olsson, G., Carlsson, B., Comas, J., Copp, J., Gernaey, K. V., Ingildsen, P., Jeppson U., Kim C., Rieger L., Rodriguez-Roda I., Steyer J-P., Takàcs I., Vanrolleghem P. A., Vargas A., Yuan Z. & Åmand, L. (2014). Instrumentation, control and automation in wastewater–from London 1973 to Narbonne 2013. *Water Science and Technology*, *69*(7), 1373-1385.

Osada, T., Haga, K., & Harada, Y. (1991). Removal of nitrogen and phosphorus from swine wastewater by the activated sludge units with the intermittent aeration process. *Water Research*, *25*(11), 1377-1388.

Paul, E., Plisson-Saune, S., Mauret, M., & Cantet, J. (1998). Process state evaluation of alternating oxic-anoxic activated sludge using ORP, pH and DO. *Water Science and Technology*, *38*(3), 299-306.

Rieger, L., Gillot, S., Langergraber, G., Ohtsuki, T., Shaw, A., Takacs, I., & Winkler, S. (2012). *Guidelines for using activated sludge models*. IWA publishing.

Rubio-Rincón, F. J., Lopez-Vazquez, C. M., Welles, L., Van Loosdrecht, M. C. M., & Brdjanovic, D. (2017). Cooperation between Candidatus Competibacter and Candidatus Accumulibacter clade I, in denitrification and phosphate removal processes. *Water Research*, *120*, 156-164.

Smith S., Takács I., Murthy S., Daigger G. T. and Szabó A., (2008) Phosphate complexation model and its implications for chemical phosphorus removal. *Water Environment Research Vol. 80, No. 5, Nutrient Removal, pp. 428-438*

Szabo A., Takács I., Murthy S., Daigger G. T. and Smith S. (2006) The importance of slow kinetic reactions in simultaneous chemical P removal *Water Environment Research Vol. 80, No. 5, Nutrient Removal, pp. 407-416*

Szabó, A., Takács, I., Murthy, S., Daigger, G. T., Licsko, I., & Smith, S. (2008). Significance of design and operational variables in chemical phosphorus removal. *Water Environment Research*, *80*(5), 407-416.

Wentzel, M. C., Lötter, L. H., Loewenthal, R. E., Marais, G. v. R., 1986, Metabolic behaviour of Acinetobacter spp. in enhanced biological phosphorus removal - a biochemical model, *Water SA* 12 (4) 209-224.

2.7. Supplementary material

Figure S2. 1. Daily pattern of influent loads during measurement campaign of 2019

Chapter 3 - Iron reduction kinetics and influencing parameters in activated sludge

Highlights

- Fe(III) reduction follows first-order kinetics in activated sludge under anaerobic condition
- The influence of MLSS concentration on Fe(III) reduction rate is determined
- Fe(III) reduction rate is not limited by the organic substrate in activated sludge
- Sulphate concentration does not influence iron reduction rate
- Potential vivianite formation is maximum with the advancement of Fe(III) reduction but before sulphate reduction (1-2 day window)

Key-words

Ferrous iron, microbial-induced reduction, ferric iron, vivianite, ferrous sulfide, phosphorus recovery

3.1. Introduction

Metal salts are widely used as chemical reagents in wastewater treatment and wastewater collection systems. Iron ions can be naturally present in wastewater but are generally supplied for different purposes: to prevent hydrogen sulfide emission, capture organic compounds by coagulation, remove phosphate in physical-chemical treatment, or in combination with activated sludge treatment. More stringent limits for phosphorus in wastewater treatment plant effluent can explain the trend of increased iron dosing in some countries (Takács *et al*., 2006). In parallel considering the scarcity of phosphorus as a resource, new phosphorus recovery strategies are being developed with iron-coagulated sludge (Wilfert *et al*., 2016). Indeed the recovery of ferrous phosphate as vivianite has been demonstrated, and this new route is driven by iron reduction in the anaerobic digester (Prot *et al*., 2020). Finally, the same amount of iron can play successive roles, first in the collection system, then in wastewater treatment tanks, and finally in sludge treatment. For this reason, it was recently shown that an integrated approach should be taken when considering iron salt usage in an urban wastewater system (Rebosura *et al*., 2018). Therefore, it is important to increase our insight into iron reduction kinetics, either in the activated sludge process or in sidestream processes and sludge treatment.

Either ferric (Fe(III)) or ferrous (Fe(II)) salts can be used in wastewater treatment but ferric (especially ferric chloride) is the most commonly used for phosphorus removal. Ferric iron dosage leads rapidly to hydrous ferric oxide (HFO) formation in water, a precursor of ferrihydrite precipitation. The formation of HFO considered to be $Fe(OH)_{3(s)}$ provides a number of adsorption sites for ions on its surface, which allow both adsorption and co-precipitation of phosphate (Smith *et al*., 2008; Szabó *et al*., 2008).

As soon as anaerobic conditions are imposed, oxygen and nitrate are depleted, and ferric iron (including HFO) is progressively reduced into ferrous iron which is more soluble and produces less hydroxide. In an activated sludge system microbial iron reduction was previously observed (Nielsen *et al*., 1996; Lovley, 1997; Chen *et al*., 2003; Wang *et al*., 2019). Iron is completely reduced in an anaerobic digester in which long anaerobic retention times and low oxidation-reduction potential conditions were maintained (Cheng *et al*., 2015). Inversely iron is oxidized under aerobic (Stumm and Sulzberger, 1992; Chen *et al*., 2018) or anoxic conditions (Benz *et al*., 1998).

Regarding the general knowledge in aquatic environments, iron reduction can happen both through abiotic and biotic pathways (Roden 2003; Lovley, 2013).

However microbial reduction seems to be dominant in wastewater treatment plants (Nielsen, 1996; Nielsen *et al*., 1997; Rasmussen and Nielsen, 1996). There are several enzymatic and non-enzymatic iron-reducing pathways for microorganisms (Schultze-Lam *et al*., 1996; Southam, 2000; Nevin and Lovley, 2000). Different studies (Achtnich *et al*., 1995; Lovley and Chapelle, 1995; Zhang *et al*., 2009) suggested that iron reducers are able to outcompete sulphate reducers and methanogens under different conditions (paddy soils, deep water, and sewer biofilm conditions, respectively) while Bethke *et al*. (2011) even found proof of mutualism between iron reducers and sulphate reducers. However, the effect of sulphate on iron reduction rates in activated sludge still needs to be clarified.

Regarding the iron reduction kinetics, Nielsen (1996) determined rates ranging from 0.9 – 3.7 mg Fe g^{-1} VSS h^{-1} for six different facilities (all of which were dosing iron for phosphorus removal – either exclusively or simultaneously with biological phosphorus removal). Wang *et al*. (2019) calculated zero order rate constant from a chemical treatment (CT) and Enhanced Biological Phosphorus Removal (EBPR) facilities and obtained values equal to 2.99 mg Fe g^{-1}VSS h^{-1} and 1.02 mg Fe g^{-1}VSS h^{-1} respectively. The authors concluded that there is a correlation between zero-order reduction rate and iron concentration, and determined first-order rates which were slightly different in the two types of facilities (1.2±0.17 d^{-1} for CT and 1.44±0.02 d^{-1} for EBPR). Chen *et al*. (2003) examined the pure culture (*Shewanella putrefaciens)* and abiotic reduction as well, using different natural organic matter (NOM) as the electron donor. The iron reduction rate constant was in the range of 3.31 – 10.94 d^{-1} while in chemical reduction 0.3-1 d^{-1} at pH 3. The iron reducing capacity of natural organic matter decreases significantly with increasing pH, the abiotic reduction becoming negligible compared to the microbial reduction. These studies provided general insight into iron reduction kinetics but did not scrutinize influencing parameters.

Considering the whole plant system, ferric iron is being completely reduced into ferrous iron in the anaerobic digester tanks, this reduction modifies the iron speciation and its mobility as well as the iron interactions with phosphate and sulfur. Phosphate can be released in the digester liquor or precipitated with ferrous iron. Speciation of ferrous iron in anaerobic digesters is controlled through a primary reaction (sulfide precipitation to form pyrite and ferrous sulfide) and a secondary reaction (phosphate precipitation to form vivianite) (Roussel and Carliell-Marquet, 2016). The formation of ferrous phosphate and ferrous sulfide was both confirmed experimentally in digested sludge (Wang *et al*., 2019; Prot *et al*., 2019; Wilfert *et al*., 2020). Finally, vivianite can be collected from digested sludge due to its magnetic properties (Prot *et al*., 2019). Iron phosphate and iron sulfide production would depend on the S and P availability. Despite iron sulfide being theoretically favored in thermodynamics, it has been demonstrated that iron forms

vivianite in the majority of the phosphate-rich digester (Roussel and Carliell-Marquet, 2016). Iron reduction in anaerobic digestion was implemented in recent models for anaerobic digesters (Hauduc *et al*., 2019). Moreover, studies revealed that iron reduction and vivianite crystallization can even be realized with a much lower retention time than those of anaerobic digester (Azam and Finneran, 2014; Priambodo *et al*., 2017; Liu *et al*., 2018; Varga *et al*., 2020). As a consequence knowing accurately iron reduction kinetic is important for predicting possible phosphorus recovery strategies, as well as hydrogen sulfide mitigation.

The objective of this study is to determine iron reduction rates and clarify the interactions between iron reduction, sulphate reduction, and phosphate release in activated sludge. Experiments were designed in anaerobic conditions with activated sludge receiving ferric chloride. The following influencing parameters were scrutinized: the dependence on suspended solids concentration, the possible effect of biodegradable organic matter, and the influence of sulphate concentration on both iron reduction and phosphate release.

3.2. Materials and methods

3.2.1. Batch assay setup

The batch reactors used for these experiments contained 1000 ml or 500 ml of activated sludge with sealed screw caps and inserted sampling tubes into the gas and liquid phase. Constant mixing was maintained via magnetic stirrers. Prior to sealing the reactors, sludge samples were flushed with nitrogen gas for five minutes.

For the sampling, 20 ml plastic syringes were used, and to ensure the accurate sampling of the mixed sludge, the tubes were flushed with the sludge multiple times prior to sampling. Moreover, dinitrogen gas was added to the reactor headspace to maintain constant pressure and ensure anaerobic conditions. The reactors were kept at room temperature (25±1°C). For most of the experiments, additional Fe(III) was initially added to the reactor as $FeCl_3$ (100 mg Fe L^{-1}).

Each batch test was systematically duplicated. Samples (volume: 15 - 20 ml where 10 ml was used for total Fe^{2+} measurement by acidification and the rest for soluble components by centrifugation and filtration) were taken at increasing time intervals: 0, 15, 30, 60, 90 minutes, then at 2h, 4h, 6h, 8h, and 24h following with one sample per day until the end of the experiment (14 days).

In most cases, sludge samples (type A) were taken from the biological tank of an activated sludge process in Villefranche de Lauragais (France) treating 9500 PE. This facility is designed to perform simultaneous biological and physical-chemical P removal, with a pre-anaerobic zone followed by an intermittently aerated basin. Nitrification, denitrification, and phosphorus removal are carried out by combined physical-chemical, and biological processes with $FeCl_3$ dosed in the aeration tank. For a specific comparison, sludge samples (type B) were collected from a second facility (Seine Amont, Valenton, France, 2.600.000 PE). This plant is designed with denitrification-nitrification activated sludge, followed by physical-chemical phosphorus removal (clariflocculation) and anaerobic digestion as sludge treatment. The sludge samples were sieved (2mm) and stored at 4°C until the start of the batch tests during transporting and storage time of a maximum of 24 hours.

In order to determine influencing parameters, different scenarios with parameter adjustments were included in the study (Table 3.2-1). Each experiment included two simultaneous reference reactors, to reflect current conditions at the facility and parameter-adjusted reactors to monitor the impact on the reduction rate.

Table 3.2-1. Experimental scenarios of iron reduction batch tests

Scenario/question	Parameter	Required adjustments	Number of tests
Biomass concentration dependency	Total suspended solids	TSS concentration changed by settling or dilution (with supernatant) in the range 1.5 – 11 g TSS L^{-1}	24
Confirm biological reaction	Substrate addition	200 mg/l acetate as $NaC_2H_3O_2$	2
	Substrate addition	100 mg/l lactate as $NaC_3H_5O_3$	2
	Inhibition of biological processes	Autoclaved samples: 30 minutes at 121 °C	2
Sulphate dependency	Initial sulphate concentration	Addition of 30 mgS/l sulphate as Na_2SO_4	4
Effect of Fe(III) concentration	No additional Fe(III) vs. additional Fe(III)	Initial Fe(III) varies from 40 to 150 mg L^{-1}	4
Sludge origin effect	Inoculum	Sludge A v.s. sludge B for initial Fe(III) 150 mg L^{-1}	4
Temperature dependency*	Temperature	Controlled temperature: 16°C and 30°C	4

*Temperature dependency is presented in 3.7 Supplementary material

3.2.2. Analysis

Total iron and total phosphate concentrations in sludge samples were determined by Inductively Coupled Plasma Atomic Emission Spectrometry (ICP-AES - Horiba Jobin Yvon - Ultima2). Before analysis, a hot acid attack (HNO3 - DigiPREP HT high-temperature digestion system - SCP science) was carried out to allow the complete dissolution of the precipitates contained in the samples. HNO_3 (69-70% PlasmaPURE) was added in a mineralization tube, and digestion was performed at room temperature for 1h, and at 95 °C for one hour. Samples were diluted and measured in the range of 0-10 mg L^{-1} after calibration with SPEX CertiPrep 1000µg/ml for Fe and P.

Total and soluble Fe(II) concentrations were measured with a 1.10-phenanthroline spectrometric method adapted from water quality standards (NF T 90-017, AFNOR, qualité de l'eau, 1994). Soluble iron was measured after filtration (0.2 µm pore size). For total Fe(II), the HCl extraction method was applied. 0.65 ml HCl (1 M) was added to a 10 ml sample for lowering the pH to 1-1.5, before mixing for 10 min. The sample was then centrifuged and filtered (0.2 µm pore size) and the supernatant was analyzed. Prepared samples were stored in sealed containers until analysis. Fe(III) was calculated by the difference between total iron and Fe(II). The HCl extracted Fe(II) measured at the end of the anaerobic assay was compared to total iron which confirmed the high extraction efficiency.

Total suspended solids (TSS) and volatile suspended solids (VSS) were determined according to APHA (1992) protocol. Soluble COD was measured with the dichromate method using spectrophotometric determination according to NF T90-101 (Hanna Instruments, Woonsocket, RI, USA). The analysis of phosphate and sulfate was conducted on an ionic chromatography system with a suppressor and conductivity detector (ThermoFisher Scientific, DX 320, Waltham, MA, USA) according to the water quality standard method (NF EN ISO 10304-1, AFNOR qualité de l'eau). Chromatographic separation was performed using an AS19, 2 × 250mm column (ThermoFisher Scientific, Waltham, MA, USA) at 30°C. The volume injected was 10µL of samples. The flow rate was 0.25 mL/min. The mobile phase was a multi-step gradient of KOH. The sample preparation consisted to centrifuge 5mL of sludge at 13000 rpm for 15 min and filtered at 0.2 µm cellulose acetate membrane. For all measurements, a maximum storage time of 24 hours was applied to prevent the re-oxidation of soluble Fe(II) and subsequent possible hydroxide precipitation.

3.2.3. Calculation

Iron and phosphorus speciation were estimated in order to scrutinize the effect of reduction on both sulfur and phosphorus compounds. A calculation method was used based on measurements during kinetics and assumptions related to reactions stoichiometry (Figure S3. 1, Table S3. 1). First the reduced iron and reduced sulfate were used for estimating iron sulfide formation, assuming that this compound is thermodynamically favored (Roussel and Carliell-Marquet, 2016; Wilfert *et al*., 2020). Secondly, the available ferrous iron was compared to available phosphate for estimating the ferrous phosphate potentially formed as vivianite.

The following components were assumed:

- Total iron is composed of Fe(III) and Fe(II). Fe(III) is in particulate form (HFO). Fe(II) is composed of soluble Fe(II), FeS precipitate, vivianite, and other Fe(II) precipitates.
- Total phosphorus is composed of Fe(III) bound P, soluble orthophosphate, P content of biomass, vivianite, and other particulate phosphorus (including stored polyphosphate).

Fe(III) bound P was assumed initially with measurements of Fe and P with a molar ratio of 1.5. Initial SO_4-S concentration was considered as the potential for sulfide production (samples were initially flushed with pure dinitrogen). With closed stirred reactors, the gas phase was assumed to be in equilibrium with the liquid phase, and H_2S gas was not removed. Sulphate reduction directly causes FeS precipitation with a molar ratio of 1:1. Dosed Fe(III) adsorbs with gradually released PO_4 (based on P release without iron dose). Fe(II) captured by sulfide is assumed to induce PO_4 release.

3.3. Results

3.3.1. Iron reduction kinetics

Figure *3.3-1* shows the evolution of Fe(II) concentration over time (relative to final) during typical experiments with sludge A and sludge B. Fe(III) was dosed at a similar concentration (100 mg/L) initially, and a similar MLSS concentration was chosen (TSS= 3.4 g L^{-1} for sludge A - Villefranche; TSS= 3.5 g L^{-1} for sludge B - Valenton). Both experiments showed a very similar pattern. 68±5% of iron was reduced after 24 hours, and more than 90% of iron was reduced after 2 days.

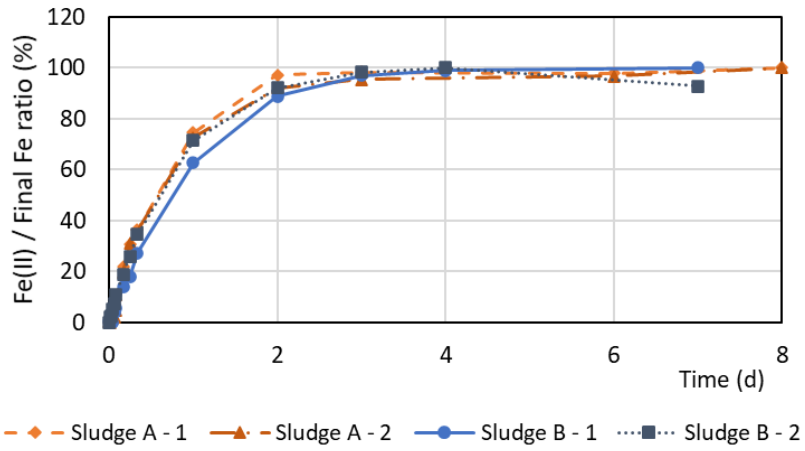

Figure 3.3-1. Total Fe(II) to final Fe(II) concentration ratio in sludge A (Villefranche de Lauragais) and sludge B (Seine Valenton)

The initial kinetic rate (k_o) of iron reduction was determined (in mg Fe g^{-1}VSS h^{-1}) using the measurements realized during the first 24 hours. Considering that the rate was proportional to the iron concentration 7 days of kinetic test results were used to determine the kinetic rate (k) of a first-order model (13 data points on average):

$$\frac{d[Fe^{3+}]}{dt} = -k.[Fe^{3+}]$$

The first-order model gives a very good fit for the overall dataset as indicated by the logarithmic representation (R^2=0.99) (Figure 3.3-2). The k value was 1.399 ± 0.053 d^{-1} for sludge A and 1.135 ± 0.162 d^{-1} for sludge B. The average zero-order rate determined with the initial measurements was 1.068 ± 0.364 mg Fe g^{-1}VSS h^{-1} for sludge A and 1.226 ± 0.162 mg Fe g^{-1}VSS h^{-1} for sludge B. Correlation coefficients for the rate calculations were excellent in most cases (R^2>0.95). The initial rates (k_0) show more variation compared to the first order rate (k), which was possibly due to the sensitivity of k_0 to the initial sludge condition and preparation (iron concentration, degassing, and pH drop).

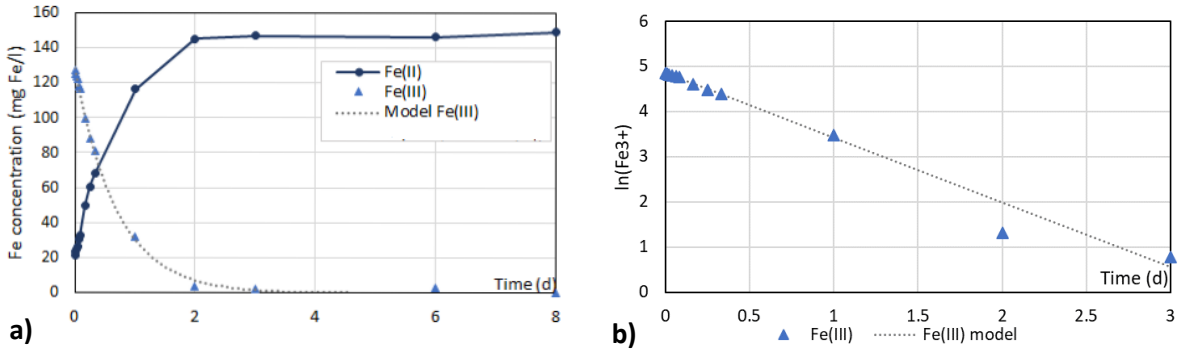

Figure 3.3-2. a) measured and calculated iron concentrations in a selected batch reactor (sludge A, TSS=3.442 g TSS/l) b) first-order kinetics illustrated on a logarithmic scale (up to day 3).

To confirm the dominance of biological reduction over chemical reduction during the tests (sludge A), a first experiment was done after autoclaving the sludge (non-biotic reference), and two experiments were performed (both in duplicate) with the addition of lactate and acetate (Figure 3.3-3). After autoclaving, almost no reduction was detected during 24 h which confirmed that iron reduction was mainly biologically induced. Regarding the assays with lactate and acetate, the Fe(II) production rate was comparable to the reference test. It seems that substrate addition slightly encouraged reduction during the first hours (Figure 3.3-3), but the total amount of Fe(II) at 24 hours and later was not significantly different from the endogenous condition. Moreover, the kinetic rates determined for lactate addition (k= 1.502±0.366 d^{-1}) and acetate addition (k= 1.305±0.072 d^{-1}) were not statistically different from the value obtained at the reference conditions (sludge A) without any organics addition. This result shows that the iron reduction in the endogenous condition was not significantly limited by organic matter after 24 hours and in the long term.

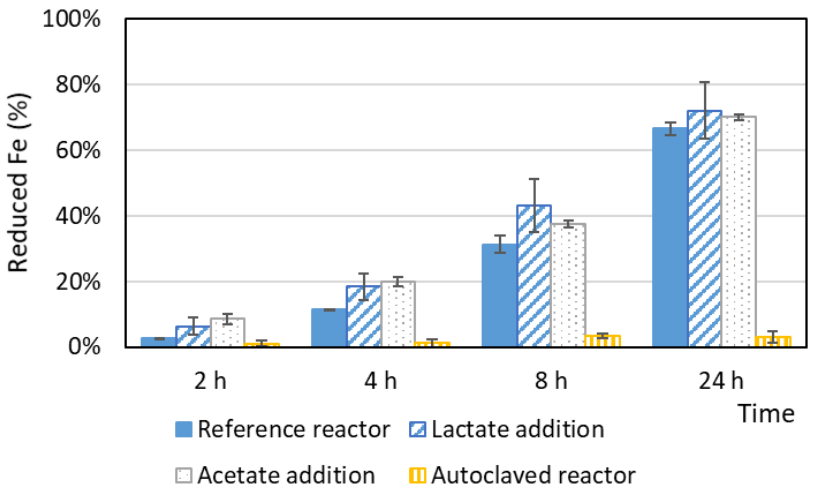

Figure 3.3-3. Reduced fraction of Fe(III) dosed at the beginning of the experiment (duplicated tests) for different organic substrates addition

3.3.2. Influence of sludge concentration on the kinetic rate

As it was previously established, iron(III) reduction in activated sludge is dominantly a biological process. While biomass speciation was not carried out, it is appropriate to use VSS as an indicator for biological activity, considering the available dataset. A number of batch tests were carried out with different sludge concentrations in the range of 1.1 – 9.5 g VSS L^{-1}. The first order rate constant (k) ranged from 0.5 to 1.9 d^{-1} (0.021 – 0.08 h^{-1}), increased very significantly with VSS concentration from 1.1 to 4 g VSS L^{-1}, and was relatively constant from 4 to 9.5 g VSS L^{-1} (Figure 3.3-4). Considering such a typical pattern for a biological reaction with saturation phenomena, a Michaelis-Menten expression was proposed to describe this tendency (eq. 1) where VSS dependency implies enzymatic activity.

$$k = k_{max} * \frac{X_{VSS}}{(K_{VSS}+X_{VSS})} \qquad \textit{Equation 1}$$

Where k_{max} is the maximum reduction rate constant in d^{-1}

K_{VSS} is the half-saturation parameter for the VSS effect in g L^{-1}

X_{VSS} is volatile suspended solids concentration in g L^{-1}

The parameter estimation was performed by minimizing the Root Mean Square Error (RMSE) using the generalized reduced gradient method as an optimization procedure. The optimal value of k_{max} was 2.65 d^{-1} and the optimal value for saturation parameter K_{VSS} was 3.23 g L^{-1}.

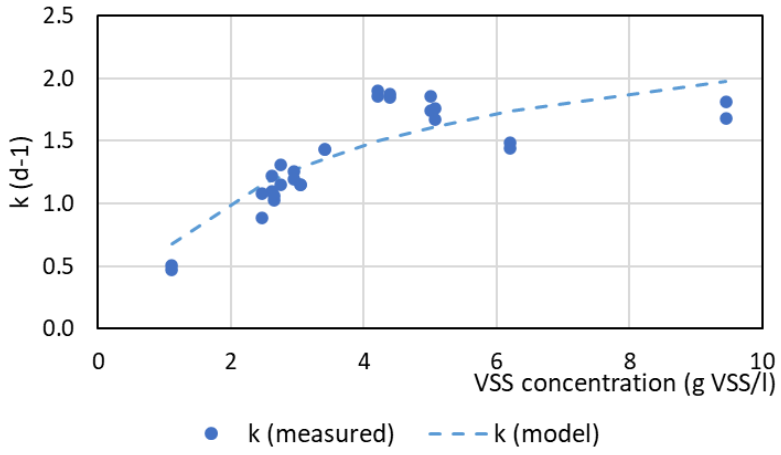

Figure 3.3-4. Iron reduction rate constant as a function of VSS concentration.

3.3.3. Effect of sulphate on reduction kinetics and phosphate release

To investigate the interactions between iron and sulphate reduction, four scenarios were compared, by combining a low and high level of iron concentration (40 - 150 mg Fe(III) L^{-1}) with low and high levels of sulphate concentration (15 – 50 mg SO_4-S L^{-1}). Results are shown on Figure 5.

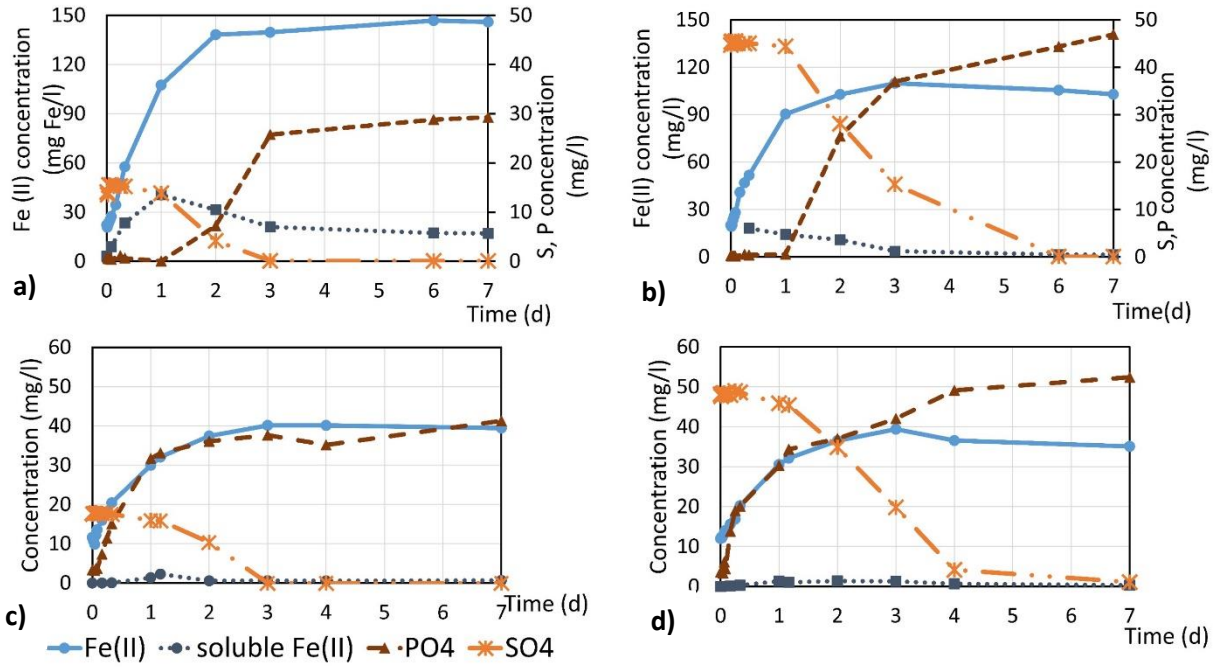

Figure 3.3-5. Iron and sulphate reduction, phosphate release, and soluble iron for different SO_4 to Fe ratios. a) high Fe - low S; b) high Fe – high S; c) low Fe - low S; d) low Fe - high S.

In all the experiments sulphate reduction accelerated after 24 hours whereas it was not significant during the first day. During the tests with a low level of iron (only the original iron dosed on the plant) phosphate was released (40 mg P L^{-1}) during the first 24 hours simultaneously as iron was reduced. With additional sulphate a secondary release of phosphate was observed after sulphate was reduced between days 3 and 4 (Figure *3.3-5*.d). For higher iron dosage, phosphate release was observed to start only after 24 hours after most of the Fe(III) was reduced. Finally, in case of additional iron dosing, phosphate release occurs concomitantly to sulphate reduction which was observed to start after iron reduction. On the contrary, phosphate release at low levels of iron (endogenous) happened parallel to iron reduction but a secondary phosphate release was observed after sulphate reduction. During the experiments with additional iron, significant soluble Fe^{2+} was measured in the reactors after 24 hours (up to 30% of total Fe(II) at 24 hours). This soluble fraction of iron decreases progressively after 24 hours which coincides with the beginning of sulphate reduction.

Sulphate reduction was observed as the main process between 24 h and 3 to 6 days. Although the sulphate reduction started parallel with Fe(III) reduction, it is clear that Fe was the more favored electron acceptor during the first day, whereas sulphate reduction accelerated after Fe(III) abundance decreased. As phosphate release seemed to correspond with sulphate reduction, with additional iron dosage, it was expected that higher concentrations of phosphate can be achieved with higher initial sulphate concentrations and these observations were similar to lower iron concentrations (i.e. endogenous iron reduction). This result is confirmed on Figure *3.3-5* b) compared to Figure *3.3-5* a), indicating 50% additional phosphate release when the initial sulphate was 45 mg S L^{-1} instead of 15 mg S L^{-1}.

An important question is to evaluate if the concentration of sulphate could have an influence on the iron reduction rate. The values of the k constant obtained are plotted as a function of S: Fe molar ratios on Figure 6. Despite the variation of sulphate to iron ratio, the rate constant (k) did not show any significant variation and was maintained around 1.2 ± 0.2 d^{-1}. This indicates that sulphate did not inhibit nor enhance iron reduction kinetics. Moreover, sulphate reduction happened at a similar rate during these experiments despite the different levels of iron concentrations used.

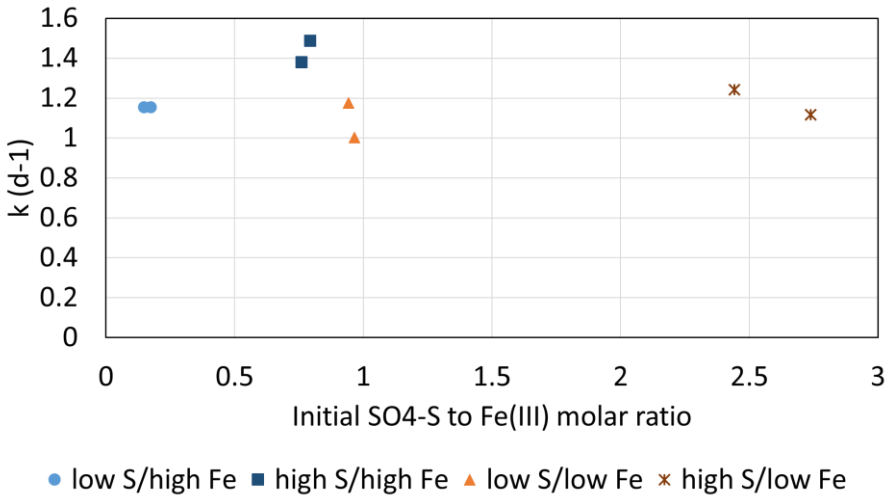

Figure 3.3-6. Iron reduction rates measured for different SO_4 to Fe molar ratios (Fe concentrations: 40 – 150 mg Fe/l and sulphate concentrations: 15 – 50 mg S/l)

3.3.4. Calculation of iron and phosphorus speciation

As described earlier (Chapter 3.2.3), based on the measured data, an estimation of iron and phosphorus chemical fractionation was performed. Figure 3.3-7 shows the iron fractions for the four anaerobic tests with different sulphate-to-iron ratios.

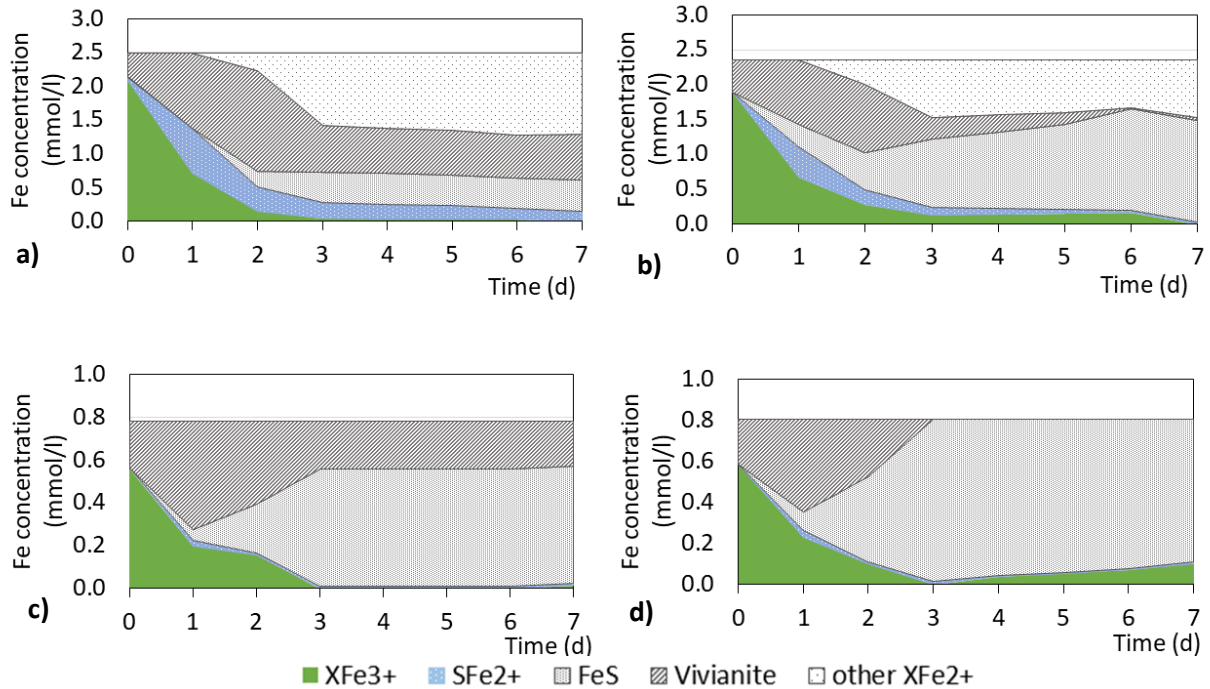

Figure 3.3-7. Estimated iron fractions in different S to Fe ratio reactors; a) high Fe -low S; b) high Fe – high S; c) low Fe -low S; d) low Fe - high S. Components are particulate iron(III) hydrous oxide (XFe^{3+}), soluble iron(II) (SFe^{2+}), iron(II) sulfide (FeS), iron(II) phosphate (vivianite), other particulate iron(II) (XFe^{2+}).

Figure 3.3-8 shows P fractionation in the same batch reactors. Without additional iron (Figure *3.3-8*.c and Figure *3.3-8*.d) the initial P release (<8 h) can be attributed to polyphosphate (PP) cleavage and not necessarily to a consequence of iron reduction. Indeed, in the first 4 hours, nearly 1 mmol L^{-1} P was released while only 0.2 mmol L^{-1} of iron was reduced (compared to Fe: P=1.5 assumed for chemical P capture). This indicates that the release of phosphate is related to other processes than reduction (eg. PP cleavage, hydrolysis). With additional iron dosage, phosphate was assumed to be similarly released by bacteria but did not appear in solution due to its sorption by Fe(III) (hydrous ferric oxide-HFO). In accordance with available iron and assumed P release (approximately 0.038 mmol P/h) the fraction of Fe(III) bound P was increased at the beginning of the reduction. With the iron reduction, the amount of Fe(II) bound P increased (assumed to be vivianite) and this amount was higher for additional iron dosage. The Fe(II) bound P was progressively solubilized as the iron sulfide was produced during sulphate reduction. The maximal vivianite formation was reached after 24 h at a low level of iron, and 48 h at a high level of iron.

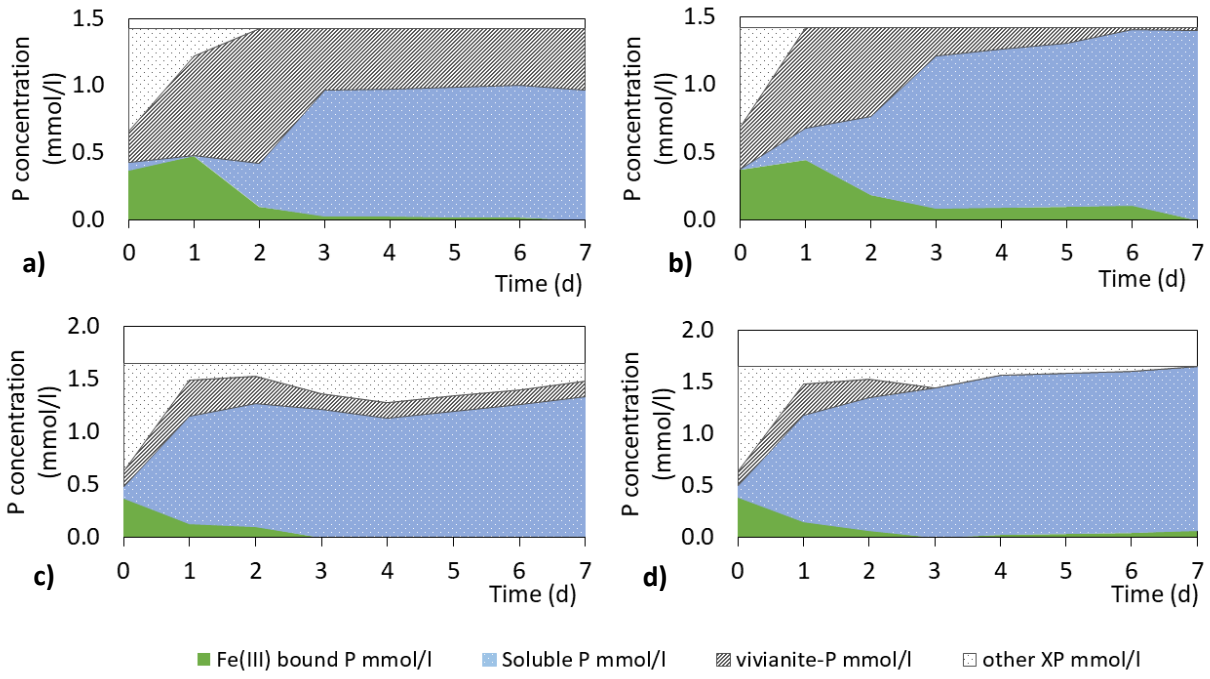

Figure 3.3-8. Estimated phosphorus fractions in different S to Fe ratio reactors a) high iron-low S b) high iron – high S c) low iron-low S d low iron- high

3.4. Discussion

3.4.1. Iron reduction kinetic rates

In this study, zero-order reduction rates (k_0) and first-order rate constants (k) were determined to reflect the initial part and the totality of the reduction kinetics, respectively. The values obtained for k_0 in this study were added to the synthetic chart of Wang *et al*. (2019) which includes data from previous studies (Nielsen, 1996; Nielsen *et al*., 1997; Rasmussen and Nielsen, 1996). Note that the variation of concentration expressed in mg Fe g^{-1}VSS was due to variation of either Fe or VSS concentrations. Endogenous iron also varied widely in the literature data whereas, in this study, iron was dosed at the beginning of batch experiments. Our values confirmed the global tendency indicating that the initial specific iron reduction rate primarily depends on iron (Fe(III)) concentration, which justifies further examination of first-order rates. The values of the first order rate constant (k) ranged in this study from 0.5 to 2.0 d^{-1} (0,021 - 0,083 h^{-1}) for a range of VSS concentration from 1.0 to 9.5 g L^{-1}. The average value for standard conditions (3.4-3.5 g VSS L^{-1}) was 1.399 ± 0.053 d^{-1} for sludge A and 1.135 ± 0.162 d^{-1} for sludge B. These values were in the range of literature studies (0.178 – 10.9 d^{-1}) from natural sediments (Roden and Wetzel, 2003) to pure Fe reducer culture (Chen *et al*., 2003), and within the range of 1.2 – 1.44 d^{-1} which is the reference for activated sludge (Wang *et al*., 2019).

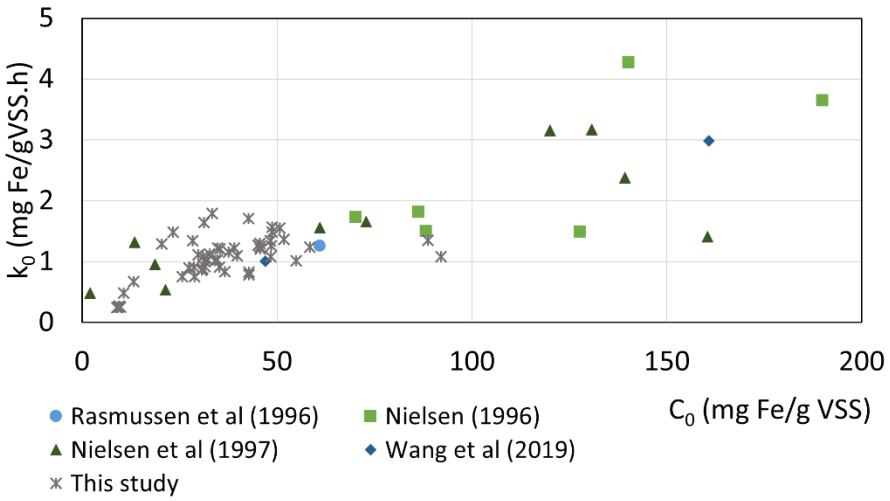

Figure 3.4-1. Zero-order iron reduction rate constants as a function of iron concentration in different studies (based on Wang *et al*., 2019 – using average values to display Nielsen, 1996)

The parameter most influencing the reduction rate is the mixed liquor concentration indicating that the reduction was logically intensified by the biomass concentration. This effect was less significant for MLSS concentrations higher than 4 g L^{-1}. This can be explained by the poorly soluble nature of Fe(III) mainly present as hydroxide precipitates (HFO) which are adsorbed on suspended solids. Therefore the reduction rate is surface limited and may be no longer influenced by additional biomass as soon as iron is totally adsorbed. Logically it was observed that no iron reduction occurred with autoclaved sludge sample (during 24h), which confirmed the dominance of the microbial process as an iron reduction mechanism in activated sludge.

Two experiments were performed with additional substrates (lactate and acetate) to stimulate different groups of microorganisms, but a very similar iron reduction rate was obtained. This result showed that organic matter was not limiting for the iron reduction in the activated sludge sample.

Organic matter naturally available or produced by fermentation was sufficient for playing the role of electron donor during iron reduction. It should be mentioned that the amount of iron reduced in the batch tests (100 mg L^{-1}) corresponds to an equivalent oxygen demand of only 14.3 mg L^{-1}. An increase of soluble COD during batch tests (measurements not shown) indicated that hydrolysis and fermentation produced organic electron donors. As acetate is naturally produced by fermentation, its addition does not increase the reduction rate. Lactate may be less abundant in fermentation products which may explain a slight accelerating effect when it was dosed.

In this study, the genealogical composition of the biomass was not determined, but a range of microorganisms are able to use Fe(III) as an electron acceptor with various electron donors in wastewater treatment communities (Lovley, 2013). Many of these are fermenters and/or facultative iron reducers, utilizing the electron acceptor that yields the highest energy. Nielsen (1996) stated that not all Fe(III) reducers use Fe(III) as the exclusive electron acceptor, some may use oxygen and nitrate facultatively and some sulphate reducers also showed iron-reducing capabilities. This can explain the rapid initial reduction, as various electron donors can be used for iron reduction even at very low concentrations (Lovley and Chapelle, 1995). The availability of these electron donors can also drive the competition between anaerobic microorganisms (Achtnich *et al*., 1995; Lovley and Chapelle, 1995).

3.4.2. Relation and comparison between iron and sulphate reduction

In this work, iron and sulphate reduction kinetics were compared on the same activated sludge. Results revealed that sulphate reduction rate was very low during the first 24 hours and accelerated only after the majority of Fe(III) was reduced, whereas the Fe(III) reduction rate was the highest at the start of the experiment.

Less than 5% of sulphate was reduced during the first 24 hours while more than 70% of iron was reduced in parallel. This observation appears in line with the thermodynamic sequence theory used in geomicrobiology (Achtnict *et al*, 1995; Bethke *et al*, 2011; EPA, Groundwater, 2013) even though little information can be found to support this in activated sludge literature. Ingvorsen *et al*. (2003) observed that sulphate reduction could start immediately in anaerobic conditions but at a low rate during the first 20 hours, before the kinetics became exponential. This rate was accelerated by adding an organic substrate indicating that sulphate-reducing bacteria were limited by electron donors. Most sulphate reduction bacteria (SRB) are unable to degrade high molecular mass compounds and depend on fermentation products for their metabolism (Ingvorsen *et al*., 2003). Our measurements also revealed that iron reduction starts more rapidly and does not suffer from similar organic matter limitations. After the sample storage period (24 h) iron was mainly found in Fe^{2+} form (~25 mg Fe L^{-1}) while sulphate concentration was still significant around 15 mg SO_4-S L^{-1}. An on-site sampling showed that at the sampling point in the aeration tank Fe^{2+} concentration was negligible whereas sulphate concentration was also close to 15 mg SO_4-S L^{-1}.

In addition, our study demonstrates that the iron reduction rate constant (k) is not influenced by the concentration of sulphate. This clearly supports the idea that Fe(III) reduction is not inhibited by sulphate. Conversely, the sulphate reduction kinetics were not modified by the variation of the initial iron dose. The sequence between both reduction processes is not completely exclusive, as an overlapping period can be observed. When sulphate reduction begins (at 24 hours), there is still substantial Fe(III) present (~40 mg Fe/l) and iron reduction continues parallel with sulphate reduction. This supports neither a complete inhibition of sulphate reduction by ferric iron nor the exclusively sequential nature of the electron-accepting processes. As Lovely and Chapelle (1995) studied the zoning of anaerobic groundwater systems, they found that the competing groups of microorganisms (Fe(III) reducers, sulphate reducers, and methanogens) are able to utilize available electron donors (acetate or dihydrogen) in increasing concentrations only, giving the “higher rung” groups an advantage.

Thus, this sequence could be interpreted by a lower affinity constant for organic electron donors for iron reducers in comparison with sulphate reducers. Regarding this competition, Bethke *et al*. (2011) found that the initial structure of the Fe(III) precipitate is crucial for the reduction. They explained that whereas ferrihydrite is a preferred electron acceptor over sulphate, more crystalline iron structures (eg. Goethite) are not naturally reduced as rapidly. And finally, they found proof of mutualism between functional groups of reducing microorganisms as opposed to competitive exclusion. According to Achtnich *et al*. (1995) sulphate to iron ratio may also have an impact on the competition for electron donors.

However, in the range explored in the current study (SO_4: Fe range of 0.15 – 2.75 mol S/mol Fe) this ratio was not an influencing factor either in sulphate and iron reduction kinetics. Finally, it appears that the reduction of sulphate and iron can happen at the same time independently, but the rate of SRB was initially more limited by an organic substrate.

3.4.3. Implications for phosphate and iron recovery

Both iron and sulphate reduction affect phosphate immobilization and phosphate release as well as mineral speciation, depending on the S: Fe ratio (Figure *3.3-7* and Figure *3.3-8*). Similarly, Kleeberg *et al*. (2015) have shown the importance of the S: Fe ratio for indicating vivianite occurrence in natural sediments. In our study phosphate release was rapid and concomitant with Fe reduction at a low level of iron, whereas at a higher iron dose phosphate release was delayed by 24 h and correlated to sulphate reduction. In that case, phosphate was captured by Fe(II) but was progressively solubilized due to iron capture by iron sulfide precipitation. The speciation estimation showed that the maximum amount of Fe(II) phosphate (assumed to be vivianite) was systematically obtained after 1 or 2 days when most of the iron was reduced but iron sulfide was still minimized. This indicates that an optimal condition could be obtained in an anaerobic reactor with a lower retention time than conventional AD for recovering vivianite. Alternatively, Prott *et al*. (2020) demonstrated that overdosing the iron was possible to increase vivianite production in anaerobic digestion, but a part of iron was naturally captured by sulfide.

Finally, an optimal saturation index (SI) for vivianite can be reached after iron reduction but before accumulating too much sulfide. It seems that such a condition could be reached by controlling the retention time and the organic electron donor availability, as iron reduction appeared less limited than sulphate reduction for a similar condition in our experiments. It was important to show that decoupling iron and sulphate reduction was possible.

To the author's knowledge, this is the first time such a possibility is supported by experimental evidence, and it constitutes a promising perspective for vivianite recovery.

Alternatively, phosphate recovery can be improved by solubilizing phosphate before precipitating it as struvite or hydroxyapatite. In the current study, the catalyzing effect of sulphate reduction on phosphate release was shown. In previous studies, the addition of sulfide to digested sludge or activated sludge was performed to provoke phosphorus release (Suschka *et al*., 2001; Wilfert *et al*. 2020; Lippens and de Vrieze, 2019).

Lippens and de Vrieze (2019) recently showed that sulphate injection in an anaerobic digester can release phosphate but reduce methane production. In contrast, phosphate extraction before anaerobic digestion, either by extracting vivianite or releasing the phosphate thanks to sulfide production could also be explored.

According to our observation, the phosphate captured by Fe(II) (although further work is needed to demonstrate the exact crystallization level and composition) can be rapidly solubilized thanks to sulfide, without consuming much organic matter. This could be an emerging way to release phosphate before the anaerobic digestion without reduction of the methane potential.

3.5. Conclusions

These findings clarify the iron reduction kinetics in activated sludge under anaerobic conditions, as well as some influencing parameters and the consequence on Fe-S-P interactions. Most of the Fe(III) was reduced into Fe(II) within two days. The iron reduction was described by first-order kinetics and rates were similar for two sludges from different sources. Results revealed that iron reduction was not limited by organic matter as an electron donor. The effect of MLSS concentration on the rate constant was described by a non-linear function. The study further revealed that sulphate concentration did not influence iron reduction rates, and the iron dose did not influence sulphate reduction as well. Sulphate reduction started slower than iron reduction, probably due to higher sensitivity to organic substrate limitation. Phosphate release depended on the initial iron dose but was quantitatively affected by sulphate reduction. As a consequence, ferrous phosphate precipitation, supposed to produce vivianite, potentially reached a maximum for a time of 1 to 2 days. These results could help to define strategies for phosphorus recovery in presence of iron.

3.6. References

Achtnich, C., Bak, F., Conrad, R. (1995). Competition for electron donors among nitrate reducers, ferric iron reducers, sulfate reducers, and methanogens in anoxic paddy soil. *Biology and fertility of soils*, *19*(1), 65-72.

AFNOR. Qualité de l'eau, (1994). Association française de normalisation. Éditeur: AFNOR, *Paris-La Défense*, 1994. Recueil de normes française en environnement. 1ère édition.

APHA (1992). Standard Methods for the examination of water and wastewater *18th Edition. American Public Health Association, Washington D.C.*

Azam, H. M., Finneran, K. T. (2014). Fe (III) reduction-mediated phosphate removal as vivianite (Fe3 (PO4) 2· 8H2O) in septic system wastewater. *Chemosphere*, *97*, 1-9.

Benz, M., Brune, A., Schink, B. (1998). Anaerobic and aerobic oxidation of ferrous iron at neutral pH by chemoheterotrophic nitrate-reducing bacteria. Archives of Microbiology, 169(2), 159-165.

Bethke, C. M., Sanford, R. A., Kirk, M. F., Jin, Q., Flynn, T. M. (2011). The thermodynamic ladder in geomicrobiology. *American Journal of Science*, *311*(3), 183-210.

Chen, J., Gu, B., Royer, R. A., Burgos, W. D. (2003). The roles of natural organic matter in chemical and microbial reduction of ferric iron. *Science of the total environment*, 307(1-3), 167-178.

Chen R. Liu H., Tong M., Zhao L., Zhang P., Liu D., Yuan S. (2018) Impact of Fe(II) oxidation in the presence of iron-reducing bacteria on subsequent Fe(III) bio-reduction *Science of The Total Environment Volume 639, 15 October 2018, Pages 1007-1014*

Cheng, X., Chen, B., Cui, Y., Sun, D., Wang, X. (2015). Iron (III) reduction-induced phosphate precipitation during anaerobic digestion of waste activated sludge. *Separation and Purification Technology*, 143, 6-11.

Hauduc, H., Wadhawan, T., Johnson, B., Bott, C., Ward, M., Takács, I. (2019). Incorporating sulfur reactions and interactions with iron and phosphorus into a general plant-wide model. *Water Science and Technology,* 79(1), 26-34.

Kleeberg, A., Grüneberg, B., Friese, K., Pérez-Mayo, M., Hupfer, M. (2015). Sedimentary sulphur: iron ratio indicates vivianite occurrence: a study from two contrasting freshwater systems. *Plos one*, *10*(11), e0143737.

Ingvorsen, K., Yde Nielsen, M., Joulian, C. (2003). Kinetics of bacterial sulfate reduction in an activated sludge plant. FEMS Microbiology Ecology, 46(2), 129–137.

Lovley, D. R., Chapelle, F. H. (1995). Deep subsurface microbial processes. *Reviews of Geophysics*, 33(3), 365-381.

Lovley, D. R. (1997). Microbial Fe(III) reduction in subsurface environments. *FEMS Microbiology Reviews*, *20*(3-4), 305-313.

Lovley D. (2013) Dissimilatory Fe(III)- and Mn(IV)-Reducing Prokaryotes. In: Rosenberg E., DeLong E.F., Lory S., Stackebrandt E., Thompson F. (eds) *The Prokaryotes. Springer, Berlin, Heidelberg*

Lippens, C., De Vrieze, J. (2019). Exploiting the unwanted: Sulphate reduction enables phosphate recovery from energy-rich sludge during anaerobic digestion. *Water Research*, 163, 114859

Liu, J., Cheng, X., Qi, X., Li, N., Tian, J., Qiu, B., Xu K. and Qu, D. (2018). Recovery of phosphate from aqueous solutions via vivianite crystallization: Thermodynamics and influence of pH. *Chemical Engineering Journal*, 349, 37-46.

Nevin, K. P., Lovley, D. R. (2000). Lack of production of electron-shuttling compounds or solubilization of Fe (III) during reduction of insoluble Fe (III) oxide by Geobacter metallireducens. *Applied and environmental microbiology,* 66(5), 2248-2251.

Nielsen P. H. (1996) The significance of microbial Fe(III) reduction in the activated sludge process. *Wat. Sci. Tech.* Vol. 34. No.s-e. pp. 129-136.

Nielsen, P. H., Frølund, B., Spring, S., Caccavo Jr, F. (1997). Microbial Fe (III) reduction in activated sludge. *Systematic and applied microbiology*, 20(4), 645-651.

Priambodo, R., Shih, Y. J., and Huang, Y. H. (2017). Phosphorus recovery as ferrous phosphate (vivianite) from wastewater produced in manufacture of thin film transistor-liquid crystal displays (TFT-LCD) by a fluidized bed crystallizer (FBC). *RSC advances*, 7(65), 40819-40828.

Prot, T., Nguyen, V. H., Wilfert, P., Dugulan, A. I., Goubitz, K., De Ridder, D. J., Korving L. Rem P., Bouderbala A. Witkamp G.J. and Van Loosdrecht, M. C. M. (2019). Magnetic separation and characterization of vivianite from digested sewage sludge. *Separation and Purification Technology*, 224, 564-579.

Prot, T., Wijdeveld, W., Eshun, L. E., Dugulan, A. I., Goubitz, K., Korving, L., van Loosdrecht, M. C. M. (2020). Full-scale increased iron dosage to stimulate the formation of vivianite and its recovery from digested sewage sludge. *Water Research*, 182.

Rasmussen, H., Nielsen, P. H. (1996). Iron reduction in activated sludge measured with different extraction techniques. *Water Research*, 30(3), 551-558.

Rebosura Jr, M., Salehin, S., Pikaar, I., Sun, X., Keller, J., Sharma, K., Yuan, Z. (2018). A comprehensive laboratory assessment of the effects of sewer-dosed iron salts on wastewater treatment processes. *Water research,* 146, 109-117.

Roden, E. E. (2003). Fe (III) oxide reactivity toward biological versus chemical reduction. *Environmental Science Technology*, *37*(7), 1319-1324.

Roden, E. E., Wetzel, R. G. (2003). Competition between Fe (III)-reducing and methanogenic bacteria for acetate in iron-rich freshwater sediments. *Microbial Ecology*, 45(3), 252-258.

Roussel, J., Carliell-Marquet, C. (2016). Significance of vivianite precipitation on the mobility of iron in anaerobically digested sludge. Frontiers in Environmental Science, 4, 60.

Schultze-Lam, S., Fortin, D., Davis, B. S., Beveridge, T. J. (1996). Mineralization of bacterial surfaces. *Chemical Geology,* 132(1-4), 171-181.

Smith S., Takács I., Murthy S., Daigger G. T. and Szabó A., (2008) Phosphate complexation model and its implications for chemical phosphorus removal. *Water Environment Research Vol. 80, No. 5, Nutrient Removal, pp. 428-438*

Southam, G. (2000). Bacterial surface-mediated mineral formation. Environmental microbe-metal interactions, 257-276.

Stumm, W., Sulzberger, B. (1992). The cycling of iron in natural environments: considerations based on laboratory studies of heterogeneous redox processes. *Geochimica et Cosmochimica Acta, 56(8), 3233-3257.*

Suschka, J., Machnicka, A., Poplawski, S. (2001) Phosphates Recovery from Iron Phosphates Sludge, Environmental Technology, 22:11, 1295-1301

Szabó, A., Takács, I., Murthy, S., Daigger, G. T., Licsko, I., Smith, S. (2008). Significance of design and operational variables in chemical phosphorus removal. *Water Environment Research*, *80*(5), 407-416.

Takács, I., Murthy, S., Smith, S., McGrath, M. (2006). Chemical phosphorus removal to extremely low levels: experience of two plants in the Washington, DC area. *Water Science and Technology*, 53(12), 21-28.

Varga E., Bounouba M., Takacs I. and Sperandio M. (2020) Significance of Fe(III) reduction and consequence on phosphate binding capacities *IWA Nutrient Removal and Recovery Virtual Conference presentation 1-3 September 2020*

Wang, R., Wilfert, P., Dugulan, I., Goubitz, K., Korving, L., Witkamp, G. J., van Loosdrecht, M. C. (2019). Fe (III) reduction and vivianite formation in activated sludge. *Separation and Purification Technology*, *220*, 126-135.

Wilfert, P., Mandalidis, A., Dugulan, A. I., Goubitz, K., Korving, L., Temmink, H., Witkamp G.J. and Van Loosdrecht, M. C. M. (2016). Vivianite as an important iron phosphate precipitate in sewage treatment plants. *Water research*, *104*, 449-460.

Wilfert, P., Meerdink, J., Degaga, B., Temmink, H., Korving, L., Witkamp, G. J., Goubitz K., van Loosdrecht, M. C. M. (2020). Sulfide induced phosphate release from iron phosphates and its potential for phosphate recovery. Water Research, 171, 115389.

Zhang, L., Keller, J., Yuan, Z. (2009). Inhibition of sulfate-reducing and methanogenic activities of anaerobic sewer biofilms by ferric iron dosing. *Water Research, 43(17), 4123-4132*.

3.7. Supplementary material

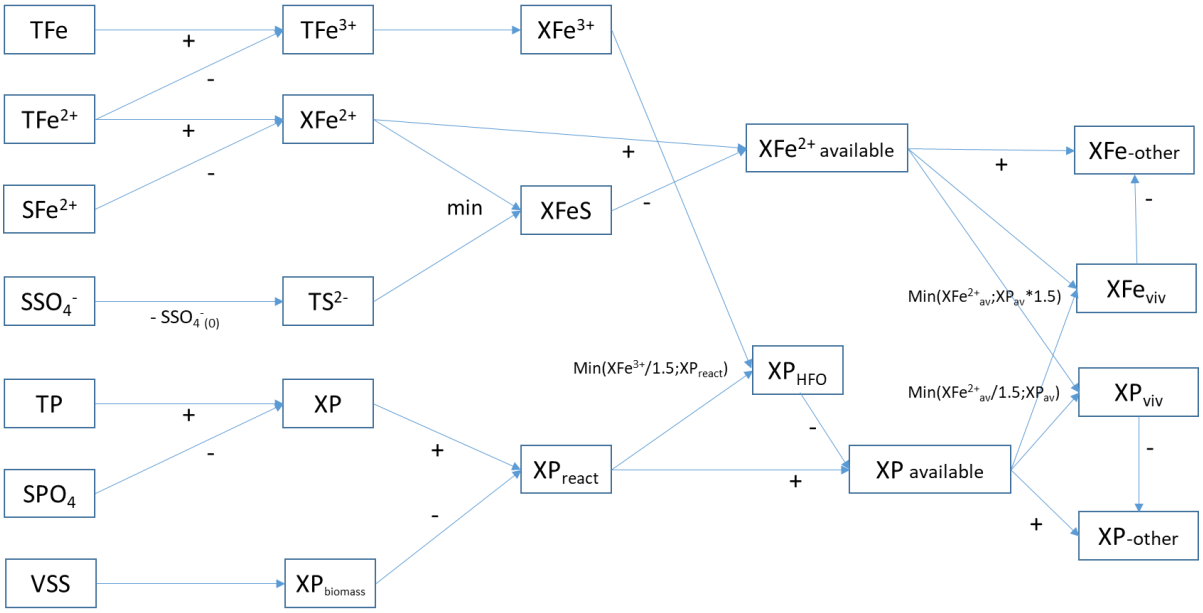

Figure S3. 1. Schematic diagram of the calculation method for determination of Fe, P fractionation. Notation: T for total concentrations particulate with X and soluble with S. Measured components: Total iron (TFe); Total iron(II) (TFe^{2+}); soluble Fe(II) (SFe^{2+}); Total phosphorus (TP); orthophosphate (SPO_4); sulphate (SSO_4). Calculated components: Ferric iron (XFe^{3+}); particulate ferrous (XFe^{2+}); consists of FeS (XFeS), vivianite (XFe_{viv}), and other precipitates, and Particulate phosphorus (XP) consists of Fe^{3+} bound Phosphorus, P in biomass (assumed to be constant); vivianite bound P and other P particulates.

Table S3. 1 Calculation for Fe, P fractionation

Component	Symbol	Calculation	Unit	Comment
Particulate iron(II)	XFe^{2+}	$TFe^{2+} - SFe^{2+}_i$	mmol Fe/l	
Particulate iron(III)	XFe^{3+}	$TFe - XFe^{2+}_i$	mmol Fe/l	Considered as HFO
Sulphide	TS^{2-}	$SSO4_{max} - SSO4_i$	mmol S/l	
FeS precipitate	XFeS	$Min(XFe^{2+}; TS^{2-})$	mmol Fe/l	Dependent on both available Fe and S
Available Fe for vivianite	XFe^{2+}_{av}	$XFe^{2+} - XFeS$	*mmol Fe/l*	*Including vivianite and other particulates*
Fe in Vivianite	XFe_{viv}	$Min(XFe^{2+}_{av}; XP_{av})$	mmol Fe/l	Dependent on available iron and P
Other particulate iron(II)	XFe^{2+}_{other}	$XFe^{2+} - XFeS - XFe_{viv}$	mmol Fe/l	Unspecified precipitates
Particulate P	XP	TP - SPO4	mmol P/l	
P in biomass	$XP_{biomass}$	0.02 * VSS	mmol P/l	Assumed to be constant
Reactive P particulates	XP_{react}	$XP - XP_{biomass}$	mmol P/l	Particulate P including various precipitates and stored PP
HFO precipitated P	XP_{HFO}	$Min(XP_{react}; X_{HFO}\text{-}P_{ini} + P_{released}; XFe^{3+}/1.5)$	mmol P/l	Dependent on available P (released and initial) and HFO
Available P for vivianite	XP_{av}	$XP_{react} - XP_{HFO}$	*mmol P/l*	
P in vivianite	XP_{viv}	$Min(XFe^{2+}_{av}/1.5; XP_{av})$	mmol P/l	Dependent on available Fe and P
Other particulate P	XP_{other}	$XP_{av} - XP_{viv}$	mmol P/l	

Temperature dependency of Fe(III) reduction

To assess the temperature dependency of iron reduction processes, a set of experiments were carried out at a controlled temperature. Reference cases at room temperature (~25°C), and two different scenarios: at 15°C and 35 °C.

Figure S3.2 presents the calculated reduction rates for different temperatures.

Due to a malfunction in the equipment in the low-temperature scenario, there is no duplicate available for that case, but it is still visible that colder temperature results lower rate whereas higher temperature results in a higher reduction rate. This phenomenon is expected during biological processes and this set of experiments confirms that. However, a significant variation was observed therefore the authors do not recommend a specific temperature dependency function (Arrhenius coefficient) at this stage, further experiments would be necessary.

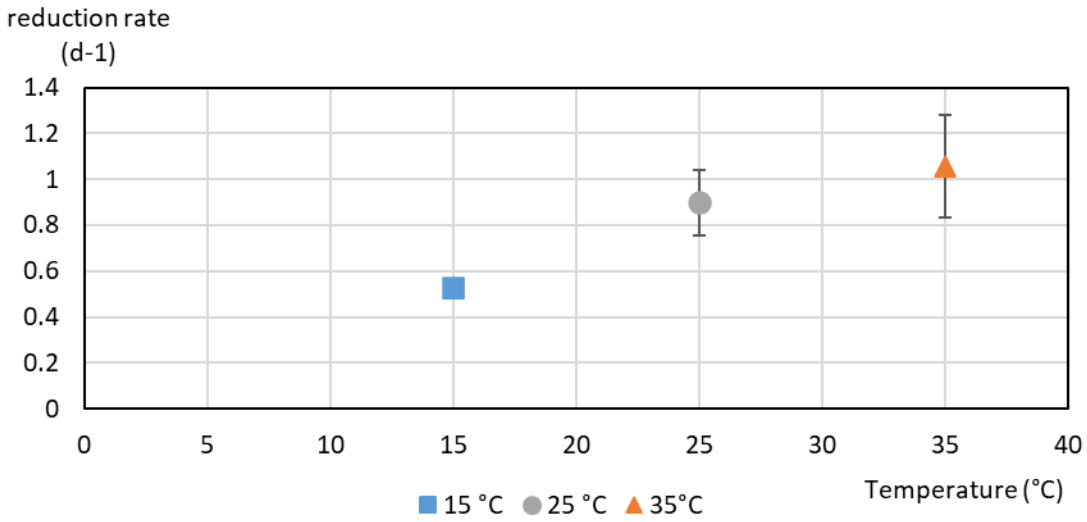

Figure S3. 2 Temperature dependency of iron reduction rate

Chapter 4 - Modelling combined biological and physical-chemical P removal in an intermittent aeration system

Highlights

- Process unit development and model calibration was carried out to simulate a highly dynamic control system of combined biological and physical-chemical P removal system
- Laboratory batch tests and full-scale data were used for calibration
- Variation of aeration pattern and the impact on P removal were simulated
- Iron redox reactions were adjusted and the impact of chemical dose on biological activity was introduced
- Detailed dynamic interactions were successfully simulated

Keywords

Combined P removal, aeration control, iron dose, model complexity

4.1. Introduction

In Chapter 2, a highly dynamic operational strategy of small/medium plants was presented using intermittent aeration and a specific chemical dosage strategy through the example of the Villefranche de Lauragais facility. This type of facility is fairly common in France and most cases optimized to complete nitrogen removal through nitrification-denitrification (Deronzier and Choubert, 2004). If an anaerobic zone is available, the P removal is carried out via combined biological and physical-chemical methods. The combination (i.e. the chemical dose) is necessary as there is not sufficient experience to rely on purely biological means in these systems. However, it is assumed that chemical doses may impose detrimental effects on biological processes (i.e. PHA storage). Therefore it is important to optimize the system to ensure proper effluent quality for ecological and economic reasons as well.

Intermittent aeration for nitrification and denitrification has a long history and uses different strategies, control methods, and cycle optimization to achieve high removal with minimizing energy use. The advanced control system implemented at the observed facility Villefranche de Lauragais (France) is based on bending points of continuously monitored operational parameters: dissolved oxygen (DO) and oxidation-reduction potential (ORP) which indicate the end of nitrification and denitrification, respectively. The theory is based on Paul *et al.* (1998) and the controller and monitoring system (*Inflex*) was developed by INSA Toulouse and commercialized by Biotrade.

The modeling of such an activated sludge system with combined physical-chemical treatment is feasible with different modeling frameworks (Hauduc *et al*., 2015; Solon *et al*., 2017; Mbamba *et al*., 2016). Hauduc *et al.* (2015) introduced a comprehensive dynamic model for chemical P removal which was included in the full-plant models on different platforms. The concepts consider five types of kinetic processes: Chemical Equilibrium dissociation (CED); Chemical Ion Pairing (CIP); Physical Mineral Precipitation (PMP) meaning the formation of hydrous ferric oxide (HFO) and co-precipitation of $FePO_4$; Chemical Surface Complexation (CSC) and HFO aging processes.

Further iron reactions and interactions with other components were considered by Hauduc *et al.* (2018). In this more recent work, sulfur reactions and interactions with iron and phosphorus in the plantwide model were considered. This model framework (SUMO2S) includes different oxidation states: three for sulfur (sulphate - SO_4^{2-}, elemental sulfur - S°, and reduced sulfide - S^-) and two for iron (ferric as particulate HFOs, ferrous as soluble Fe^{2+} and Fe(II) precipitates in separate processes).

Iron reduction is carried out via two pathways: sulfide and organic matter oxidation. This latter process represents microbially mediated reduction without the introduction of a new biomass. Reduced soluble Fe(II) precipitates with phosphate or sulfide and forms vivianite and ferrous sulfide (FeS) respectively. FeS and soluble Fe^{2+} are re-oxidized in aerobic zones chemically with oxygen as the electron donor.

Reduction processes were calibrated to sewer and digester conditions (Hauduc *et al.*, 2018) but a practical observation (Chapter 3) revealed that it may hold special significance in the anaerobic zones of the mainstream reactor or during sludge handling. The oxidation process and precipitation were not discussed in detail but recommendations were given based on observations at the facility and during experiments.

Regarding biological phosphorus removal, Varga *et al.* (2018) introduced PAO-GAO competition in the full plant model used by Sumo. Both groups use VFA as substrate and store PHA and glycogen respectively, a fraction being able to use nitrate as an electron acceptor. The major drivers of the competition were ORP (deep anaerobic conditions favor fermenting PAOs) as well as temperature (higher temperatures favor GAO) and micro-aerated conditions (that favor PAOs). This modeling concept can describe a wide range of configurations and is especially advantageous for side-stream processes. However, the competition needed to be described more accurately, and therefore the general concept was restructured. A major group of carbon-storing organisms (CASTO) was introduced in Sumo21 and this group is differentiated into PAO-GAO groups as opposed to two, parallel competitors. This change unifies the growth (aerobic and anoxic, considering both carbon storage components) maintenance (aerobic and anoxic), and decay processes of both groups while fractionating the group into PAO and GAO based on individual storage components (PHA for PAO coupled with P release and GLY for GAO), anaerobic maintenance (PP cleavage for PAO and GLY for GAO). Polyphosphate storage under aerobic and anoxic conditions and fermentation under deep ORP conditions are specific to PAOs.

In the model, interactions between biological and chemical processes are not included but they are presented as independent processes (with only metabolic limitation for phosphorus that may represent). However, the literature suggests that chemical dose may be detrimental to biological processes. This chapter considers the effect of iron dose exclusively. Different studies (de Haas *et al*, 2000, Valve *et al*, 2002, Liu *et al.* 2011, Fan *et al*, 2018) found that the presence of iron has adverse effects on VFA uptake.

Modeling such a complex system is not without its challenges. The aim of this chapter is to define the bottlenecks of the full-plant model regarding this highly dynamic activated sludge facility and propose modifications/extensions to the current model structure.

It is important to consider these types of facilities in modeling, as intelligent control systems are gaining more attention not only for large plants but also for smaller ones as well. Moreover, the overall impact of small/medium facilities must not be underestimated as they serve a significant fraction of the population and digital solutions that are calibrated for large plants often need to be readjusted.

4.2. Process unit development

4.2.1. Influent characterization and influent Process Unit

The plant model was developed in Sumo software (version 21) using the Sumo2S focus model, which was modified and renamed as Sumo2Fe (to indicate the additional focus on iron reactions). Sumo21 provides influent process units and fractionation tools for each Sumo model in a different version to properly fit the available data of the users.

A Series of experiments (sampling and monitoring) were carried out in order to characterize influent patterns at the Villefranche de Lauragais facility. The plant configuration and operation were described in detail in chapter 2.2.1. The dates were chosen without additional external sludge and without precipitation prior to the sampling dates (due to significant infiltration, this could have altered the profile). During a 24-hour period, hourly samples were taken with an automatic sampler (Reseau31) which was later analyzed at the laboratory (TBI). Standard methods were used to measure: total and soluble COD, total suspended solids (TSS), total phosphorus and orthophosphate, total Kjeldahl nitrogen, nitrite, nitrate, and ammonia.

For these simulations, Sumo2S concentration-based influent was modified. To better describe the observed patterns, instead of influent concentrations of specific parameters (influent flow, total suspended solids, total COD, total Kjeldahl nitrogen, and total phosphorus), an average value was added as an input parameter with a pattern fraction parameter. This is convenient for seasonal or diurnal variation. Here, the diurnal pattern is implemented, i.e. the daily average concentrations (composite samples from the facility) and correlating daily fraction parameters as a dynamic input table.

Observing the diurnal variations allows us to check other indicators of the impact of the influent composition on the operating and efficiency potential. Rieger *et al.* (2012) present typical ratios of influent fractions at several wastewater treatment plants.

Additionally, it is interesting to look at the pattern of these ratios as well, as typically small facilities have higher amplitudes in their daily patterns. As the P removal is carried out in a combined way, it is important to consider influent COD fractionation to assess bioP potential (and possibly adapt chemical dose or other operational parameters). It is well observed that the fraction of soluble COD changes significantly during the day which can have an impact on bioP removal, especially regarding that during these otherwise high load periods, aerated time phases are longer and unaerated is shorter, hence efficient COD supply is necessary for PHA storage. The measured soluble COD profile was thus implemented to calculate the diurnal variation of the COD fraction.

4.2.2. Operational inputs: alternated aeration and sludge wastage

A general description of the A/O process with alternated aeration which was simulated on SUMO software is presented on Figure 4.2-1.

Intermittent aeration. The activated sludge system is composed of an anaerobic basin followed by the main basin with alternated aeration. For piloting intermittent aeration, *Inflex* control system was operated as such during the period of the CircRural 4.0 project: a) in case of high load (the α bending point is not found within the cycle), aeration time is set to maximum (1h) and unaerated time to a minimum (1h) b) in case of low/medium load (the bending point is detected within the cycle) aeration time varies between 15-59 min (15 being the minimum) and unaerated time is set to maximum (1.5 h).

To simulate the operation of the *Inflex* controller, a simplified approach to the definition of low/high load periods was implemented within the CSTR unit based on influent ammonia load. This feature compares the moving average (24 hours-moving average by default) of the influent ammonia load (kg/d) to the current influent and by parameters (0.25 and 1.45 by default) distinguishes between high and low load. During the high load period, the aeration time is set to maximum and unaerated time to a minimum while in low load periods the opposite is true: aeration time is minimum and unaerated time is maximum. The length of the periods that fall between these load conditions is proportional to the load. The code in SumoSlang can be found in Supplementary Material.

MLSS control and sludge wastage. MLSS in the aeration tank was set between 4800-5000 g/m^3 for the steady state in normal conditions or adapted to specific date measurements. Sludge wastage was controlled according to automatic regulation in order to maintain the desired MLSS setpoint.

Sludge dewatering was carried out by centrifuge (dewatered sludge of 20% solid content) and extended with a small reactor to simulate observed phosphate release. Return sludge liquor passes through a small "mixing tank" for the purpose of HFO reactions (reactive volume is required in Sumo).

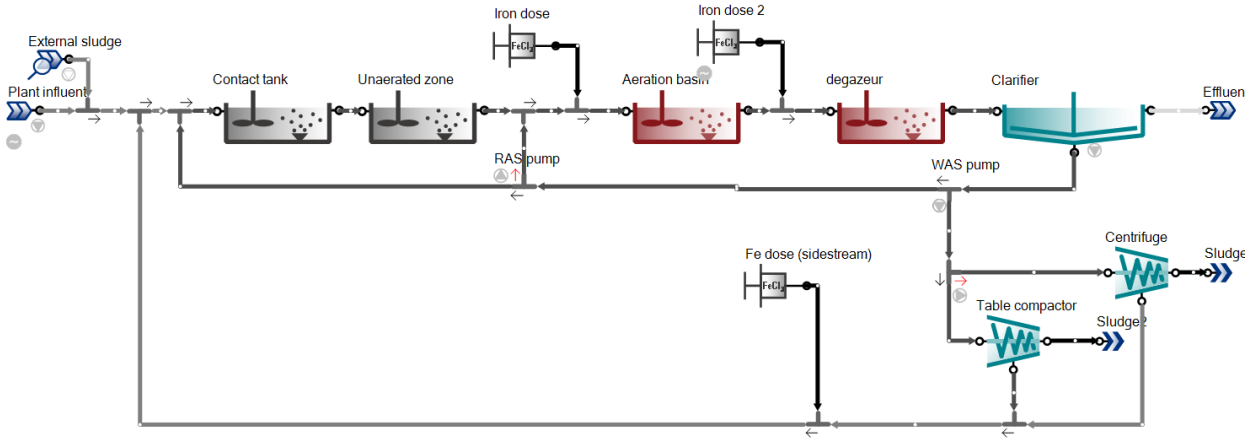

Figure 4.2-1 Villefranche de Lauragais plant configuration in Sumo21. ($V_{contact\ tank}$=33 m^3; V_{ana}= 350 m^3; $V_{aeration}$= 2410 m^3; V_{degas}= 24 m^3)

4.3. Process model basis and extension

4.3.1. Calibration Overview

Concerning the specific challenges of the facility and the results of the measurement campaign, laboratory experiments, and initial simulations with the default model, the calibration protocol of Figure 4.3-1 was followed for the model development.

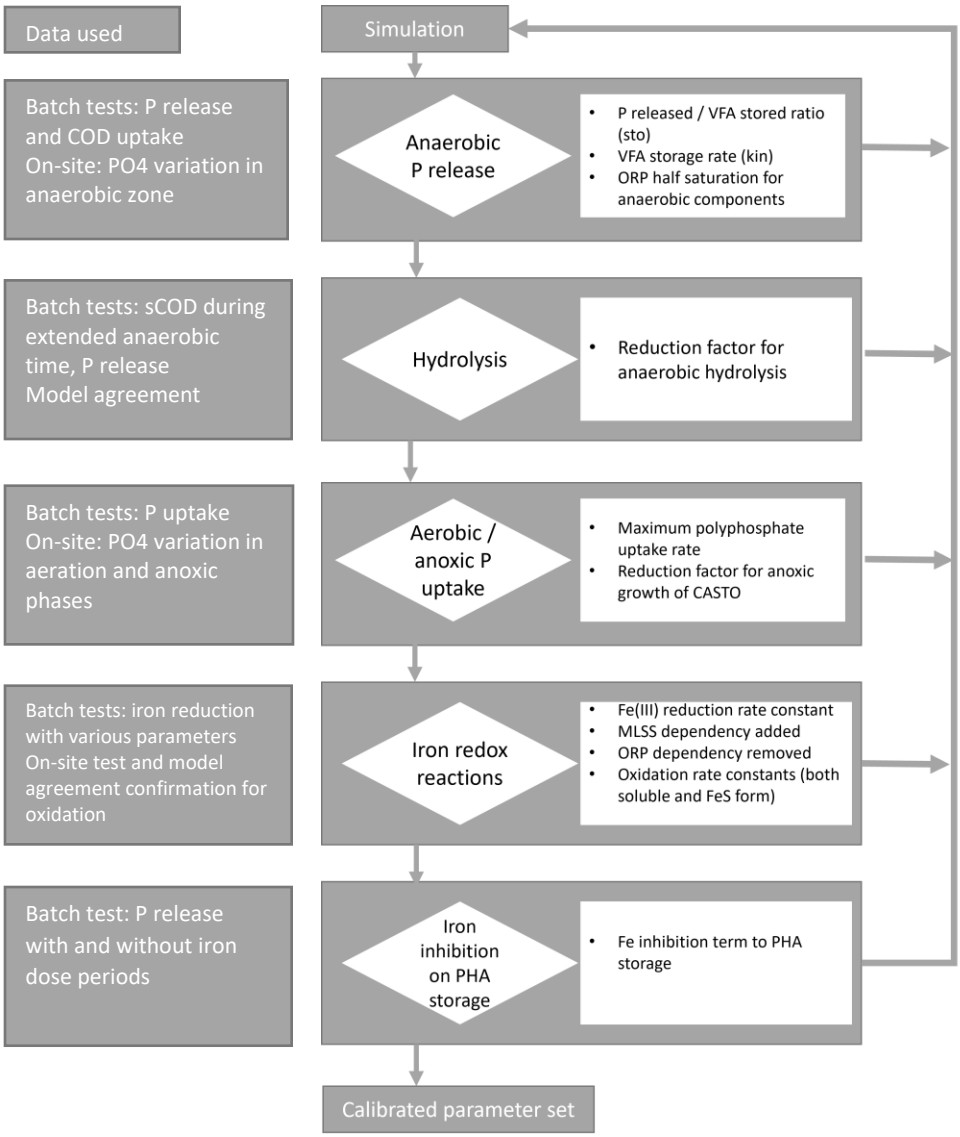

Figure 4.3-1 Calibration steps for model extension

4.3.2. Biological P removal processes

As explained in the introduction the adapted PAO/GAO model (Varga *et al*., 2018) was used in this study, but considering a single carbon-storing organism category (CASTO). PHA storage from VFA and PP cleavage is one of the main anaerobic processes of PAOs. Stored PHA drives aerobic and anoxic growth and polyphosphate storage, and therefore is crucial for phosphate removal efficiency. The major processes and all the parameters are given in Table 4.3-2 and Table 4.3-4.

Different experimental data were obtained to assess the biological phosphorus removal processes. P release and uptake tests were performed with VFA dose to determine the maximum P release rate at the facility.

When biological and physical-chemical treatment is combined, the processes in activated sludge systems are complex and interconnected in every stage of the process. During the initial simulations, the overestimated anaerobic P release (and subsequent uptake) was observed and synergies between biological and chemical processes were evaluated. While the introduction of Fe inhibition mitigates this effect, there are more parameters to consider under these specific conditions: 1) PAO-GAO competition in the anaerobic zone and 2) OHO fermentation which is a direct result of anaerobic hydrolysis.

PAO and GAO are competing for substrate under anaerobic conditions; each can store a single carbon storage component (PHA and glycogen respectively) with specific storage rates. The competition is driven by the uptake rates and the saturation of the storage pools. Moreover, under low ORP conditions, VFA uptake by PAOs is the dominant process, and fermentation by PAOs begins. ORP calculations are based on DO, nitrate concentrations for aerobic and anoxic conditions, and anaerobic conditions are represented by the combined concentration of dissolved H_2 (fermentation product), dissolved H_2S (product of sulphate reduction), and dissolved CH_4 (methanogenesis). This serves as an indicator for ORP conditions, however, cannot simulate the exact measured pattern.

The general setup of the configuration would theoretically allow deep ORP conditions and therefore the encouragement of the related processes, however, these do not align with the observations at the facility. In fact, the observations of the anaerobic zone indicate significant, but not as enhanced PAO activity as one would expect. To mitigate the impact of the ORP-dependent processes that probably cause a discrepancy between the model and measured concentration, half-saturation coefficients of the anaerobic redox-active components have been increased. This means that a higher concentration of these products would influence the ORP values.

This modification helps to describe the actual observations at this facility without re-calibrating related anaerobic process, however, the exact interactions are not well understood therefore using this parameter change need to be handled with caution for other facilities with less real-time data.

The following tables (Table 4.3-1, Table 4.3-2, Table 4.3-3, and Table 4.3-4,) include all parameters and variables that were considered during the model calibration. The nomenclature used in this thesis is consistent with the one used in Sumo21 software and is based on Corominas et al (2010)

4.3.3. Hydrolysis

During the initial simulation, a high variation of biomass activity was observed in the anaerobic zone. This was indirectly the result of high hydrolysis that occurred according to the model as the retention time is high at the facility. Due to this high anaerobic hydrolysis, fermentable organic matter and hydrogen were produced, which then encouraged phosphate release as well as lowered the ORP (the main driver in PAO-GAO competition, therefore causing higher amplitudes of P concentration during cycles). While the hydrolysis rate is rather consistent in different models, the anaerobic reduction factor defines the slow/fast rate of hydrolysis. This parameter in Sumo is tending to faster hydrolysis and it was decreased to simulate our conditions.

4.3.4. HFO kinetics

Based on the surface complexation model (Smith *et al*, 2008) which is implemented in this full plant model, (Hauduc *et al*. 2015) $FeCl_3$ precipitates as high and low surface HFO immediately depending on the velocity gradient (mixing) at the dosage point. Phosphorus binds to HFO by two processes: fast binding on the high surface HFO (coprecipitation) and slow binding on low surface HFO. Desorption and aging occur from both complexes with different kinetic rates. Aging limits the active sites but in itself does not cause a change in P concentration, while a dissolution process is also included. These processes are included here to demonstrate all iron processes included in the model. Only a specific change was proposed for a local parameter in the dewatering process in order to simulate the observed phosphate release from HFOs.

4.3.5. Fe reduction

In Chapter 3 experiments, it was concluded that Fe(III) reduction starts as soon as anaerobic conditions are provided and follows first-order kinetics. The findings have been implemented in the full plant Sumo model (extension named: Sumo2Fe to distinguish between the original Sumo2S model). The kinetic rate constant and VSS dependency were implemented according to the finding. Temperature dependency of the process was confirmed by experiments (Supplementary Material, Chapter 3), but a significant standard deviation was observed and the set of results was not conclusive enough for parameter calibration and validation, therefore the default Arrhenius coefficient was used throughout the simulations. The description of iron reduction based on ORP dependency proposed in the Sumo2S model was changed. The iron reduction rate was preferably related to anaerobic indicators (inhibition terms by O_2, NO_2, and NO_3) and a single electron donor component (as VFA + readily biodegradable substrate) was introduced. The final reduction rate expression can be found in Table 4.3-4.

4.3.6. Iron oxidation

Fe(II) oxidation is included in Sumo2S full-plant model as two distinct processes: 1) Oxidation of soluble Fe^{2+} and 2) Oxidation of FeS. Both reactions are abiotic and use oxygen as the sole electron donor and are carried out at the same rate. Exact oxidation rates of soluble Fe(II) and precipitates in activated sludge are not well characterized, however, based on literature findings, it is assumed that iron oxidation takes a higher rate than iron reduction. While literature suggests several pathways for Fe(II) oxidation (abiotic, microbially mediated aerobic, nitrate-reducing) current work aims to adjust the current model structure through parameters due to the lack of comprehensive study on activated sludge. On-site measurements show negligible Fe(II) concentration in the aeration basin, which is not the case in the long-term simulation with the default Sumo2S model. Indeed, the model initially contained lower oxidation rates than reduction rates, which (especially in the alternated aeration systems with long SRT) would overestimate the Fe(II) components, specifically precipitates. It is also assumed that soluble and precipitated ferrous iron reduction rates vary significantly. The parameters have been adjusted in accordance with the literature data and on-site observations.

Table 4.3-1 Model state variables

Symbol	Name	Unit
S_{VFA}	Volatile fatty acids (VFA)	g COD.m^{-3}
S_B	Readily biodegradable substrate (non-VFA)	g COD.m^{-3}
X_{PHA}	Stored polyhydroxyalkanoates (PHA)	g COD.m^{-3}
X_{GLY}	Stored glycogen (GLY)	g COD.m^{-3}
X_{CASTO}	Carbon storing organisms (CASTO)	g COD.m^{-3}
S_{PO4}	Orthophosphate (PO_4)	g P.m^{-3}
X_{PP}	Stored polyphosphate (PP)	g P.m^{-3}
S_{O2}	Dissolved oxygen (O_2)	g O_2.m^{-3}
S_{CH4}	Dissolved methane (CH_4)	g COD.m^{-3}
S_{H2}	Dissolved hydrogen (H_2)	g COD.m^{-3}
S_{CO2}	Total inorganic carbon (CO_2)	g TIC.m^{-3}
S_{H2S}	Hydrogen sulfide (H_2S)	g S.m^{-3}
S_{SO4}	Sulfate (SO_4)	g S.m^{-3}
S_{Fe2}	Ferrous ion (Fe^{2+})	g Fe.m^{-3}
$X_{HFO,H}$	Active hydrous ferric oxide, high surface (HFO,H)	g Fe.m^{-3}
$X_{HFO,L}$	Active hydrous ferric oxide, low surface (HFO,L)	g Fe.m^{-3}
$X_{HFO,old}$	Aged unused hydrous ferric oxide (HFO,old)	g Fe.m^{-3}
$X_{HFO,H,P}$	P-bound hydrous ferric oxide, high surface (HFO,H,P)	g Fe.m^{-3}
$X_{HFO,L,P}$	P-bound hydrous ferric oxide, low surface (HFO,L,P)	g Fe.m^{-3}
$X_{HFO,H,P,old}$	Aged used hydrous ferric oxide, high surface (HFO,H,P,old)	g Fe.m^{-3}
$X_{HFO,L,P,old}$	Aged used hydrous ferric oxide, low surface (HFO,L,P,old)	g Fe.m^{-3}
X_{Vivi}	Vivianite (Vivi)	g TSS.m^{-3}
X_{FeS}	Iron sulfide (FeS)	g TSS.m^{-3}

Table 4.3-2 Model parameters

Symbol	**Name**	**Default**	**Unit**
Carbon storing organism kinetics (CASTO)			
$q_{PAO,PHA}$	Rate of VFA storage into PHA for PAOs	7.0	d^{-1}
$Logrange_{PP,PAO,AS,sat}$	Effective range of logistic switch for PP cleavage by PAOs	0.40	-
$K_{PHA,cle}$	Half-saturation of PHA for PAOs at PP cleavage	0.10	g COD.g COD^{-1}
K_{PHA}	Half-saturation of PHA for PAOs	0.01	g COD.g COD^{-1}
K_{STC}	Half-saturation of PHA and GLY for PAOs	0.10	g COD.g COD^{-1}
$K_{O2,CASTO,AS}$	Half-saturation of O_2 for CASTOs (AS)	0.05	g O_2.m^{-3}
$K_{VFA,CASTO,AS}$	Half-saturation of VFA storage for CASTOs (AS)	5.0	g COD.m^{-3}
K_{PP}	Half-saturation of PP for PAOs	0.01	g COD.g COD^{-1}
$Ki_{PP,PAO,max}$	Half-inhibition of maximum PP content of PAOs	0.35	g P.g COD^{-1}
$Ki_{HFO,PAO}$	Half-inhibition of Fe(III) on VFA uptake	30.00	g Fe.g COD^{-1}
$Logrange_{PP,PAO,inh}$	Effective range of logistic switch for PP/PAO inhibition term	0.17	-

$X_{PP,PAO,min}$	PAO PP uptake booster denominator limiting term	0.10	g COD.m^{-3}
$Ki_{PHA,PAO,max}$	Half-inhibition of maximum PHA content of PAOs	0.60	g COD.g COD^{-1}
$Logrange_{PHA,PAO,inh}$	Effective range of logistic switch for PHA/PAO inhibition term	0.10	-
$Logsat_{ORP,PAO,Half}$	Logistic half-saturation of ORP switching in fermentation of PAO	-170.0	mV
$Logsat_{ORP,PAO,Slope}$	Logistic slope of ORP switching in fermentation of PAO	0.1	mV^{-1}
$\eta_{bGLY,ana}$	Reduction factor for anaerobic maintenance of GAOs on glycogen	0.10	unitless
K_{GLY}	Half-saturation of glycogen for GAOs (AS)	0.05	g COD.g COD^{-1}
$Ki_{GLY,GAO,max}$	Half-inhibition of maximum glycogen content of GAOs (AS)	0.5	g COD.g COD^{-1}
$Logrange_{GLY,GAO,inh}$	Effective range of logistic switch for GLY/GAO inhibition term	0.12	-
$Logsat_{ORP,GAO,Half,15}$	Half-value of ORP switch of glycogen storage by GAO at 15°C / 59°F	-30	mV
$Logsat_{ORP,GAO,Half,25}$	Half-value of ORP switch of glycogen storage by GAO at 25°C / 77°F	-110	mV
$Logsat_{ORP,GAO,Slope}$	Logistic slope of ORP switching of GAOs	0.035	mV^{-1}
Precipitation kinetics			
$q_{Vivi,PREC}$	Rate of vivianite precipitation	0.01	g.m^{-3}.d^{-1}
$q_{Vivi,DISS}$	Rate of vivianite dissolution	0.01	g.m^{-3}.d^{-1}
$q_{FeS,PREC}$	Rate of FeS precipitation	2.00E-07	g.m^{-3}.d^{-1}
$q_{FeS,DISS}$	Rate of FeS dissolution	2.00E-07	g.m^{-3}.d^{-1}
$K_{FeS,DISS}$	Half-inhibition of FeS redissolution	0.010	g TSS.m^{-3}
$K_{Vivi,DISS}$	Half-saturation of vivianite redissolution	0.01	g TSS.m^{-3}
HFO kinetics			
$q_{HFOH,AGING}$	Rate of $X_{HFO,H}$ aging	250	d^{-1}
$q_{HFOL,AGING}$	Rate of $X_{HFO,L}$ aging	1.00	d^{-1}
$q_{P,HFO,COPREC}$	Rate of P binding and coprecipitation on XHFO,H	150	d^{-1}
$q_{P,HFO,BIND}$	Rate of P binding on XHFO,L	1.00	d^{-1}
$q_{HFOH,DESORP}$	Rate of $X_{HFO,H,P}$ desorption	100	d^{-1}
$q_{HFOL,DESORP}$	Rate of $X_{HFO,L,P}$ desorption	10	d^{-1}
$q_{HFO,DISS}$	Rate of $X_{HFO,H,P,old}$ and $X_{HFO,L,P,old}$ redissolution	100	d^{-1}
$q_{HFO,RED}$	Rate of HFO reduction with organics	2.7	d^{-1}
$K_{VSS,HFO,red}$	Half-saturation of VSS in HFO reduction	3230.0	g VSS. m^{-3}
$K_{edonor,HFO,red}$	Half-saturation of organic matter in HFO reduction	0.010	g COD. m^{-3}
$Ki_{P,HFO,DISS}$	Half-inhibition of PO_4 in HFO redissolution	0.010	g P.m^{-3}
$Logrange_{P,HFO,DISS}$	Effective range of logistic switch for HFO redissolution	1.00	-
$Ki_{P,HFO,DESORP}$	Half-inhibition of PO_4 in HFO desorption	0.100	g P.m^{-3}
$K_{P,HFO,BIND}$	Half-saturation of PO_4 in binding on HFO	0.10	g P.m^{-3}
$q_{HFO,H2S,RED}$	Rate of HFO reduction with H_2S	2.0	d^{-1}
$q_{Fe2,OX}$	Rate of Fe_2 oxidation	1.0	d^{-1}
$q_{FeS,OX}$	Rate of FeS oxidation	1.0	d^{-1}
$Ki_{SO4,RED}$	Half-inhibition of SO_4 in HFO reduction with SO_4	0.20	g S.m^{-3}
HFO stoichiometry			
$ASF_{HFO,H}$	Active site factor for HFO,H	1.2	mol P.mol Fe^{-1}
$ASF_{HFO,L}$	Active site factor for HFO,L	0.2	mol P.mol Fe^{-1}

$f_{H2O,HFO,TSS}$	Fraction of H_2O loss in TSS test for HFO	0.0829	g H2O.g $FeOH^{-1}$
$f_{H2O,HFO,VSS}$	Fraction of H2O loss in VSS test for HFO	0.17	g H2O.g $FeOH^{-1}$
Stoichiometric yields			
$f_{P,VFA}$	Ratio of P released per VFA stored	0.65	g X_{PP}.g S_{VFA}^{-1}
Temperature dependency			
$\theta_{q,PAO,PHA}$	Arrhenius coefficient for PHA storage	1.040	unitless
$\theta_{q,Fe2,OX}$	Arrhenius coefficient for ferrous iron oxidation kinetics	1.040	unitless
$\theta_{q,FeS,OX}$	Arrhenius coefficient for ferrous iron sulfide oxidation kinetics	1.040	unitless
$\theta_{q,HFO,RED}$	Arrhenius coefficient for ferric iron reduction kinetics	1.040	unitless
$\theta_{q,HFO,H2S,RED}$	Arrhenius coefficient for ferric iron reduction with sulfide kinetics	1.000	unitless
T_{base}	Arrhenius base temperature	20.0	C^o
Oxidation-reduction potential constants			
ORP_{base}	Base ORP value	-300	mV
$ORP_{max,SO2}$	ORP max for dissolved oxygen	300	mV
$ORP_{max,SNOx}$	ORP max for dissolved nitrate	70	mV
$K_{ORP,SO2}$	Half-saturation of dissolved oxygen for ORP	0.05	g O2.m^{-3}
$K_{ORP,SNOx}$	Half-saturation of NO_x for ORP	0.1	g N.m^{-3}
$K_{ORP,H2,CH4,H2S}$	Half-saturation of dissolved hydrogen, methane and hydrogen sulfide for anaerobic ORP	5	g COD.m^{-3}

Table 4.3-3 Sumo functions for calculated variables

Symbol	**Name**	**Expression**
Msat(var; k)	Monod saturation	var / (k + var)
Minh(var; k)	Monod inhibition	k / (k + var)
MRsat(s;x;k)	Monod ratio saturation	(s/x)/(s/x+k)
MRinh(s;x;k)	Monod ratio inhibition	(k)/(s/x+k)
Logisticslope(halfval; range)	Slope for logistic saturation and inhibition functions	(-1)*(2 / (halfval * range)) * Ln((1/19) * (1 + (1/2) * (halfval * range / halfval)))
Logsat(var; halfval; slope)	Logistic saturation	var / (var + halfval * Exp((halfval - var) * slope))
Loginh(var; halfval; slope)	Logistic inhibition	1 - var / (var + halfval * Exp((halfval - var) * slope))
Logsatswitch(var; halfval; slope)	Logistic saturation switch	1 / (1 + Exp((halfval - var) * slope))
Loginhswitch(var; halfval; slope)	Logistic inhibition switch	1 / (1 + Exp((var - halfval) * slope))
Arrh(theta;temp;tbase)	Temperature sensitivity	theta^(temp-tbase)

Note: the described calculation of the functions in this table later refers to specific values indicated in the symbol. Eg. $Msat_{SO2,KO2,CASTO}$ refer to Monod saturation term of dissolved oxygen for CASTO. All related parameters have been introduced in these tables.

Table 4.3-4 A selection of kinetic rates

Process	Kinetic rate expression
Biological P removal	
CASTO growth on PHA and GLY, O_2	$\mu_{CASTO,T} * X_{CASTO} * MRsat_{XSTC,XCASTO,KSTC} * Msat_{SO2,KO2,CASTO} * Msat_{SNHx,KNHx,BIO} * Msat_{SPO4,KPO4,BIO} * Msat_{SCAT,KCAT} * Msat_{SAN,KAN} * Msat_{SCa,KCa,PAO} * Msat_{SMg,KMg,PAO} * Msat_{SSO4,KSO4,BIO} * Bellinh_{pH}$
CASTO growth on PHA and GLY, NO_3	$\mu_{CASTO,T} * X_{CASTO} * \eta_{CASTO,anox} * MRsat_{XSTC,XCASTO,KSTC} * Msat_{SNO3,KNO3,CASTO} * Minh_{SO2,KO2,CASTO} * Minh_{SNO2,KNO2,CASTO} * Msat_{SNHx,KNHx,BIO} * Msat_{SPO4,KPO4,BIO} * Msat_{SCAT,KCAT} * Msat_{SAN,KAN} * Msat_{SCa,KCa,PAO} * Msat_{SMg,KMg,PAO} * Msat_{SSO4,KSO4,BIO} * Bellinh_{pH}$
PAO polyphosphate storage, O_2	$q_{PAO,PP,T} * X_{PAO}/(X_{PP}+X_{PP,PAO,min}) * X_{PAO} * Msat_{SO2,KO2,CASTO} * Logsat_{SPO4,KPO4,PAO} * Loginh_{XPP,XPAO,max} * Msat_{SCa,KCa,PAO} * Msat_{SMg,KMg,PAO} * Msat_{SK,KK,PAO} * Bellinh_{pH}$
PAO polyphosphate storage, NO_3	$q_{PAO,PP,T} * X_{PAO}/(X_{PP}+X_{PP,PAO,min}) * X_{PAO} * \eta_{CASTO,anox} * Msat_{SNO3,KNO3,CASTO} * Minh_{SO2,KO2,CASTO} * Minh_{SNO2,KNO2,CASTO} * Logsat_{SPO4,KPO4,PAO} * Loginh_{XPP,XPAO,max} * Msat_{SCa,KCa,PAO} * Msat_{SMg,KMg,PAO} * Msat_{SK,KK,PAO} * Bellinh_{pH}$
PAO's PHA storage from VFAs and PO_4 release	$q_{PAO,PHA,T} * X_{CASTO} * act_{sto,PAO,ORP} * Msat_{SVFA,KVFA,CASTO} * MRsat_{XPP,XPAO,KPP} * Minh_{HFO,PAO} * Loginh_{XPHA,XPAO,max}$
GAO's GLY storage from VFAs	$q_{GAO,GLY,T} * X_{CASTO} * act_{sto,GAO,ORP} * Msat_{SVFA,KVFA,CASTO} * Loginh_{XGLY,XGAO,max}$
Physical-chemical processes for P removal	
Aging of active HFO,H	$q_{HFOH,AGING} *(X_{HFO,H}+X_{HFO,H,P})$
Aging of active HFO,L	$q_{HFOL,AGING} *(X_{HFO,L}+X_{HFO,L,P})$
Fast binding of P on active HFO,H	$q_{P,HFO,COPREC} * X_{HFO,H} * Msat_{SPO4,KP,HFO,BIND}$
Slow binding of P on active HFO,L	$q_{P,HFO,BIND} * X_{HFO,L} * Msat_{SPO4,KP,HFO,BIND}$
Desorption of P from $X_{HFO,H,P}$	$q_{HFOH,DESORP} * X_{HFO,H,P} * Minh_{SPO4,KiP,HFO,DESORP}$
Desorption of P from $X_{HFO,L,P}$	$q_{HFOL,DESORP} * X_{HFO,L,P} * Minh_{SPO4,KiP,HFO,DESORP}$
Dissolution of P from $X_{HFO,H,P,old}$ and $X_{HFO,L,P,old}$	$q_{HFO,DISS} *(X_{HFO,H,P,old}+X_{HFO,L,P,old}) * Loginh_{SPO4,KiP,HFO,DISS}$
Reduction of X_{HFO} with organic matter	$q_{HFO,RED,T} * X_{HFO} * Minh_{SO2,KO2,OHO} * Minh_{SNO2,KNO2,OHO} * Minh_{SNO3,KNO3,OHO} * Msat_{edonor,XHFO,red} * Msat_{XVSS,XHFO,red}$
Reduction of X_{HFO} with sulfide	$q_{HFO,H2S,RED,T} * X_{HFO} * Minh_{SO2,KO2,OHO} * Minh_{SNO2,KNO2,OHO} * Minh_{SNO3,KNO3,OHO} * Minh_{SSO4,KiSO4,RED} * Hsat_{SH2S,KH2S,SOO}$
Oxidation of Fe^{2+}	$q_{Fe2,OX,T} * S_{Fe2} * Msat_{SO2,KO2,CASTO}$
Oxidation of FeS	$q_{FeS,OX,T} * X_{FeS} * Msat_{SO2,KO2,CASTO}$
Vivianite precipitation	$q_{Vivi} *((([Fe^{2+}]^{(3/5)} * [PO_4^{3-}]^{(2/5)} - K_{sp,Vivi}^{(1/5)})/K_{sp,Vivi}^{(1/5)}))^2$
Iron sulfide precipitation	$q_{FeS} *((([Fe^{2+}]^{(0.5)} * [HS^-]^{(0.5)} - K_{sp,FeS}^{(0.5)})/K_{sp,FeS}^{(0.5)})^2$

4.4. Results and discussion

4.4.1. Modeling aeration control and nitrogen removal

The calibrated configuration is able to show general trends in the operation settings, including the aeration intermittency. To illustrate standard operation, online data of the aeration tank was compared with simulation results. Specifically, the dates of 17-18 June 2019 were chosen as during these dates, a 24-hour sampling event took place and the influent load was then characterized. For this time, not the average, but the specific daily pattern was implemented as well as the MLSS concentration observed at that time.

Figure 4.4-1 presents the phase times in each cycle, assigned to the corresponding time when it was observed (2 days, measured data starting at 00:00 on 17. 06. 2019). Positive values correspond to aeration times and negative values to unaerated times. It is visible that the model values correspond to the measured values, although there is an oscillation in the unaerated phase time at the online measurement which occurs at the facility from time to time.

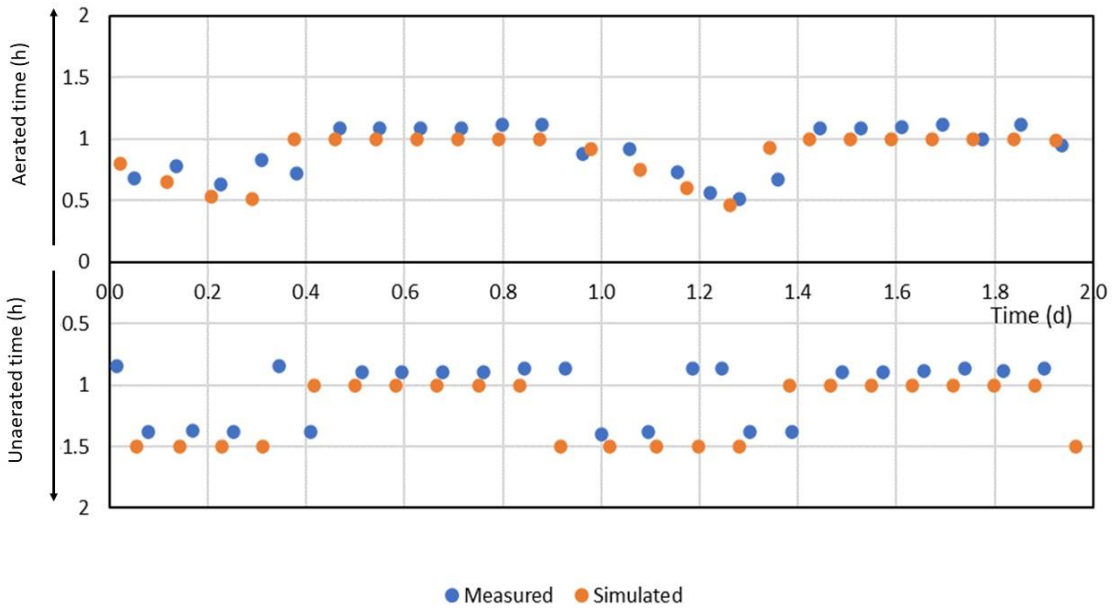

Figure 4.4-1 Aerated/unaerated phase time presentation (+ aerated, - unaerated) over 2 days. Measured data:17-18. 06. 2019

As there are slight differences in the phase times, it is expected that an offset is also present in the DO, ammonia, and nitrate patterns, therefore the simulated and measured results are presented separately. The pattern of cycle variation is still visible.

Figure 4.4-2 shows measured and simulated DO concentrations. It is clear that while the load is calibrated to the plant conditions with time, nitrification appears to be finished with each cycle in the process model while the bending point cannot be detected at the measured figure (although even during this time, ammonia concentration is rather low).

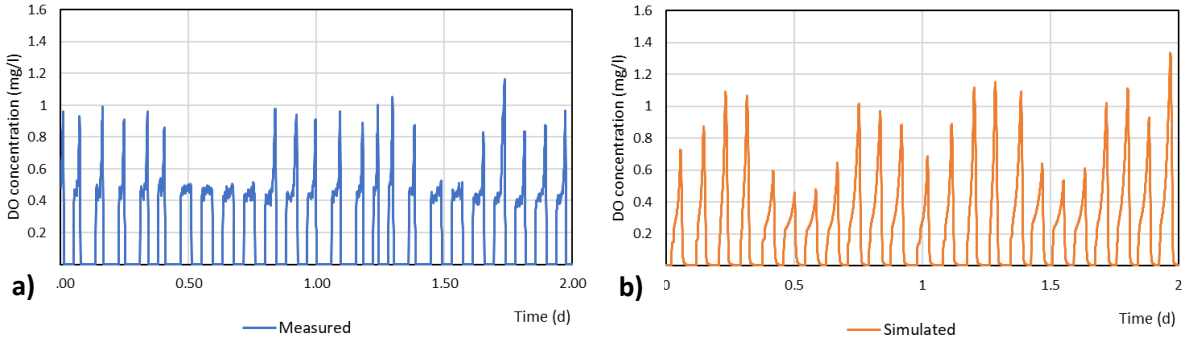

Figure 4.4-2 DO concentration in aeration basin a) measured Inflex sensor) b) simulated (Sumo) values

Nitrogen removal corresponds with aeration cycles. Globally the model describes well the average residual concentration in ammonia and nitrate as well as the maximum punctual concentration (generally around 1.5 mgN/L), corresponding to very high nitrification and denitrification efficiency. A slight daily increase in concentration can be observed in measurements (Figure 4.4-3) and simulation (Figure 4.4-4), however slightly higher variations in both monitored nitrogen components are simulated within the cycle.

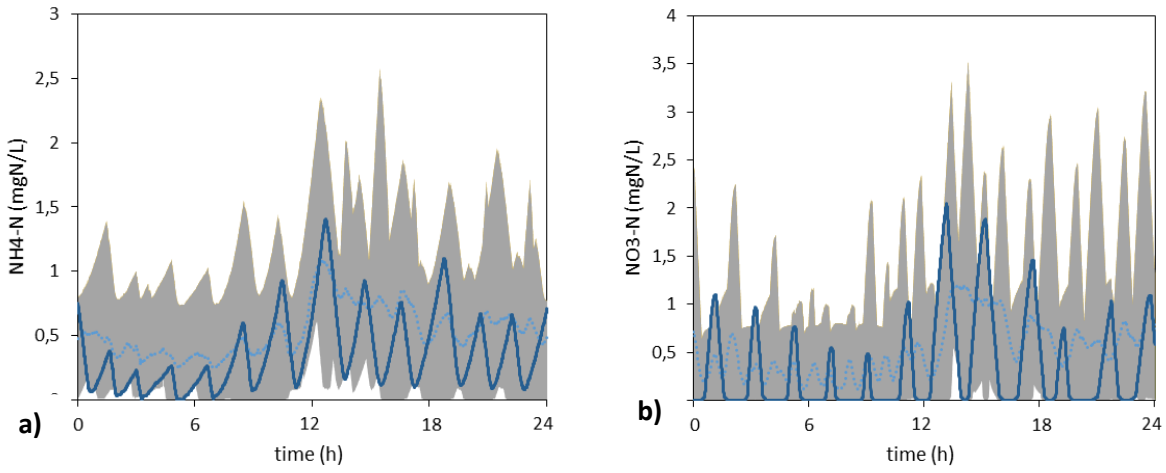

Figure 4.4-3 Typical daily profile measured with online sensors in the aerated basin. Ammonia (a) and nitrate (b). Dark blue: one typical example (2019), Grey zone: Min and max of a one-month period, blue light dot: average value.

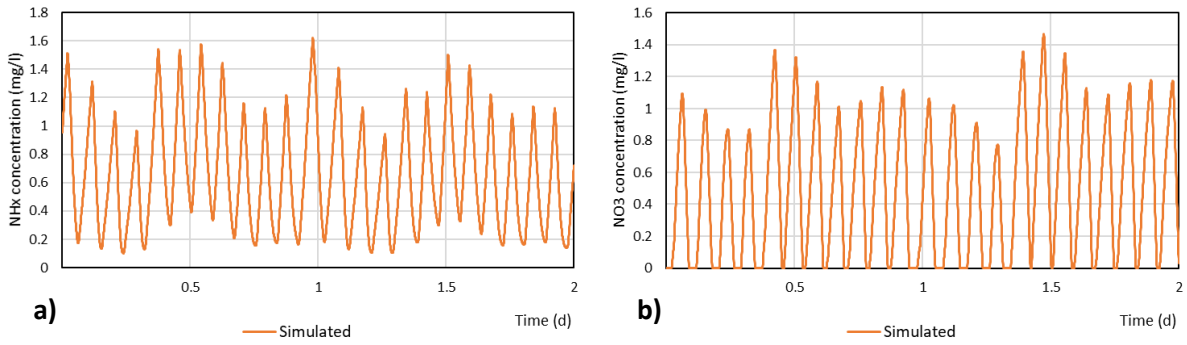

Figure 4.4-4 Simulated ammonia (a) and nitrate (b) concentrations (2 days)

Some aspects of the difference in variation can partially be explained with the calibration of the online sensors and process models. For instance at some moments, while at the facility measured nitrate concentrations can reach a minimum of around 0.2 mg N/L, the simulation shows almost complete nitrate removal. However such difference was relatively minor when we consider all the possible uncertainties.

4.4.2. Initial results for phosphorus removal with default parameters and calibration approach

Phosphorus removal was globally overestimated with default parameters both in the presence or absence of iron dosage. The effort was first dedicated to biological reaction adaptation while parallel work was finally done for chemical phosphorus removal. And finally, synergetic effects were discussed.

Biological P removal processes. As for phosphate uptake, the initial simulated P release in the anaerobic zone was much higher than observed at the facility (36 ± 1.9 mg P/L instead of 10-15 mgP/L). Lab measurements (batch anaerobic tests) with and without additional VFA both indicated that the default model overestimated VFA uptake and P release. Initially, it was assumed that the overestimation of anaerobic fermentation activity was responsible for that in the majority (by both OHO and PAO in the anaerobic tank, as default conditions would allow that). The P release test with acetate addition tended to disprove that, as substrate abundance did not result in a similar extent of released P concentration.

While PAO-GAO competition is always an important consideration for bioP removal, a bad prediction of such competition was also possible, but information on the relative abundance of each group was not available.

Note that in Sumo2S, P uptake occurs under anoxic and aerobic conditions as well. The anoxic uptake is controlled by the denitrifying fraction of PAO (η_{anox}). Regarding the phosphate dynamics in the alternated aeration basin, the initial simulation clearly overestimated the anoxic uptake (leading to a low difference between aerobic and anoxic phases). Moreover, the laboratory tests confirmed that the maximal anoxic uptake rate was also much lower than the aerobic one (by 45%). As a consequence, the anoxic reduction factor was reduced in order to predict more correctly the observed difference between P uptakes.

Chemical processes. When combined with iron dosage, the discrepancy with the observation could be likely due to the limited PHA storage and PO4 release, which can be due to the presence of iron (De Haas *et al.*, 2000). Indeed the effect of iron on PHA storage was also considered as a possible inhibiting factor. This would explain similarly both the limited P release and P uptake as well.

Moreover, according to the simulation, only about 50% of total iron was initially in the form of HFO in the aerobic reactor whereas a part of iron was reduced into Fe(II). Iron reduction (and consequent FeS and vivianite formation) was simulated whereas it was unlikely to achieve in such an intermittent aeration system, despite the anaerobic zone. Finally, measurements of total iron and iron(II) were performed on the site and confirmed that the reduced iron (Fe^{2+}) was poorly observed, no more than 7-10 % of the total iron. In Sumo2S, the kinetic rate for reduction was initially higher than the kinetic rate for oxidation, which was poorly supported by the literature. Moreover, an abundance of electron donors may increase the maximum reduction rate even more. Literature suggests that oxidation (especially the oxidation of soluble ferrous iron) is more rapid than reduction. Therefore in such a system, negligible Fe(II) forms are expected in the mainstream. While this model does not contain vivianite oxidation (in case of redissolution, it may oxidize from soluble Fe^{2+}) the first-order kinetic rates of the existing processes needed to be revised.

Finally, it was also observed in practice that return sludge liquor had a much higher phosphate concentration compared to the simulated one (additional release during the process). This was possibly due to either release of biologically stored phosphorus or the chemically captured one. This mechanism is insufficiently understood and as a first assumption, it was assumed that it was due to desorption from HFO (because anaerobic phosphate release was not that significant in endogenous batch tests).

This phenomenon was included in the model as a specific local parameter during dewatering. This observation needs to be confirmed from similar facilities and studied more deeply in the future.

It was observed during the model calibration, that during the period without iron dose, some H2S was produced in the anaerobic tank, while with iron dose this amount is negligible. As ORP is calculated based on this component and PAO-GAO fractionation is sensitive to ORP. To avoid the interference of this component, during these full-plant simulations the Fe(II) precipitation processes were not considered for full-scale simulation with the exception of an initial simulation to verify Fe oxidation and reduction calibration based on the on-site measurement.

The calibrated parameters are given in Table 4.4-1

Table 4.4-1 Calibrated model parameters

Symbol	Name	Default	Calibrated	Unit
Biological process parameters				
$\eta_{HYD,ana}$	Reduction factor for anaerobic hydrolysis	0.5	0.1	-
$K_{HYD,AS}$	Half-saturation of particulates in hydrolysis (AS)	0.05	0.1	g COD.g COD^{-1}
$f_{P,VFA}$	Ratio of P released per VFA stored	0.65	0.5	g XPP.g $SVFA^{-1}$
$q_{PAO,PP}$	Maximum polyphosphate uptake rate of PAOs	0.1	0.065	d^{-1}
b_{CASTO}	Decay rate of CASTOs	0.08	0.05	d^{-1}
$q_{PAO,PHA}$	Rate of VFA storage into PHA for PAOs	7	5	d^{-1}
$q_{GAO,GLY}$	Rate of VFA storage into GLY for GAOs	4	2	d^{-1}
$\eta_{CASTO,anox}$	Reduction factor for anoxic growth of CASTOs	0.66	0.45	-
$K_{PO4,PAO,AS}$	Half-saturation of PO4 for PAOs (AS)	0.3	0.5	g P/m^3
$Lograng e_{PO4,PAO,AS,sat}$	Effective range of logistic switch for PO4 uptake by PAOs	80	180	%
$K_{ORP,H2,CH4,H2S}$	Half-saturation of dissolved hydrogen, methane and hydrogen sulfide for anaerobic ORP	5	25	g COD/m^3
Chemical process parameters				
$Ki_{HFO,PAO}$	Half-inhibition of Fe(III) on VFA uptake (PAO)	-	75	g Fe /g COD
$q_{Fe2,OX}$	Rate of Fe^{2+} oxidation	1	10	d^{-1}
$q_{FeS,OX}$	Rate of FeS oxidation	1	4	d^{-1}
$q_{HFO,RED}$	Rate of HFO reduction with organics	2	2.65	d^{-1}
$K_{VSS,HFO,red}$	Half-saturation of VSS in HFO reduction	-	3230	g VSS/m^3
$K_{edonor,HFO,red}$	Half-saturation of organic matter in HFO reduction	-	0.01	g COD/m^3

Figure 4.4-5 shows a boxplot of measured data, simulation with the default model, and with the calibrated model including all processes for a selected period. This period was selected based on the normal average MLSS and iron dose, as those operational parameters are shown to have a significant impact on P removal. It is clear, that at a full-scale facility, even more so at a small/medium size plant, in an extent of one month, significant variation and disturbance can be observed. As the diurnal influent pattern in the simulation represents an average pattern observed throughout the measurement campaign, the differences can be explained by that. However, the calibrated model captures better the variation and the average P concentrations. An important difference between the calibrated model and measured values is the extent of the variation within each cycle. Measurements show lower amplitudes during aeration cycle phases than the model. These differences in short dynamic cycles can be originated for numerous reasons, and some of that reasons (aeration, discontinuous wastage) are explained later.

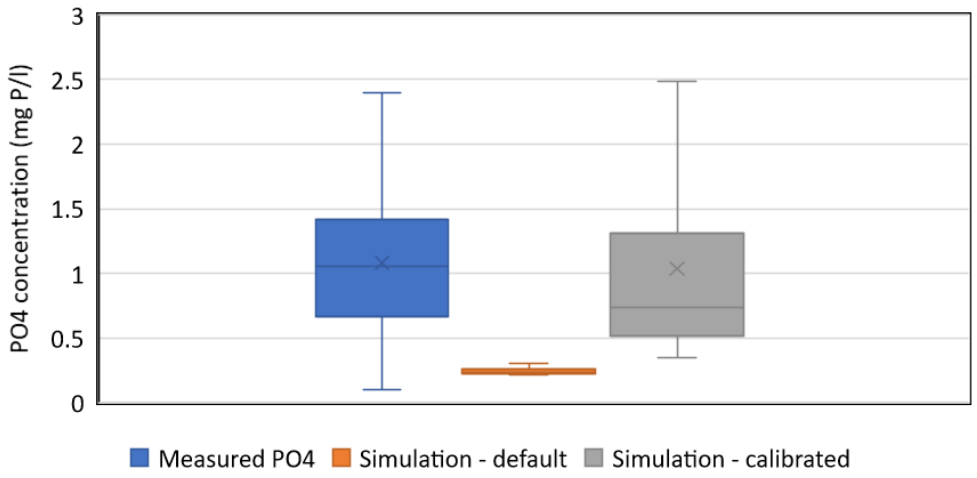

Figure 4.4-5 Effluent phosphate concentration values: online measurement (May 2020), simulation with default model, and simulation with the calibrated model

4.4.3. Phosphorus release and uptake tests

In order to gain a more detailed insight into the potential P release and uptake in the activated sludge from the facility, batch test experiments were carried out. Modeling such batch tests allows us to assess the relevance of kinetics parameters for CASTO regarding specific rates and maximal phosphate release and accumulation.

These experiments showed an average release of 5.6 ± 1.7 (n=5) mgP.gVSS^{-1}.h^{-1} within 50 minutes of anaerobic time. P release was also observed during Fe(III) reduction assays (chapter 3). In this case, however, the additional substrate was not provided, and the apparent release included the effect of iron reduction. Moreover, in batch reactor fermentation, other anaerobic processes occur that can induce further release. From the endogenous iron reduction, the released orthophosphate was 38% of total phosphorus after 24 hours and 50% after 7 days (MLSS= 4.4 g TSS/L).

The dedicated P release and uptake tests were discussed in detail in Chapter 2.2.5. Figure 4.4-6 presents the P release test with simulation results.

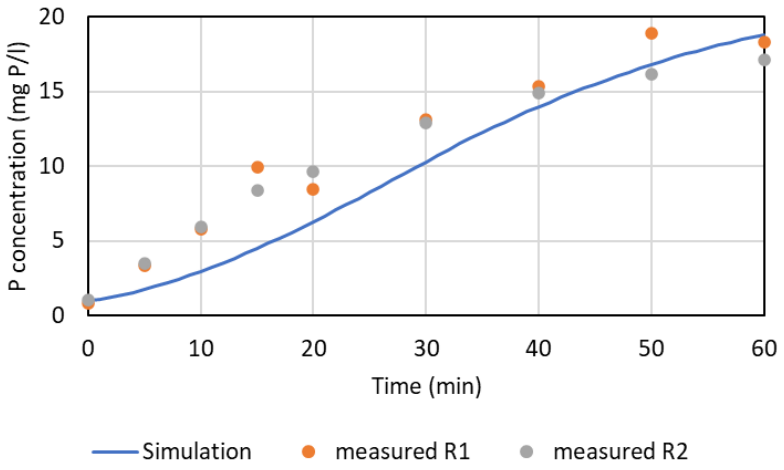

Figure 4.4-6. Phosphate release batch test and simulation with the calibrated model

Figure 4.4-7 presents P release and uptake batch tests and simulation for two different uptake cases: aerobic conditions and anoxic conditions. The release and uptake rates were calibrated together with the full-plant observations which results in some deviation from the laboratory measurements and the model. Moreover, condition change at the respirometer (anaerobic-aerobic scenario) occurred with some offset which does not appear in the simulation. The general agreement in the release and uptake prediction is acceptable nonetheless.

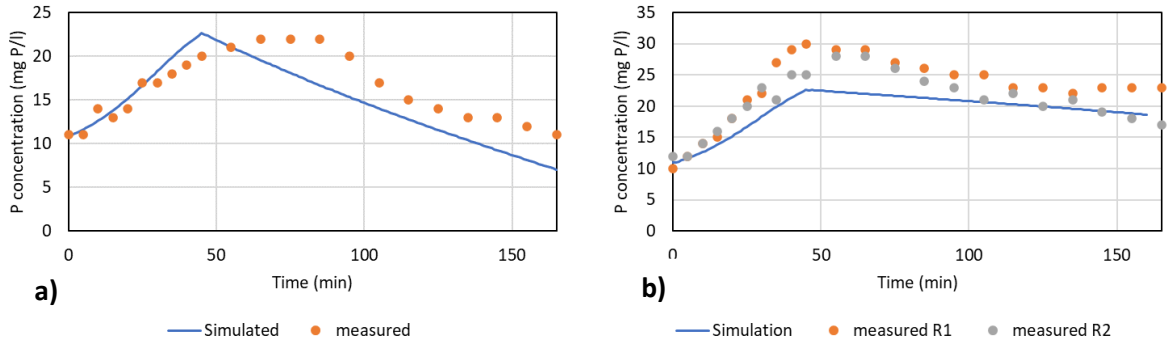

Figure 4.4-7 P release and uptake batch tests and simulation with calibrated model (a) anaerobic-aerobic cycle (b) anaerobic anoxic cycle

Whereas the batch test results were first used for parameter calibration, specific dynamic data monitored in the plant could be used for validation. First of all the anaerobic release in the anaerobic zone was much better predicted by the adaptations. Indeed the phosphate concentration measured around (10-15 mg P/L) whereas the simulations give a range of 15 ± 1.4 mg P/L after calibration, whereas it was higher at 36.7 ± 1.9 mg P/L with initial default parameter values.

4.4.4. Intermittent aeration and phosphorus removal

The different aeration strategies of an intermittent aeration system influence the biological P removal, as demonstrated in Chapter 2. Different aeration strategies were applied in the following simulations with purely biological P removal. The aerated fraction of the cycles was determined to give a general pattern which was used as an input parameter in the simulation to demonstrate the sensitivity of the model to this interaction. First, different fractions of the same aeration cycles were simulated over several days dynamically changing the periods, and then a combination of these fractions to represent an aeration pattern that was described in Chapter 2.

The simulated aeration time fractions were 20%, 28%, 35%, and 41% of the cycle. It is clear from Figure 4.4-8, that with increasing aeration time, lower P concentration can be achieved. Moreover, daily variation as well as variation within cycles are lower (indicated with light orange areas on the figure). It is important to note, that it appeared in the dynamic simulations that dynamically decreasing the aeration time suddenly causes a disturbance in bio-P removal which may take a couple of days to stabilize.

This effect was not included in the presentation. However, significant variation can be observed in the simulations with lower aeration times.

One common feature of these figures is the increased DO concentration in the night/early morning hours. This indicates that the system is over-aerated. Moreover, typically the influent P during this period is rather low, and also most cases of the simulation. Figure 4.4-8 (c) and (d) shows the lowest variation during this time, reaching the minimum values of the simulation due to the excessive aeration and the low influent load.

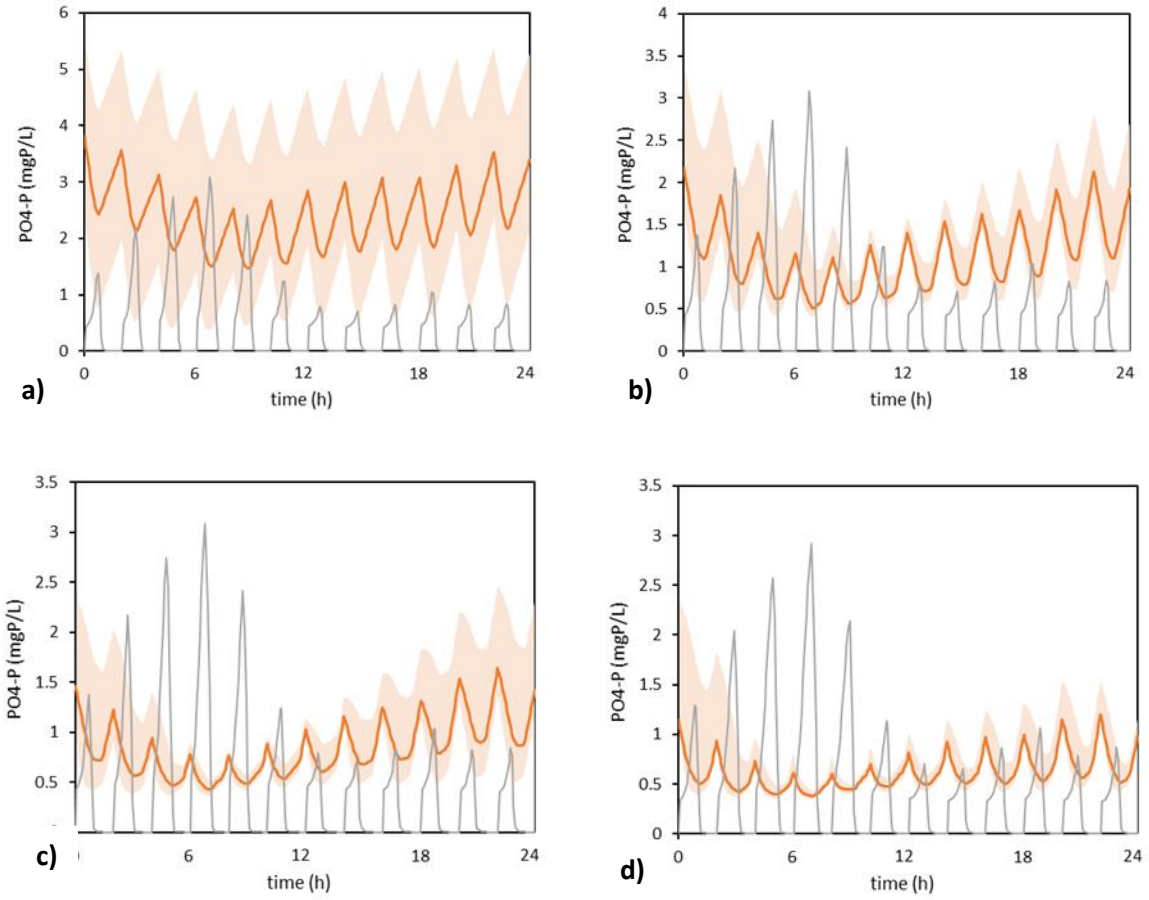

Figure 4.4-8 P pattern with different aeration fractions within cycles. (a) 20% (b) 28% (c) 35% (d) 41%. Corresponding aeration cycles are represented by DO concentration (gray line)

In average phosphate concentration reaches the following values: (a) 20%: 2.40 mg P/l; (b) 28%: 1.12 mg P/L; (c) 35%: 0.83 mg P/L; (d) 41%: 0.61 mg P/L; Dynamic: 0.69 mg P/L.

It is clear that none of these aeration options are energy efficient nor optimized by the aeration controller. *Inflex* aeration control system does not operate with fix aeration time ratio and allows variable aeration times depending on the load, for adapting the nitrification/denitrification performance.

For simulating such a daily dynamic aeration time, as defined in Chapter 2 a typical cycle can be described as 0-8 h: 28%, 8-20h: 41%, and 20-24h: 33%. Figure 4.4-9 shows the profile of the simulation with this aeration pattern. This pattern gives a comparable average to Figure 4.4-8 (d) but with lower aeration time (hence more energy efficient). During the morning phosphate increase is observed and after this morning peak, phosphate concentration returned progressively as the aeration time ratio increases, but finally, phosphate increased again in the evening with the aeration time decrease. This type of dynamic behavior is very comparable to those observed in practice (Figure 2.2-2) and illustrates how sensitive the phosphate removal is regarding the aeration controller.

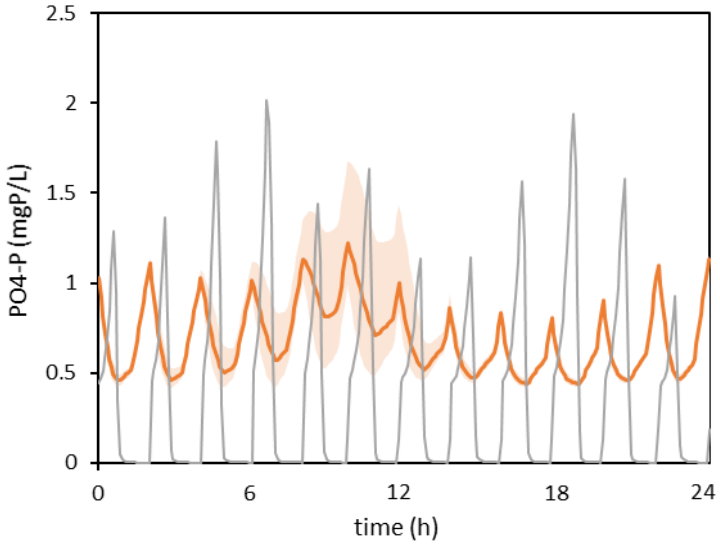

Figure 4.4-9 Phosphate profile in the aerated basin with varying aeration time

4.4.5. Modeling the effect of iron dose on P removal efficiency

During the period of the project, four different iron dosing strategies were implemented (as described in Chapter 2): iron dose A - regular iron dose, intermittent dose to the aeration basin Iron dose B - increased dose to the aeration basin iron dose C – iron dose to sludge liquor and period without iron dose.

The simulations were carried out for the full-scale facility for different iron dosage strategies with the calibrated model. This model included inhibition of VFA uptake by iron. However, this option is here assessed and discussed by comparing the simulation results with and without inhibition. This is an important interaction in combined processes, but the introduction into such a complex model holds different uncertainties. This inhibition has been included in PHA storage by PAO with a half inhibition constant of 75 mg Fe/L (a large variation of the degree of inhibition was found in literature, De Haas (2000) found 3-20% inhibition at the presence of 10-20 mg Fe/l as $FeCl_3$). To test the sensitivity of this process, the simulation was carried out with and without this inhibition (Figure 4.4-10).

The average concentrations predicted for iron dose A and iron dose B were 1.04 and 0.93 mg P/L with inhibition, and 0.81 and 0.65 mg P/L respectively without inhibition. From a comparison with the experimental campaigns with these levels of iron dosage (dose A: 1.08 mg P/L, dose B: 0.494 mg P/L), it comes that the simulation with inhibition matches better for the dose A, whereas simulation without inhibition fits better to the results obtained for dose B. This indicates that while iron inhibition may be an important interaction in activated sludge systems, a more detailed experimental calibration would be necessary with various Fe:P ratios to determine the parameters more accurately and potentially reconsider the inhibition model typology.

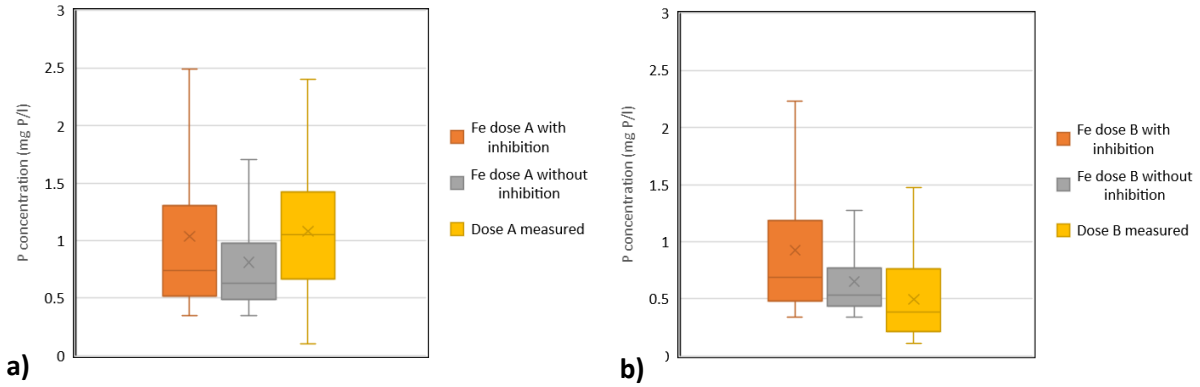

Figure 4.4-10. Simulation of the effect of iron dose on phosphate concentration in the aerated basin a) regular dose on the left (dose A) and b) increased dose on the right (dose B)

4.4.6. Effect of sludge wastage and MLSS concentration on P removal

Compared to simulation with continuous wastage, the consideration of discontinuous wastage leads to a higher cyclic variation of phosphate concentration. A higher phosphate peak is also predicted after the wastage period due to phosphate release in sludge dewatering and sludge liquor recirculation, and this is in line with the practical observation of the plant. It is assumed that during the dewatering process (due to mechanical or chemical impact) phosphate desorption occurs at a higher rate. This has been implemented as a local parameter for the simulations (for the combined biological and physical-chemical scenario). Figure 4.4-11 presents the effect of variation of intermittent wastage on the phosphate concentration. During the 10 days cycles, the last three days, a small, gradual increase can be observed. During wastage, an instantaneous decrease is observed at first and followed by a higher peak. This short-term increase in concentrations is caused by the additional P load arriving from the sludge liquor. As a mitigation strategy, it was proposed to dose iron directly to the return sludge liquor.

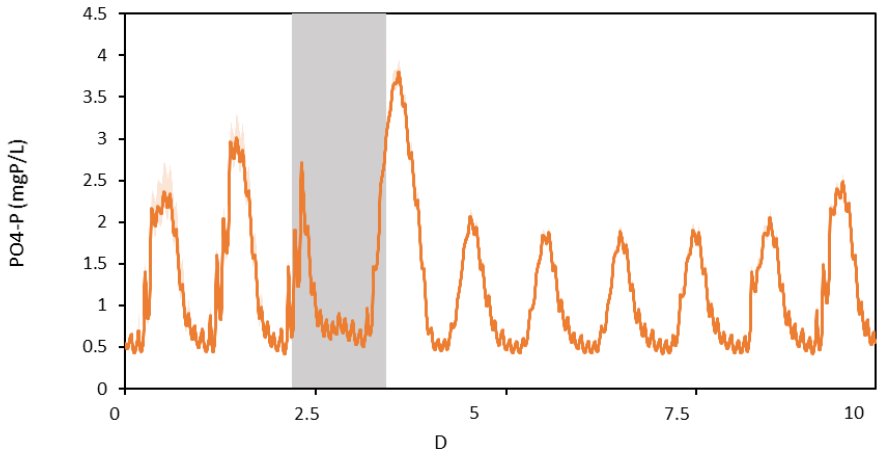

Figure 4.4-11 Simulation of phosphate concentration with discontinuous sludge wastage (grey zone: period of wastage and sludge dewatering)

Indeed, in comparison with the monitoring campaign presented in chapter 2 (Figure 2.3-9) very similar range of variations was observed. Therefore the discontinuous wastage makes the results of the simulation more realistic. On the long term, the simulated average phosphate concentration and the variation amplitude are both sensitive to discontinuous wastage.

4.4.7. Model complexity and remaining challenges

Table 4.4-2 summarizes the parameter adjustments with their added benefits and remaining challenges.

Table 4.4-2 Calibration outcomes and remaining challenges

Process/Parameter	Impact	Challenges
P release/VFA uptake rate (decreased)	More realistic P release in batch tests	Without the VFA characterization in the influent, the verification of full scale is lacking
Kinetic rate of VFA storage (decreased)	More fitting soluble COD and P pattern in batch tests	Extensive specific calibration is necessary to confirm
ORP half saturation for anaerobic components (increased)	Stabilizing the PAO-GAO competition which was a little unrealistic due to the highly dynamic changes	ORP function is indicative of the conditions, a more accurate ORP function would be advantageous for developing further ORP parameters (e.g. Nernst equation)
Reduction factor for anaerobic hydrolysis (decreased)	The complex interactions (sCOD, PO4, ORP) and observations support the need for adjustment. COD and ORP values are mitigated therefore false PAO dominance is reduced	Calibration is based on observation, and parameters from other models, validation from targeted new experiments could be beneficial
Maximum polyphosphate uptake rate (decreased)	Calibrated with batch and full-scale data	Better prediction of PO4 dynamics in intermittent aeration tanks
Reduction of growth factor for anoxic growth (CASTO) (decreased)	Based on batch tests, the calibration could take into account the anoxic reduction and therefore better match the observation during anoxic phase	It is a reduction factor for CASTO but based on PAO activity only
Iron kinetic reduction rate constant (increased)	More realistic kinetics in activated sludge	The current model structure indicates biological reduction (“iron reduction with organic matter”) but does not generate biomass
Redox ORP dependency (removed)	Iron reduction starts with anaerobic conditions and not with ORP switch	
MLSS dependency of iron reduction (introduced)	Iron reduction kinetics more adapted to different conditions	
Iron(II) oxidation kinetic rates (increased)	More realistic fit to the on-site observations	Need to be verified in batch tests
Iron inhibition on PHA uptake (introduced)	Conceptual introduction of iron inhibition on biological processes	The parameter needs to be carefully calibrated. Moreover, GAO interactions need to be considered in order to prevent a false advantage for GAOs

The most important difference that was observed in the initial simulation with default parameters was the significant overestimation of biological removal through PAO activity. Initially, it was assumed that the presence of iron inhibition of PHA storage by PAOs would help to make the simulation more accurate. While in certain cases it was true, it was also observed during the calibration process, that with the default parameter set for HFO kinetics (P precipitation and adsorption, re-dissolution and desorption and aging processes) and the introduced inhibition term, increasing Fe dose was, in fact, detrimental for the P removal, while pure biological phosphorus removal would show excellent performance (with the elimination of the inhibition).

In reality, during the extended periods without iron dose (although a low level of residual iron may be present), the effluent concentration was around 1.5 to 2 mg P/l with significant variation while with increasing iron dose (2 different dosages) the effluent phosphate decreases.

This anomaly in the model was revised by using the experimental information on P release and uptake rates for the calibration of biological processes. While interference of residual iron may be still present, these tests may give an insight into other processes. Based on the available data from the batch experiments, the depletion of soluble COD (dosed as acetate) was carried out in the model too rapidly. While the P release could be adjusted in agreement with the measurement results, it appeared that overall VFA uptake was too high by both CASTO-type groups.

Some of the necessary modifications can be explained by the fact that the model framework was not developed for a such system with a very long SRT (more than 50 days), and long HRT (about 48 hours). As a consequence, the initial default model parameters significantly overestimated the processes related to long anaerobic time: hydrolysis and fermentation, the reduction rate of iron, as well as the benefit of low ORP on PAO competition with GAO.

Indeed, in Sumo, hydrolysis is relatively fast. This provides to substrate for fermentation (by OHO and PAO) and fermentation products are VFA and H_2. CASTO may utilize VFA, while H_2 is an important component in the ORP calculation (the higher the H_2 concentration, the lower the ORP).

Low ORP conditions favor PAOs over GAOs and in the Sumo21 version, CASTO speciation for storage depends exclusively on ORP. In such a dynamic system with alternating aeration, this may cause higher variation during the simulation than what was observed in the facility.

Finally, while it was not possible to completely exclude the potential effect of iron in our measurements, biological P removal needed to be calibrated first. It is already interesting general progress for such a dynamic system. Whereas much better predictions were obtained, the consideration of some influential parameters remains, such as the temperature which is an important factor in the PAO-GAO competition. The initial calibration was done at 20°C, i.e. the average spring temperature of the plant. The effect of temperature was tested, and the simulations showed that as expected, lower temperatures (15°C) favor PAO and higher temperatures (23°C) favor GAO resulting in deteriorated P removal. These initial simulations show how the balance between these groups is heavily influenced by temperature. This does not necessarily reflect the observations at the facility as the seasonal disturbances are significant namely during winter periods when the intense hydraulic load causes dilution.

As discussed in Chapter 2, in this highly dynamic system, there are complex interactions and several influencing parameters. Capturing these in a model and confronting online measured data was a challenging task. In combined systems, the quantification of the biological and physical-chemical contribution of overall P removal needs more attention.

4.5. Conclusions and outlook

Villefranche de Lauragais wastewater treatment plant is operated with a highly dynamic aeration system, optimally designed for complete nitrogen removal via nitrification-denitrification. The simulation of phosphorus removal in a such system with automatic adaptation of aeration time is quite complex. Two different approaches to the model were presented in this chapter, one with dynamic aeration time control and one with automatic adaptation to the influent ammonia load. Both give a good estimation of the control system of the facility which is data-driven control.

Recent process models include several biokinetic and chemical reactions. However, the interactions of these reactions were insufficiently considered until now.

This chapter introduced model parameters and adjusted processes to start representing these interactions in a full-plant model using experimental, lab, and full-scale data. Some benefits were demonstrated by this approach but further investigation would be necessary to validate the model.

While the default model severely overestimated biological P removal, in this configuration, the introduced adjustments in PAO activity (regarding the release and aerobic and anoxic uptake processes) resulted in a much more realistic simulation.

In addition, the biological iron reduction process was extended by using data from detailed laboratory experiments and oxidation processes were calibrated based on full-scale observations. This allowed a better description of iron speciation and phosphate capture.

During the calibration process, a sensitivity of CASTO fractionation was observed, which can have a detrimental impact on the accuracy of a simulation in such a dynamic system. ORP dependency of PAO-GAO competition may be exaggerated in the model. As iron reduction processes were extended, the question of terminal electron-accepting processes (TEAP) was raised. To keep the model complexity at a practical level, the existing structure was simplified, but the authors suggest a more detailed description of TEAP, especially regarding the competition of ferric and sulphate reduction as it can be a crucial interaction for the emerging recovery process of vivianite separation from the sludge in the future.

4.6. References

Corominas, L. L., Rieger, L., Takács, I., Ekama, G., Hauduc, H., Vanrolleghem, P. A., ... & Comeau, Y. (2010). New framework for standardized notation in wastewater treatment modelling. *Water Science and Technology*, *61*(4), 841-857.

de Haas, DW, Wentzel, MC & Ekama, G. A. (2000). The use of simultaneous chemical precipitation in modified activated sludge systems exhibiting biological excess phosphate removal Part 4: Experimental periods using ferric chloride. *Water Sa*, *26*(4), 485-504.

Deronzier, Gaëlle, Choubert, Jean-Marc. 2004. Traitement du phosphore dans les petites stations d'épuration à boues activées. Cemagref, Document Technique FNDAE, n° 29.

Fan, J., Zhang, H., Ye, J., & Ji, B. (2018). Chemical stress from Fe salts dosing on biological phosphorus and potassium behavior. *Water Science and Technology*, *77*(5), 1222-1229.

Hauduc, H., Takács, I., Smith, S., Szabó, A., Murthy, S., Daigger, G. T., & Spérandio, M. (2015). A dynamic physicochemical model for chemical phosphorus removal. *Water Research*, *73*, 157-170.

Hauduc, H., Wadhawan, T., Johnson, B., Bott, C., Ward, M., & Takács, I. (2019). Incorporating sulfur reactions and interactions with iron and phosphorus into a general plant-wide model. *Water Science and Technology*, *79*(1), 26-34.

Paul, E., Plisson-Saune, S., Mauret, M., & Cantet, J. (1998). Process state evaluation of alternating oxic-anoxic activated sludge using ORP, pH and DO. *Water Science and Technology*, *38*(3), 299-306.

Rieger, L., Gillot, S., Langergraber, G., Ohtsuki, T., Shaw, A., Takacs, I., & Winkler, S. (2012). *Guidelines for using activated sludge models*. IWA publishing.

Varga, E., Hauduc, H., Barnard, J., Dunlap, P., Jimenez, J., Menniti, A., ... & Takács, I. (2018). Recent advances in bio-P modelling–a new approach verified by full-scale observations. *Water Science and Technology*, *78*(10), 2119-2130.

4.7. Supplementary material

Table S4. 1 Additional model variables used in highlighted expressions

Stoichiometric calculated variables			
Symbol	**Name**	**Expression**	**Unit**
$S_{edonor,HFO,red}$	COD equivalent of electron donors in biological Fe(III) reduction	$S_B + S_{VFA}$	g COD.m^{-3}
$X_{HFO,TSS}$	Total HFOs in TSS unit	$(1-f_{H2O,HFO,TSS})*X_{HFO}*MM_{FeOH3}/AM_{Fe}+(X_{HFO,L,P}+X_{HFO,L,P,old})*ASF_{HFO,L}*(MM_{PO4}/AM_{Fe})+(X_{HFO,H,P}+X_{HFO,H,P,old})*ASF_{HFO,H}*(MM_{PO4}/AM_{Fe})$	g TSS.m^{-3}
X_{HFO}	Total HFOs	$X_{HFO,H}+X_{HFO,L}+X_{HFO,L,P}+X_{HFO,H,P}+X_{HFO,old}+X_{HFO,L,P,old}+X_{HFO,H,P,old}$	g Fe.m^{-3}
T_{Fe}	Total iron	$X_{HFO} + S_{Fe2}+X_{FeS}*AM_{Fe}/MM_{FeS}+X_{Vivi}*3*AM_{Fe}/MM_{Vivi}$	g Fe.m^{-3}
$X_{vivi,Fe}$	Vivianite as iron(II)	$X_{Vivi}*3*AM_{Fe}/MM_{Vivi}$	g Fe.m^{-3}
$X_{FeS,Fe}$	FeS as iron(II)	$X_{FeS}*AM_{Fe}/MM_{FeS}$	g Fe.m^{-3}
$X_{HFO,P}$	Total phosphorus in HFOs	$(X_{HFO,L,P}+X_{HFO,L,P,old})*ASF_{HFO,L}*(AM_P/AM_{Fe})+(X_{HFO,H,P}+X_{HFO,H,P,old})*ASF_{HFO,H}*(AM_P/AM_{Fe})$	g P.m^{-3}
CASTO related kinetic calculated variables			
X_{STC}	PHA and GLY stored in CASTO	$X_{PHA} + X_{GLY}$	g COD.m^{-3}
act_{PAO}	PAO activity of CASTOs	X_{PHA} / X_{STC}	-
act_{GAO}	GAO activity of CASTOs	X_{GLY} / X_{STC}	-
X_{PAO}	PAO (Phosphate accumulating organisms) fraction of CASTO	$act_{PAO} * X_{CASTO}$	g COD.m^{-3}
X_{GAO}	GAO (Glycogen accumulating organisms) fraction of CASTO	$act_{GAO} * X_{CASTO}$	g COD.m^{-3}
$act_{sto,GAO,ORP}$	ORP dependent VFA storage activity of GAOs	$Logsat_{ORP,GAO,T}$	-
$act_{sto,PAO,ORP}$	ORP dependent VFA storage activity of PAOs	$(1 - Logsat_{ORP,GAO,T})$	-
ORP calculated variables			
ORP_{O2}	Oxidation-reduction potential due to dissolved oxygen	$ORP_{base}+(ORP_{max,SO2}-ORP_{base})*S_{O2}/(K_{ORP,SO2}+S_{O2})$	mV

ORP_{NOx}	Oxidation-reduction potential due to dissolved nitrate	$ORP_{base}+(ORP_{max,SNOx}-ORP_{base})*S_{NOx}/(K_{ORP,SNOx}+S_{NOx})$	mV
$S_{H2,CH4,H2S}$	Combined concentration of hydrogen, methane and hydrogen sulfide in COD	$S_{H2} + S_{CH4} + S_{H2S}$	g COD.m^{-3}
$ORP_{H2,CH4,H2S}$	Oxidation-reduction potential due to dissolved hydrogen, methane and hydrogen sulfide (anaerobic)	$ORP_{base} * (S_{H2,CH4,H2S})/(K_{ORP,H2,CH4,H2S} + S_{H2,CH4,H2S})$	mV
ORP	Oxidation-reduction potential	$Max(ORP_{O2};ORP_{NOx};ORP_{H2,CH4,H2S})$	mV
$Loginh_{ORP,PAO}$	ORP switch of fermentation by PAOs	$Loginhswitch(ORP; Logsat_{ORP,PAO,Half}; Logsat_{ORP,PAO,Slope})$	-
$sl_{ORP,GAO,Half,T}$	Slope of logistic half-saturation of ORP switching of GAOs temperature correction	$(Logsat_{ORP,GAO,Half,25} - Logsat_{ORP,GAO,Half,15}) / (25 - 15)$	mV.°C^{-1}
$y_{ORP,GAO,Half,T}$	Intercept of logistic half-saturation of ORP switching of GAOs temperature correction	$Logsat_{ORP,GAO,Half,25} - sl_{ORP,GAO,Half,T} * 25$	mV
$Logsat_{ORP,GAO,Half,T}$	Temperature correction of ORP switch of glycogen storage by GAO	$sl_{ORP,GAO,Half,T} * T + y_{ORP,GAO,Half,T}$	mV
$Logsat_{ORP,GAO,T}$	ORP switch of glycogen storage by GAO	$Logsatswitch(ORP; Logsat_{ORP,GAO,Half,T}; Logsat_{ORP,GAO,Slope})$	-
Precipitation/redissolution rates			
PrecipDrivingForce$_{FeS}$	Rate expression of FeS precipitation (driving force)	$([Fe^{2+}]^{(0.5)} * [HS^-]^{(0.5)} - K_{sp,FeS}^{(0.5)})/K_{sp,FeS}^{(0.5)}$	Unitless
q_{FeS}	Rate of FeS precipitation	$If(PrecipDrivingForce_{FeS}>0;q_{FeS,PREC};-q_{FeS,DISS}*Msat_{XFeS,KFeS,DISS})$	d-1
PrecipDrivingForce$_{Vivi}$	Rate expression of vivianite precipitation (driving force)	$(([Fe^{2+}]^{(3/5)} * [PO_4^{3-}]^{(2/5)} - K_{sp,Vivi}^{(1/5)})/K_{sp,Vivi}^{(1/5)})$	Unitless
q_{Vivi}	Rate of vivianite precipitation	$If(PrecipDrivingForce_{Vivi}>0;q_{Vivi,PREC};-q_{Vivi,DISS}*Msat_{XVivi,KVivi,DISS})$	d-1
Slope calculations for logistic saturation/inhibition functions			
$Logslope_{PHA,PAO,inh}$	Logistic slope of inhibition term for PHA/PAO	$Logisticslope(Ki_{PHA,PAO,max}; Logrange_{PHA,PAO,inh})$	g COD.g COD^{-1}
$Logslope_{P,HFO,DISS}$	Logistic slope of PO_4 in HFO redissolution	$Logisticslope(Ki_{P,HFO,DISS}; Logrange_{P,HFO,DISS})$	m^3.g P^{-1}
Saturation/inhibition terms			

$Minh_{SNO2,KNO2,OHO}$	Inhibition term for NO_2 (OHO)	$Minh(S_{NO2};K_{NO2,OHO})$	-
$Minh_{SNO3,KNO3,OHO}$	Inhibition term for NO_3 (OHO)	$Minh(S_{NO3};K_{NO3,OHO})$	-
$Minh_{SO2,KO2,OHO}$	Inhibition term for O_2 (OHO)	$Minh(S_{O2};K_{O2,OHO})$	-
$Minh_{HFO,PAO}$	Inhibition term for PO4 (PAO)	$Minh(X_{HFO};Ki_{HFO,PAO})$	-
$MRsat_{XPP,XPAO,KPP}$	Saturation term for PP storage in (PAO)	$MRsat(X_{PP};X_{PAO};K_{PP})$	-
$Msat_{SO2,KO2,CASTO}$	Saturation term for O_2 (CASTO)	$Msat(S_{O2};K_{O2,CASTO})$	-
$Msat_{SVFA,KVFA,CASTO}$	Saturation term for VFA storage (CASTO)	$Msat(S_{VFA};K_{VFA,CASTO})$	-
$Loginh_{XPHA,XPAO,max}$	Logistic inhibition term for PHA (PAO)	$Loginh(X_{PHA}/X_{PAO};\ Ki_{PHA,PAO,max};\ Logslope_{PHA,PAO,inh})$	-
$Loginh_{SPO4,KiP,HFO,DISS}$	Inhibition term for PO_4 in redissolution of HFO	$Loginh(S_{PO4};Ki_{P,HFO,DISS};Logslope_{P,HFO,DISS})$	-
$Minh_{SPO4,KiP,HFO,DESORP}$	Inhibition term for PO_4 in desorption of HFO	$Minh(S_{PO4};Ki_{P,HFO,DESORP})$	-
$Msat_{SPO4,KP,HFO,BIND}$	Saturation term for PO_4 binding on HFO	$Msat(S_{PO4};K_{P,HFO,BIND})$	-
$Loginh_{SPO4,KiP,HAO,DISS}$	Inhibition term for PO_4 in redissolution of HAO	$Loginh(S_{PO4};Ki_{P,HAO,DISS};Logslope_{P,HAO,DISS})$	-
$Minh_{SPO4,KiP,HAO,DESORP}$	Inhibition term for PO_4 in desorption of HAO	$Minh(S_{PO4};Ki_{P,HAO,DESORP})$	-
$Msat_{SPO4,KP,HAO,BIND}$	Saturation term for PO_4 binding on HAO	$Msat(S_{PO4};K_{P,HAO,BIND})$	-
$Minh_{SSO4,KiSO4,RED}$	Inhibition term for SO_4 (HFO reduction)	$Minh(S_{SO4};Ki_{SO4,RED})$	-
$Msat_{XFeS,KFeS,DISS}$	Saturation term for FeS dissolution	$Msat(X_{FeS};K_{FeS,DISS})$	-
$Msat_{XVivi,KVivi,DISS}$	Saturation term for vivianite dissolution	$Msat(X_{Vivi};K_{Vivi,DISS})$	-
$Msat_{XVSS,XHFO,red}$	Saturation term for VSS dependency in XHFO reduction	$Msat(X_{VSS};K_{VSS,HFO,red})$	-
$Msat_{edonor,XHFO,red}$	Saturation term for electron donors in XHFO reduction	$Msat(S_{edonor,HFO,red};K_{edonor,HFO,red})$	-

Temperature dependency correction

$q_{PAO,PHA,T}$	Rate of VFA storage into PHA for PAOs (temperature corrected)	$q_{PAO,PHA}$*Arrh($\theta_{q,PAO,PHA}$; T; T_{base})	d^{-1}
$q_{Fe2,OX,T}$	Rate of Fe_2 oxidation (temperature corrected)	$q_{Fe2,OX}$*Arrh($\theta_{q,Fe2,OX}$; T; T_{base})	d^{-1}
$q_{FeS,OX,T}$	Rate of FeS oxidation (temperature corrected)	$q_{FeS,OX}$*Arrh($\theta_{q,FeS,OX}$; T; T_{base})	d^{-1}
$q_{HFO,RED,T}$	Rate of HFO reduction with organics (temperature corrected)	$q_{HFO,RED}$*Arrh($\theta_{q,HFO,RED}$; T; T_{base})	d^{-1}
$q_{HFO,H2S,RED,T}$	Rate of HFO reduction with H2S (temperature corrected)	$q_{HFO,H2S,RED}$*Arrh($\theta_{q,HFO,H2S,RED}$; T; T_{base})	d^{-1}

Conclusion and perspectives

The main objective of this thesis was to define the challenges of water resource recovery facilities with combined biological and physical-chemical phosphorus removal in order to optimize performance and identify nutrient recovery potential.

In Chapter1 a detailed literature review presented the established basis and current state of the field, especially regarding biological and combined physical-chemical P removal, nutrient recovery pathways, interactions with iron dose, and modeling advancements.

Biological processes became better characterized, and different functional groups of micro-organisms were isolated which provide a deeper understanding of the processes in order to control the environment to achieve the desired effect (e.g. selection of PAOs over GAOs in S2EBPR). Parallel to this development, mathematical modeling also started to include more processes. Different approaches of agent-based and metabolic models were presented.

Numerous facilities operate with combined biological and physical-chemical phosphorus removal. These plants implement different strategies of iron dosing. However, the optimization of the dosage is a crucial question at these facilities. Full-plant models include metal precipitation processes, namely the surface complexation model, which incorporates P precipitation with iron(III) (HFO).

Although iron is the most common element on the earth (by mass) and is widely used during wastewater treatment, there are still several interactions that are lacking research. Redox reactions, for example, extended a wider context to terminal electron-accepting processes. These can define important conditions in anaerobic reactors, such as precursors for different crystallization processes, however, the kinetics are not well described in activated sludge systems. The authors borrowed knowledge from natural aquatic environments (sediments and paddies) and while we believe the same interactions are present in activated sludge, a more detailed investigation would be necessary to precisely describe these processes.

As there are various conditions present in wastewater collection and treatment systems, redox transformations need to be considered. Moreover, iron redox transformations directly influence P removal and recovery potential.

As a deeper understanding of reduction (previously in digested sludge) and precipitation processes is gained, an emerging phosphorus recovery product appears, namely vivianite. To design and optimize the separation of this magnetic precipitate, a detailed understanding of iron reduction processes is necessary.

After conducting a literature review on the different areas of the field, three different approaches were elaborated to get closer to understanding these complex systems.

Starting with the most practical, field approach, in Chapter 2 a case study of a rural facility using an intermittent aeration system was presented (Villefranche de Lauragais). This plant represents a typical process configuration of its size (~10000 PE), where the aeration control is optimized for complete nitrogen removal via nitrification and denitrification and phosphorus removal is carried out by combined biological and physical-chemical means. The dedicated monitoring campaign and analysis of the performance of the facility was part of a regional European project (CircRural 4.0) aiming to optimize nutrient removal and recovery at rural plants while maintaining high energy efficiency.

While iron dose is present at the facility and was applied for the most part of the study, it was important to determine the biological contribution to the overall phosphorus removal. Dedicated periods without iron dose confirmed, that with solely biological removal, the requirement of an average <2 mg P/l can be met, however, it depends on operating parameters, such as aeration cycles and sludge management.

As the facility operates with an anaerobic zone and aeration basin with variable aeration cycles, it was important to determine P release (through polyphosphate cleavage) and aerobic and anoxic P uptake (confirming the presence of denitrifying PAO). Laboratory batch tests confirmed that anoxic uptake is significantly lower than aerobic uptake. Additionally, during long unaerated periods nitrate may be completely depleted, causing anaerobic conditions, which, if sufficient substrate is present, may result in additional P release. Therefore, in order to achieve good and reliable biological phosphorus removal a minimal aeration ratio needs to be maintained. With adequate aeration control, biological P removal contributes to 71% of the total P removal (resulting in an effluent P concentration of 1.61±0.49 mg P/L.)

To ensure good effluent quality at all times, Fe is dosed to complement the biological system. Different strategies were tested in order to find a reliable sustainable solution. A minor chemical dose (50% lower than the theoretical recommended dose) showed to be enough to maintain good quality.

Empirical observation of the additional load of the return sludge liquor upon intermittent wastage and the high biological P removal efficiency lead to the newly implemented Fe dose strategy of dosing iron directly to the return sludge liquor. This schedule maintains the desirable effluent while further decreasing chemical use (and therefore cost).

The facility operates with extended retention times (both HRT and SRT) and the anaerobic volume is nearly 15% of the biological reactor, the redox transformations of the dosed iron need to be examined. In Chapter 3 the results of a comprehensive series of experiments were carried out to determine iron reduction kinetics and major influencing parameters. As a start, the biological nature of the reduction process was confirmed and it was established, that the endogenous electron donors, (present in the activated sludge) batch are not limiting, and while additional substrate (lactate and acetate) slightly increases initial (zero order) reduction rates, overall improvement was negligible. Additionally, the overall reactions were described with first-order kinetics. It was previously assumed that it takes several days for the reaction to be completed, however, a significant fraction of total iron was already reduced after 24 h and the majority after 48 h. To determine the parameter dependency of Fe(III) reduction, different scenarios were experimented. The largest extent was the MLSS dependency, where a comprehensive set of results provided good data to introduce a mathematical model for the reaction. Sludges from two different plants were analyzed and gave comparable results. Temperature dependency was tested and while due to the small number of batch tests the exact parameter was not determined, temperature dependency was conclusive.

Throughout the experiments, P release was observed parallel to the reduction processes. This can be explained by different stoichiometry at the different valence of iron or, with competing ions at precipitation. Literature has suggested that sulphate may induce additional P release.

A dedicated scenario for the impact of sulphate concentration on iron reduction was carried out, and while different Fe:S ratios gave similar Fe(III) reduction rates, an increased P release (due to reduction processes) was observed with higher initial sulphate concentration. This interaction needs more detailed attention in activated sludge in order to exploit during recovery processes. The salinity of the wastewater may be an important factor to consider when developing P recovery strategies.

During the number of experiments with reference cases and different scenarios, it was consistently observed that sulphate reduction starts after around 24h when the majority of Fe was already reduced. This observation induced the author's interest in Terminal Electron Accepting Processes (TEAP).

Regardless of the iron concentration or the Fe:S ratio, the sulphate reduction was delayed. Literature suggests that it can be due to the availability of electron donors, which favors Fe(III) reduction under the examined batch conditions, or the facultative nature of the microorganisms that can utilize different electron acceptors. While the TEAP hierarchy could be an interest for operational purposes, the exact determination of the microbial mediation of the process is for novelty modeling.

Finally, Chapter 4 summarizes the findings on the full-scale and laboratory-scale observations by integrating them into a full-plant focus model. In this work, a complex full-plant model ("Focus model" in Sumo21) was chosen to be extended as it has a structure that involves the components and the mechanisms (or pre-cursor of mechanism) that were considered in this work. This way Fe(III) reduction studies and simulation of a full-scale plant could be done on the same model. The observed interactions of the full-scale plant (Villefranche de Lauragais) were demonstrated with the calibrated process units and model. The impact of the aeration pattern, different iron dosage strategies, and the additional dose of the return sludge liquor were adequately simulated.

However, the interactions are too complex to properly calibrate the model on a more global scale. Interactions between chemical and biological processes are complex and not well understood. The full-plant model presented here took the first step in that direction regarding the suggestion for VFA uptake inhibition and terminal electron accepting processes. In such a complex model with detailed processes and a lot of interactions, it is difficult to introduce a parameter that only has an impact on the specific process. However, in this case, for example, PHA storage by PAO is a competing process with glycogen storage by GAO, therefore if only PHA storage is inhibited (to which there is more evidence in literature) the competition could be deteriorated resulting in poor P removal despite of the actual observations of improved performance.

The increasing model complexity seems to be a double edge sword. On one side, the series of experiments revealed certain interactions (such as the hierarchy of TEAP) that could be important to include in the model and the applied model (ie. the extension of Sumo2S) could provide a good basis as it already contains the model components and some of the interactions. However, there is not sufficient data available to properly calibrate these new observations, and including a new type of competition may derail the initial, properly calibrated process accuracy.

After my experience of fitting a new process/parameter into a complex model and trying to understand the interactions which approach holds several uncertainties and limitations, a different approach would be to take a more simplistic model and extend that by calibrating the potential interactions with each existing process.

After all, this work presented the challenges of the operation of a special facility and aimed to introduce new concepts. It is recommended to further analyze the significance of these processes and evaluate the benefit of the model accuracy for other types of configurations. While the case study represented a conventional activated sludge process at a small/medium-scale facility, the findings of this thesis are likely to be applicable to other technologies and sizes.

As George E.P. Box said, “all models are wrong but some are useful”

List of Figures

Figure 1.2-1. Simplified visualization of anaerobic (A) and aerobic (B) processes of PAO (Seviour et al., 2003) 3
Figure 1.2-2. Simplified presentation of Tetrasphaera and typical PAO processes and interactions under anaerobic and aerobic conditions (Barnard et al., 2017) 4
Figure 1.2-3 Anoxic processes of denitrifying GAO and PAO synergy according to Rubio-Rincon et al. (2017) 5
Figure 1.2-4 Conventional EBPR configurations (a) A2O (b) Bardenpho (c) mUCT (d) VIP, designed in SUMO21 software 7
Figure 1.2-5 Examples of S2EBPR configurations (Tooker et al., 2018). (a) Side-stream RAS fermentation (SSR) (b) Side-stream RAS fermentation with external carbon addition (SSRC) (c) Side-stream MLSS fermentation (SSM), (d) Unmixed, in-line MLSS fermentation (UMIF) 9
Figure 1.2-6 Detailed anaerobic metabolism of different PAO and GAO by Oehmen et al. (2010) 10
Figure 1.2-7 EBPR model framework proposed by Dunlap et al. (2016) 11
Figure 1.3-1 Pourbaix diagram for iron, adapted from Kappler and Straub (2005) 15
Figure 1.3-2 Basic presentation of iron redox mechanism 16
Figure 1.3-3 Description of adsorption and co-precipitation of phosphate on hydrous ferric oxides - HFO (Hauduc et al., 2015) 22
Figure 1.3-4 A simplified version of the HFO model coupled to ASM2d (Solon thesis, 2017) 22
Figure 1.3-5 Fe-P-S interactions by Hauduc et al. (2019) 23
Figure 1.4-1 “Biological window” of Eh-pH diagram where redox transformation occurs in AS systems (Charpentier et al., 1998) 24
Figure 1.4-2 ORP, DO and pH curves presenting specific bending points associated with nitrogen removal (α: end of nitrification, β beginning of denitrification, and χ end of denitrification) in aeration cycles (figure by Michel Mauret, personal communication, 2018) 25
Figure 1.4-3 Dominant electron-accepting processes (EPA 542-R-13-018) 26
Figure 1.4-4 Chemical dosage strategies presented by Minton and Carlson (1972) 27
Figure 2.2-1 Picture (site and sensors) and Flow scheme of Villefranche de Lauragais wastewater treatment plant with potential iron dosage points 49
Figure 2.2-2. Typical cycles (DO, ORP, NH4, NO3) with various phase lengths (aerated and unaerated), and associated DO and ORP bending point corresponding to NH4 or NO3 removal indicators (downloaded form: myinflex.com) 50
Figure 2.2-3 P release and uptake test schedule 52
Figure 2.3-1 daily pattern of soluble COD to total COD, and total phosphorus to soluble COD ratio in Villefranche de Lauragais wastewater 55
Figure 2.3-2 Typical daily variation and cycles in the aeration tank (01/12/2018, iron dose A). Aeration time ratios are indicated for three periods: 0-8h, 8h-20h, and 20h-24h. 56
Figure 2.3-3 a) Phosphorus and b) nitrogen removal efficiency as a function of loading rate 57
Figure 2.3-4 Phosphate removal as a function of a) P loading rate and b) influent TP concentration (2019-2021) 57
Figure 2.3-5 Phosphate versus total phosphorus concentration in the effluent (2019-2021) 58

Figure 2.3-6 Two periods with zero iron dosage. (a) 24/07/2019 $P_{average}$ = 1.74 mg P/l (b) 25/07/2021 $P_{average}$ = 1.61mg P/l. (c) 04/04/2021 $P_{average}$ = 1.16 mg P/l (d) 06/04/2021 $P_{average}$ = 0.92 mg P/l. The aeration time ratio is given for 0-8h, 8-20h, 20-24h. 59
Figure 2.3-7 Batch tests (a) anaerobic for phosphate release (Sept 2019, June 2020) ; (b) anoxic and aerobic for phosphate uptake after anaerobic release (Sept 2019). Dot lines for the first-order model. . 61
Figure 2.3-8 a) Correlation between MLSS concentration (g/L) and cumulated aeration time per day (h/days) in 2019 and b) related energy demand for aeration 63
Figure 2.3-9 Effect of sludge wastage and centrifuge (grey lines) on PO4 (mgP/L) and MLSS concentration (g TSS/l) 64
Figure 2.3-10 Phosphate levels for different periods with various iron dosages. Pure biological treatment (Fe: P=0) during two periods in 2019 and 2021; dosage in the biological reactor at two dosage levels (A, B); the dosage on sludge liquor only (C). 65
Figure 3.3-1. Total Fe(II) to final Fe(II) concentration ratio in sludge A (Villefranche de Lauragais) and sludge B (Seine Valenton) 81
Figure 3.3-2. a) measured and calculated iron concentrations in a selected batch reactor (sludge A, TSS=3.442 g TSS/l) b) first-order kinetics illustrated on a logarithmic scale (up to day 3). 82
Figure 3.3-3. Reduced fraction of Fe(III) dosed at the beginning of the experiment (duplicated tests) for different organic substrates addition 83
Figure 3.3-4. Iron reduction rate constant as a function of VSS concentration. 84
Figure 3.3-5. Iron and sulphate reduction, phosphate release, and soluble iron for different SO_4 to Fe ratios. a) high Fe - low S; b) high Fe – high S; c) low Fe - low S; d) low Fe - high S. 84
Figure 3.3-6. Iron reduction rates measured for different SO_4 to Fe molar ratios (Fe concentrations: 40 – 150 mg Fe/l and sulphate concentrations: 15 – 50 mg S/l) 86
Figure 3.3-7. Estimated iron fractions in different S to Fe ratio reactors; a) high Fe -low S; b) high Fe – high S; c) low Fe -low S; d) low Fe - high S. Components are particulate iron(III) hydrous oxide (XFe^{3+}), soluble iron(II) (SFe^{2+}), iron(II) sulfide (FeS), iron(II) phosphate (vivianite), other particulate iron(II) (XFe^{2+}) 86
Figure 3.3-8. Estimated phosphorus fractions in different S to Fe ratio reactors a) high iron-low S b) high iron – high S c) low iron-low S d low iron- high 87
Figure 3.4-1. Zero-order iron reduction rate constants as a function of iron concentration in different studies (based on Wang et al., 2019 – using average values to display Nielsen, 1996) 88
Figure 4.2-1 Villefranche de Lauragais plant configuration in Sumo21. ($V_{contact\ tank}$=33 m^3; V_{ana}= 350 m^3; $V_{aeration}$= 2410 m^3; V_{degas}= 24 m^3) 105
Figure 4.3-1 Calibration steps for model extension 106
Figure 4.4-1 Aerated/unaerated phase time presentation (+ aerated, - unaerated) over 2 days. Measured data:17-18. 06. 2019 114
Figure 4.4-2 DO concentration in aeration basin a) measured Inflex sensor) b) simulated (Sumo) values 115
Figure 4.4-3 Typical daily profile measured with online sensors in the aerated basin. Ammonia (a) and nitrate (b). Dark blue: one typical example (2019), Grey zone: Min and max of a one-month period, blue light dot: average value. 115
Figure 4.4-4 Simulated ammonia (a) and nitrate (b) concentrations (2 days) 116
Figure 4.4-5 Effluent phosphate concentration values: online measurement (May 2020), simulation with default model, and simulation with the calibrated model 119

Figure 4.4-6. Phosphate release batch test and simulation with the calibrated model..... 120
Figure 4.4-7 P release and uptake batch tests and simulation with calibrated model (a) anaerobic-aerobic cycle (b) anaerobic anoxic cycle..... 121
Figure 4.4-8 P pattern with different aeration fractions within cycles. (a) 20% (b) 28% (c) 35% (d) 41%. Corresponding aeration cycles are represented by DO concentration (gray line)..... 122
Figure 4.4-9 Phosphate profile in the aerated basin with varying aeration time..... 123
Figure 4.4-10. Simulation of the effect of iron dose on phosphate concentration in the aerated basin a) regular dose on the left (dose A) and b) increased dose on the right (dose B)..... 124
Figure 4.4-11 Simulation of phosphate concentration with discontinuous sludge wastage (grey zone: period of wastage and sludge dewatering) 125

List of Tables

Table 1.3-1 Microbial groups catalyzing iron redox transformations (Kappler and Staub, 2005) 17
Table 1.3-2 Kinetic rates for iron reduction in different studies 20
Table 2.2-1 Data monitoring during the 3-year study 51
Table 2.2-2 $FeCl_3$ dose during different periods of the study 53
Table 2.3-1 Villefranche raw influent concentration ratios compared to typical ratios from Rieger et al. (2012) 54
Table 2.3-2 Summary of phosphate concentration (based on a daily average, i.e. 24h average measurement in the aerated basin) for different periods with various iron dosages. 65
Table 3.2-1. Experimental scenarios of iron reduction batch tests 78
Table 4.3-1 Model state variables 110
Table 4.3-2 Model parameters 110
Table 4.3-3 Sumo functions for calculated variables 112
Table 4.3-4 A selection of kinetic rates 113
Table 4.4-1 Calibrated model parameters 118
Table 4.4-2 Calibration outcomes and remaining challenges 126

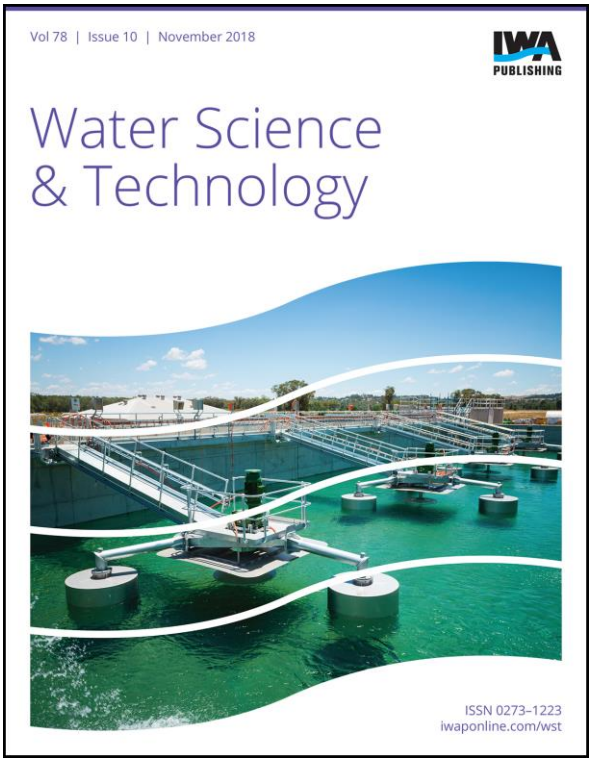

Recent advances in bio-P modelling – a new approach verified by full-scale observations

Erika Varga, Hélène Hauduc, James Barnard, Patrick Dunlap, Jose Jimenez, Adrienne Menniti, Peter Schauer, Carlos M. Lopez Vazquez, April Z. Gu, Mathieu Sperandio and Imre Takács

ABSTRACT

This paper summarizes recent developments in biological phosphorus removal modelling, with special attention to side-stream enhanced biological phosphorus removal (S2EBPR) systems on which previous models proved to be ineffective without case-by-case parameter adjustments. Through the research and experience of experts and practitioners, a new bio-kinetic model was developed including an additional group of biomass (glycogen accumulating organisms – GAOs) and new processes (such as aerobic and anoxic maintenance for PAO and GAO; enhanced denitrification processes; fermentation by PAOs which – along with PAO selection – is driven by oxidation-reduction potential (ORP)). This model successfully described various conditions in laboratory measurements and full plant data. The calibration data set is provided by Clean Water Services from Rock Creek Facility (Hillsboro, OR) including two parallel trains: conventional A2O and Westbank configurations, allowing the model to be verified on conventional and side-stream EBPR systems as well.

Key words | glycogen accumulating organisms, oxidation-reduction potential, phosphorus accumulating organisms, side-stream EBPR

Erika Varga (corresponding author)
Mathieu Sperandio
LISBP, INSA Toulouse,
135 av. de Rangueil 31077, Toulouse,
France
E-mail: *erika.varga@insa-toulouse.fr*

Erika Varga
Hélène Hauduc
Imre Takács
Dynamita,
7 Lieut-dit Eoupe, La Redoute, 26110 Nyons,
France

James Barnard
Patrick Dunlap
Black and Veatch,
8400 Ward Parkway, Kansas City, MO 64114,
USA

Jose Jimenez
Brown and Caldwell,
2301 Lucien Way, Suite 250, Maitland, FL,
USA

Adrienne Menniti
Peter Schauer
Clean Water Services,
16060 SW 85th Av. Tigard, Oregon 97224,
USA

Carlos M. Lopez Vazquez
IHE Delft,
Westvest 7, Delft 2611 AX,
The Netherlands

April Z. Gu
Cornell University,
263 Hollister Hall, Ithaca, NY,
USA
and
Northeastern University,
360 Huntington Ave,
Boston, MA 02115,
USA

INTRODUCTION

As there is an increasing need for phosphorus removal from wastewaters, a wide range of treatment technologies are implemented in order to satisfy the required limits. Conventional enhanced biological phosphorus removal (EBPR), with alternating anaerobic/aerobic conditions is a widely used process. However, its stability mostly relies on the availability of influent readily degradable carbon source, especially volatile fatty acids (VFAs). Carbon supply in the anaerobic zone often needs to be supplemented from an external source such as fermentation. An alternative solution to increase process stability where influent VFAs are not available is the implementation of an anaerobic

doi: 10.2166/wst.2018.490

side-stream reactor for sludge hydrolysis and fermentation (S2EBPR). Tooker *et al.* (2017) reviewed various side-stream configurations and compared performance to conventional facilities. The authors reported higher phosphorus removal efficiency in S2EBPR systems.

Clean Water Services (CWS) is investing in infrastructure to be able to operate using multiple side-stream EBPR configurations (e.g. Westbank and return activated sludge – RAS- fermentation), while retaining the use of a conventional anaerobic-anoxic-oxic (A2O) system (Schauer *et al.* 2017). A process model is an ideal tool for utilities with flexible infrastructure because the model can support the decision on which configuration is optimal for the observed influent and operating conditions. An operational model is mostly beneficial when it can further be used to support the choice of key operational parameters such as determining the optimal anaerobic detention time for RAS fermentation.

Dunlap *et al.* (2016) studied a full-scale side-stream facility (Westside Regional) and reported that, with existing models, a significant parameter adjustment was necessary to meet nutrient profiles especially regarding P uptake and release parameters. In order to incorporate the observed behavior, three different modeling approaches have been suggested: a multiple species metabolic model; new PAO mechanisms and multiple PAO parameters. Combining new PAO mechanisms, and multiple PAO parameters, Dunlap *et al.* (2016) proposed a new model. As in S2EBPR, the PAO populations may differ from those in conventional EBPR systems, and they exhibit different metabolic traits, a second group of PAOs were introduced representing these conditions. The competition between the modeled PAO groups was dependent on the specific conditions. The first, a conventional group of PAOs (PAO1) includes a wide range of species that behave similarly to those observed in conventional EBPR. Under low ORP conditions, PAO1 is outcompeted by the second phenotypic group of PAOs (PAO2). In the PAO2 culture, fewer glycogen accumulating organisms (GAOs) are assumed to be present and PAOs with fermentation ability, such as Tetrasphaera, are assumed to be the dominant PAO species. Fermentation by PAO2 is introduced to this model under low ORP conditions. Parameters, such as growth rate, P:VFA release ratio, anoxic growth factor, aerobic and anoxic P:PHA uptake ratio, were adjusted (Dunlap *et al.* 2016).

In the ASM standard models (ASM2d, ASM2d + TUD; ASM3 + bio-P; Barker-Dold model; UCTPHO+) only one population of PAO is considered (Hauduc *et al.* 2013). In these models, the kinetic and stoichiometric parameters are calibrated to include the impact of GAO presence instead of considering the competition with GAOs. The ability of PAOs to use a wider range of substrates and the fermentation capability under specific conditions are not considered either. Moreover, anaerobic maintenance is only considered by Barker & Dold (1997); UCTPHO+ (Hu *et al.* 2007) and ASM2 + TUD (Meijer 2004).

GAO population has been introduced in some metabolic research models (Gu *et al.* 2008; Oehmen *et al.* 2010; Lanham *et al.* 2014). The competition between the two populations has been described based on the effect of temperature, pH and carbon source (Lopez-Vazquez *et al.* 2008).

According to recent research, intracellular compounds have a major effect on both the stoichiometric and kinetic parameters of PAOs, thus affecting EBPR predictability. Welles *et al.* (2017) demonstrated that a higher poly-P content correlates with higher anaerobic kinetic rates (P release) of PAO, and as the poly-P content increased the glycogen content decreased showing that poly-P is the preferred storage compound for PAOs. In addition, lower poly-P contents resulted in a higher glycogen utilization and lower poly-P hydrolysis rates under anaerobic conditions, slowing down the anaerobic kinetic rates of PAO, which can be interpreted as an increasing use of glycogen accumulating metabolism in PAOs. HAc (acetic acid) uptake rate may increase with high P/C influent ratio or return phosphorus of the sludge line, aerobic P uptake may decrease because the PAO storage pool is saturated (Welles *et al.* 2017).

The denitrifying capability of PAOs and GAOs has been observed in laboratory and full-scale plants (Kuba *et al.* 1997). Also, the electron acceptor under anoxic conditions may differ within PAO species (Ahn *et al.* 2001a, 2011b). Rubio-Rincon *et al.* (2017) documented that the denitrifying activity of a pure PAO culture (as *Candidatus* Accumulibacter clade I) is less significant on nitrate, whereas they show higher uptake on nitrite. On the contrary, a mixed PAO-GAO culture showed higher activity under anoxic conditions using nitrate, leading to the conclusion that GAOs (as *Candidatus* Compatibacter) reduce nitrate to nitrite in A2O systems. According to that study, GAOs are not only competitors to PAOs in the anaerobic zone, but also provide electron acceptors (NO_2^-) in the anoxic zone.

EBPR treatment plants are designed with aeration zones operated at high dissolved oxygen (DO) levels (i.e. 2 mg/L) following unaerated zones. Low DO operation has been considered unfavorable for biological aerobic uptake of phosphorus by PAOs and is avoided in biological P removal plants. However, there are instances where low DO operation (e.g. with DO around 1 mg/L or less) has been proven successful for EBPR operation (Downing *et al.* 2014; Jimenez *et al.* 2014). The low DO environment at St Petersburg, Florida,

has led to phosphate uptake rates under anoxic/low DO conditions similar to aerobic conditions. Multiple studies (Camejo *et al.* 2016; Keene *et al.* 2017) examined phylogenetic abundance variations and found that in a low DO environment GAO clade are detectable, but with low relative abundance (<0.2% of total biomass according to Keene *et al.* 2017) with Accumulibacter being the dominant PAO species. Jimenez *et al.* (2017) demonstrated simultaneous biological nutrient removal (SBNR) efficiency in a full scale facility with DO concentrations ranging from 0.2 to 0.7 mg O2/L. This approach with aeration control strategy can lead to substantial energy savings while maintaining good bio-P performance.

To describe these new findings, a new model has been developed including those processes based on the proposal of Dunlap *et al.* (2016). The new calibrated model differentiates PAOs and GAOs and introduces ORP as an indicator for dominance. The biomasses therefore represent the two extremes (from a diverse PAO community e.g. with fermenting capabilities to non-poly-P accumulating GAOs) and the mixture represents the competition between the two populations, whereas GAO presence reduces the performance of conventional EBPR systems due to the competition for VFA. The model was calibrated based on full plant measurements from the Rock Creek and Durham advanced wastewater treatment plants (AWWTP) operated by Clean Water Services (Hillsboro, Oregon) and batch tests performed with sludge from the Rock Creek AWWTP. Attention was paid to make sure that the new model also predicts the performance of existing calibrated systems in typical, well characterized situations.

MATERIALS AND METHODS

Model description

The new bio-P model that has been extended was based on the Barker-Dold model (Barker & Dold 1997) approach for biological phosphorus removal. The model was developed trying to keep the structure as simple as possible while still describing a wide range of processes. As the model was extended, the structure of the components has been changed alongside the corresponding parameters.

The changes affect PAO and GAO processes (growth, maintenance, decay, carbon storage, phosphorus release and uptake, and fermentation). Stoichiometric matrix and kinetic rates can be found in Supplementary Tables A1–A5 (available with the online version of this paper), the complete model file including parameters, calculated variables, ionic species and full stoichiometric matrix is available at http://www.dynamita.com/wp-content/uploads/Sumo1.xlsm.

Model concepts and processes included in the new model are as follows:

- *One biomass (GAO)* is added to the widely used Barker-Dold (Wentzel) model. GAOs have been separated as a facultative anaerobic biomass, storing glycogen (GLY) under anaerobic conditions.
- *Temperature dependency* is introduced to favor GAO growth at higher temperatures.
- *A constant fraction of PAOs and GAOs are able to denitrify*. The denitrifying fraction of PAOs and GAOs is determined by using a reduction factor for anoxic growth.
- *Each microbial group uses a single carbon storage component* (PHA is stored by PAOs only and glycogen (GLY) is stored by GAOs only), and only VFA is stored.
- *Aerobic and anoxic maintenance* were added to precede PAO and GAO decay, which use PHA and GLY, respectively. Active biomass loss occurs only once the storage pools are exhausted.
- *Glycogen storage is inhibited under low ORP conditions* (e.g. side-stream EBPR processes), reducing or completely eliminating GAOs and providing a more optimal PAO performance. The PAO-GAO competition under extended anaerobic conditions is partially driven and captured by oxidation-reduction potential (ORP) conditions. Under low ORP conditions (e.g. long anaerobic retention time, side-stream processes), the difference in the intracellular polymer usage sequence and onset of biomass decay between PAOs and GAOs led to a biomass dominated by PAOs (Tooker *et al.* 2016, 2017).
- *PAO are able to ferment readily biodegradable substrate (S_B) under low ORP conditions*, in order to simulate the behavior of putative *Tetrasphaera* genus type of organisms when subjected to longer anaerobic SRT conditions.
- *Polyphosphate stored by PAOs are considered as one variable, as opposed to the previous model, where the stored polyphosphate was fractioned into a non-releasable and a releasable part*. This change allows PAOs to completely deplete the poly-phosphate (PP) storage pool.

Experimental data used for calibration and validation

In this project, data from aeration basins 4 and 5 of the Rock Creek AWWTP were considered. The configuration for aeration basins 4 and 5 is shown in Figure 1. High operational flexibility is available at the facility. During the calibration period, AB4 operated as A2O (primary clarifier effluent

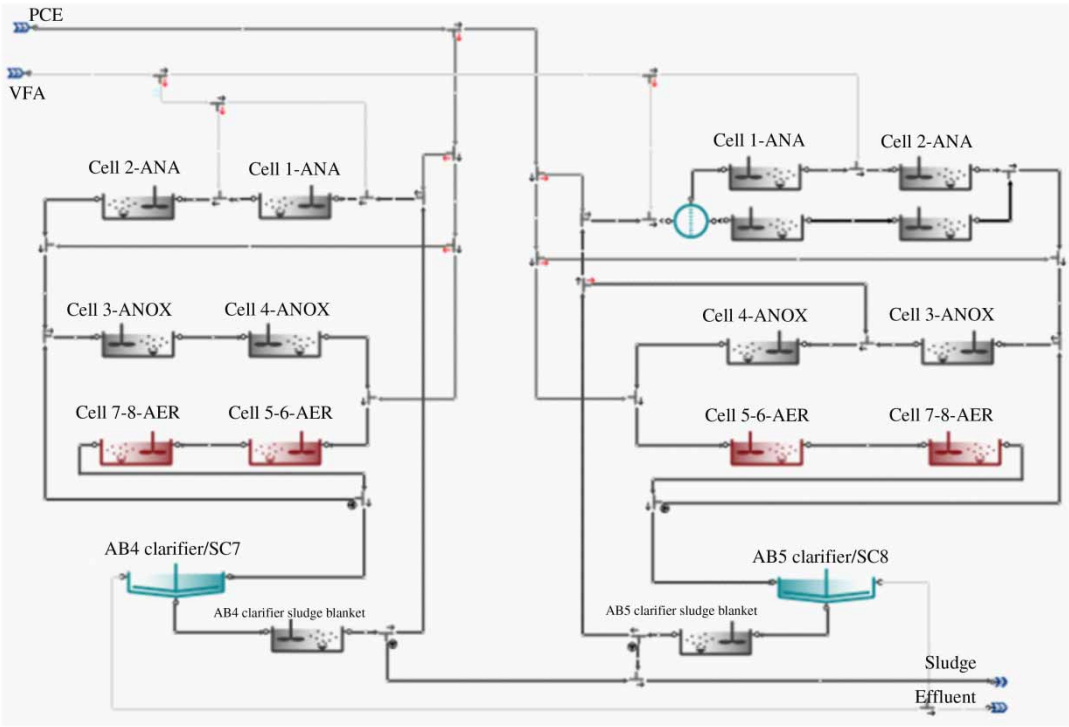

Figure 1 | Aeration basin 4 (AB4 based on A2O configuration) and aeration basin 5 (AB5 cased on Westbank configuration) configuration for simulation.

(PCE) flows to anaerobic zones – cell 1), AB5 as Westbank (PCE flows to anoxic zone – cell 3, bypassing anaerobic zones).

Table 1 summarizes the detailed aeration basin volumes in unaerated and oxic zones (the anaerobic fraction may vary based on the operational settings).

Table 1 | Aeration basin volumes of Rock Creek facility

	Basin 4	Basin 5	Unit
Total basin volume	6,380	6,380	m^3
Total anaerobic volume	620	620	m^3
Cell 1	307	307	m^3
Cell 2	313	313	m^3
Total anoxic volume	620	620	m^3
Cell 3	310	310	m^3
Cell 4	310	310	m^3
Total oxic volume	5,140	5,140	m^3
Cell 5	1,285	1,285	m^3
Cell 6	1,285	1,285	m^3
Cell 7	1,285	1,285	m^3
Cell 8	1,285	1,285	m^3
% Oxic	80.6%	80.6%	
% Unaerated	19.4%	19.4%	
% Anaerobic	9.7%	9.7%	

Operational settings at Rock Creek facility and model configuration

For the model calibration, two parallel trains of the Rock Creek wastewater treatment plant were considered with different operational settings (Figure 1).

During the period of August 2016, the AB4 train operated as an A2O system, where all the PCE flow and return activated sludge were directed to the anaerobic cell 1 and mixed liquor recirculation to the anoxic cell 3. The flow rates were adjusted to the average of the selected period.

The AB5 train during this period is operated in the Westbank configuration with side-stream anaerobic reactors. In this type of configuration, PCE and mixed liquor recycle is directed to the anoxic reactor, whereas the RAS flow and VFA addition flow to the anaerobic zones.

The anaerobic reactors are intermittently (rarely) mixed. To reflect this situation in the model, each anaerobic zone is split into two parts: a lower part with more concentrated sludge (concentration ~2.5% in the PAO-GAO model) and an upper part with lower mixed liquor suspended solids (MLSS) concentration. This is the 'compartmental approach' applied by Le Moullec *et al.* (2010). It is assumed that the samples were taken from this upper part of the reactor. Regarding the flow and volumes, 30% of the volume is

considered in the settled zone. The internal mass flow splitting can be adjusted to the current conditions.

Schauer *et al.* (2017) demonstrated the effect of different configurations on the effluent PO_4 concentration and concluded that the Westbank process with mixers turned off is beneficial for biological phosphorus removal. Even though there were uncertainties in the sampling locations, the calibration data set had been selected for this period. Figure 2 presents the effluent PO_4 concentration in each train versus the influent VFA to PO_4 ratio. The performance of the Westbank train does not depend on the influent VFA as much as the conventional, A2O train, which could be explained by the fermentation that may be occurring in the anaerobic zone, more specifically in the settled sludge phase.

In the clarifier underflows, reactors have been inserted to simulate the effect of the sludge blanket (anaerobic conditions) in secondary clarifiers. The sludge blanket plays a significant role, especially regarding phosphorus release for side-stream processes. This simplified approach was chosen to avoid having to calibrate settling properties and slowing down the model with a reactive layered clarifier. These reactors (AB4 clarifier sludge blanket and AB5 clarifier sludge blanket) therefore are not considered as part of the anaerobic zones in the basins.

The calibration period was determined based on the plant performance. In June 2016, operational changes were implemented in the facility. During the following period, significant effluent variation occurred on the AB4 train (operating as a conventional A2O system). The performance of both examined trains can be considered stable in August 2016; therefore, this period was selected for model calibration.

The calibration data set includes the following:

1. One month of operational data regarding PCE, flows and concentrations for AB4 and AB5.
2. Phosphorus and nitrogen profiles through the basins, focusing on AB4 and AB5 in the selected period (weekly grab samples).
3. P release and uptake batch test.

During calibration, the average values of the selected period have been used to meet steady-state conditions for the facility. Dynamic simulations have only been performed for the batch tests. Batch phosphorus release and uptake kinetic tests were performed at the Northeastern University.

Batch activity tests

A side-stream reactor influent (RAS) sample from the AB5 train was taken on the 28th October 2016 and shipped on ice overnight for further analysis. The sample was brought to room temperature then aerated for 1 hour, and kept under anaerobic conditions for up to 36 hours. Mixing only occurred for sample collection. Every 6 hours, a sample was collected for a P release and uptake tests.

In the simulation, the following assumptions were considered:

- Samples are diluted to ~4,000 mg VSS/L concentration with secondary effluent.
- Testing takes place at room temperature (20 °C).
- Nitrification is inhibited.

The general schedule of the test:

- After the storage period, an 800 ml sample was taken, 3 hours' aerobic conditions (nitrification inhibitor added).
- Forty-five minutes of anaerobic phase (sodium acetate addition at the start of the phase).
- Three hours of aerobic phase.

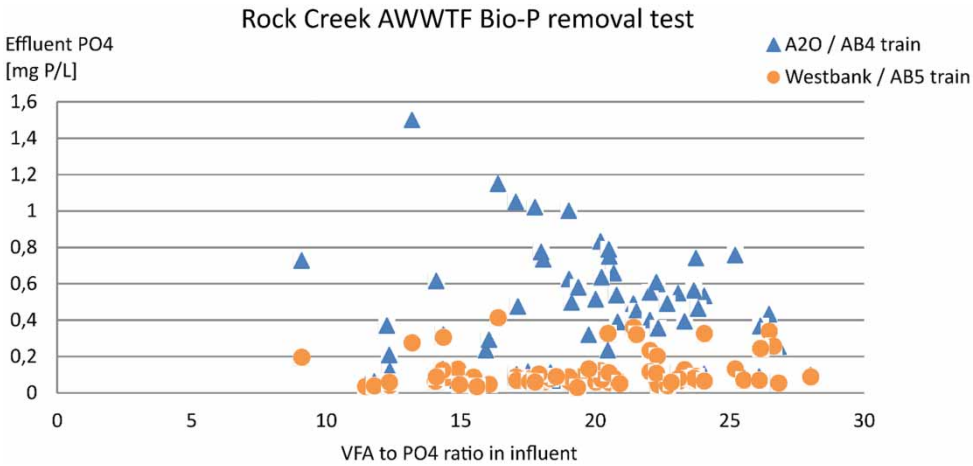

Figure 2 | Effluent PO4 versus influent VFA:PO4 during testing period (Schauer *et al.* 2017).

During the aerobic phase, DO concentrations reach saturation.

Parameter estimation and calibration procedure

As a new biomass variable and new processes have been introduced to the new model, new stoichiometric and kinetic parameters have been added and some of the existing ones recalibrated.

The model calibration was carried out based on the following.

Full plant configurations managed by Clean Water Services: 1. Rock Creek Facility: data sets from the plant for AB4 and AB5, including PCE variation, full plant P profiles and operational changes; 2. Durham AWWTP: primary effluent, nutrient profile and effluent data for the selected time period as well as operational settings.

Batch tests: data sets from Northeastern University, including phosphorus uptake and release tests under controlled conditions.

The parameter calibration procedure focuses on the following (only manual trial and error tuning was followed):

1. *Maximum specific growth rate for PAOs and GAOs*
   Formerly, the base model was calibrated to the mixed culture of PAOs, including GAOs. In the new model, the maximum specific growth rate was determined to have a similar weighted average for PAO-GAO growth as the mixed culture in general configurations (although this may vary in specific configurations).
2. *Fermentation rate for PAOs*
   The fermentation rate was determined to ensure the VFA concentration and biomass activity for the required performance in PAO culture that did not contain GAOs (e.g. Westbank).
3. *Anoxic reduction rates for PAO and GAO growth and decay*
   Anoxic reduction for PAO growth was increased to match the P profile within the aeration basin and enable denitrification under specific conditions.
4. *Maintenance*
   Maintenance processes for both PAOs and GAOs have been introduced and considered to occur at the same rate as decay processes, but preceding decay until the storage pool is exhausted.
5. *P:VFA release ratio*
   During the laboratory tests, a high P to VFA release ratio was observed. The separation of GAOs justifies raising the previously used default value for this parameter.
6. *Aerobic PHA:PP uptake ratio*
   Aerobic PHA to PP uptake ratio was adjusted to the batch test results with PAO cultures.
7. *Oxygen half saturation*
   Oxygen half saturation terms were determined to ensure PAO dominance under micro-aerobic conditions.
8. *Stoichiometric yields for GAOs*
   Aerobic and anoxic yields for GAO on glycogen were calibrated to encourage GAOs in the PAO-GAO competition in the aerobic and anoxic zones.
9. *ORP parameters*
   ORP calculations are based on dissolved O_2, NO_x and CH_4. CH_4 was chosen as an indicator for low ORP conditions as this model does not consider sulfur reactions to further characterize ORP in anaerobic zones. The default value for ORP inhibition for storage in GAOs and the saturation term for PAO fermentation was determined during the calibration, and the parameters may require adjustments for the specific configuration.
10. *Temperature dependency*
    GAO growth and maintenance has a higher temperature dependency than PAOs. The selected default parameter values are based on Lopez-Vazquez *et al.* (2009).

RESULTS AND DISCUSSION

Data set and sampling

The PCE fractions and hydraulic settings were calibrated based on a daily average data set provided by Clean Water Services (Table 2). Table 3 summarizes the calibrated PCE concentrations. The selected period was August 2016, where both studied trains showed a stable performance. Nutrient profiles are compared to grab sample data. As these samples were taken weekly, inconsistencies to the average data set in the aerobic zone effluent may occur based on the sampling time. As mentioned before, there are uncertainties about the representativeness of sampling locations in the unmixed anaerobic zone of the AB5 train. Additionally, some back-mixing from the anoxic zone can cause an apparent P uptake (see Figure 4).

AB4 results

Table 4 summarizes the average measured data set for AB4 secondary effluent in the calibration period and the

Table 2 | Calibration data set

	Variable	Unit	Numbers of measurements	Average	Minimum	Maximum
Primary clarifier effluent	COD	mg COD/L	19	297	260	368
	TSS	mg TSS/L	14	77	60	102
	VSS	mg VSS/L	4	58.5	52	68
	Alkalinity	mg CaCO3/L	19	224	203	240
	TKN	mg N/L	4	42.4	37.1	46.2
	NHx	mg N/L	31	32.1	25.0	37.6
	NOx	mg N/L	9	0.53	0.10	1.59
	TP	mg P/L	4	3.83	3.50	4.16
	PO4	mg P/L	31	2.30	1.52	3.59
Secondary clarifier effluent (SCE) of AB4	COD	mg COD/L	9	27.4	21.1	32.5
	TSS	mg TSS/L	19	3.97	1.60	5.40
	pH		9	6.74	6.55	6.89
	Alkalinity	mg CaCO3/L	19	103.5	75.2	128.0
	NHx	mg N/L	19	0.081	0.038	0.159
	NOx	mg N/L	19	18.2	13.0	21.6
	TP	mg P/L	5	0.50	0.26	1.21
	PO4	mg P/L	31	0.23	0.04	1.50
Secondary clarifier effluent (SCE) of AB5	COD	mg COD/L	9	27.7	23.6	32.0
	TSS	mg TSS/L	19	3.3	2.4	5.2
	pH		9	6.70	6.54	6.85
	Alkalinity	mg CaCO3/L	19	107	79	131
	NHx	mg N/L	19	0.17	0.09	0.38
	NOx	mg N/L	19	17.5	12.0	19.8
	TP	mg P/L	5	0.28	0.19	0.49
	PO4	mg P/L	31	0.104	0.031	0.414

Table 3 | Rock Creek primary clarifier effluent concentrations

Variable	Unit	Measured average	PAO-GAO model	Difference	Barker-Dold model	Difference
COD	mg COD/L	297.05	297.05	0%	294.15	−1%
TSS	mg TSS/L	76.86	118.80	+54.57%	129.50	+68.5%
VSS	mg VSS/L	58.5	100.86	+72.4%	109.60	+87.3%
Alkalinity	mg CaCO3/L	224.16	250.00	+11.53%		–
TKN	mg N/L	42.4	42.4	0.0%	42.5	+ 0.24%
NHx	mg N/L	32.14	32.14	0.0%	32.14	0.0%
NOx	mg N/L	0.53	0.53	0 mg N/L	0.53	0 mg N/L
TP	mg P/L	3.83	3.83	0%	3.5	−8.59%
PO4	mg P/L	2.3	2.3	0%	2.3	0%

simulation results of the PAO-GAO and Barker-Dold models. Due to different heterotrophic kinetics in the Barker and Dold model, a lower MLSS is observed.

Figure 3 presents nutrient profiles within the A2O system in aeration basin 4. As mentioned before, the measured data are based on weekly grab samples, thus the differences in NOx concentration at the end of the aeration basin. Regarding the simulations, in general the PAO-GAO model shows satisfactory agreement with the measured data. However, the P release is overestimated in anaerobic zones, and nitrate concentration is generally lower. The Barker and Dold model simulates the NOx profile in the A2O process properly. However, it shows a slight P release in the anoxic zone (due to decay and PP lysis) where P uptake is expected. According to literature experiments, the PAOs decay rate is higher under aerobic conditions,

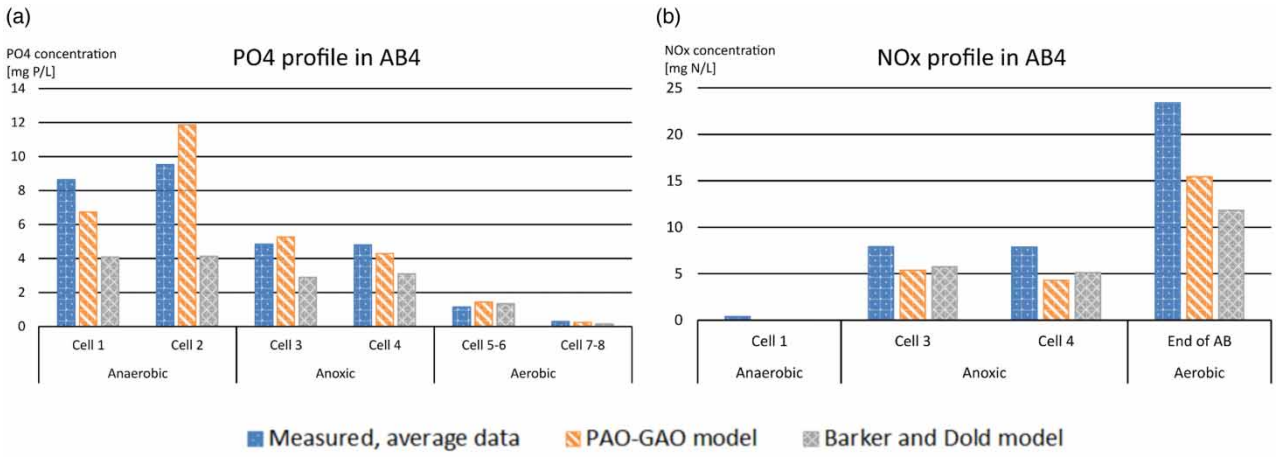

Figure 3 | Nutrient profiles in AB4 (a) PO4 profile; (b) NOx profile.

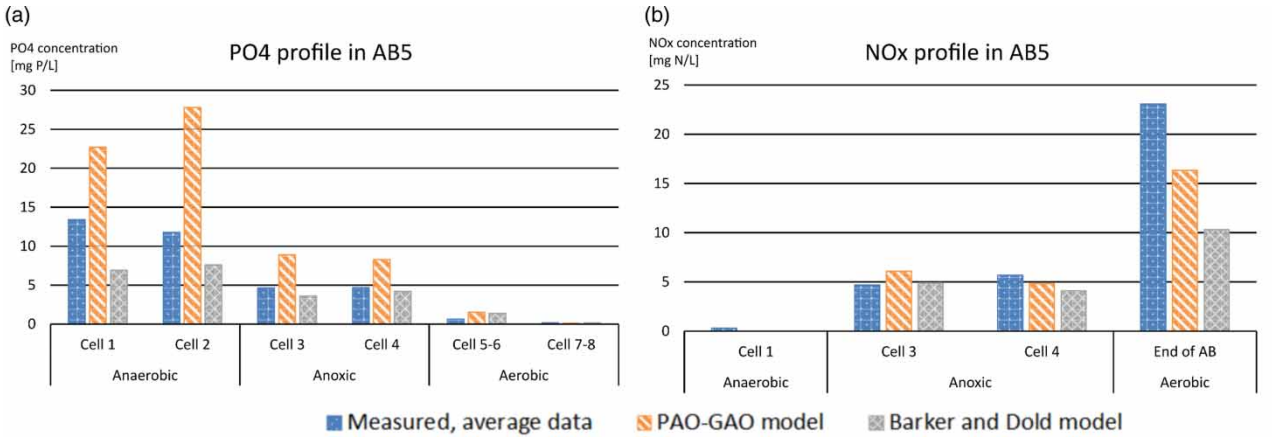

Figure 4 | Nutrient profiles in (a) PO4 profile; (b) NOx profile.

Table 4 | AB4 secondary effluent performance

Variable	Unit	Measured average	PAO-GAO model	Difference	Barker-Dold model	Difference
COD	mg COD/L	27.4	26.5	−3.28%	28.8	+5%
TSS	mg TSS/L	3.97	4.00	+0.76%	4.00	+0.76%
pH		6.74	6.46	−4.15%	–	–
Alkalinity	mg CaCO3/L	103.5	103.3	+0.19%	–	–
NHx	mg N/L	0.08	0.16	+0.079 mg N/L	0.20	+0.12 mg N/L
NOx	mg N/L	18.23	16.67	−8.56%	12.00	−34.1%
TP	mg P/L	0.50	0.48	−0.02 mg P/L	0.32	−0.17 mg P/L
PO4	mg P/L	0.23	0.24	+0.01 mg P/L	0.15	−0.08 mg P/L

and is low/negligible under anoxic and anaerobic conditions (Siegrist *et al.* 1999; Lu *et al.* 2007) and maintenance seems to be the main endogenous process. In the PAO-GAO model, aerobic and anoxic maintenance precede decay where no P release occurs.

According to the simulation, 81% of the combined PAO-GAO population (which was formerly considered as PAO) is PAO, resulting in good EBPR performance.

As observed during the simulations, in A2O configurations, the expected CH_4 production in the anaerobic zone (used as an indicator of deep anaerobic conditions) is relatively low, which has a major impact on the ORP. Under these conditions (ORP~ −50 mV), a PAO-GAO competition is observed. The dominant PAO population is considered to use VFA as a substrate.

AB5 results

Table 5 summarizes the average measured data for secondary effluent in aeration basin 5, operating as Westbank, with the simulation results.

Figure 4 shows the measured data with simulation results regarding the nutrient profile through the reactor. As discussed before, the anaerobic zones of the train were unmixed at this period, therefore part of the differences between the simulation results and measurement data may be due to that (however, as presented in the AB4 simulation results, a slight overestimation of the P release was observed). Moreover, as seen in Figure 4(a), the measurements show P uptake in the anaerobic zone that is probably due to some back-mixing from the anoxic zone around the sampling point. The

Table 5 | AB5 secondary effluent performance

Variable	Unit	Average	PAO-GAO model	Difference	Barker-Dold model	Difference
COD	mg COD/L	27.7	25.8	−6.9%	28.2	+1.8%
TSS	mg TSS/L	3.3	3.3	0%	3.3	0%
pH		6.7	6.45	−3.73%	–	–
Alkalinity	mg CaCO3/L	107	100.2	−6.4%	–	–
NHx	mg N/L	0.17	0.18	0 mg N/L	0.21	+0.04 mg N/L
NOx	mg N/L	17.50	16.35	−6.57%	10.31	−41.1%
TP	mg P/L	0.28	0.33	+0.05 mg P/L	0.32	+0.04 mg P/L
PO4	mg P/L	0.104	0.12	+0.016 mg P/L	0.15	+0.046 mg P/L

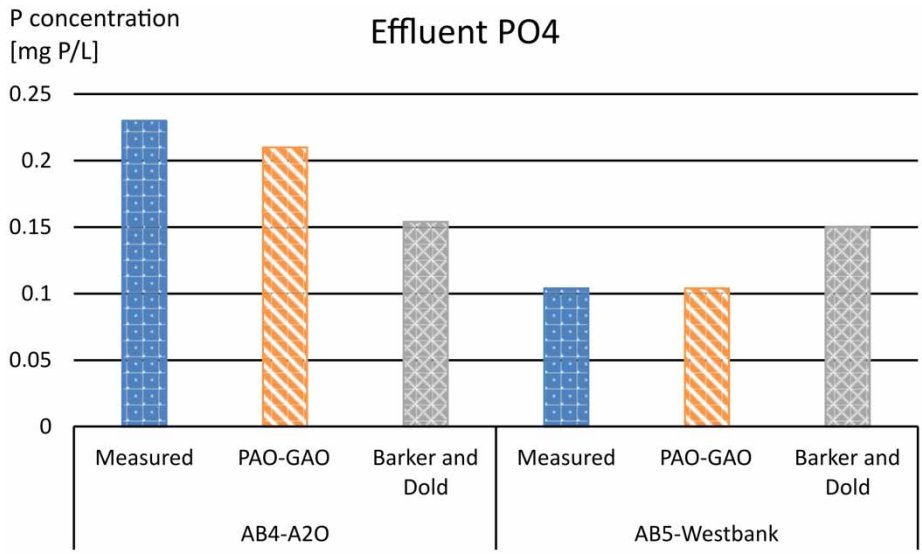

Figure 5 | Secondary effluent P concentrations.

measured phosphorus profile in the AB5 train (Westbank) was deemed not to be representative due to the sampling uncertainties, therefore was not taken into account during calibration.

The observed deep ORP conditions (ORP <– 100 mV) typically are a disadvantage for the substrate uptake of GAOs. The PAO species present are able to ferment under these conditions and also show nitrate uptake in the anoxic zone. The changing functionality according to the specific conditions cannot be properly described with previous models. Figure 5 summarizes the effluent PO_4 measurements and simulation results on the two trains. According to the simulations, the PAO-GAO model shows a closer correlation regarding the difference in the effluent values, which is due to the different processes in the basins.

Batch tests

Phosphorus release and uptake tests have been performed with sludge from the AB5 train, as described in the materials and methods section, in order to determine the kinetics in side-stream systems. Figure 6(a)–6(f) display the results of the laboratory measurements and the dynamic simulation.

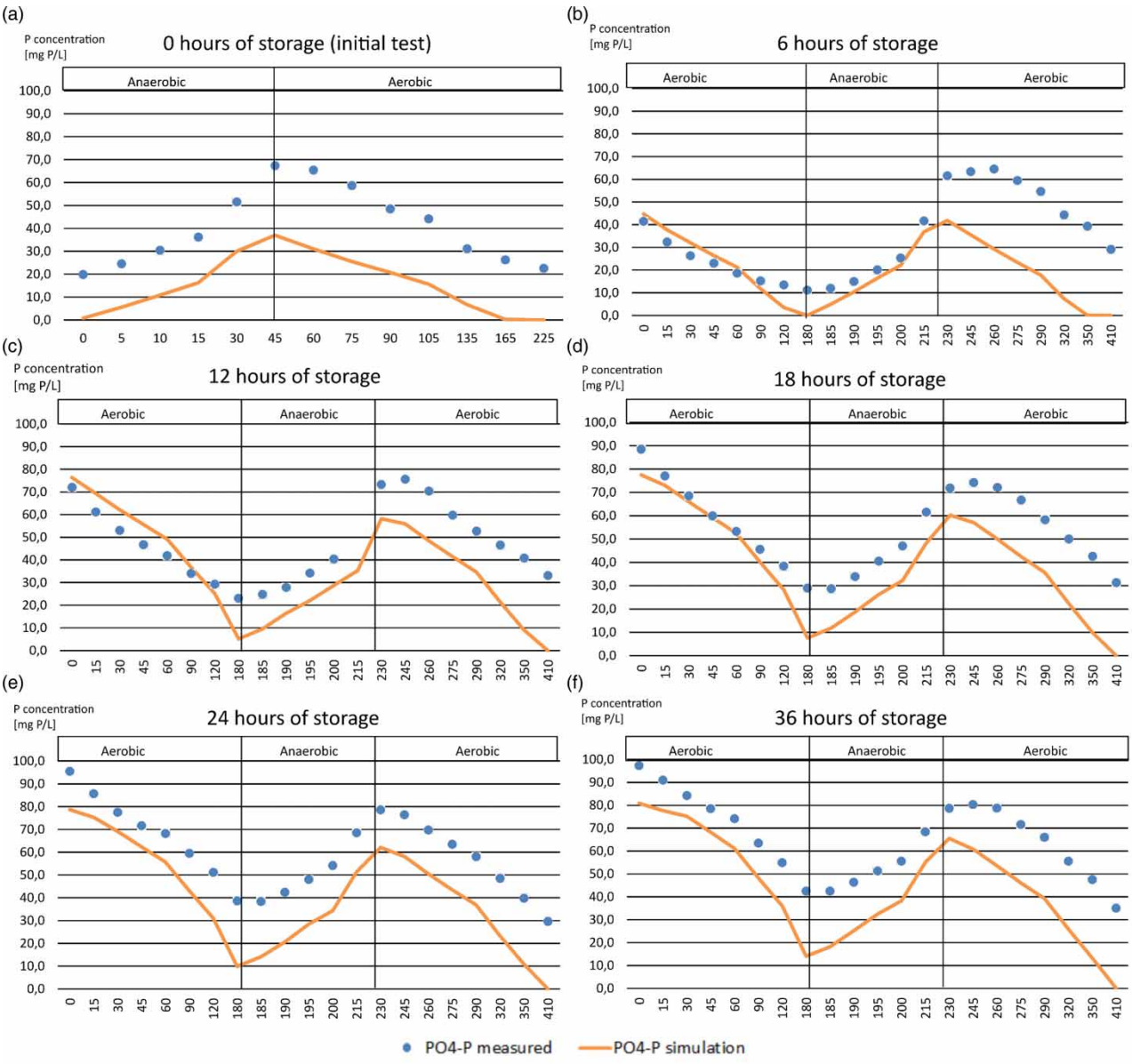

Figure 6 | Phosphorus uptake and release tests with alternating aerobic/anaerobic periods after the indicated anaerobic storage period (X axis represents the time of the experiment in minutes).

In the simulations, the biomass was taken from AB5 RAS during the calibration period (steady state simulation). In the S2EBPR systems, low abundance of GAOs was observed in several cases (Tooker *et al.* 2017) and also the model predicts negligible GAO concentration due to the discussed side-stream conditions. The tests, therefore, represent a biomass where PAO-GAO competition does not have an impact on the simulation results.

Phosphorus release and uptake tests were performed in a controlled laboratory environment; the pH level target is 7.00–7.15, controlled by HCl or NaOH addition. Moreover, nitrification inhibitor was added to the sample to facilitate the creation of anaerobic conditions during the unaerated phase.

Figure 6(a)–6(f) show the simulation results for the initial testing, 6-12-18-24-36 hours of storage time, respectively. The initial difference between the simulation and the measured data in Figure 6(a) can be explained by uncertainties regarding storage prior to the experiments. For the simulation, diluted sludge from AB5 (Westbank) simulation was taken (note that the sampling for the calibration period was not at the same time as the batch test experiments, thus differences in the exact sludge composition may occur. That may be the reason for the discrepancies between the maximum phosphorus released in the simulation (~80 mg P/L) vs. the batch test results (~95 mg P/L).

As discussed before, in the new model stored polyphosphate is represented by one variable, which allows PAOs to release all stored phosphorus unlike in the Barker-Dold model where a fraction of PP is non-releasable. This may require additional parameter adjustment in order to match the P release and uptake tests.

SUMMARY

As pointed out by Dunlap *et al.* (2016), a new approach in biological phosphorus removal modeling is necessary in order to successfully simulate S2EBPR configurations that do not depend on the presence of influent VFA.

The proposed PAO-GAO model shows an improvement in bio-P performance prediction due to the introduced processes based on recent research and modified by detecting the extent of anaerobic conditions using an ORP estimator (ORP is estimated for all zones, not only the anaerobic zone). Under normal ORP conditions, up to −100 mV range in anaerobic zones, the model allows the coexistence of PAOs and GAOs. This, through the loss of VFA to non-P removing GAOs, hampers the performance of the bio-P system, as experienced in the A2O configuration.

Under extreme low ORP conditions (lower than −150 to −200 mV) GAOs are disappearing through substrate storage limitation in the model and more stable bio-P performance can be observed in agreement with experimental and full-scale results.

There are conditions where GAOs are able to outgrow PAOs (e.g. under high temperatures), simulating the loss of biological phosphorus removal experienced in plants from time to time even when anaerobic zones are present.

The model, coded in Sumo© was successfully calibrated against typical bio-P plant configurations, as well as detailed data from Clean Water Services' Rock Creek facility including both full scale operational data and specific batch P release and uptake tests. The full model file (including parameter values, etc.) is available at the following link: http://www.dynamita.com/wp-content/uploads/Sumo1.xlsm.

ACKNOWLEDGEMENTS

This project was carried out with Sumo© modeling and simulation software (Dynamita 2017) based on the data provided by Clean Water Services (Hillsboro, OR) and Northeastern University (Boston, MA).

REFERENCES

Ahn, J., Daidou, T., Tsuneda, S. & Hirata, A. 2001a Metabolic behavior of denitrifying phosphate accumulating organisms under nitrate and nitrite electron acceptor conditions. *Journal of Bioscience and Bioengineering* **92** (5), 442–446.

Ahn, J., Daidou, T., Tsuneda, S. & Hirata, A. 2001b Selection and dominance mechanisms of denitrifying phosphate-accumulating organisms in biological phosphate removal process. *Biotechnology Letters* **23** (24), 2005–2008.

Barker, P. S. & Dold, P. L. 1997 General model for biological nutrient removal activated-sludge systems: model presentation. *Water Environment Research* **69** (5), 969–984.

Camejo, P. Y., Owen, B. R., Martirano, J., Ma, J., Kapoor, V., Domingo, J. S., McMahon, K. D. & Noguera, D. R. 2016 *Candidatus* Accumulibacter phosphatis clades enriched under cyclic anaerobic and microaerobic conditions simultaneously use different electron acceptors. *Water Research* **102**, 125–137.

Downing, L., Young, M., Cramer, J., Nerenberg, R. & Bruce, S. 2014 Low level DO operation: impacts on energy, nutrient and ecology. In: *Proceedings of the 87th Annual Water Environment Federation Technical Conference and Exhibition*, Chicago, IL.

Dunlap, P., Martin, K. J., Stevens, G., Tooker, N., Barnard, J. L., Gu, A. Z., Takacs, I., Shaw, A., Onnis-Hayden, A. & Li, Y. 2016 Rethinking EBPR: what do you do when the model will not fit real-world evidence? *Presented at the 5th IWA/WEF Wastewater Treatment Modelling Seminar, Annecy, France*.

Gu, A. Z., Saunders, A., Neethling, J. B., Stensel, H. D. & Blackall, L. L. 2008 Functionally relevant microorganisms to enhanced biological phosphorus removal performance at full-scale wastewater treatment plants in the United States. *Water Environment Research* **80**, 688–698.

Hauduc, H., Rieger, L., Oehmen, A., van Loosdrecht, M. C. M., Comeau, Y., Héduit, A., Vanrolleghem, P. A. & Gillot, S. 2013 Critical review of activated sludge modeling: state of process knowledge, modeling concepts, and limitations. *Biotechnology and Bioengineering* **110**, 24–46.

Hu, Z. R., Wentzel, M. C. & Ekama, G. A. 2007 A general kinetic model for biological nutrient removal activated sludge systems: model development. *Biotechnology and Bioengineering* **98** (6), 1242–1258.

Jimenez, J., Dold, P., Du, W. & Burger, G. 2014 Mainstream nitrite-shunt with biological phosphorus removal at the city of St. Petersburg Southwest WRF. In: *Proceedings of the Water Environment Federation, WEFTEC 2014*, pp. 696–711.

Jimenez, J., Stensel, D. & Daigger, G. 2017 Simultaneous nutrient removal through low dissolved oxygen operation: application, pitfalls and design. In: *WEFTEC 2017 Proceedings*, pp. 1308–1313.

Keene, N. A., Reusser, S. R., Scarborough, M. J., Grooms, A. L., Seib, M., Domingo, J. S. & Noguera, D. R. 2017 Pilot plant demonstration of stable and efficient high rate biological nutrient removal with low dissolved oxygen conditions. *Water Research* **121**, 72–85.

Kuba, T., van Loosdrect, M. C. M., Brandse, F. A. & Heijnen, J. J. 1997 Occurrence of dentirifying phosphorus removal bacteria in modified UCT type wastewater treatment plants. *Water Research* **31** (4), 777–786.

Lanham, A. B., Oehmen, A., Saunders, A. M., Carvalho, G., Nielsen, P. H. & Reis, M. A. M. 2014 Metabolic modelling of full-scale enhanced biological phosphorus removal sludge. *Water Research* **66**, 283–295.

Le Moullec, Y., Gentric, C., Potier, O. & Leclerc, J. P. 2010 Comparison of systemic, compartmental and CFD modelling approaches: application to the simulation of a biological reactor of wastewater treatment. *Chemical Engineering Science* **65**, 343–350.

Lopez-Vazquez, C. M., Hooijmans, C. M., Brdjanovic, D., Gijzen, H. J. & van Loosdrecht, M. C. M. 2008 Factors affecting the microbial populations at full-scale enhanced biological phosphorus removal (EBPR) wastewater treatment plants in the Netherlands. *Water Research* **42**, 2349–2360.

Lopez-Vazquez, C. M., Oehmen, A., Hooijmans, C. M., Brdjanovic, D., Gijzen, H. J., Yuan, Z. & van Loosdrecht, M. C. M. 2009 Modeling the PAO-GAO competition: effects of carbon source, pH and temperature. *Water Research* **43**, 450–462.

Lu, H., Keller, J. & Yuan, Z. 2007 Endogenous metabolism of *Candidatus* Accumulibacter phosphatis under various starvation conditions. *Water Research* **41**, 4646–4656.

Meijer, S. C. F. 2004 *Theoretical and Practical Aspects of Modelling Activated Sludge Processes*. Department of Biotechnological Engineering. Doctoral thesis, Delft University of Technology, The Netherlands, 218.

Oehmen, A., Lopez-Vazquez, C. M., Carvalho, G., Reis, M. A. M. & van Loosdrecht, M. C. M. 2010 Modelling the population dynamics and metabolic diversity of organisms relevant in anaerobic/anoxic/aerobic enhanced biological phosphorus removal processes. *Water Research* **44**, 4473–4486.

Rubio-Rincon, F. J., Lopez-Vazquez, C. M., Welles, L., van Loosdrect, M. C. M. & Brdjanovic, D. 2017 Cooperation between *Candidatus* Compatibacter and *Candidatus* Accumulibacter clade I, in denitrification and phosphate removal processes. *Water Research* **120**, 156–164.

Schauer, P., Menniti, A. & Maher, C. 2017 Testing the limits of EBPR for stable operation. In: *WEFTEC 2017 Proceedings*, pp. 1581–1594.

Siegrist, H., Brunner, I., Koch, G., Phan, L. C. & Van Le, C. 1999 Reduction of biomass decay rate under anoxic and anaerobic conditions. *Water Science and Technology* **39**, 129–137.

Tooker, N. B., Barnard, J. L., Bott, C., Carson, K., Dombrowski, P., Dunlap, P., Martin, K., McQuarrie, J., Menniti, A., Phillips, H., Schauer, P., Shaw, A., Stevens, G., Takács, I., Onnis-Hayden, A. & Gu, A. Z. 2016 *Side-Stream Enhanced Biological Phosphorus Removal As A Sustainable And Stable Approach For Removing Phosphorus From Wastewater WEF/IWA Nutrient Removal and Recovery Conference, Denver, CO, USA*.

Tooker, N. B., Li, G., Bott, C., Dombrowski, P., Schauer, P., Menniti, A., Shaw, A., Barnard, J. L., Stinson, B., Stevens, G., Dunlap, P., Takacs, I., Phillips, H., Analla, H., Russell, A., Ellsworth, A., McQuarrie, J., Carson, K., Onnis-Hayden, A. & Gu, A. Z. 2017 Rethinking and reforming enhanced biological phosphorus removal (EBPR) strategy – concepts and mechanisms of side-stream EBPR. In: *WEFTEC 2017 Proceedings*, pp. 2547–2564.

Welles, L., Abbas, B., Sorokin, D. Y., Lopez-Vazquez, C. M., Hooijmans, C. M., van Loosdrecht, M. C. M. & Brdjanovic, D. 2017 Metabolic response of '*Candidatus* Accumulibacter phosphatis' clade II C to changes in influent P/C ratio. *Frontiers in Microbiology* **7**, 2121.

First received 30 June 2018; accepted in revised form 16 November 2018. Available online 4 December 2018